UAB
Universitat Autònoma de Barcelona

The Role of Low-Density Lipoprotein Cholesterol and 27-Hydroxycholesterol in Epithelial Thyroid Cancer

Giovanna Revilla Senra

PhD Thesis • 2023

The Role of Low-Density Lipoprotein Cholesterol and 27-Hydroxycholesterol in Epithelial Thyroid Cancer

Giovanna Revilla Senra

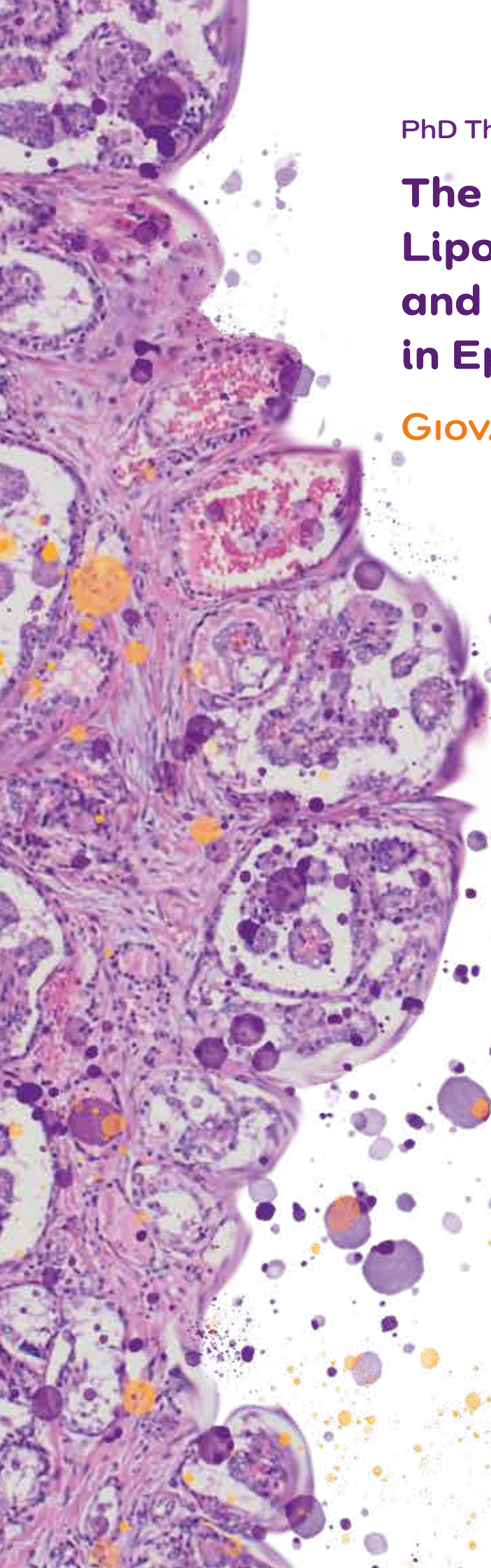

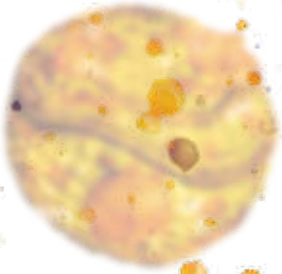

UAB
Universitat Autònoma de Barcelona

This thesis was researched and written in the **Pathophysiology of Lipid-related diseases group** and in the **Experimental Endocrinology Department** of the Research Institute, Hospital de la Santa Creu i Sant Pau

The Role of Low-Density Lipoprotein Cholesterol and 27-Hydroxycholesterol in Epithelial Thyroid Cancer

PhD Thesis

Doctoral Program in Biochemistry, Molecular Biology and Biomedicine

Department of Biochemistry and Molecular Biology
Universitat Autònoma de Barcelona
Institut de Recerca de l'Hospital de la Santa Creu i Sant Pau

Directors

Eugènia Mato Matute **Joan Carles Escolà Gil**

Tutor

Francisco Blanco Vaca

Barcelona, 2023

Autonomous University of Barcelona
Department of Biochemistry and Molecular Biology
Doctoral Program in Biochemistry, Molecular Biology and Biomedicine

The Role of Low-Density Lipoprotein Cholesterol and 27-Hydroxycholesterol in Epithelial Thyroid Cancer

Thesis presented by Giovanna Revilla Senra to apply for the degree of Doctor by the Autonomous University of Barcelona in the program of PhD in Biochemistry, Molecular Biology and Biomedicine.

This thesis has been carried out in the Pathophysiology of Lipid-related diseases group and in the Experimental Endocrinology Department of the Research Institute, Hospital de la Santa Creu i Sant Pau, co-directed by Dra. Eugènia Mato and Dr. Joan Carles Escolà Gil and supervised by Dr. Francisco Blanco Vaca.

Dra. Eugènia Mato
Senior Researcher
CIBER BBN

Dr. Joan Carles Escolà Gil
Senior Researcher
Institut de Recerca de l'Hospital de la Santa Creu i Sant Pau

Dr. Francisco Blanco Vaca
P.I. of Molecular Bases of Cardiovascular Disease group.
Servei de Bioquímica, Hospital de la Santa Creu i Sant Pau. Departament de Bioquímica i Biologia Molecular. Universitat Autònoma de Barcelona (UAB)

Giovanna Revilla Senra

Institut de Recerca de l'Hospital de la Santa Creu i Sant Pau

Barcelona, September 2023

A mis padres

A mi abuelo

A estudiar que es la ciencia tesoro,
más valiosa que el rico metal,
es la ciencia la joya preciada
que enaltece y eleva la moral.
Y si el tiempo de niños perdemos,
no tendremos jamás bienestar.
Estudiando seremos mañana,
hombres buenos de sano ideal.

TABLE OF CONTENTS

ACKNOWLEDGEMENTS

I finalment, ha arribat el moment d'escriure l'apartat que potser em fa més respecte redactar. I és que si la meva etapa com a doctorand ha permès tancar la meva formació acadèmica amb felicitat i nostàlgia, ha sigut gràcies a tota la gent que m'ha acompanyat. Per això espero que aquestes paraules estiguin a l'alçada de totes aquestes persones.

Vull començar agraint a qui m'han brindat l'oportunitat de fer aquesta tesi doctoral. Gràcies Eugènia per confiar en mi des del principi, per ensenyar-me com un líder és millor líder quan som tots un equip. Gràcies perquè m'has fet sentir com a casa i per ajudar-me no només al laboratori sinó també en l'aspecte personal. Gràcies Joan Carles, per haver lluitat tant per aconseguir la PFIS, per aportar serenor en els moments de caos i per sempre animar-me. Em fascina el teu amor per la ciència. Gràcies Xisco, per haver confiat en mi quan pràcticament ni em coneixies. Gràcies per donar-me l'oportunitat de fer la tesi doctoral en aquest grup. Gracias Dr. Leiva, tu insaciable sed de conocimiento y perseverancia me fascinan. Gracias por acompañarme todos estos años y por siempre estar dispuesto a ayudarme en lo que fuera necesario.

Gràcies Dr. Moral i Dra. Fina per acompanyar-me durant aquests anys. Gràcies per sempre tenir paraules agradables cap a mi i animar-me a cada reunió. Per mi ha sigut un honor tenir-vos a la meva comissió de seguiment.

Rosi, hasta hace poco mi única compañera diaria de laboratorio. Gracias por ser así, por desprender alegría en cada poro de tu piel, por darle vida al laboratorio y alegrarme todas las mañanas. Te quiero mucho y no sabes cuánto te echaré de menos. Gràcies a tots els companys de Bioquímica: Núria, Raquel, Carla, Sònia i José Luis, per fer-me sentir sempre com una més del grup i ajudar-me en tot moment. Gràcies a les "padeleres científiques"; Noe, Mireia i Marina, per totes les tardes de pàdel, riures i per deixar-me compartir moments amb vosaltres fora del lab. David, qué te voy a decir… Gracias por todos los momentos divertidos en el lab, por siempre estar dispuesto a ayudarme en las "no pocas" dudas que he tenido. Ojalá haberte tenido más en mi día a día.

Gràcies a tots els companys del IR: Marga, Esther, Josep, Rosa, Carmen, Edu, Pablo, Virtu, Lara i Eli. Gràcies per fer-me sentir tan estimada i per ajudar-me sempre que ho he necessitat.

Gràcies als cirurgians de l'hospital i als companys d'anatomia patològica, sense vosaltres aquesta tesi no hagués estat possible. Gràcies Vicky per sempre acollir-me amb un somriure i per dedicar-me tant de temps quan et faltaven hores al dia. Aquesta portada també és teva.

Thanks to my labmates in New York. Vera, thank you for teaching me and caring about me during my fellowship. That July 4th will always be in my memory. Thank you Katherine, for being my everything buddy there, I miss you a lot. Gracias Dr. Fagin por acogerme como lo hiciste y por brindarme la oportunidad de vivir la que hasta ahora ha sido la mejor experiencia de mi vida. Mi admiración a tu carrera científica es máxima.

Gràcies a tot el grup de "pollos", que per mi són família, amb qui he crescut des de la guarderia i, tot i que les trobades siguin impossibles, sabem que ens tenim sempre. Al grup de "Coia", i és que la vida universitària no hagués sigut la mateixa sense vosaltres. Gràcies per sempre ser-hi, i per estimar-me tot i la meva "independència". Anna i Alba, què dir-vos si em coneixeu més del que em conec jo mateixa, gràcies per moltes coses i per ser-hi absolutament sempre. Oriol i Lídia, gràcies per tots els cafès d'actualitzacions i de compartir penes doctorals.

Gràcies a les integrants del "Last Dance", i a tothom del món del bàsquet. Heu fet que tingui moltes nits èpiques per recordar, i les que queden. Gràcies Ari i Eva, i és que no puc estar més agraïda a aquest esport per haver-me donat a dues persones que ja són imprescindibles per mi. Erika, por casualidades de la vida llegaste a mi vida, y bendito día. Gracias por desprender felicidad a todas horas, por siempre estar dispuesta a todo y por ser mi confidente. Adriana, Llançà siempre será nuestra casa, gracias por ser como mi hermana mayor. Aina, gràcies es queda molt curt. No concebo la meva vida sense tu. Gràcies per ser la meva meitat i la meva màxima confident.

Gracias a mi familia Nebredeña, porque "El pueblo" siempre será nuestro mejor punto de encuentro y que nunca nos falte. A las "pris"; Fabiola, Anna, María, Paty, Virgi y Laura, gracias por los viajes, los carnavales, las confidencias y por seguir siendo las Revis en esencia. Gracias Abuelo, hoy estás malito y aún así nunca pierdes tu espíritu luchador y la devoción por tu familia. Gracias por tenerme siempre tan presente y preocuparte tanto a pesar de la distancia. Ojalá haberte tenido más cerca. A la familia Figuerenca, porque sois mi día a día. Eca, gracias por ser mi segunda madre, por haberme cuidado como a una hija, es imposible

no emocionarme. Pepe, gracias también por haberme cuidado tanto y tan bien. Laura, Fernando, Isa, Fran, Eri y Tivi, la palabra primos se queda muy corta. Gracias por hacerme sentir que siempre estáis ahí, por quererme tanto, por ser como mis hermanos. Lluc, Biel y Gerard, gràcies per ser l'alegria de la família, per fer-me madrina i per tornar-me a fer sentir aquella il·lusió per les coses més senzilles. Gracias Maico y Javi, por estar tan presente a pesar de la distancia. Luis y Lourdes, porque para mi sois familia, gracias por estar siempre. Carlos y Maria, por ser mis papis de Barcelona. Gracias junto con Carlos junior por todas esas cenas italianas tan ricas.

A mis padres, mis pilares, os lo debo absolutamente todo. Siempre habéis confiado en mi y habéis dejado que escogiera mi camino. Mama, aunque a veces nos mataríamos, gracias por siempre cuidarme como la que más, por tu esfuerzo y dedicación, y es que el amor a veces hasta duele. Papa, las palabras de agradecimiento se quedan muy cortas. Gracias por siempre remar a favor, por confiar en mi, apoyarme y hacerlo todo más fácil.

Pepe, gràcies per ser el meu suport diari, per fer-me sentir que res és impossible, per confiar en mi més que ningú. Gràcies per creure en nosaltres i per mai desistir. Em sento molt afortunada de tenir-te al meu costat, de que m'estimis tant però sobretot, tan bé. Gràcies per fer-me riure cada dia, per compartir passions conflictives i seguir-les per millors reconciliacions (vinagret). Gràcies per fer-me sentir més lliure que mai. La següent tesi és la teva, i jo no puc estar més il·lusionada per seguir creixent junts, i amb el millor que tenim, la Kiaris.

ABBREVIATIONS

AJCC	American Joint Committee on Cancer
ANOVA	Analysis Of Variance
Apo	Apolipoprotein
ATC	Anaplastic Thyroid Cancer
BBM	Brush Border Membrane
BHT	Butylated hydroxytoluene
BMI	Body Mass Index
BMR	Basal Metabolic Rate
BTT	Benign Thyroid Cancer
cDNA	Complementary DNA
CM	Chylomicrons
CT	Computer Tomography
DHGTC	Differentiated High-Grade Thyroid Carcinoma
DiI	1,1'-Dioctadecyl-3,3,3',3'-Tetramethylindocarbocyanine Perchlorate
DTC	Differentiated Thyroid Carcinoma
EDTA	Ethylenediaminetetraacetic Acid
EGF	Epidermal Growth Factor
EMA	European Medicine Agency
ER	Endoplasmic Reticulum
FDA	Food and Drug Agency
FDR	False Discovery Rate
FNA	Fine Needle Aspiration
FPP	Farnesyl Pyrophosphate
FTC	Follicular Thyroid Carcinoma
GDNF	Glial cell line-derived Neurotrophic Growth Factor
GDP	Guanosine Diphosphate
GTP	Guanosine Triphosphate
HC	Hydroxycholesterol
HDL	High-Density Lipoprotein
I^{13}	Iodine-13
IDL	Intermediate-Density Lipoprotein
IDOL	Inducible Low-Density Lipoprotein

IEFV	Invasive Encapsulated Follicular Variant
LDL	Low-Density Lipoprotein
LDL-C	LDL-Cholesterol
LDLR	Low-Density Lipoprotein Receptor
LPL	Lipoprotein Lipase
LXR	Liver X Receptor
LXRE	Liver X Receptor Responsive Element
MMP	Matrix Metalloproteinases
MTC	Medullary Thyroid Carcinoma
MVB	Multivesicular Bodies
NIFTP	Non-invasive Follicular Thyroid Neoplasm with Papillary-like Nuclear Feature
NIS	Sodium Iodine Symporter
NP	Nanoparticles
OCA	Oncocytic Carcinoma
OCT	Optimal Cutting Temperature
ORP	Oxysterol-related Protein
OSBP	Oxysterol-Binding Protein
PBS	Phosphate-buffered saline
PCR	Polymerase Chain Reaction
PDTC	Poorly Differentiated Thyroid Cancer
PI (4,5) P_2	Phosphatidylinositol-(4,5)-Bisphosphate
PMSF	Phenylmethylsulfonyl Fluoride
PTC	Papillary Thyroid Carcinoma
PyMT	Mammary tumor virus-polyomavirus middle T antigen
RAI	Radioactive Iodine Treatment
RAI-R	RAI-refractory
RNS	Reactive Nitrogen Species
ROS	Reactive Oxygen Species
RT-PCR	Quantitative Real-Time PCR
RTK	Receptor Tyrosine Kinases
RXR	Retinoid X Receptor
SCAP	SREBP Cleavage-activating Protein
SERM	Selective Estrogen Receptor Modulator
SNX	Sorting Nexins

SRE	Sterol Regulatory Element
SSD	Sterol Sensing Domain
TBST	Tris Buffer Saline containing 0.05% of Tween-20
TC	Thyroid Cancer
TG	Triglycerides
TKI	Tyrosine Kinase Inhibitors
TL	Ipsilteral Thyroid Lobectomy
TM	Transmembrane
TME	Tumor Microenvironment
TSH	Thyroid-Stimulating hormone
TT	Total Thyroidectomy
VDA	Vascular Disrupting Agents
VEGF	Vascular Endothelial Growth Factor
VLDL	Very-Low Density Lipoprotein
VPS	Vacuolar Protein-Sorting
WASH	Wiskott–Aldrich Syndrome Protein and SCAR homolog
WDTC	Well-Differentiated Thyroid Carcinoma
WHO	World Health Organization

INDEX OF FIGURES

INDEX OF TABLES

ABSTRACT

Thyroid cancer (TC) represents 3% of all cancer cases globally, and its incidence has increased significantly in recent decades. Papillary thyroid carcinoma (PTC) is the most common subtype, accounting for 80%–90% of diagnosed cases. While PTC generally responds well to treatment, certain subtypes may have a high risk of recurrence and advanced disease and can ultimately become resistant to radioactive iodine treatment.

Obesity and dyslipidemias (e.g., hypercholesterolemia) have been linked to worse cancer progression, including TC. Additionally, the *BRAF*^{V600E} mutation in the MAPK signaling pathway, present in 60% of PTC cases, is associated with more aggressive PTC. The overall aim of this thesis was to investigate the role of cholesterol in TC and the molecular mechanisms involved.

The first objective was to examine the association between low-density lipoprotein (LDL) receptor (LDLR) expression, intratumoral 27-hydroxycholesterol (HC) levels, and the malignancy of TC tumors. Patients with high-risk PTC, poorly differentiated TC (PDTC), and anaplastic TC (ATC) showed low levels of LDL-cholesterol (LDL-C) in their serum. These TC subtypes displayed higher LDLR expression and increased levels of intratumoral 27-HC due to the downregulation of the CYP7B1 enzyme responsible for 27-HC degradation. *In vitro* studies showed that LDL promoted cellular proliferation and migration, and these effects were influenced by the CYP27A1 and CYP7B1 enzymes.

The second objective was to explore whether the *BRAF*^{V600E} mutation in an environment rich in LDL could enhance LDLR-mediated oncogenic processes through the RAS/RAF/MAPK (MEK)/ERK pathway. The results revealed differential regulation of LDLR expression in PTC cell lines (TPC1 and BCPAP) based on *BRAF*^{V600E} mutational status, which significantly affected LDL uptake capacity. Treatment with the *BRAF*^{V600E} inhibitor, vemurafenib, partially blocked the oncogenic effects of *BRAF*^{V600E}, leading to downregulated LDLR expression and attenuated LDL-induced proliferation. These findings suggest a potential synergistic effect between LDL and tumors harboring *BRAF*^{V600E}. Furthermore, LDL has the ability to act as a coadjutant with *BRAF*^{V600E}, accelerating oncogenic processes by hyperactivating the RAS/RAF/MAPK (MEK)/ERK signaling cascade in cells with *BRAF*^{V600E} mutations compared to wild-type cells.

Overall, this study demonstrated that LDL and its metabolite, 27-HC, play a role in promoting malignancy in TC. In the context of BRAF mutant tumors, the exposure to high LDL levels can lead to hyperactivation of the RAS/RAF/MAPK (MEK)/ERK signaling cascade, resulting in a worse tumor prognosis.

RESUMEN

El cáncer de tiroides (CT) representa el 3% de todos los casos de cáncer a nivel mundial. Su incidencia ha aumentado significativamente en las últimas décadas, siendo el carcinoma papilar de tiroides (CPT) el subtipo más común con el 80%-90% de los casos diagnosticados. Aunque el CPT suele responder bien al tratamiento, existen ciertos subtipos que pueden presentar un alto riesgo de recurrencia y progresión a etapas avanzadas, volviéndose resistentes al tratamiento con yodo radiactivo.

La obesidad y las dislipidemias (por ejemplo, la hipercolesterolemia) se han relacionado con una peor progresión del cáncer, incluido el CT. Además, la mutación de *BRAF*^{V600E} en la vía de señalización MAPK, presente en el 60% de los casos de CPT, se asocia con CPT más agresivos. El objetivo general de esta tesis fue investigar el papel del colesterol en el CT y los mecanismos moleculares involucrados.

El primer objetivo fue examinar la asociación entre la expresión del receptor de lipoproteínas de baja densidad (LDLR), los niveles intratumorales de 27-hidroxicolesterol (27-HC) y la malignidad de los tumores de CT. Los pacientes con CPT de alto riesgo, CT poco diferenciados (PDTC) y CT anaplásicos (ATC) mostraron bajos niveles de colesterol de lipoproteínas de baja densidad (LDL-C) en su suero. Estos subtipos de CT mostraron una mayor expresión de LDLR y niveles elevados de 27-HC intratumoral debido a la regulación a la baja de la enzima CYP7B1, responsable de la degradación del 27-HC. Los estudios *in vitro* mostraron que la LDL promovía la proliferación y migración celular, y estos efectos estuvieron influenciados por las enzimas CYP27A1 y CYP7B1.

El segundo objetivo fue explorar si la mutación *BRAF*^{V600E} en un ambiente rico en LDL podría mejorar los procesos oncogénicos mediados por LDLR a través de la vía RAS/RAF/MAPK (MEK)/ERK. Los resultados revelaron una regulación diferencial de la expresión de LDLR en líneas celulares de CPT (TPC1 y BCPAP) según el estado mutacional de *BRAF*^{V600E}, lo que afectó significativamente a la capacidad de captación de LDL. El tratamiento con el inhibidor de *BRAF*^{V600E}, vemurafenib, bloqueó parcialmente los efectos oncogénicos de *BRAF*^{V600E}, lo que condujo a una regulación a la baja de la expresión de LDLR y una proliferación atenuada. Estos hallazgos sugieren un posible efecto sinérgico entre la LDL y los tumores que albergan la mutación de *BRAF*^{V600E}. Además, la LDL tiene

la capacidad de actuar como coadyuvante con *BRAF*^{V600E}, acelerando los procesos oncogénicos al hiperactivar la cascada de señalización RAS/RAF/MAPK (MEK)/ERK en células con mutaciones de *BRAF*^{V600E}.

En general, este estudio demostró que la LDL y su metabolito, 27-HC, desempeñan un papel en la promoción de la malignidad en el CT. En el contexto de tumores con mutación BRAF, la exposición a altos niveles de LDL puede promover la hiperactivación de la cascada de señalización RAS/RAF/MAPK (MEK)/ERK, lo que resulta en un peor pronóstico del tumor.

RESUM

El càncer de tiroides (CT) representa el 3% de tots els casos de càncer a nivell mundial. La seva incidència ha augmentat significativament en les últimes dècades, essent el carcinoma papil·lar de tiroide (CPT) el subtipus més comú amb el 80%-90% dels casos diagnosticats. Encara que el CPT sol respondre bé al tractament, hi ha certs subtipus que poden presentar un alt risc de recurrència i progressió a etapes avançades, fent-se resistents al tractament amb iode radioactiu.

L'obesitat i les dislipèmies (per exemple, la hipercolesterolèmia) s'han relacionat amb una pitjor progressió del càncer, incloent-hi el CT. A més, la mutació de *BRAF*^{V600E} en la via de senyalització MAPK, present en el 60% dels casos de CPT, s'associa amb CPT més agressius. L'objectiu general d'aquesta tesi va ser investigar el paper del colesterol en el CT i els mecanismes moleculars involucrats.

El primer objectiu va ser examinar l'associació entre l'expressió del receptor de lipoproteïnes de baixa densitat (LDLR), els nivells intratumorals de 27-hidroxicolesterol (27-HC) i la malignitat dels tumors de CT. Els pacients amb CPT d'alt risc, CT poc diferenciat (PDTC) i CT anaplàsic (ATC) van mostrar baixos nivells de colesterol de lipoproteïnes de baixa densitat (LDL-C) en el seu sèrum. Aquests subtipus de CT van mostrar una major expressió de LDLR i nivells elevats de 27-HC intratumoral a causa de la regulació a la baixa de l'enzim CYP7B1, responsable de la degradació del 27-HC. Els estudis *in vitro* van mostrar que la LDL promovia la proliferació i migració cel·lular, i aquests efectes van estar influïts pels enzims CYP27A1 i CYP7B1.

El segon objectiu va ser explorar si la mutació de *BRAF*^{V600E} en un ambient ric en LDL podria millorar els processos oncogènics mitjançant el LDLR a través de la via RAS/RAF/MAPK (MEK)/ERK. Els resultats van revelar una regulació diferencial de l'expressió de LDLR en línies cel·lulars de CPT (TPC1 i BCPAP) segons l'estat mutacional de *BRAF*^{V600E}, la qual cosa va afectar significativament a la capacitat de captació de LDL. El tractament amb l'inhibidor de *BRAF*^{V600E}, vemurafenib, va bloquejar parcialment els efectes oncogènics de *BRAF*^{V600E}, i conseqüentment, una regulació a la baixa de l'expressió de LDLR i una proliferació atenuada. Aquests resultats suggereixen un possible efecte sinèrgic entre la LDL i els tumors portadors de la mutació de *BRAF*^{V600E}. A més, es proposa la capacitat de

la LDL d'actuar com a coadjuvant amb *BRAF*^{V600E}, accelerant els processos oncogènics mitjançant la hiperactivació de la cascada de senyalització RAS/RAF/MAPK (MEK)/ERK en cèl·lules amb la mutació de *BRAF*^{V600E}.

En general, aquest estudi va demostrar que la LDL i el seu metabòlit, 27-HC, juguen un paper en la promoció de la malignitat en el CT. En el context de tumors amb mutació de BRAF, l'exposició a alts nivells de LDL pot promoure la hiperactivació de la cascada de senyalització RAS/RAF/MAPK (MEK)/ERK promovent un pitjor pronòstic del tumor.

GRAPHICAL ABSTRACT

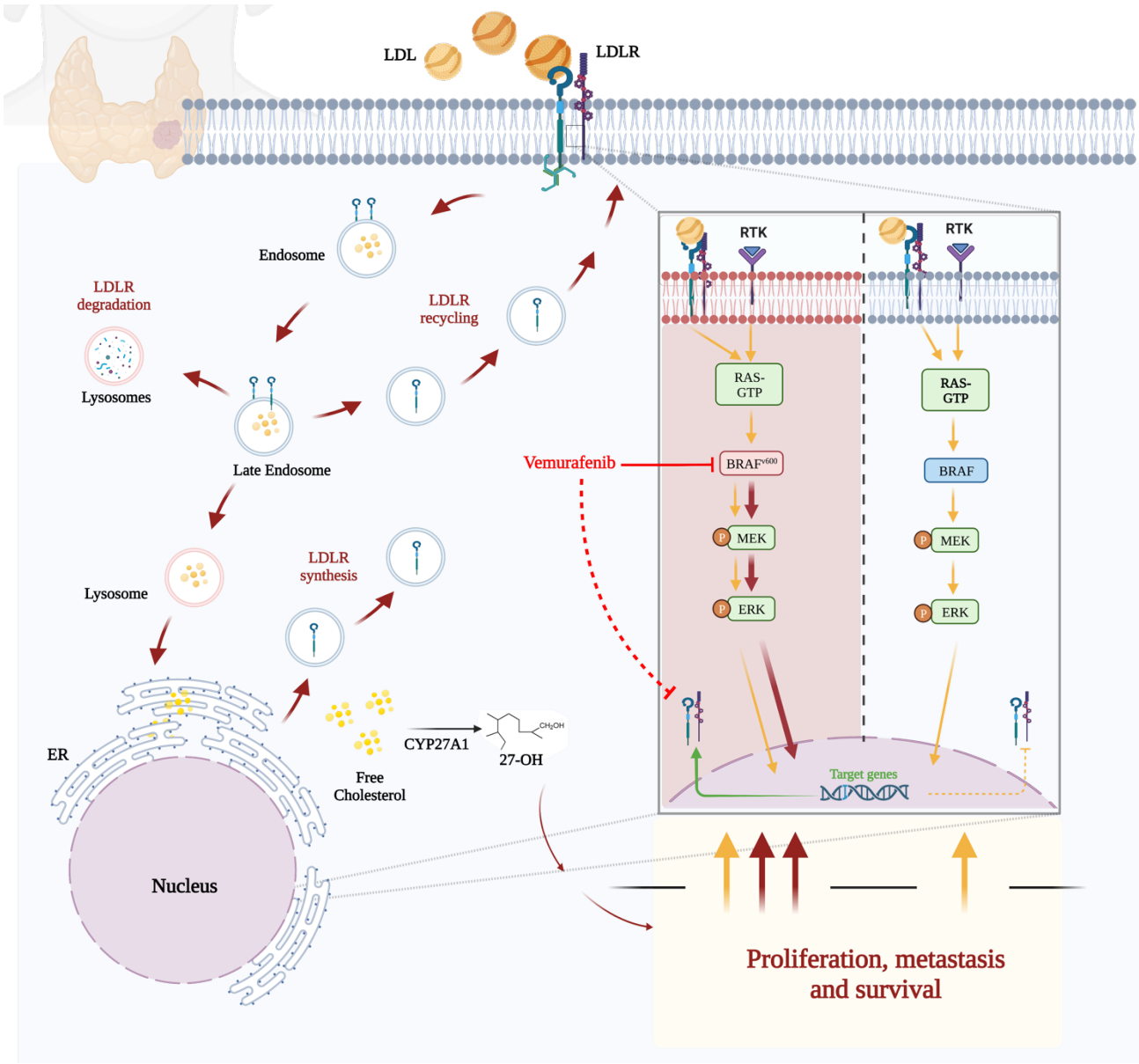

Chapter I

- INTRODUCTION -

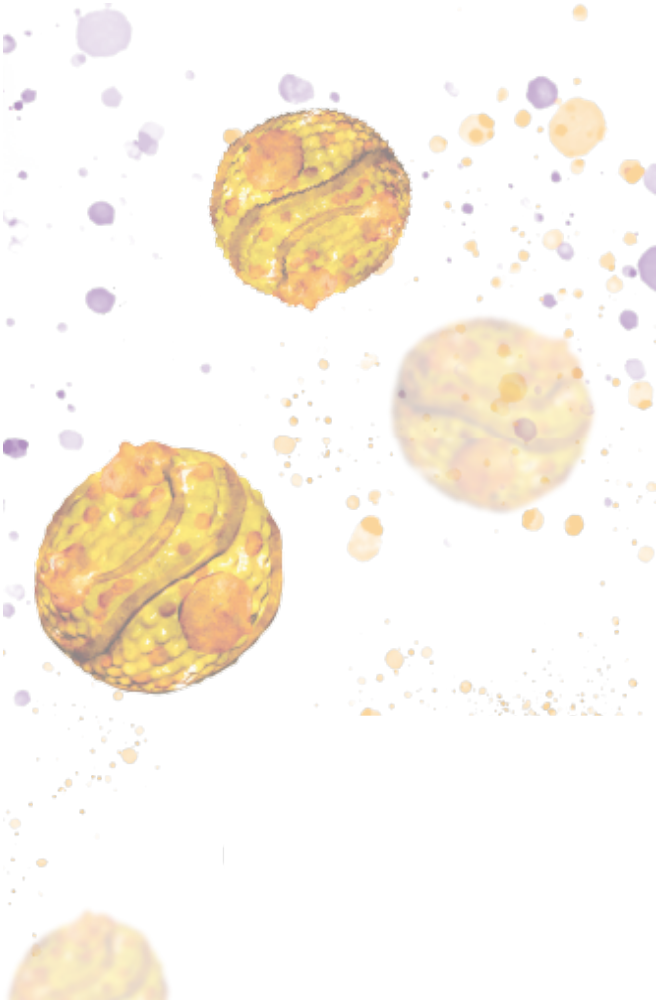

1. Thyroid Gland

1.1 Morphology and Functions

The thyroid is an endocrine gland located in the lower, anterior part of the neck that is formed as two lobes (right and left) joined by an intermediate structure named the isthmus. The lobes are 5 x 2.5 x 2.5 cm in dimension, weigh around 25 g, and become bigger in women during the menstruation and pregnancy. These lobes consist of structural and functional units called thyroid follicles, which are 0.02–0.9 mm diameter and spherical, and the wall is made of cuboidal cells called follicular cells, responsible for the secretion of thyroid hormone[1]. Therefore, 70% of this gland is composed of follicular cells, 20% correspond to endothelial cells, and the rest are fibroblasts and C cells (Figure 1)[2].

The thyroid gland has a key role in the regulation of the body basal metabolic rate (BMR), together with many other important cellular functions such as: the homeostasis of calcium metabolism, the stimulation of somatic and physical growth, the regulation of heart rate and contraction, and so on. The thyroid gland produces three types of iodothyronines, T4, T3 and rT3, being the thyroglobulin the protein precursor. This is a protein within the colloid in the follicular lumen originally created within the rough endoplasmic reticulum of follicular cells and then transported into the follicular lumen. Thyroglobulin contains 123 units of tyrosine, which reacts with iodine in the follicular lumen. When thyroid hormones are needed, thyroglobulin is uptake from the colloid into the cells to obtain T4 and T3. Finally, the thyroid releases the hormones by passing from the cells into the circulation.

T4 is known as thyroxine; it corresponds to 90% of the inactive thyroid hormone and is the prohormone of triiodothyronine (T3), which belongs to 10% of the active thyroid hormone. The T4 hormone is converted peripherally to T3 by type 1 deiodinase in tissues with high blood flow (e.g., kidneys and liver). The third iodothyronine, rT3 (reverse T3), is inactive and is a metabolite from T4 formed by type 3 deiodinase activity[1,3]. It is believed the body produces rT3 when there is a severe illness or when the body enters starvation mode as a mechanism for saving energy[4]. However, there are many ideas around rT3 that have not been consistently proven, and the precise significance of this hormone function is still being teased out.

Between follicular cells there are parafollicular cells (also called the small C cells) that secrete a polypeptide hormone known as calcitonin, which plays a role in calcium homeostasis lowering serum calcium concentrations[1].

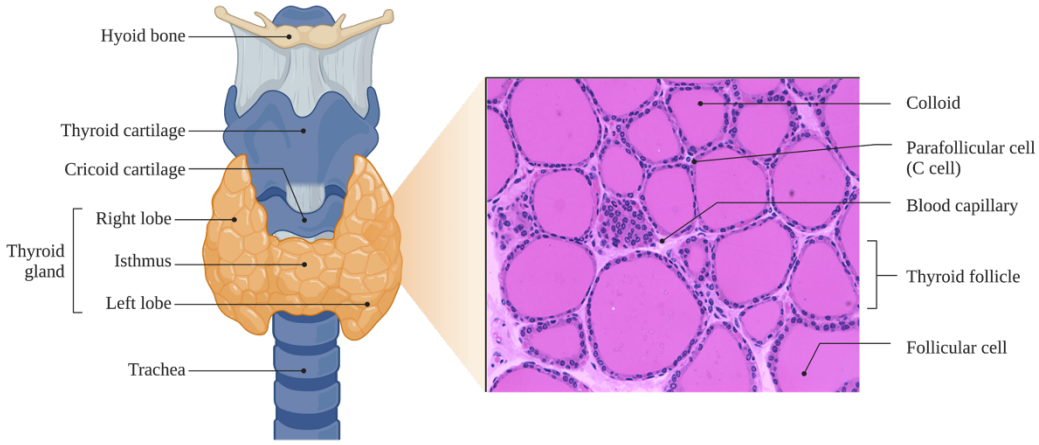

Figure 1. Thyroid gland anatomy and histology. Created with BioRender.com

2. Thyroid Cancer

2.1 Histological Classification (progression and prognosis)

Thyroid cancer (TC) is characterized by a wide spectrum of morphologies and behaviors including indolent tumors as well as the most aggressive and lethal malignancies. For this reason, an exact identification, diagnosis, and prognosis of TC are crucial. Figure 2 presents the 2022 World Health Organization (WHO) classification of thyroid tumors, which are divided into benign, low-risk, and malignant neoplasms[5].

Benign tumors are classified as follicular adenomas as well as variant adenomas that are clinically significant. The low-risk follicular cell-derived neoplasms include non-invasive follicular thyroid neoplasms with papillary-like nuclear features (NIFTP), thyroid tumors of uncertain malignant potential, and hyalinizing trabecular tumors[5]. Finally, the worst malignancies are classified as malignant follicular cell-derived neoplasms and are subdivided based on molecular profiles and aggressiveness, as follows:

- Well-Differentiated Thyroid Carcinomas (WDTC)
    - Papillary Thyroid Carcinomas (PTCs): this is the most common subtype, accounting for about 80%–90% of TC. It is characterized by the presence of

papillary structures, which are finger-like projections. It tends to grow slowly and has a good prognosis.

  - Follicular Thyroid Carcinomas (FTCs): represent the 10%–15% of TC. It typically forms follicular structures resembling closed sacs. These type of tumors have a higher tendency to invade blood vessels and spread to distant organs.

- Oncocytic carcinomas (OCAs): also known as Hürthle cell carcinoma, it is a variant of FTC characterized by the presence of oncocytic or Hürthle cells. These cells are large, granular cells with abundant eosinophilic cytoplasm due to the accumulation of mitochondria. This type of neoplasm accounts for a small percentage of TC, around 3%–5% of cases. It is more common in older people and tends to have a higher recurrence rate and a slightly worse prognosis compared to typical FTC.

- Differentiated high-grade thyroid carcinomas (DHGTCs): this is a term used to describe a subset of TC that exhibit aggressive behavior and have histological features indicating a higher grade of malignancy compared to typical differentiated thyroid carcinomas (DTCs). However, in some cases, certain thyroid tumors may exhibit features of high-grade malignancy, such as increased cellularity, nuclear atypia, mitotic activity, and invasion beyond the thyroid capsule. These tumors may have more aggressive behavior, higher rates of recurrence, and a poorer prognosis compared to typical DTCs.

- Invasive encapsulated follicular variant papillary thyroid carcinomas (IEFV-PTCs): this is characterized as a thyroid tumor with nuclear features of PTC but with a follicular growth pattern. This type of tumor is the second most common variant of PTC, accounting for 7–23% of all PTCs[6].

- Poorly differentiated thyroid carcinomas (PDTCs): this is a subtype of TC that falls between WDTC and undifferentiated TC in terms of cellular features and behavior, and it is therefore considered an intermediate stage of TC. Its most common histological features are cellular atypia, decreased differentiation, solid growth pattern

and increased mitotic activity. PDTC is associated with a higher risk of aggressive behavior, local invasion, and distant metastasis compared to WDTC.

- Anaplastic thyroid carcinomas (ATCs): this is a rare type but an aggressive form of TC, accounting for less than 2% of cases. It can develop from differentiated TC cells (PTC or FTC) or de novo from undifferentiated cells within the thyroid gland. It is characterized by undifferentiated, rapidly growing cells. ATC often has a poor prognosis due to its invasiveness and resistance to treatment with a five-year survival rate of less than 10%[7].

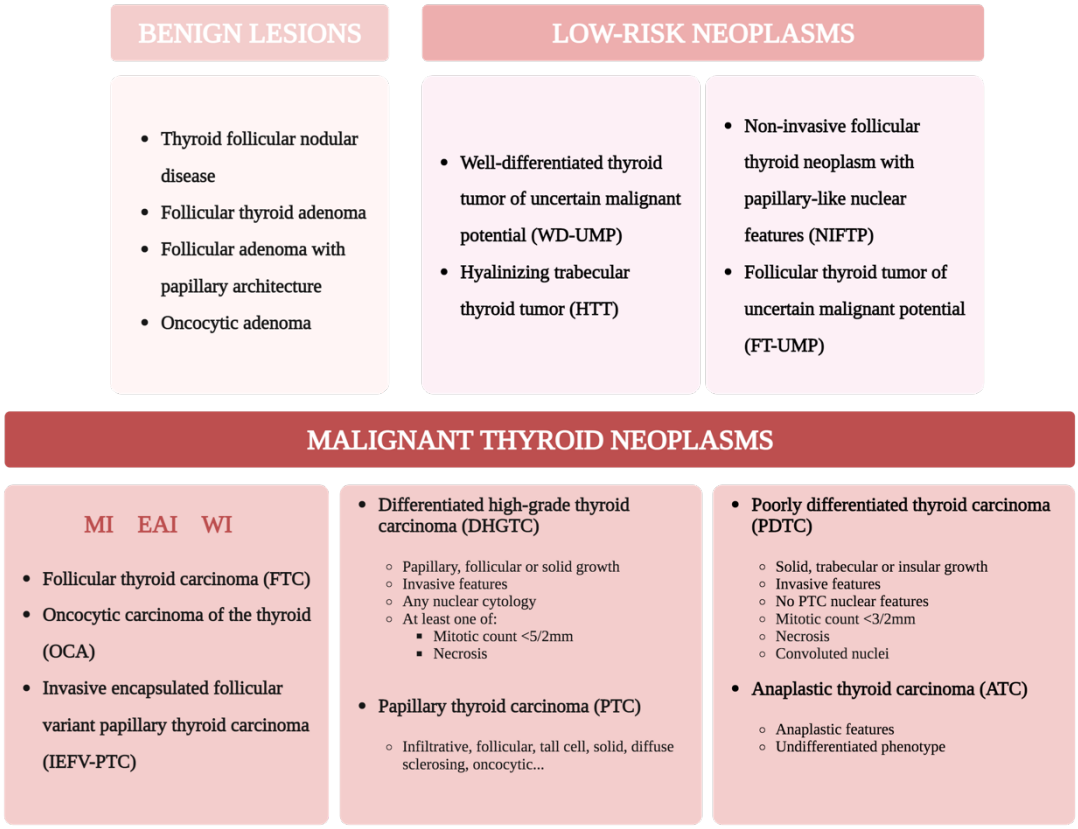

Figure 2. Overview of the main diagnostic groups of the 2022 World Health Organization (WHO) classification of thyroid tumors. MI, minimally invasive; EAI, encapsulated angioinvasive; WI, widely invasive. Created with BioRender.com. Modified from[5]

There are also other thyroid malignancies that are non-follicular cell-derived and have different histological and molecular features compared to the most common types of TC that arise from follicular cells:

- Medullary thyroid carcinomas (MTCs): arises from parafollicular or C cells, and it accounts for about 5%–10% of TCs.

- Thyroid lymphoma: is a rare type of TC that originates from lymphatic tissue within the thyroid gland. It can be classified as either Hodgkin's lymphoma or non-Hodgkin's lymphoma.

After someone is diagnosed with a subtype of TC, the next step is to determine the stage of the malignancy. TC ranges from stages I (less spread) through IV (more cancer spread). The staging system most often used is the **AJCC** (American Joint Committee on Cancer) **TNM** system, which consists of three key pieces of information:

- The extent (size) of the **t**umor **(T):** how large is the cancer? Has it grown into nearby structures?
- The spread to nearby lymph **n**odes **(N):** has the cancer spread to nearby lymph nodes?
- The spread (**m**etastasis) to distant sites **(M):** has the cancer spread to distant organs such as the lungs or liver?

People younger than 45 who are diagnosed with WDTC have a low likelihood of dying. In this case, the **TNM** stages for these people are I if they have no distant spread and II if they have distant spread. Regarding ATC, all these tumors are considered stage IV due to the poor prognosis for people with this type of cancer (Figure 3)[8].

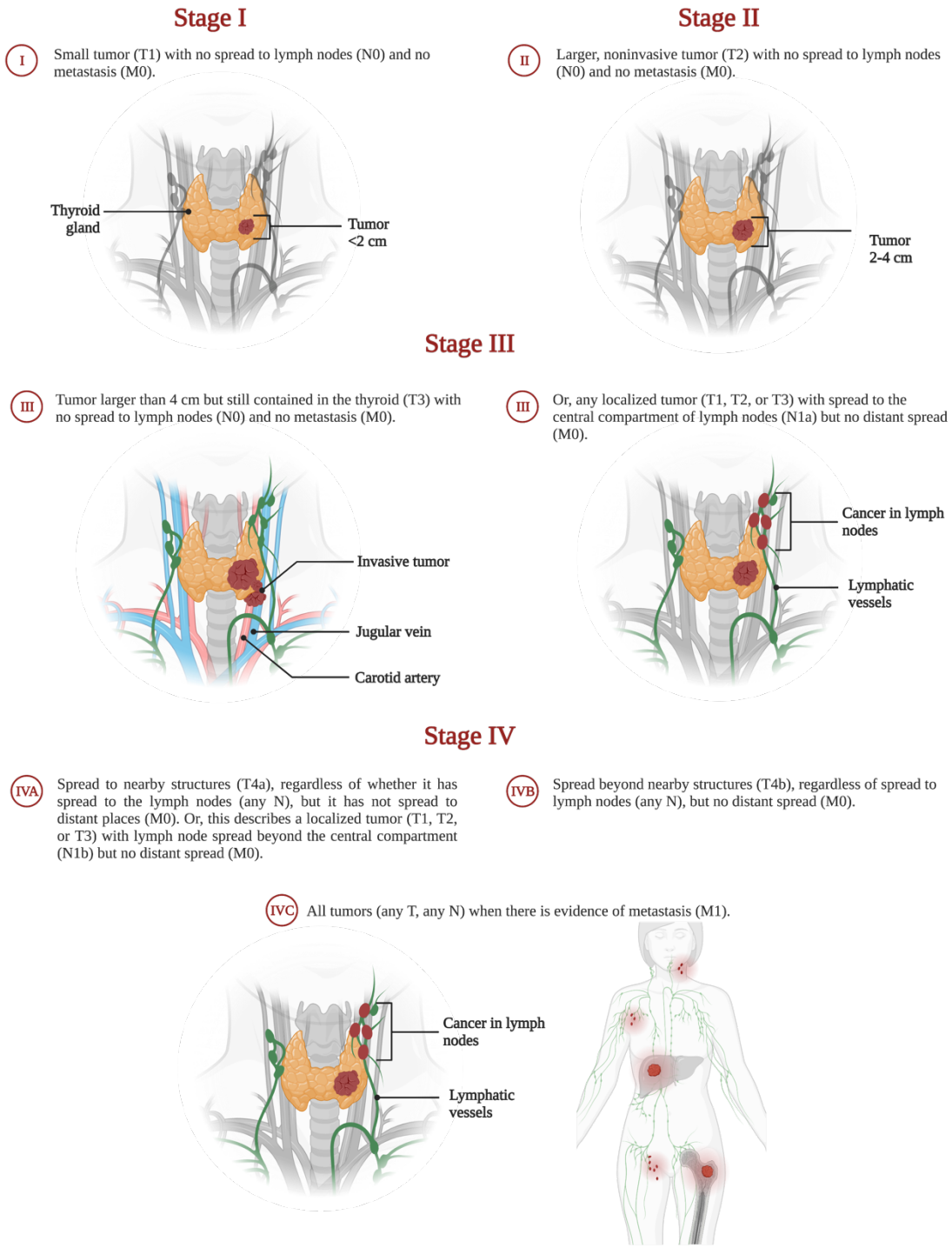

Figure 3. TNM staging classification for papillary thyroid carcinoma (PTC) in a 55-year-old person and older. Created with BioRender.com

2.2 Epidemiology Data of Thyroid Cancer

TC represents 3% of the global incidence of all cancers and its incidence has risen dramatically over the past decades. Although it is characterized as a rare disease, currently it is the 13th most common cancer diagnosis overall, the 6th most common in women, and the

most common form of endocrine tumor. Its incidence is about three-fold higher in women than in men, peaking around 55 years in women and 65 years in men and declining with older age. As such, women may have more opportunities for an incidental detection of thyroid nodules during the reproductive years and around menopause[9].

Nevertheless, these higher incidence trends have been mostly attributed to a widespread use of diagnostic imaging and better diagnostic tools available in higher-income countries. Because of this, TC incidence varies by geographic location in relation to care access and diagnostic practices, although environmental exposures could also play a role. In contrast with the increased incidence in certain places, mortality rates tend to be much lower or remained stable and vary much less geographically, along with less evidence of a sex disparity[9].

2.3 Risk Factors

2.3.1 Modifiable Risk Factors

- Ionizing radiation

Nowadays, the most well-established modifiable risk factor for TC is childhood exposure to ionizing radiation. Radiation exposure among the general population has increased in recent decades due to a dramatic increase in the use of diagnostic imaging, specifically computed tomography (CT)[9]. Thyroid tissue is very sensitive during the early years of life, and for that reason, ionizing radiation is especially harmful in children[10]. Around 5%–15% of the 63% total radiation exposure from CT in the United States impacted children. Additionally, repeated CT scans are common, and each scan promotes a greater cumulative thyroid dose and a greater risk of TC. For instance, a single head CT scan before age 20 has been associated with a 33–53% increased risk of TC[9]. Ionizing radiation causes DNA strand breaks and somatic mutations, inducing carcinogenesis. It has been demonstrated that exposure of thyroid cells to ionizing radiation can induce RET/PTC rearrangements. Aside from this, the most common point mutations (*BRAF* and *RAS* genes) found in the population do not seem to be associated with radiation-related tumors.

- Benign thyroid conditions

Some epidemiologic evidence suggests that TC is often preceded by benign thyroid disease such as thyroid nodules, goiter, hyperthyroidism, hypothyroidism, and thyroiditis. However, it remains unclear if thyroid diseases are the real cause of progression and development of TC. It is thought that diagnostic work-up of benign thyroid diseases may lead to an incidental detection of TC, though it is difficult to disentangle whether an association for a particular benign condition is because of the disease itself or its treatment[9].

- Dietary factors (iodine)

Iodine is a crucial element in the formation of thyroid hormones. Iodine deficiency is a risk factor for benign thyroid diseases like goiter and hypothyroidism, while iodine excess can induce thyroid dysfunction. However, it is difficult to establish whether iodine insufficiency or excess causes TC. A meta-analysis about the radioiodine treatment with iodine[131] concluded that using radioiodine for hyperthyroidism increased the risk of TC[11]. However, further investigation is needed because the included studies had low quality scores and lacked rigorous data analysis to establish a strong association[9].

- Metabolic factors

The global prevalence of excess weight and obesity has drastically increased in the recent decades. The excess of body fat promotes adverse metabolic conditions such as insulin resistance, hormonal fluctuation, and inflammation, leading to diseases such as diabetes, cardiovascular disease, and different types of cancer. In terms of TC, a positive association has been observed for all major histologic types. Moreover, a recent case-control study carried out in Australia demonstrated that body mass index (BMI) was positively associated with *BRAF*^{V600E} -mutated PTC, while no association was observed for *BRAF*-negative PTC[12].

- Reproductive factors/sex steroid hormones

Finally, reproductive factors such as the use of exogenous hormones (thyroid-stimulating hormone [TSH]), age at menopause, and age at menarche, as well as other factors related to perinatal and *in utero* exposures or environmental pollutants, could be associated with TC risk. However, several of these findings are novel, and they require further investigation to reach strong conclusions[9].

2.3.2 Non-modifiable Risk Factors

Two types of evidence support that TC could also be promoted by genetic factors. Firstly, studies carried out using United States cancer registry data reveal an important familial risk. Three first-degree relatives with TC indicates that a genetic factor is causing a particular family cluster. Secondly, different studies have identified germline polymorphisms that can contribute to the development of TC. For instance, several polymorphisms in the gene *FOXE1* have been identified as a risk factor in thyroid carcinogenesis[9]. Hence, more than 90% of TCs are sporadic because of somatic genetic alterations, while approximately 3%–9% is due to hereditary conditions[10].

2.4 Molecular Pathogenesis and Mechanisms of Thyroid Cancer

A wide range of genetic abnormalities are implicated in the development of thyroid neoplasms. The most relevant alterations are specific mutations or rearrangements related to processes such as proliferation, survival, and differentiation through different signaling pathways. Approximately 90% of mutations are considered mutually exclusive, activating mutation in oncogenes such as $BRAF^{V600E}$ (around 60%) and *RAS* (around 13%) as well as rearrangements involving *RET*, *ALK,* and *NTRK* genes (around 5%). The remaining 10% belongs to the loss-of-function mutations affecting tumor suppressor genes like *PTEN, PPARγ* and *TP53*. Additionally, these somatic point mutations promote the activation of MAPK and PI3K/AKT/mTOR signaling pathways. The most common oncogenic drivers of these pathways are *BRAF* and *RAS* point mutations signaling pathways, which are relevant in tumoral processes (Figure 4)[13,14].

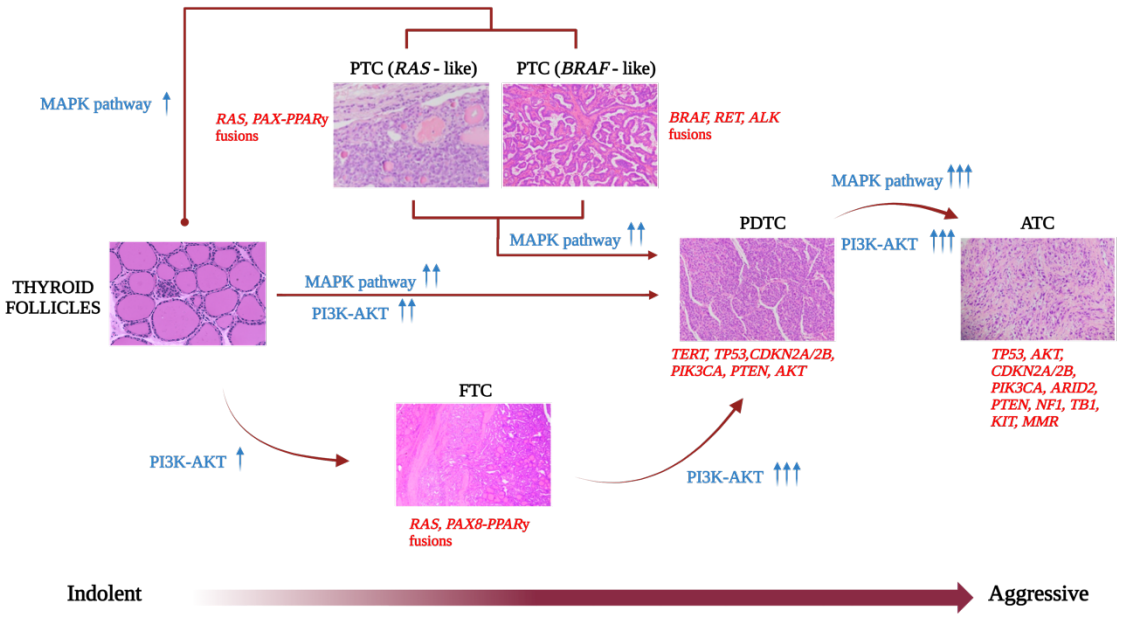

Figure 4. Schematic representation of multistep carcinogenesis in thyroid cancer (TC). This model suggests a stepwise dedifferentiation process from mature thyroid cells to well-differentiated TC (WDTC) up to poorly differentiated TC (PDTC) and anaplastic TC (ATC) as a result of progressive accumulation of somatic genetic alterations and driven by the MAPK and PI3K/AKT/mTOR pathways (H&E stain, original magnification: 200×) Modified from[14,15]. Created with BioRender.com

The MAPK and PI3K/AKT/mTOR signaling pathways depend on the mutually exclusive *RAS*, *BRAF* and *RET/PTC* point mutations and rearrangements (*RET/PTC* and *TRK*). This prevalence of these genetic aberrations differs for the different TC subtypes, with a 62% prevalence related to $BRAF^{V600E}$ in PTC. These *BRAF* mutations are most common in infiltrative PTC with aggressive behavior, whereas less fatal *RAS* mutations are generally found in encapsulated PTC and adenomas.

The Wnt signaling pathway also plays a crucial role in TC progression. This pathway includes genes such as *CTNNB1*(β-catenin), *AXIN1,* and *APC,* which play a role in cell adhesion and transcription. In non-disease situations, β-catenin is linked to APC and recruits CK1 and GSK3, which phosphorylate β-catenin followed by ubiquitination and degradation by the proteasome. When the Wnt pathway is overactivated or there is a defect in the GSK3-β-axin-APC-mediated degradation of β-catenin (due to mutations in *APC* or *CTNNB1* genes), β-catenin degradation is inhibited, and is translocated to the nucleus, acting as a transcription factor (Figure 5). These aberrations are present in 25% of PDTCs and 65% of ATCs, being more infrequent in DTCs[14].

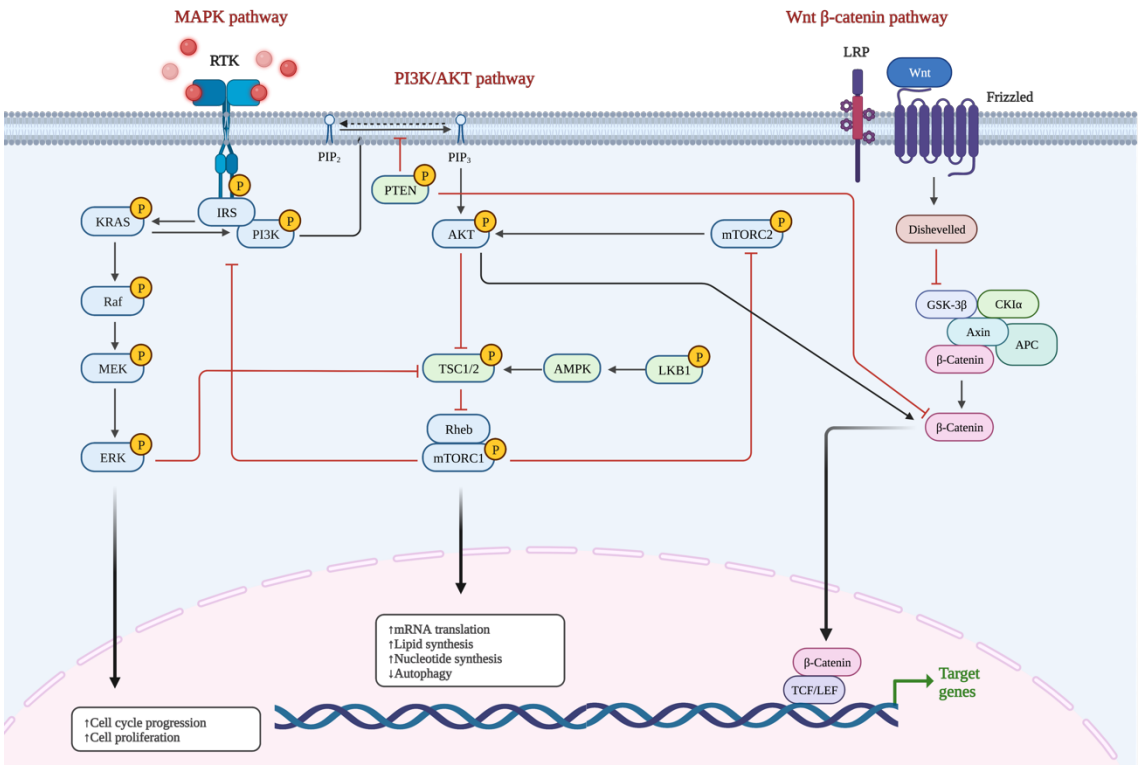

Figure 5. Commonly dysregulated cell signaling MAPK, PI3K/AKT/mTOR and Wnt pathways in TC. Created with BioRender.com

2.4.1 Point mutations

- *BRAF*^{V600E} mutation

  BRAF serine-threonine kinase belongs to the family of RAF proteins that are intracellular effectors of the MAPK signaling pathway. Protein recruitment to the cell membrane activates BRAF, which in turn phosphorylates and activates MEK and consequent effectors of the MAPK cascade[16] (Figure 5). Point mutations in the *BRAF* gene are found in about 60% of patients with PTC. It has been identified more than 40 mutations in *BRAF* gene, but the most frequent hot spot event accounting for over 95% of all *BRAF* mutations is the T1799A BRAF transversion nucleotide, originating a V600E mutant protein. Several studies have demonstrated a correlation between *BRAF*^{V600E} with more aggressive PTC and the dysregulation of sodium iodide symporter (NIS) functioning, which decreases the ability of tumors to trap radioiodine and leads to treatment failure. Moreover, tumors harboring *BRAF* and *TERT* promoter mutations usually demonstrate extrathyroidal extension together with lymph node and distant metastases. Although BRAF activation promotes TSH-dependent cell growth, the resultant balance is no net growth due to the acquisition of secondary genetic events that decrease the expression of TSH

receptors. In clinical settings, the use of MEK inhibitors in addition to BRAF inhibitors are highly recommended to inhibit MAPK pathway-driven growth. For these reasons, *BRAF*^{V600E} mutation has been included as a factor to be consider in stratification for the risk of poor prognosis in stages III and IV[13,14,16,17].

- *RAS* mutation

RAS genes (*H-RAS, N-RAS* and *K-RAS*) are the responsible for encoding highly related G-proteins located at the inner surface of the cell membrane. When RAS protein is inactive, it is bound to guanosine diphosphate (GDP); upon activation, GDP is released, and RAS binds to guanosine triphosphate (GTP), inducing different signaling pathways such as MAPK and PI3K/AKT/mTOR (Figure 5). Point mutations occur in the *RAS* gene domains and result in either an increased affinity for GTP or inactivation of the autocatalytic GTPase function, causing a permanent switch in the active position and a constitutive activation of its downstream signaling pathways[16]. These *RAS* point mutations are found in FTC (40%–53%), PTC (20%), PDTC and ATC (20%–60%). *N-RAS* has been identified four times more frequently in follicular tumors than in papillary malignancies, and tumors with *RAS* mutations together with *TERT* promoter mutations are more aggressive, especially in PTC[13]. Selpercatinib is a highly selective RET kinase inhibitor used in PTC patients with RET fusions and MTC patients with RET mutations[14].

- *EIF1AX* mutation

EIF1AX encodes an essential eukaryotic translation initiation factor for change-of-function or gain-of-function mutations. The *EIF1AX* gene was recently described as a new TC-related gene and occurs in both benign and malignant TC. These mutations were mainly reported in PDTC (11%) and ATC (9–30%), but also occur in WDTC (FTC [17%], OCA [11%] and PTC [1%–2%]) and benign thyroid lesions[14]. Usually, there is co-expression between *EIF1AX* and *RAS* mutations in advanced tumors. Using inhibitors of EIF1AX such as BRD4, in combination with mTOR and MEK inhibitors result in a reduction in tumor size. However, *in vivo* studies are required to further elucidate the use of these inhibitors in humans[14].

2.4.2 Vascular Endothelial Growth Factor (VEGF)

The Vascular Endothelial Growth Factor (VEGF) and the Notch signaling axis are related to angiogenesis and lymphangiogenesis, which are crucial for tumor progression and tumor dissemination. These processes are initiated and regulated by the matrix metalloproteinases (MMP) that participate in the disruption of the basement membrane, followed by the action of the VEGF receptor, which is a TK receptor expressed by endothelial cells; and the VEGF-A produced by tumoral and immune cells in tumor microenvironment (TME)[18] (Figure 6). TC is related to increased angiogenesis, and the overexpression of VEGF has been associated with local and distant metastasis in 50% of PTC, 39% of FTC, and 12% of PDTC[19,20].

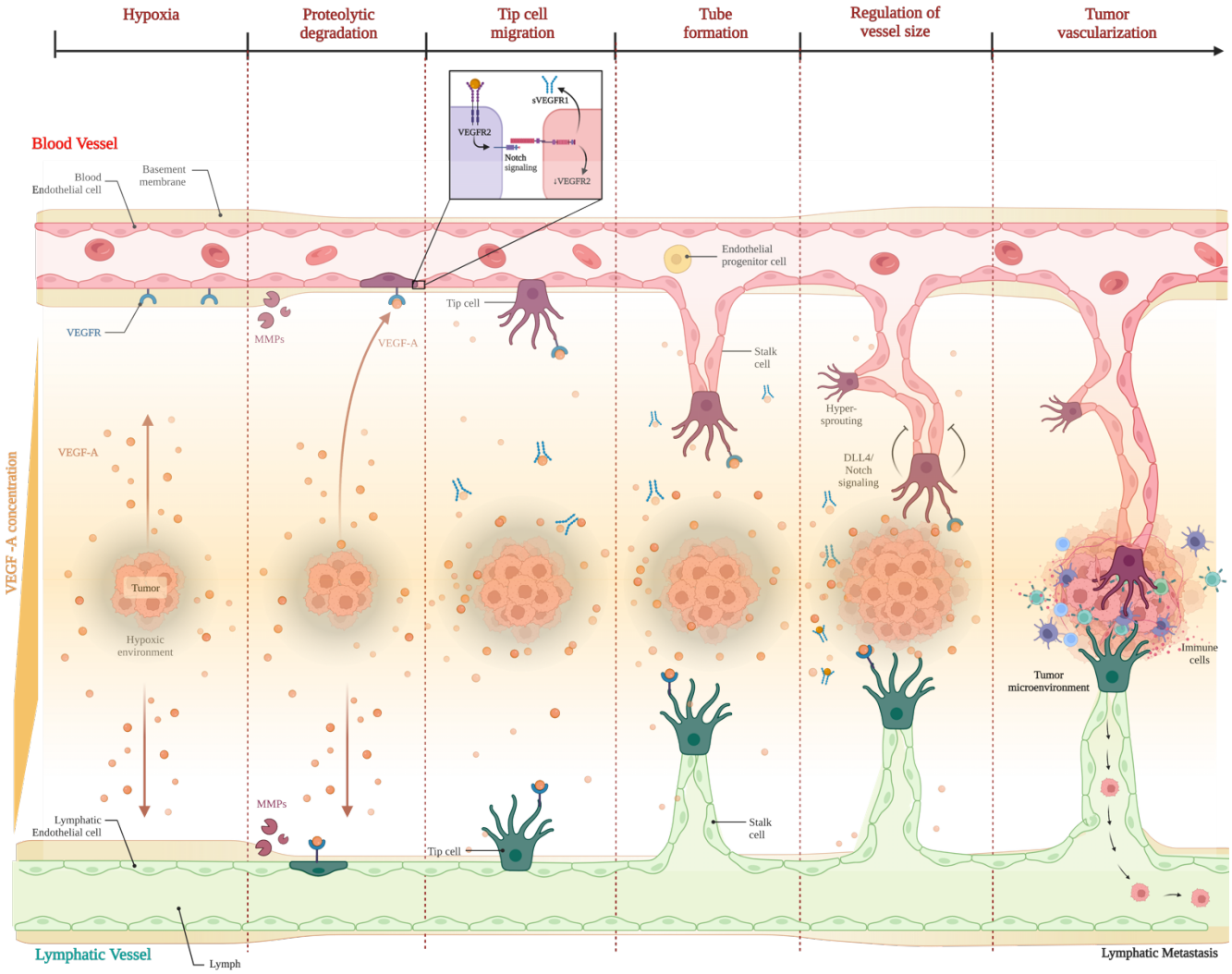

Figure 6. Schematic representation of vascular angiogenic and lymphangiogenic growth factors and their receptors expressed by endothelium. MMP: Matrix Metalloproteinases. Created with BioRender.com

2.4.3 Tumor suppressor genes

Mutations in tumor suppressor genes such as *TXNIP*, *TP53*, *RASAL1*, and *PTEN*, promote the loss of their expression, impairing the control of cell growth and apoptosis[19]. For instance, mutations in PTEN promote a constitutive activation of the PI3K/AKT/mTOR pathway that leads to the development of many carcinomas. Inhibitors of specific PI3K/AKT/mTOR pathway effectors have been found to be suitable for use in combination with chemotherapeutic agents[14]. Inactivating point mutations of *TP53* are common in PDTC and ATC, with a prevalence of 8–35% and 73%, respectively. Otherwise, they are infrequent in metastatic PTC (13%) or FTC (8%).

Therefore, *p53* inactivation in combination with other oncogenes, such as $BRAF^{V600E}$, promotes a malignant phenotype[14].

2.4.4 *TERT* promoter mutations

TERT is the catalytic subunit of the telomerase enzyme, which is essential for telomerase activity. The *TERT* promoter mutation, which is mutually exclusive with *TERT* rearrangements, is present in approximately 90% of malignancies. This mutation can consist of CpG promoter methylations, histone tail modifications, copy number amplifications, alternative splicing, and others, resulting in an unregulated proliferation due to an upregulation of *TERT* expression[21]. *TERT* mutations co-exists with $BRAF^{V600E}$ or *RAS* mutations and are associated with aggressive behavior, including higher invasive and metastatic ability, treatment resistance, and poor prognosis. So, *TERT* prevalence is around 60% in metastatic PTC and around 10% in non-metastatic PTC. In terms of PDTC, the prevalence of *TERT* mutations is around 40% and 60–70% in ATC. Therefore, a well-established implementation of molecular diagnosis assessment of these mutations could help in the identification of high-risk patients[14].

2.4.5 Gene fusions

- *RET* Gene Rearrangements *(RET/PTC)*

The *RET* gene encodes a transmembrane receptor with tyrosine kinase activity, and it is stimulated by ligands of the glial cell line-derived neurotrophic growth factor (GDNF) family belonging to the TGFβ superfamily. In PTC, *RET* rearrangements (*RET-PTC)* are an early event in carcinogenesis, and 10%–20% of PTC patients are detected with *RET* fusions and consequently characterized with stage III/IV disease and recurrence. However, somatic *RET* mutations are more frequent in sporadic MTC (40%–50%) and are linked to a poor prognosis for patients[22].

- Rearrangements of *PAX8-PPARγ, ALK* and *NTRK*

The *PAX8-PPARγ* fusion protein is the consequence of a chromosomal translocation (t(2;3) (q13;p25)) that fuses the *PAX8* gene to the *PPARγ* gene. Tumors harboring these translocations present higher vascular and capsular invasion in comparison to *RAS*-positive tumors. Rearrangements of *PAX8-PPARγ* are present in 4%–33% of follicular adenomas,

30%–58% of FTC, and 37.5% of PTC[14,23]. *ALK* rearrangements are common in PDTC (16%), and *NTRK* rearrangements are recognized in up to 26% of PTC[14].

2.4.6 Others

Apart from the main oncogenic events described above, other modifications can also be found in TC development, such as epigenetic modifications (including DNA methylation and histone deacetylation), copy number variations and mismatch repair gene deficiencies[14,19].

2.5 Treatment Strategies for Thyroid Cancer

2.5.1 Surgical intervention

Radiographic and cytologic features together with family history and symptomatology help to determine the risk of malignancy in a thyroid nodule. Additionally, nodules with a specific size and with certain features obtained by ultrasound undergo fine needle aspiration (FNA) and cytologic evaluation. Following the FNA results, the nodule is stratified following the Bethesda System, which places the lesion into one of six categories of increasing likelihood of malignancy. Based on Bethesda results, the grade of thyroidectomy is established. A total thyroidectomy (TT) is the procedure that provides the most favorable outcomes. TT are carried out in patients with a diagnosis of high suspicion of malignancy in tumors greater than 1 cm (Bethesda V and VI). Nevertheless, some data report that an ipsilateral thyroid lobectomy (TL) has equivalent long-term outcomes to TT in patients with PTC and without node dissemination. For Bethesda III and IV lesions and without a malignant diagnostic, TL is performed to avoid the thyroid hormone replacement treatment. Asymptomatic lesions categorized as Bethesda II (benign category), do not usually undergo surgery. Finally, lesions that fall into Bethesda I are characterized as non-diagnostic, and repeated FNA is usually indicated. Given that radioactive iodine (RAI) treatment is an effect therapy, the primary tumors as well as the remainder of the thyroid gland need to be removed to facilitate the use of this treatment. The decision-making process regarding undergoing surgery in patients with ATC is significantly more complex due to the poor survival rate and the involvement of surrounding neck structures[24].

2.5.2 Thyroid hormone suppression therapy

Hormone therapy consists of adding, blocking, or removing hormones to decrease or inhibit the growth of cancer cells that need hormones to grow. In that case, hormone levels can be modified or blocked by drugs, surgery, or radiation therapy. In terms of TC, when a TT takes place, hormone therapy is needed to replace thyroxine (T4). TSH is obtained from the pituitary gland, and it controls the thyroid functions and growth as well as the growth of cancer cells. For this reason, hormone therapy is used to control TSH levels, which in turn helps to prevent cancer cells from growing and reduces the risk of TC recurrence. Levothyroxine is the standard hormone therapy used for these patients and is usually given as a pill once a day for the rest of one's life[25]. However, this therapy is not free from side effects. Levothyroxine may cause a fast or irregular heartbeat, skin rash, hair loss, weight loss, nervousness, shakiness or tremors, sleep problems such as insomnia, or osteoporosis (with the likelihood of this developing increasing the longer one takes the drug)[25].

Nevertheless, over recent decades different opinions have emerged regarding the need for long-term thyroid hormone suppression as a therapeutic strategy to reduce TSH levels, with the aim of improving outcomes. Nowadays, recent findings establish that the TSH target therapy should be based on the severity of the disease and the response to therapy weighted against the individual's risk factors for taking excess thyroid hormone therapy. Consequently, there would be no reason to maintain a low TSH level in these patients. For patients with more advanced TCs, there is evidence that TSH therapy might result in improved results. In this respect, the most recent arguments maintain that TSH suppression therapy is not necessary for the average person with TC[26–28].

2.5.3 Radioactive Iodine Therapy

WDTC could receive RAI ablation therapy thanks to cells' capacity to uptake iodine. RAI treatment is recommended as an adjuvant in patients with an incomplete resection, locally advanced disease, or distant metastasis. RAI therapy consists of the uptake of iodine-131 (I^{131}) radioisotope by thyroid follicular cells via the NIS in the same process of uptake natural iodine (precursor of thyroglobulin and thyroid hormone). In this therapy, targeted iodine is absorbed by thyroid glandular tissue and DTC cells in order to cause radiation-induced cytotoxicity in all residual thyroid tissue and TC cells to reduce tumor recurrence. Moreover, this treatment is more effective for the *RAS*-mutated PTC than *BRAF*-mutated tumors, possibly because *BRAF* mutation decreases the expression of the genes required for iodine

transport (e.g. ABC transporters) and metabolism, thereby reducing the radioiodine uptake[24]. However, only one third of patients have a complete response to RAI therapy; the remaining two thirds become RAI-refractory (RAIR)-DTC, and have a poor overall prognosis, which is an inevitable challenge in the current medical management of the disease[29].

2.5.4 Chemotherapy

Currently, there are more than 50 clinical trials in TC that combine chemotherapy drugs with targeted or immunotherapy drugs; this is because cytotoxic chemotherapy alone is rarely indicated for WDTC. Nevertheless, despite their limited efficacy, paclitaxel and docetaxel, anthracyclines (doxorubicin), and platins such as cisplatin and carboplatin are often used in *BRAF* wild-type ATC in combination with external radiotherapy. However, the lack of durable anti-tumor efficacy of the cytotoxic chemotherapy for *BRAF* wild-type ATC demonstrates a critical need to identify novel effective treatments[24].

2.6 Targeted Therapies in Thyroid Cancer

Understanding the dysregulated signaling pathways in TC is crucial for identifying effective treatment approaches, tailoring treatments based on molecular profiles, and stratifying patients based on disease risk. Recent advancements related to the molecular mechanisms underlying TC progression have led to the development of a new generation of drugs targeting these dysregulated pathways. Several targeted anticancer agents, such as tyrosine kinase inhibitors (TKI), immune checkpoint inhibitors (PD-L1), NOTCH1 inhibitors, and mTOR pathway inhibitors, have emerged as promising monotherapy options. These therapies demonstrate potential for blocking the functions of molecules involved in the transformation of indolent tumors into aggressive tumors. The following sub-sections provide an overview of the major groups of targeted therapies in TC.

2.6.1 Tyrosine Kinase Inhibitors

TKIs are a crucial type of small molecule inhibitor and have been extensively studied in TC. Receptor tyrosine kinases (RTKs) play an important role in several regulatory processes in normal and cancer cells as they participate in transmembrane signaling. Upon ligand binding, RTKs undergo dimerization and autophosphorylation, and they activate downstream signaling cascades, thus promoting cancer initiation and progression. These TKIs competitively inhibit the ATP-binding site within the tyrosine kinase domain, impeding

its functioning and subsequently blocking downstream signaling pathways. TC with *BRAF*^{V600E} and *P53* mutations led to activation of the MAPK pathway. Multiple-targeted TKIs can be found, such as anti-angiogenic, BRAF-targeting, MEK-targeting, and mTOR-targeting, which can suppress the progression of these tyrosine kinase-driven oncogenic pathways, leading to tumor regression[30]. Figure 7 depicts several TKIs that have been investigated in TC[24].

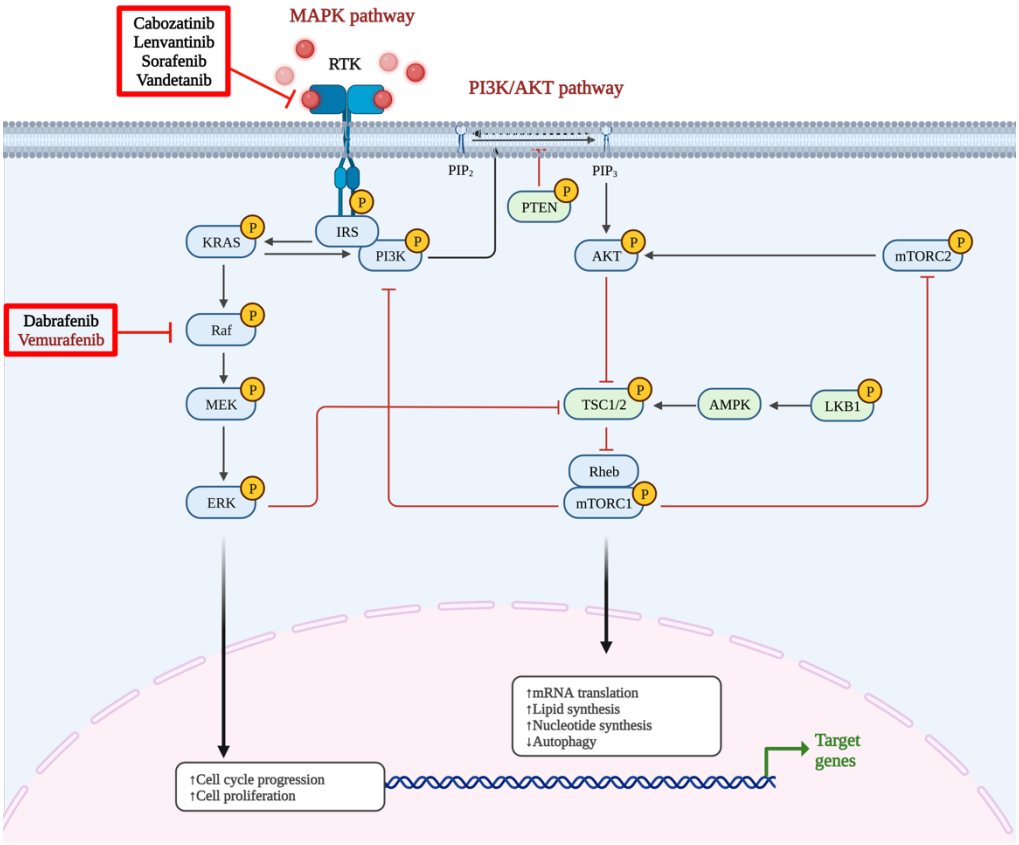

Figure 7. Some of the tyrosine kinase inhibitors (TKI) used clinically for treatment of radioactive iodine-refractory (RAI-R) TC with the goal of arresting uncontrolled proliferation. Created with BioRender.com

Although the TKIs sorafenib and lenvatinib are standard treatments for patients with RAI-R TC, a limitation of these therapies is the need for continuous dosing and the accompanying drug toxicities[31,32]. Vemurafenib is a kinase inhibitor specific to mutated *BRAF*, and it has been approved for the management of *BRAF*^{V600E}-positive melanoma[33]. Data from preliminary studies suggest that vemurafenib might be effective in *BRAF*^{V600E}-positive PTC[34,35].

2.6.2 Vascular Disrupting Agents

TC, like many other endocrine cancers, is highly dependent on its blood supply for nutrients and oxygen. Vascular disrupting agents (VDAs) are a class of drugs that target and disrupt the blood vessels supplying tumors. These agents are designed to cut off or reduce the blood supply to tumors, leading to a decrease in nutrients and oxygen delivery. By disrupting the tumor's blood vessels, VDAs can inhibit tumor growth and induce tumor cell death. VDAs work by targeting the endothelial cells that line the blood vessels, as well as the structure and function of the blood vessels themselves. They can cause vascular shutdown, leading to ischemia (lack of blood flow) and subsequent tumor cell death. Some examples of VDA include CA4P, efatutazone, and crolibulin that act by depolymerizing microtubules, which are important for maintaining the structure and function of blood vessels. By disrupting microtubules, VDAs can cause the collapse and destruction of tumor blood vessels[24].

2.6.3 Immunotherapy

Immunotherapy uses the body's immune system to fight against diseases, particularly cancer. It involves using substances or treatments that stimulate, enhance, or suppress the immune system's response to recognize and attack cancer cells more effectively. However, cancer can sometimes evade or suppress the immune system's response; for that reason, immunotherapy aims to overcome these barriers and activate the immune system to target and eliminate cancer cells. There are various approaches to immunotherapy, including the use of immune checkpoint inhibitors, adoptive cell transfer, cancer vaccines, and cytokines. Immune checkpoint inhibitors work by blocking proteins on immune cells or cancer cells that inhibit the immune response, allowing the immune system to attack cancer cells more effectively. Adoptive cell transfer involves modifying a patient's own immune cells, such as T cells, to enhance their ability to recognize and destroy cancer cells. Immunotherapy can lead to durable responses, fewer side effects compared to traditional treatments, and improved overall survival rates for some patients.

An increasing number of studies have focused on the role of PD-L1 as a crucial regulator of T cell function following antigen stimulation. Notable immune checkpoint inhibitors include pembrolizumab, nivolumab, cemiplimab, avelumab, atezolizumab, and durvalumab. In recent studies, high expression of PD-L1 has been observed in WDTC and ATC.

Additionally, CTLA-4, another immunosuppressive marker, has been identified as an important target due to its negative correlation with thyroid differentiation and immunosuppressive markers. Notably, the expression of PD-L1 in TC subtypes has been found to be heterogeneous, and its expression is associated with clinicopathological features such as mutations in the *TERT* promoter and *BRAF*, which indicate disease progression in ATC[24].

2.6.4 Nanomedicine-mediated Targeted Therapy

Nanomedicine is a term that emerged from nanotechnology, and it is defined as the creation and use of materials at the level of molecules and atoms (generally less than 100 nm). Nanoparticles (NPs) serve as valuable tools for establishing an accurate diagnosis or treatment for TC, and they can be classified depending on their size, shape, and surface characteristics. The most used NPs in cancer are organic (liposomes, polymer-based…), inorganic (gold, carbon-based…), and hybrid (liposome-silica, chitosan-carbon, and cell membrane-coated) particles.

In terms of diagnostic tools, gold NPs are useful to detect biomarkers (such as circulating tumor cells) in liquid biopsies using contrast agents and analyze them using fluorescence, or colorimetry detection. In TC, gold NP-bases assays have been established to detect *BRAF* mutation. For TC treatment, NPs not only improve the delivery of chemostatic treatments with poor solubility or rapid metabolization/excretion, such as doxorubicin, paclitaxel, or cisplatin, they also decrease the adverse effects on patients. Moreover, decorating NPs with monoclonal antibodies against highly expressed tumor proteins such as EGFR, can increase the efficacy of chemotherapeutic drugs by triggering their release from nanocarriers specifically in the tumor. However, the translation of engineered particles to clinical settings is slow. The approval of NPs is 1–7 NPs/year, and the submissions of the Food and Drug Agency (FDA) represent liposomes (33%), nanocrystals (23%), emulsions (14%), iron-polymer complexes (9%), and micelles (6%), with 35% of submissions focused on cancer treatment or diagnosis (Figure 8)[36]. Most of these submissions are in the pre-clinical phase of drug development and, despite the encouraging results from animal studies, their efficacy in humans is subjected to inherent limitations of the models. These limitations include, the absence of metastasis in the mouse models, subcutaneous versus orthotopic localization, the

immunodeficient status of the athymic models, and the smaller sizes of tumors in mice relative to body weight in comparison to humans[36,37].

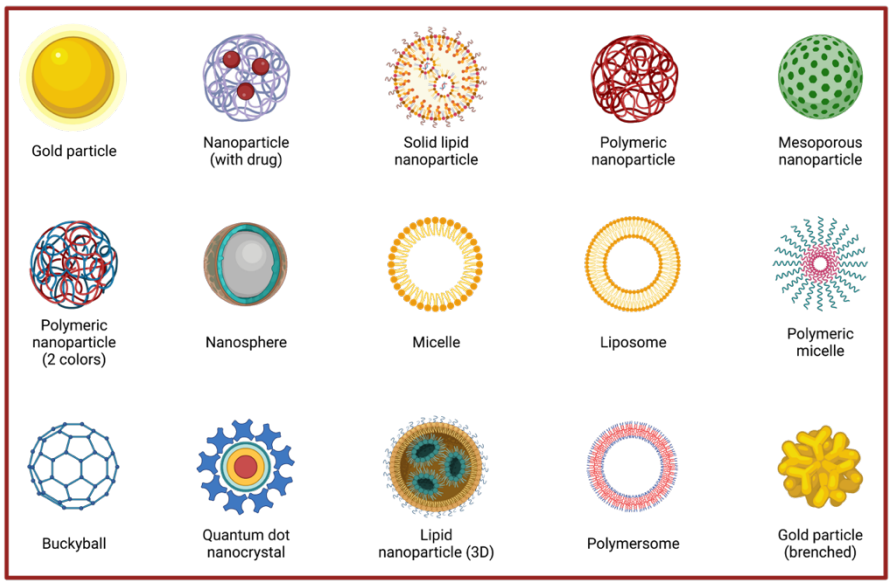

Figure 8. Different types of nanoparticles (NPs). Created with BioRender.com

3 Cellular Cholesterol Metabolism

Cholesterol and triglycerides (TGs) are the most important plasmatic lipids. Cholesterol is a fundamental lipid component in the sustenance of cell structure, maintaining cell membrane integrity and fluidity as well as regulating a plethora of biological functions[38,39]. Cholesterol is highly regulated in normal cells; intracellular homeostasis is maintained by a complex network where processes such as biosynthesis, uptake, efflux, trafficking, and esterification are critical for cellular functions[38,40]. Around the 80% of total cholesterol is biosynthesized, and 20% is obtained from the diet as free form or as a cholesterol ester together with fatty acids.

3.1 Cholesterol Synthesis

3.1.1 Endogenous Pathway

Cholesterol biosynthesis primarily occurs in the liver, which synthesizes about 50% of the cholesterol in humans[41]. The endogenous pathway involves 30 steps of reactions, beginning with the mevalonate pathway, followed by the sterol pathway. In the mevalonate pathway, the enzymes HMG-CoA synthase and HMGCR catalyze two molecules of acetyl-CoA to finally obtain mevalonate, with HMGCR being the main enzyme targeted by statins to

regulate cholesterol homeostasis. Consequently, mevalonate is converted to farnesyl pyrophosphate (FPP)[42,43]. Then, the sterol pathway begins obtaining squalene from FPP, the product of the mevalonate pathway. Subsequently, many series of oxidation and reduction steps take place to convert squalene into many different sterols, including cholesterol[43].

Cholesterol biosynthesis is subject to both short-term and long-term regulatory processes. The short-term regulation is related to the phosphorylation of the enzyme HMG-CoA reductase by an AMP-dependent protein kinase (HMG-CoA reductase kinase), which is active when ATP is low. In this way, when there are low levels of ATP, energy is not spent synthesizing cholesterol. Long-term regulation is related to the formation and degradation of HMG-CoA reductase together with other enzymes in the pathway[41]. Cholesterol, oxysterols, mevalonate, and dephosphorylated FPP stimulate HMG-CoA degradation. Each of the genes coding the cholesterol biosynthesis pathway enzymes has a sterol regulatory element (SRE) in its promotor, which is activated by the nuclear form of SREBP-2[44–46]. Hence, the enzymes are regulated at the transcription level by SREBP-2. This SREBP-2 is activated by three other proteins in response to sterol levels: the SREBP cleavage-activating protein (SCAP), which is a protein of the endoplasmic reticulum; protease S1P, which belongs to the Golgi; and protease S2P[41].

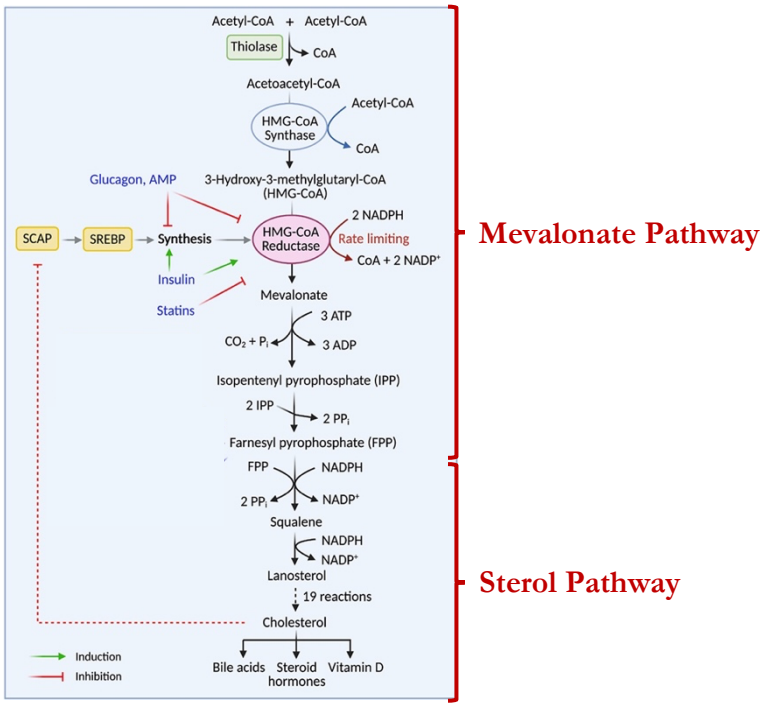

Figure 9. A schematic overview of cholesterol biosynthesis. Modified from[41].

3.1.2 Exogenous Cholesterol Uptake

Cholesterol is absorbed from the diet in the small intestine through the brush border membrane (BBM). Dietary cholesterol could be taken passively or facilitated by proteins such as NPC1L1. NPC1L1 recruits cholesterol from the diet to form a lipid raft surrounding it on the BBM. Once sufficiently substantial levels of cholesterol are aggregated into the lipid raft, NPC1L1 can sense the sterol molecule via its sterol sensing domain (SSD), thereby promoting clathrin-mediated endocytosis together with cholesterol molecules and ending up in the endoplasmic reticulum (ER). In the ER, the enzyme ACAT2 modifies cholesterol to cholesterol ester and then packages it into chylomicrons in combination with TGs from the diet. Alternatively, the heterodimer proteins ABCG5 and ABCG8 can secret the absorbed cholesterol back to the lumen. Fatty acids have different fates depending on their length. On the one hand, short- and medium-chain fatty acids move through the enterocyte and then move into circulation through the capillaries, where they are bound to albumin to be transported. On the other hand, long-chain fatty acids that correspond to re-esterified cholesterol, forming TG, phosphatidylcholine, and cholesterol esters, are packaged into chylomicrons (CMs). These CMs are too large to fit through the pores of the capillaries, but they can fit through the larger fenestrations in the lymphatic duct (Figure 10)[47].

Hence, dietary TG can be transported inside CM from the enterocytes to the blood via the lymphatic system and is subsequently absorbed by adipose tissue and muscle cells through the actions of lipoprotein lipase (LPL). The CMs remnants are enriched in cholesterol and endocytosed into the liver where they are metabolized, and cholesterol is re-packaged into very-low density lipoprotein (VLDL) and secreted into the circulation or into the lumen as unesterified cholesterol or bile acids[41] (Figure 10).

3.2 Lipoproteins and Cholesterol Transport

Cholesterol and TGs are carried in bound form within lipoproteins creating an apolipoprotein (Apo)-lipid complex. Lipoproteins are formed by a surface layer of phospholipids and free cholesterol[41]. They are classified into various types depending on their size, density, apo, or lipid composition. The main lipoproteins are CMs, high-density lipoprotein (HDL), intermediate-density lipoprotein (IDL), low-density lipoprotein (LDL), and VLDL[38,40]. The conversion of free cholesterol to the hydrophobic cholesterol ester by the enzyme LCAT ™n peripheral tissues and ACAT2 in the enterocytes bordering the

intestinal lumen allows for a greater amount of cholesterol molecules storage in individual lipoproteins than would be possible with only free cholesterol[41].

VLDL is secreted by the liver and shrinks in diameter during the lipolysis to form IDL. The TGs within the IDL are hydrolyzed by lipase, forming LDL particles. Extracellular cholesterol is acquired by peripheral cells from extracellular sources that include LDL, whereas HDL carries out the reverse cholesterol transport function through the delivery of cholesterol to the liver to remove excess cholesterol from different organs/tissues[40] (Figure 10).

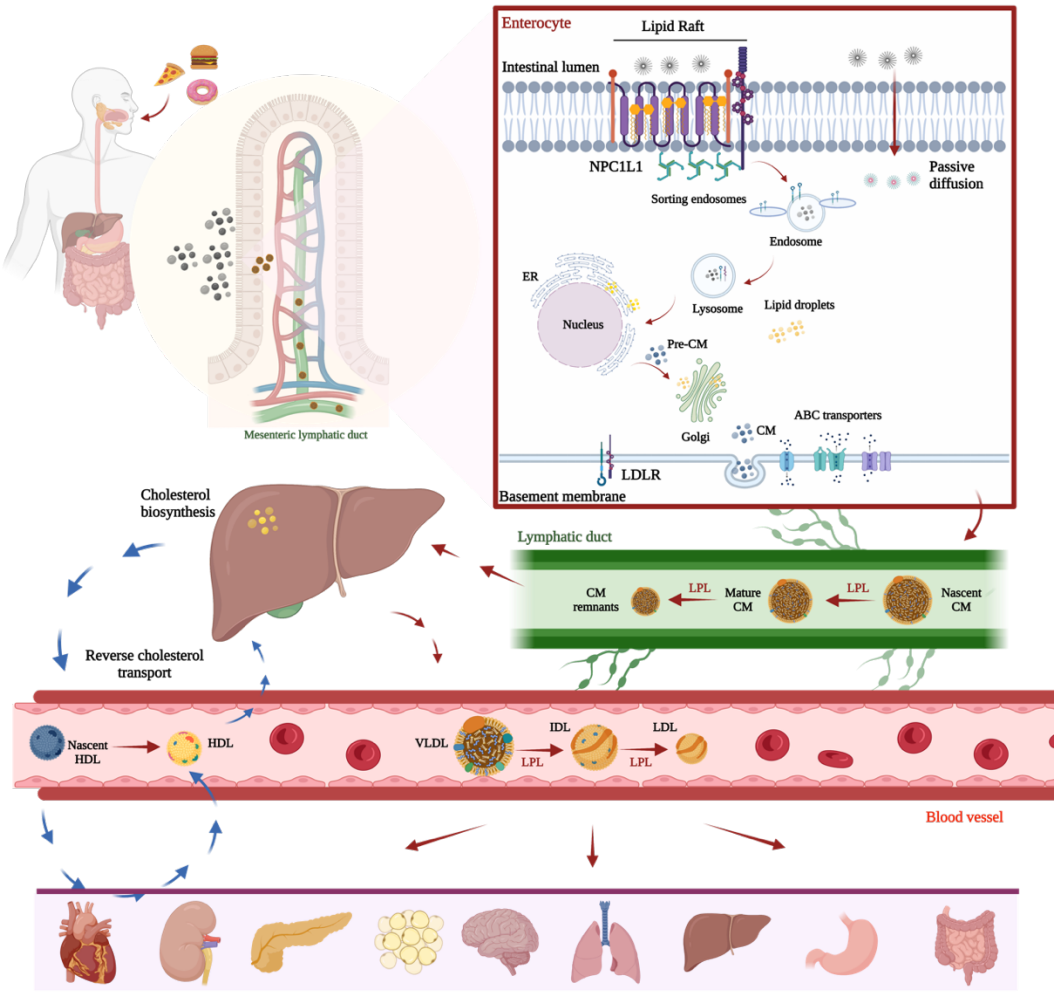

Figure 10. A schematic diagram of dietary lipids uptake, absorption, and transport in the human body. Created with BioRender.com

4 LDL: Structure and Composition

Nearly 60% of the circulating cholesterol in human plasma is LDL, and most of this cholesterol is absorbed by the liver through the LDL receptor (LDLR). LDL density ranges

from 1.019 to 1.063 g/mL in the ultracentrifuge; it has an average diameter of about 20 nm and is about three times smaller than VLDL particles[48,49]. In humans, LDL levels of <100 mg/dL are considered optimal, whereas levels of >160 mg/dL are considered elevated[41,50]. LDL is characterized as a complex particle that contains proteins and lipids. Its surface is composed of lipids and a monomeric protein, ApoB-100; each LDL lipoprotein contains only one ApoB-100, comprising over 20% of the mass of an LDL particle. Regarding the remainder of the lipoprotein, 9% corresponds to free cholesterol, 4–6% to TGs, 22%–26% to phospholipids, and 38% to cholesteryl ester (Figure 11)[49]. With a molecular weight >550 kDa and about 4,500 amino acid residues, ApoB-100 is one of the largest and most insoluble proteins in humans, with 4,536 residues[48,51]. ApoB-100 has a high-affinity ligand for LDLR, which is present in most tissues, including the liver. After binding, LDL can enter to the cell via clathrin-mediated endocytosis and can fuse with lysosomes. In lysosomes, LDL is hydrolyzed to release amino acids, fatty acids, and intracellular free cholesterol, which is catalyzed by ACAT to cholesteryl ester[41,48,52]. As mentioned above, the SREBP-2 protein regulates LDLR levels. When intracellular cholesterol levels are low, SREBP-2 is cleaved and translated to the nucleus to upregulate the LDLR expression. Otherwise, when intracellular cholesterol levels are high, SREBP-2 remains inactive, downregulating the expression of LDLR[41,52].

LDL particles contain polyunsaturated fatty acids that can be oxidized by reactive oxygen species (ROS) and reactive nitrogen species (RNS) to obtain lipid peroxides such as ox-LDL, while ox-LDL stimulates ROS production. ApoB-100 contains residues of cysteine, lysine, histidine, and tyrosine, which are oxidation targets for ROS and RNS. They can abolish the function as an LDLR ligand[53]. If this occurs, ox-LDL, which is no longer recognized by LDLR, can be identified by scavenger receptors such as LOX-1, SR-A, and CD36[52].

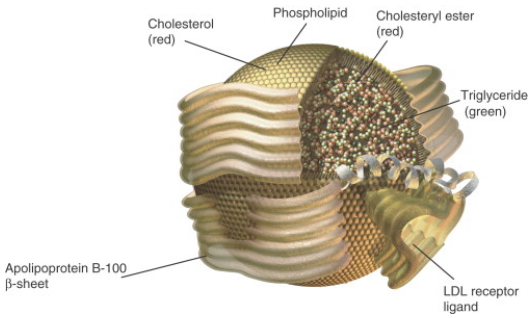

Figure 11. An illustrated model of a low-density lipoprotein (LDL) particle. Extracted from[53]

5 Low-Density Lipoprotein Receptor

The LDLR is a multi-domain transmembrane protein of 839 amino acids. Its gene is located on the short arm of chromosome 19 (19p13.1–13.3) consisting of five domains (18 exons and 17 introns) and with a length of 45 kb. The protein is encoded as a precursor with 860 amino acids. During translocation into the ER, this precursor excises the 21-residues signal sequence located at the N-terminus. Thus, the LDLR is synthesized on the ER's ribosomes, folded, partially glycosylated within the ER, and matured in the Golgi, where glycosylation is concluded[54].

LDLR is therefore composed of five functional domains organized as an ectodomain and as an intracellular domain (Figure 12). The ectodomain harbors a ligand-binding domain, an epidermal growth factor (EGF) precursor homology domain, and a C-terminal domain.

- The ligand-binding domain consists of seven cysteine-rich repeats (LR1 to LR7) of about 40 amino acids. The acidic residues from this domain interact with the basic residues of Apo-B100, allowing the binding of LDL to the LDLR. Moreover, a low-pH-induced conformational change of LDLR from an open to a closed conformation, allows the intracellular release of LDL.
- The EGF precursor homology domain is important to the LDL release in the endosome. However, this domain also plays a critical role in the LDLR degradation interacting with proteins such as PCSK9 at the cell surface. These proteins bind to the full-length receptor with greater affinity in the acidic environment of the endosome. Consequently, the receptor moves from the endosome to the lysosome for degradation instead of being recycled.
- The C-terminal domain consists of 58 amino acids and is enriched with threonine and serine residues. Its role remains uncertain, but it is thought to be critical in receptor stabilization.
- The intracellular domains constitute the transmembrane ™ and the cytoplasmic domain. The TM domain anchors the LDLR to the cell membrane, while the cytoplasmic domain is important for receptor internalization. The latter contains two sequence signals for targeting the LDLR to the cell surface and localizing the receptor's coated pits[54].

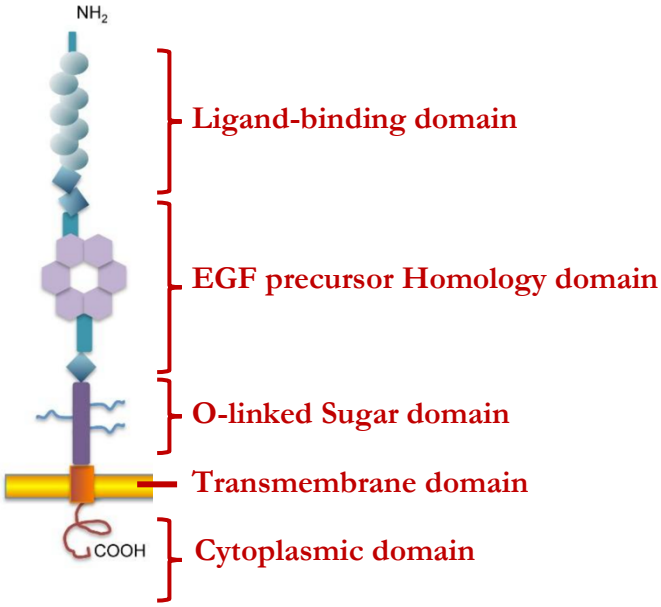

Figure 12. Schematic representation of the domain organization of the LDL receptor (LDLR). Modified from[54]

5.1 Low-Density Lipoprotein Receptor Internalization, Recycling and Degradation

LDL binds to LDLR on the cell surface creating LDL-LDLR complexes that are internalized through clathrin-mediated endocytosis. For an efficient internalization, LDLR are clustered into coated pits whose growth and maturation are regulated depending on the membrane levels of phosphatidylinositol-(4,5)-bisphosphate (PI (4,5) P_2). The internalization process begins with the formation of clathrin-coated pits once the adaptor proteins ARH or Dab2 binds to the LDLR cytoplasmatic domain. In this process, the ARH interaction with LDLR and PI(4,5) P_2 is necessary for the clathrin-coated pits' formation as well as for the recruitment of accessory proteins such as AP2 (Figure 13)[55–57].

Membrane contact sites can contribute to the regulation of LDLR internalization through two main pathways: 1) depending on the PI (4,5) P_2 amount in the membrane and 2) by regulating the vesicle formation process through direct connection with endosomes.

Membrane contact sites between the cell membrane and ER are lipid exchange routes affecting PI (4,5) P_2 levels. Oxysterol-binding protein (OSBP)-related proteins (ORP) 5 and 8 (introduced in Section 4. Oxysterols and Carcinogenesis) seem to transport phosphatidylserine to the cell membrane in exchange for PI (4,5) P_2. Hence, PI (4,5) P_2 is

transported between the cell membrane and ER through ORP5 and ORP8 proteins, with ORP5/ORP8 depletion resulting in PI (4,5) P_2 plasma membrane accumulation.

Nir2 and Nir3 are proteins that also regulate PI (4,5) P_2 generation. Nir3 maintains a basal pool of PI at the plasma membrane to generate PI (4,5) P_2 via PI 4-kinase and PI4P 5-kinase and Nir2 translocation in response to a PI (4,5) P_2 depletion by phospholipase C allows a rapid transfer of PI from the ER to the plasma membrane to PI (4,5) P_2 reformation[56,58]. When the clathrin-coated vesicle separates from the cell membrane, the coat proteins detach, and consequently PI (4,5) P_2 is hydrolyzed to PI4P. Finally, the vesicles integrate into the early endosomal system. According to Friedman et al., 80% of early endosomes are in touch with the ER, suggesting that this is the same case for those that carry the LDL-LDLR complex[59]. At this point, different trafficking paths take place, LDLR can be included in recycling endosomes, whereas LDL and some LDLR remain on a degradation path through late endosomes and lysosomes[56].

After internalization mediated by ARH, several studies have identified that the ligand and receptor dissociate in an early endosome system through the EEA1 detection, thus initiating the process of LDLR recycling. At this point, there is a conformational change in the LDLR that prevents its degradation and allows for the possibility of its recycling. It is thought that sorting nexins (SNX) and specifically SN17 are critical in redirecting LDLR towards the plasma membrane through their binding to the LDLR cytoplasmatic tail. Several studies have determined that efficient LDLR recycling also needs the Wiskott–Aldrich syndrome protein and SCAR homolog (WASH) and COMMD/CCDC22/CCDC93 (CCC) complex for LDLR endosomal sorting as well as for redirecting receptors to the cell membrane. In this instance, a retromer complex formed by vacuolar protein-sorting (VPS) proteins (VPS26), together with SN17 are responsible for recruiting the WASH and CCC complex, mediating endosomal cargo, and sorting LDLR into recycling and retrieval pathways. LDLR is enhanced by sorting SNX17 and requires the WASH and CCC complex for efficient LDLR recycling (Figure 13)[56,60]. However, further investigation is needed because it is possible that other proteins also play a role in this process.

Finally, LDLR degradation and exocytosis pathways can follow the same path as LDL molecule degradation, reaching late endosomes and lysosomes for LDLR proteolysis or multivesicular bodies (MVBs) for LDLR exocytosis. LDLR can join the late endosome and lysosome routes if it is targeted by PCSK9 or the inducible low-density lipoprotein (IDOL)

receptor or if the LDL dissociation fails. This route is preceded by MVB biogenesis, which takes place after the activation of the NDRG1 endosome protein. This pathway demonstrates a nearly 100% association between endosomes and ER, which appears to play an important role in exporting LDL-derived cholesterol from endosomes to ER[56,60]. Therefore, LDLR is regulated in two phases: transcriptional and posttranscriptional. In terms of the transcriptional level, the mRNA expression of LDLR is regulated by SREBP2, which responds to the ER's cholesterol content. At the posttranscriptional level, PCSK9 redirects the LDLR to the lysosome for degradation, while IDOL ubiquitylates the LDLR for degradation in lysosome (Figure 13)[61].

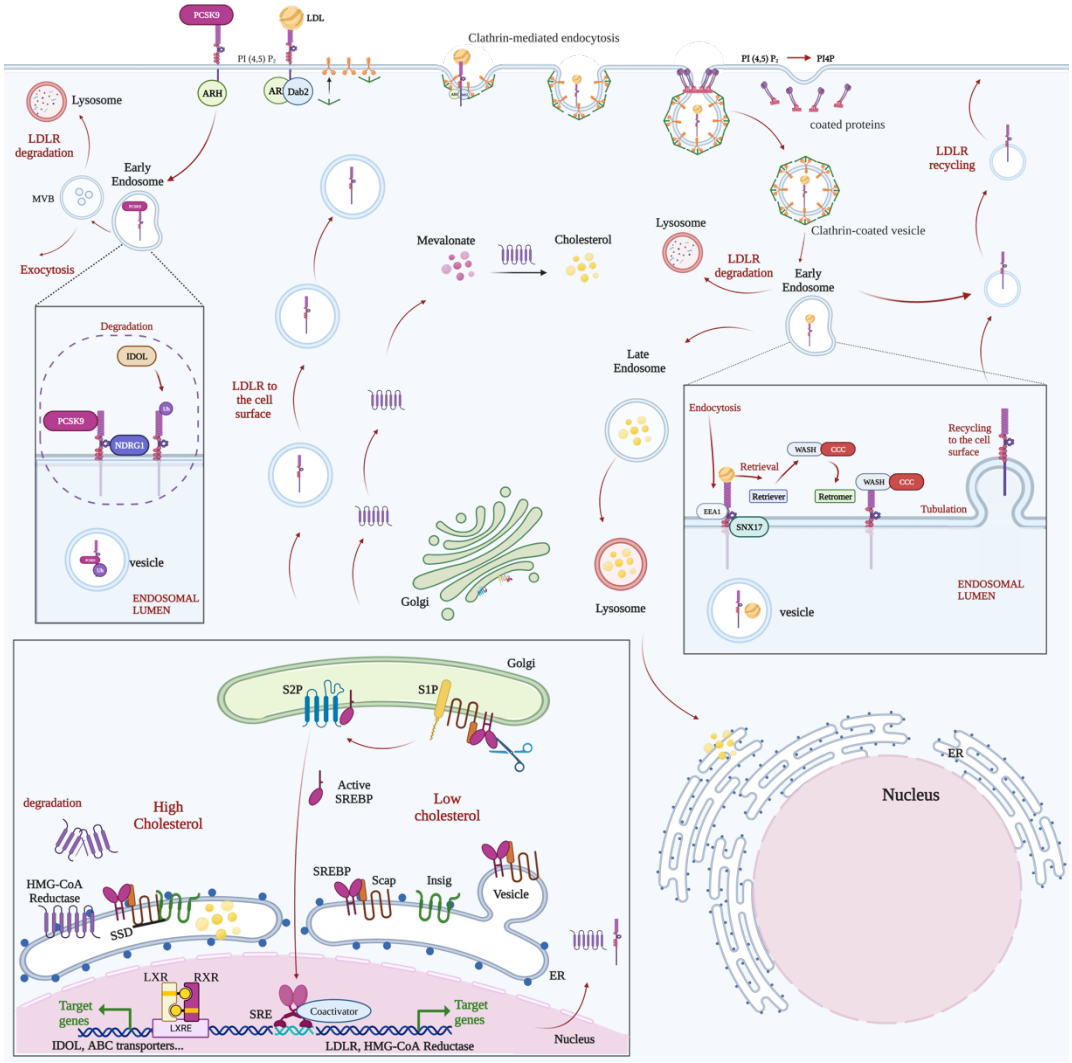

Figure 13. Schematic model of LDLR regulation: synthesis, recycling, and degradation. Created with BioRender.com

5.2 Low-Density Lipoprotein/Low-Density Lipoprotein Receptor in Cancer

A high-fat diet and consequent obesity are risk factors for several diseases, including cancer. Cholesterol plays a crucial role in the pleiotropic functions of cancer cells by enhancing cellular proliferation; invasion; and migration that mediates membrane trafficking, intracellular signal transduction, and the production of hormones and steroids, among other functions. Although it is difficult to establish a direct connection, several epidemiological studies have investigated the link between high-fat diets and dyslipidemias such as hypercholesterolemia, which is a comorbidity of obesity, with several cancers. Moreover, disturbance of cholesterol homeostasis is considered a feature of cancer[43,62–64].

In terms of LDLR, several studies have reported that increased circulating LDL cholesterol levels promote cancer growth through LDLR expression in cancer cells[65–67]. Scully et al., determined an association between circulating LDL and tumor LDLR expression with the activation of the oncogenic MAPK pathway in breast cancer, supporting tumor cell proliferation and migration[68]. However, the mechanisms by which cholesterol promotes cancer progression are not fully understood.

6 Oxysterols and Carcinogenesis

6.1 Formation of Oxysterols

The products of cholesterol metabolism are bile acids, steroid hormones, and their metabolites. While the impact of bile acids and steroid hormones in different biological processes is well known, in recent years investigations of the intermediates in the cholesterol-biosynthetic pathway as well as derivatives of cholesterol known as oxysterols have drastically increased[69]. Oxysterols are critical regulators of many biological processes in the cell. For instance, oxysterols influence the biophysical properties of lipid membranes through lipid ordering and regulating vesicular transport; interacting with membrane proteins (e.g., ABC transporters, or Na^+/K^+ ATPase) and signaling pathway proteins (Hedgehog, Wnt, MAPK pathway) and modulating their activity; and regulating the sterol metabolism through various ways, such as interacting with transcription factors or OSBP or regulating HMG-CoA reductase (Figure 14)[70].

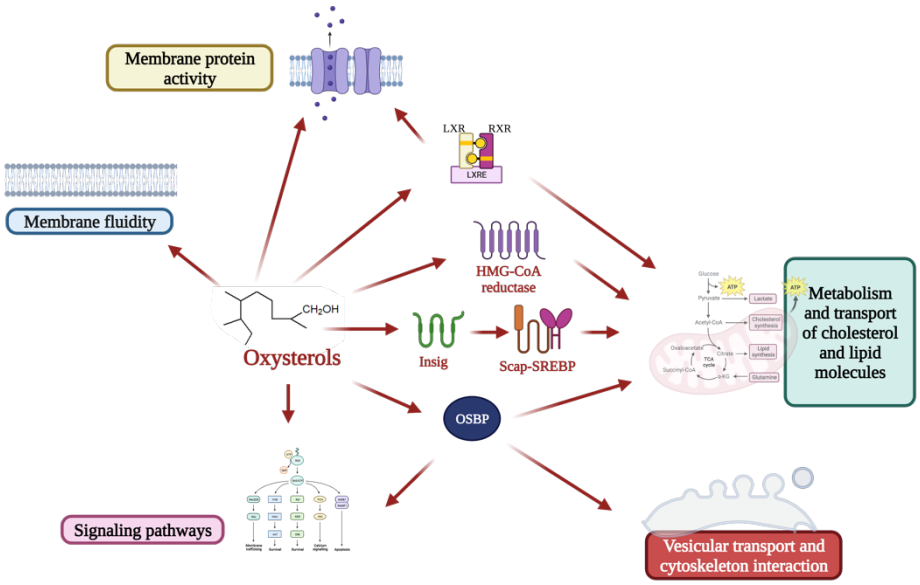

Figure 14: Schematic illustration of oxysterol functions in cells. Modified from [70]. Created with BioRender.com

Oxysterols are the products of cholesterol oxidation, and they are formed in the liver and other peripheral tissues during the first steps of cholesterol metabolism[70–73]. Oxysterols can also be absorbed in human intestines followed by esterification through the enzyme LCAT, being incorporated into CMs and later into LDL and HDL. As a result, they can be transported to different cells. However, the contribution of dietary oxysterols obtained from food products to human plasma and tissue levels remains unclear[39].

Oxysterols are 27-carbon derivatives of cholesterol formed *in vivo* in both nonenzymatic and enzymatic ways. On the one hand, the non-enzymatic cholesterol oxidation mediated by ROS leads to the acquisition of products where the sterol ring is oxidized. On the other hand, when enzymatic oxidation takes place via enzymes from the CYP450 family and cholesterol-25-hydroxylase, products with an oxidized side chain are formed. Nonetheless, oxysterols differ from cholesterol by the presence of one or several polar groups, such as hydroxyl, keto, hydroperoxy, epoxy, or carboxyl moieties[74].

The most abundant oxysterols in human serum are: 27-, 24(S)-, 7α-, and 4β-hydroxycholesterol (HC); 24(S)-HC originates from neurons and is catalyzed by the cholesterol hydroxylase CYP46A1, and 7α- and 27-HC are synthesized in the liver by CYP7A1 and CYP27A1. However, CYP27A1 is also functional in non-hepatic cells, and its expression could be associated with a good or bad prognosis in different carcinogenesis processes[74–76]. Importantly, oxysterols belong to a family of molecules where small changes in geometry can lead to significant changes in their biophysical properties[39]. They are found at very low concentrations *in vivo*, but it has been demonstrated that they could be critical

active molecules for many biological processes despite having a drastically shorter biological half-life in comparison to cholesterol[39,43,73,74,77]. Nowadays, mass spectrometry, together with liquid chromatography or gas chromatography, are used for oxysterol measurements[78].

6.2 Metabolism and Elimination of Oxysterols

There are four routes involved in the oxysterol metabolism. Firstly, cholesterol acyltransferases (ACAT and LCAT) can esterify oxysterols. Secondly, CYP7B1 can catalyze further oxidation of ring-oxidized sterols to higher oxidized oxysterols, rendering them more soluble in water. Thirdly, the enzyme 11β-HSD1 can reduce oxidized sterols. Finally, both ring and side-chain oxysterols can be sulfated by the cholesterol sulfotransferase SULT2B1b enzyme. When there is a large oxysterol accumulation, a direct elimination can take place. In this case, lyophilic transporters are required due to the hydrophobicity of oxysterols. Many transporters can transport intracellular oxysterols back to the blood, such as the ABC binding cassette transporters ABCA1 and ABCG1. Both transporters are transcriptionally regulated by the liver X receptor (LXR). However, apart from the active transport, spontaneous passive diffusion could also exist between cells and HDL or others extracellular lipid structures[39,52]. In terms of lipid transport, the ORP corresponds to a large family of lipid transfer proteins conserved from yeast to humans, and it has the capacity to bind oxysterols that are essential to sterol transfer and sterol-dependent signal transduction[79].

6.3 Oxysterol's Role in Transcriptional Control of Lipid Metabolism

It has been demonstrated that endogenous oxysterols can activate the orphan nuclear receptors LXR α (NR1H3) and β (NR1H2)[39]. These two LXR isoforms in mammals share almost 80% of their amino acid sequence. The first, LXRα (NR1H3), exists in three variants (LXRα1, LXRα2, and LXRα3) that are mainly expressed in the liver, intestine, kidney, spleen, and adipose tissue. In addition, the LXRα2 variant is expressed in the thyroid gland. In terms of LXRβ (NR1H2), it is ubiquitously expressed and is known to upregulate the ApoE expression, which is associated with inhibition of angiogenesis and metastasis in cancer cells[80,81]. LXRs are cholesterol sensors when oxysterol accumulation occurs due to an increase of cholesterol concentrations. Here, LXR promotes the transcription of genes such as *ABCA1* and *ABCG1* to protect cells from cholesterol overload, thus controlling the cholesterol homeostasis. LXR activation leads to a regulation of bile acid synthesis and

metabolism/excretion, reverse cholesterol transport, cholesterol biosynthesis, and cholesterol absorption/excretion in the intestine[81].

LXR receptors form heterodimers with the retinoid X receptors (RXRs), which are receptors for the metabolite of vitamin A, 9-cis retinoic acid[82,83]. These complex LXR/RXR regulate gene expression by binding to the DNA sequences of the genes responsible for the transcription of proteins, such as the SREBP controlling intracellular cholesterol homeostasis (Figure 13)[84]. LXR/RXR can be activated by either LXR agonists or 9-cis retinoic acid. Then, this complex binds to an LXR-responsive element (LXRE) in the promotor region of target genes regulating various biological functions such as metabolic disorders, cardiovascular diseases, skin diseases, neurodegenerative diseases, cancer, and liver steatosis[80].

6.4 Oxysterol's Role in Carcinogenesis

Oxysterols have been linked to cancer in numerous ways. However, more investigation is needed to understand the exact influence of oxysterols on carcinogenesis given their complex effect on various cell lines. Many studies declare a pro-cancerous and pro-proliferative role through the overactivation of many oncogenic pathways. However, oxysterols have also been characterized as protective molecules against cancer through a pro-apoptotic and cytotoxic effects on tumor cells related to the overproduction of ROS, changes in calcium levels in the cell, or mitochondrial membrane modifications[70].

27-HC plays a key role in cancer development. 27-HC is synthesized from cholesterol by CYP27A1 and catalyzed to 3b-HCA or to 7a,26-diHC by CYP27A1 and CYP7B1, respectively. In healthy humans 27-HC levels are between 0.2 to 0.9 mM; otherwise, its concentration increases in hypercholesterolemia and with age. CYP27A1 and CYP7B1 are mainly expressed in the liver to facilitate the metabolism of excessive cholesterol levels to bile acids, although they are also expressed in the lung, brain, adipose tissue, thyroid, and other peripheral tissues[72]. 27-HC also acts as an endogenous LXR ligand, increasing the activity of both LXRα and LXRβ in a dose dependent manner, and as a selective estrogen receptor modulator (SERM), where it demonstrates anti-estrogenic effects or pro-estrogenic effects that are cell-type-specific[69,72]. The oxysterol 27-HC is speculated to be the missing link between obesity/high-fat diet and the cancer chain[72].

However, there is some controversy in terms of 27-HC's oncogenic effects. For example, Dambai, et al., have demonstrated that 27-HC could inhibits prostate cancer by disrupting lipid rafts, reducing STAT3 activation, and consequently slowing tumor growth[85]. At the same time, Raza et al., established that 27-HC promoted cell proliferation via ERβ in prostate cancer[86]. There are a great number of studies that establish a link between CYP27A1-(27-HC)-CYP7B1 axis and tumor proliferation. The role of CYP27A1 and CYP7B1 in 27-HC homeostasis, as well as the 27-HC's role as a ligand of the LXR receptor and estrogen receptor, have been characterized as crucial in terms of various cancer's progression, such as breast cancer[87].

Indeed, 27-HC increased spontaneous breast cancer tumor growth in an ER-dependent manner in the mammary tumor virus-polyomavirus middle T antigen (PyMT) transgenic mice fed an obesogenic diet. Furthermore, a lack of the CYP27A1 enzyme attenuated the effects of this obesogenic diet on the growth of breast cancer tumors in hypercholesterolemic mice[88]. 27-HC also accelerated cancer cell metastasis to the lungs in these mice, an effect that implicated LXR activation[88,89]. The pro-metastatic actions of 27-HC also required both polymorphonuclear-neutrophils and γδ-T cells, together with an immune depletion of CD8+ T cells in obese and hypercholesterolemic mice. However, the precise signaling events involved in this process are not yet known[90]. It should be noted that 27-HC administration also increased xenografted ER-positive breast cancer tumor growth in non-obese ovariectomized female immunodeficient mice; in the referred report, 27-HC was found to be increased in ER+ human breast cancer tissues in close association with CYP7B1 downregulation, whereas CYP27A1 remained unchanged[91]. Moreover, another report demonstrated that 27-HC induces angiogenesis by promoting the expression of VEGF in an ER-dependent manner in ER-positive breast cancer cells or by activating STAT3 in an ER-independent manner[92]. 27-HC also induces the epithelial mesenchymal transition by downregulating E-cadherin and β-catenin expression as well as by upregulating the phosphorylation of STAT3, which was found to promote MMP-9 expression[93, 94].

7 Thyroid Cancer and Cholesterol

Metabolic reprogramming is a common feature of tumors, and lipid metabolism reprogramming is one of the most crucial aspects of these. Fatty acids play a critical role as essential components of lipids, including TGs, phospholipids, glycolipids, cholesterol, and their esters[95].

In this context, several studies have attempted to link various blood metabolic biomarkers to the risk of developing TC or increasing its malignancy. However, the results remain inconclusive, partly due to the cross-sectional nature of many of these studies and the large sample sizes in prospective studies that still have limited statistical power. Moreover, it is challenging to rule out the possibility that some of the analyzed biomarkers may have been modified by the disease itself, and most of these studies have been conducted on cohorts with Asiatic populations. One notable study by Zhao et al. explored a cohort of 2,021 patients with DTC from China and demonstrated that hypercholesterolemia is a risk factor for developing DTC[96]. Among these studies, the AMORIS project (a prospective study of Swedish Apolipoprotein Mortality Risk Cohort) stands out, with over 500,000 individuals and a follow-up period of more than 30 years. This project investigated the associations between metabolic abnormalities and the risk of cardiovascular disease and cancer, including TC. Interestingly, the AMORIS project revealed declining levels of all lipidic and apolipoprotein biomarkers during the 10 years before diagnosis, in contrast to the stable or increasing levels observed among controls[97]. However, this project's limitations include a predominantly Swedish population and a lack of data on specific TC subtypes (e.g., PTC, FTC, ATC, or MTC).

Focusing on PTC studies, different findings have suggested that fatty acid metabolism serves as a critical supplier of energy and substrates for cancer progression[98]. Moreover, these studies have identified a genetic signature consisting of four recurrence-related genes, namely *PDZK1IP1*, *TMC3*, *LRP2*, and *KCNJ13*, which establish a four-gene signature recurrence risk model as prognostic indicators in PTC. These genes' expression has been associated not only with clinicopathological parameters but also with the recurrence of stage T1/T2 PTC[99,100]. Furthermore, SREBP1 has been reported as a pro-proliferation gene in thyroid cancer, and its expression is upregulated with the malignancy of DTC[101]. SREBP1 binds to SRE1, a motif found in the promoter of the LDLR gene and other genes involved in sterol biosynthesis.

These few published studies suggest that body fat percentage, cholesterol levels, and adiposity could be associated with the increased incidence of PTC[64,102]. However, most of the demographic studies have been conducted on Asian populations, and the number of *in vitro* studies is quite low; this indicates that further research is needed to understand the role of cholesterol metabolism and oxysterols such as 27-HC in TC with epithelial origin.

Chapter II

- RESEARCH OBJECTIVES -

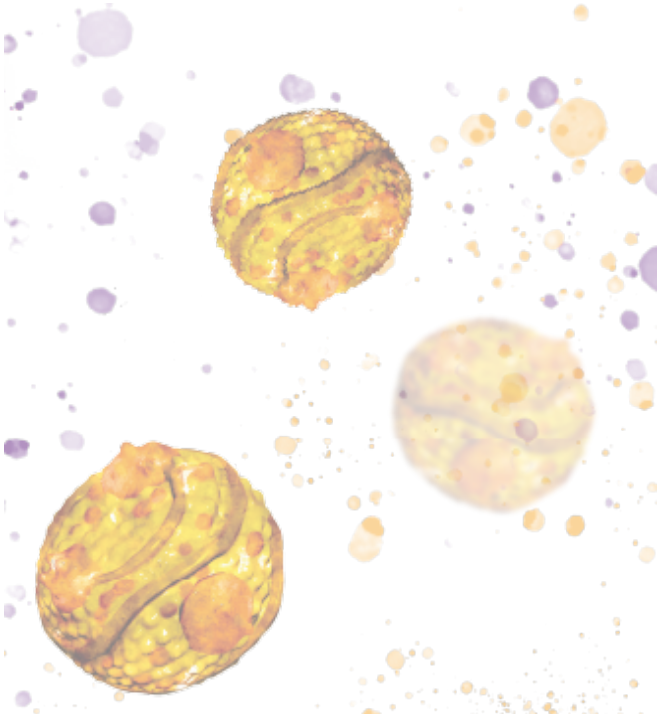

Cancer is a multifactorial disease associated with important metabolic disorders, one of which is the metabolism of cholesterol. Cholesterol and its metabolites play important roles in normal cells, actively participating in the formation of cell membranes, regulating the cell cycle as well as supplying energy requirements of tumoral cells. To meet these needs, these deregulated cells can uptake cholesterol from the bloodstream or can increase *de novo* cholesterol biosynthesis, promoting an imbalance between the accumulation of intracellular cholesterol and inhibition of the cholesterol storage machinery. Moreover, other processes related to the malignant drift of the tumors, such as cell migration and metastasis, have been demonstrated to be dependent on intracellular accumulation of cholesterol. In this regard, hypercholesterolemia has been identified as a risk factor in the development or malignant drift of some solid tumors such as breast cancer, colorectal cancer., and so on. However, in TC progression, the effects of the cholesterol metabolism and metabolite 27-HC remain unknown. Thus, the present thesis aims to study the role of cholesterol in TC aggressiveness. To achieve this goal, we have evaluated the (i) intratumoral metabolite accumulation, (ii) LDL-mediated tumorigenic effects, and (iii) the effect of on signaling pathways promoted by LDL and the oxysterol, 27-HC on TC.

Publication 1: Cholesterol and 27-Hydroxycholesterol Promote Thyroid Carcinoma Aggressiveness

Oxysterols are oxidized derivatives of cholesterol, and they are involved in the regulation of the cholesterol metabolism. One of the main oxysterols, 27-HC, has been linked to tumor progression and estrogen receptor expression in, for example, breast cancer. Moreover, low expression levels of the CYP7B1 gene, responsible for 27-HC degradation, have been correlated with worse patient survival. In this context, we aimed to analyze the association between LDL, intratumoral 27-HC levels, and TC tumors' malignancy.

In detail, the specific objectives of this publication were as follows.

In human samples of thyroid tumors

- To determine the LDL uptake and 27-HC accumulation in primary cell cultures obtained from benign thyroid tumors (BTT), PTC, PDTC, and ATC.
- To analyze the expression of genes involved in cholesterol and 27-HC metabolism: *LDLR*, *HMGCR*, *LXR*, *CYP27A1*, *CYP7B1*, *24-DHCR*, *SCARB1,* and *ABCA1*.

In thyroid cell lines (CAL-62 and Nthy-ori 3.1)

- To investigate the LDL effects on PI3K-AKT-mTOR and RAS-RAF-MAPK (MEK) ERK signaling pathways as well as on proliferation and migration processes

in the ATC cell line (CAL-62) in comparison to a benign thyroid cell line (Nthy-ori 3.1).

- To analyze the expression of genes involved in LDL and 27-HC metabolism, including *LDLR*, *HMGCR*, *CYP27A1,* and CYP7B1 in thyroid cell lines (CAL-62 and Nthy-ori 3.1).

<u>Publication 2:</u> Low-Density Lipoprotein Receptor is a Key Driver of Aggressiveness in Thyroid Tumor Cells

High intratumoral cholesterol levels have been found in a wide range of tumors. In this sense, the LDLR expression together with the abnormal lipidic metabolism have been associated with cancer progression and recurrence in hepatocellular carcinoma, lung cancer, colorectal cancer, and prostate cancer. Moreover, increased LDLR expression and LDL uptake have been linked to LDL-mediated cancer growth in mice. Studies on pancreatic cancer demonstrated that blocking LDLR decreases the proliferation of tumoral cells as well as the activation of the RAS/RAF/MAPK (MEK)/ERK pathway sensitizing cells to chemotherapeutic drugs. Interestingly, different studies have established that the degree of RAS/RAF/MAPK (MEK)/ERK signaling pathway activation determines the extent of LDLR transcription, but the potential molecular mechanisms that regulate this association in TC remain poorly understood.

Considering these points, we aimed to investigate whether $BRAF^{V600E}$ and LDL can potentiate the LDLR-mediated oncogenic processes via the RAS/RAF/MAPK (MEK)/ERK pathway.

Specifically, the main objectives of this publication were:

- To study the protein expression kinetics of LDLR and LDL uptake in response to LDL exposition in two PTC cell lines, namely TPC1 (wild type for $BRAF^{V600E}$) and BCPAP (harboring $BRAF^{V600E}$).
- To analyze the effect of LDL in PTC cell lines on cellular proliferation, migration, and adhesion processes.
- To determine the LDL-signaling pathway and the potential synergistic effect of $BRAF^{V600E}$ together with LDL.
- To study the vemurafenib effect on BCPAP cell line incubated with LDL.

Chapter III

- MATERIAL AND METHODS -

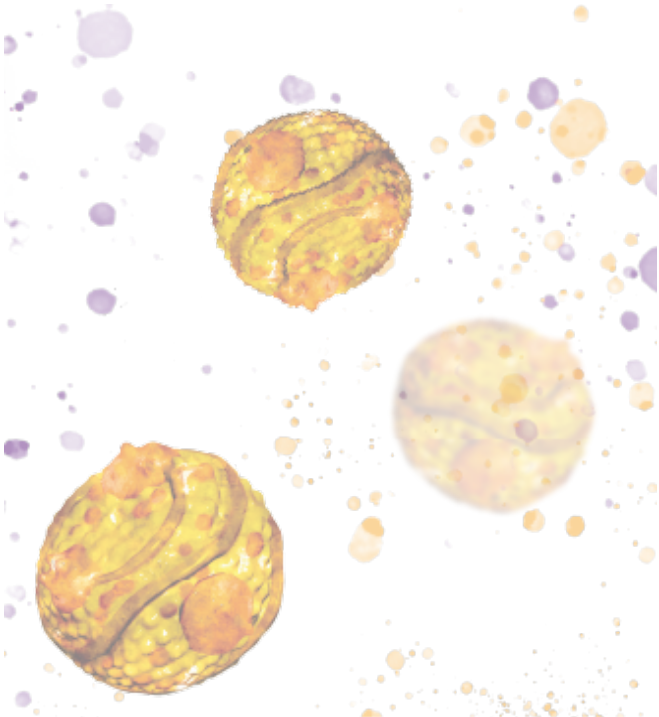

The specific methods and procedures of each research design are summarized in Table 1 and are described in detail below.

METHOD	P. 1	P. 2
1. Patients	X	
2. Human tissue		
2.1 27-hydroxycholesterol (27-HC) level determination	X	
3. Serum samples		
3.1 Lipid, lipoprotein, and apolipoprotein determinations	X	
4. Human lipoprotein isolation	X	X
5. Primary cell cultures		
5.1 Dissociation of thyroid tissue	X	
5.2 Radioactive LDL cholesterol uptake	X	
6. Human Thyroid cell cultures		
6.1 Cell lines	X	X
6.2 Proliferation assay (MTT assay)	X	X
6.3 Migration assay	X	X
6.4 Adhesion assay		X
6.5 Protein extraction and Western Blot	X	X
7. DiI-LDL analyses		
7.1 Labeling DiI-LDL		X
7.2 DiI-LDL Uptake by Fluorometric Assay		X
7.3 DiI-LDL Uptake by Confocal Microscopy		X
8. Transient transfection assay		
8.1 siRNA-mediated protein knockdown	X	X
8.2 Gene overexpression	X	
9. Quantitative RT-PCR analyses		
9.1 Tissue collection	X	
9.2 Cell collection	X	X
9.3 RNA isolation	X	X
9.4 cDNA generation	X	X
9.5 RT-PCR	X	X
10. Statistical analyses	X	X

Table 1. Methodology used in each of the publications presented. P: publication

1. Patients

The fist publication of this thesis includes a cohort of patients (n = 89) with a diagnosis of TC who were recruited at Hospital de la Santa Creu i Sant Pau in Barcelona, Spain. The following clinical information was collected from these patients: sex, age, and unhealthy habits. Additionally, dyslipidemic pathologies or statin treatments, as well as baseline TSH values (0.5–5 mlU/L), were exclusion criteria. The tumors were classified according to the histopathological diagnosis as follows: BTT, WDTC malignancies (PTC), PDTC, and ATC. The AJCC/UICC TNM staging system was used to subdivide the patients into two groups (low/intermediate and high risk; NCCN Guidelines Version 1. 2018, Staging Thyroid Carcinoma). This study was approved by the ethics committee at HSCSP, and all patients gave written informed consent to participate. All research was performed in accordance with relevant guidelines/regulations.

2. Human Tissue

Surgical snap-frozen specimens and serum were obtained from patients recruited from January 2009 at Hospital de la Santa Creu i Sant Pau in Barcelona, Spain, as described above. These belonged to the sample collection registered at Instituto de Salut Carlos III (Spain; C.000281).

2.1. 27-HC Levels Determination

Frozen thyroid samples (n = 66) included in optimal cutting temperature (OCT) compound (Tissue-Tek, Sakura Europe, Alphen den Rijn, Netherlands) were sectioned and homogenized in 1 M NaOH. Protein concentration was measured using the BCA protein assay kit (Thermo Scientific S.L.U., Spain). Lipids were then extracted as described above, resuspended in 100 µl of methanol, and transferred to a vial with 6 µl of deuterium-labeled internal standard. The 27-HC levels were measured using high-performance liquid chromatography tandem mass spectrometry.

3. Serum Samples

3.1. Lipid, Lipoprotein and Apolipoprotein Determinations

Whole blood samples from patients with TC were collected in Vacutainer® tubes and fractionated by centrifugation at 1,500 g for 15 minutes at 4 ºC to obtain serum. Afterwards, serum was aliquoted into 1.5 mL tubes and frozen at 80 ºC until analysis.

Total cholesterol, TGs, phospholipids, HDL-C, LDL-C, and ApoB levels were determined enzymatically in the autoanalyzer COBAS c501 using commercial kits (Roche Diagnostics, Basel, Switzerland). Serum HDL-C levels were measured after the precipitation of Apo B-containing lipoprotein particles with 0.44 mmol/L phosphotungstic acid (Merck, Darmstadt, Germany) and 20 mmol/L magnesium chloride (Sigma-Aldrich, Madrid, Spain).

4. Human Lipoprotein Isolation

LDL and HDL were isolated via sequential ultracentrifugation from normolipidemic human plasma obtained in EDTA-containing Vacutainer® tube and using the appropriate density. The acquisition of human plasma serum for this study was approved by the Ethics Committee of the Hospital de la Santa Creu i Sant Pau. Moreover, pooled plasma of healthy volunteers was obtained after their informed consent.

Material

- Centrifuge tubes of 20 mL maximal volume (polycarbonate plastic).
- Ultracentrifuge Beckman.
- Analytical fixed-angles rotor (55.38, Beckman Coulter).
- Lab material (Eppendorf tubes, tips, pipettes…).
- Density solutions.

Density solution (g/mL)	Composition
1.006	0.15 mM chloramphenicol, 0.15 M NaCl, 0.08 g gentamycin. Dissolve all components in distilled water in a final volume of 2 L and adjust pH at 7.4.
1.019	9.5 g of potassium bromide (KBr) to 500 mL of density solution 1.006 g/mL (KBr is just directly added to this volume of 1.006 g/mL solution).
1.050	6.54 g KBr to 100 mL of density solution 1.006 g/mL (KBr is just directly added to this volume of 1.006 g/mL solution).
1.063	8.53 g KBr to 100 mL of density solution 1.006 g/mL (KBr is just directly added to this volume of 1.006 g/mL solution).
1.340	57.40 g KBr to 100 mL of density solution 1.006 g/mL (KBr is just directly added to this volume).

Table 2. Composition of different density solutions.

All density solutions from Table 2 contained 1mM ethylenediaminetetraacetic acid (EDTA) and 2 μM butylated hydroxytoluene (BHT), and ultracentrifugation steps were performed at 4 ºC to prevent lipoperoxidation.

Lipoproteins were isolated using KBr gradients by sequential ultracentrifugation (55.38 rotor, Beckman Coulter, Fullerton, CA, USA) for 16–18 h at 36.000 g at 4 ºC in accordance with their density as shown in Table 3.

Lipoprotein	Density (g/mL)
VLDL	1.019 g/mL
LDL	1.063 g/mL
HDL	1.210 g/mL

Table 3. Lipoprotein density distributions.

The density to obtain each lipoprotein fraction was reached by adding the proper amount of KBr according to Radding and Steinberg's formula (Figure 15)[103]. The density of plasma is generally assumed to be 1.006 g/mL.

$$X = V\,(d_f - d_i) \,/\, (1 - (0.312 \times d_f))$$

Figure 15. Radding and Steinberg formula. X = g of KBr, V= mL of plasma, d_i = initial density, d_f = final density, 0.312 = partial specific volume of KBr mL/g. Taken from[103]

To carry out LDL isolation, the first isolation step at a density of 1.019 g/mL was performed to remove VLDL and IDL. Afterwards, native LDL was isolated at 1.063 g/mL. Subsequently, LDL was dialyzed against phosphate-buffered saline (PBS) through a PD-10 column (Merck, Darmstadt, Germany). The ApoB concentration was determined using commercial kits adapted to a COBAS c501 autoanalyzer (Roche Diagnostics, Minato City, Tokyo). Finally, LDL solution was filtered through a 0.2-μm filter (Merck, Darmstadt, Germany) before adding this LDL solution to the cells.

5. Primary Cell Cultures

5.1. Dissociation of Thyroid Tissue

Human thyroid tissue obtained from intraoperative pieces was dissected in the Department of Pathology, washed twice with PBS buffer at room temperature and

minced into 3–4 mm pieces with a sterile scalpel. Afterwards, these pieces were digested with collagenase type II (1 mg/mL, Gibco Invitrogen, Waltham, MA, USA) at 37 ºC for 3 h with a continuous magnetic stirring. The reaction was stopped by adding 10 mL of DMEM-F12 culture medium (ThermoFisher Scientific, Waltham, MA, USA) at room temperature, the digested tissues were centrifuged at 1,000 g for 10 min and washed two times in PBS buffer at room temperature. In the next step, the cellular pellets were suspended with Dulbecco's modified Eagle's medium F12 (DMEM-F12; Gibco, Invitrogen, Waltham, MA, USA) supplemented with 10% of FBS and 2% streptomycin/penicillin, transferred into cellular plates. The medium was changed every two days. The cultures were maintained only six days. Finally, the cells were trypsinized, and counted using an automated cell counter (TC10 Bio-Rad, Hercules, CA, USA), and cell blocks with 10^5–10^6 cells were prepared via the plasma-thrombin method. To check cell thyroid purity, thyroglobulin immunostaining with sections from cell blocks was done using the peroxidase-anti-peroxidase technique.

5.2. Radioactive LDL Cholesterol Uptake

Primary cells from human thyroid tissue were seeded at a density of 100,000 cells per 30 mm dish with DMEM-F12 supplemented with 10% of FBS and 2% streptomycin/penicillin and allowed to grow at 37 ºC in a 5% CO_2 atmosphere for 6 days, changing the media every 48 h.

Then, LDL particles (1.063 g/mL) were isolated via ultracentrifugation (protocol detailed in Section 4) and radiolabeled with [1,2-^{3}H] cholesteryl oleate (Perkin Elmer, Boston, MA). For this purpose, 50 μCi of cholesteryl-[1,2-3H(N)] oleate (Perkin Elmer, Boston, MA) and 1.8 mg of L-α-phosphatidylcholine from egg yolk (Sigma, St. Louis, MO, USA) were mixed, and the solvent was evaporated under a stream of N2. Two mL of 1.006 g/mL density solution was added, and the lipids were resuspended via vortex mixing; then, the suspension was sonicated for 10 min in a bath-type sonicator. The cholesteryl-[1,2-3H(N)] oleate emulsion was added to 2 mL of LDL and 2 mL of non-inactivated human lipoprotein depleted fraction, and then incubated for 16 to 18 h in a 37 ºC bath. The labeled LDL was reisolated by ultracentrifugation at 1.019-1.063 g/mL.

Subsequently, radiolabeled LDL (0.45 µCi [1,2-^{3}H] cholesterol oleate/50 µg LDL-ApoB) was dialyzed against PBS via gel filtration chromatography and incubated with cells in DMEN-F12 supplemented with 5% LPDS for 16 h. Then, the medium containing radiolabeled LDL was removed and centrifuged at 10,000 g for 10 min to remove detached cells. Afterwards, an aliquot of 200 µL from the upper fraction of the supernatant of cell-free medium was transferred to a scintillation vial, and 4 mL of scintillation liquid was added to the vials, vigorously mixed, and put into the radioactivity counter. The total counts in the total volume of the medium (1 mL) were calculated using a correction factor.

Simultaneously, the primary cells were washed with warm sterile PBS and lysed with 1 mL of 0.1 M NaOH after incubation at 4 ºC for 48 h. Then, all the lysate content was transferred to a scintillation vial with 4 mL of scintillation liquid, and radioactivity was measured. The [1, 2-^{3}H] LDL cholesterol uptake was expressed as the percentage of the radioactivity collected in the cells relative to the sum of radioactivity in cells and medium per µg of protein per cell (Figure 16).

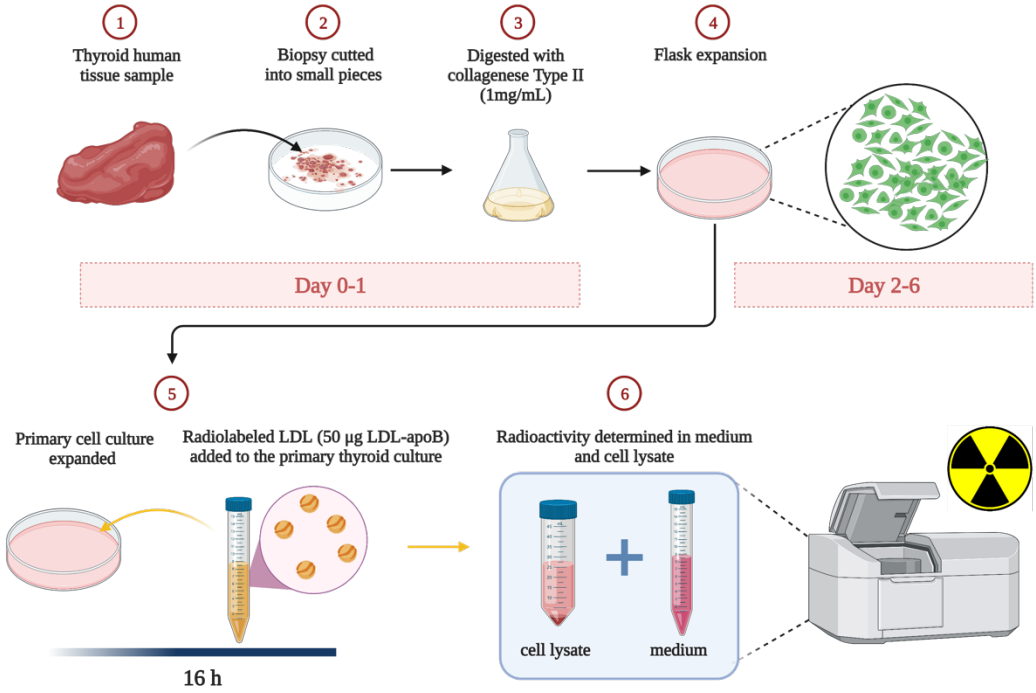

Figure 16. Methodological procedure of radioactive LDL cholesterol uptake. Created with BioRender.com

6. Human Thyroid Cell Cultures

6.1. Cell Lines

The Nthy-ori 3.1 cell line, provided by Dr. Pilar Santisteban (CSIC, Madrid) and derived from normal human primary thyroid follicular epithelial cells, was immortalized with a plasmid containing an origin-defective SV40 genome. The CAL-62 cell line, provided by Leibniz-Institute DSMZ GmbH (ACC 448) and derived from a human ATC harboring KRAS p.G12, has a epithelial-like cells stabilized in culture. The cells do not show thyroglobulin expression, and the most relevant cytogenetic data showed a gain of chromosome 20, a translocation (14q), breakpoints of centromeric chromatin without presenting any *BRAF* mutation. Nthy-ori 3.1 cell lines were cultured in RPMI 1640 (w/L-glutamine; ThermoFisher Scientific, Waltham, MA, USA) and CAL-62 in Dulbecco's modified Eagle's medium (DMEM; Gibco, Invitrogen); both media were supplemented with 10% FBS and 2% streptomycin/penicillin and maintained at 37 ºC in a 5% CO_2 atmosphere. The TPC1 cell line, provided by Paolo Vigneri of Azienda Ospedaliero Universitaria Policlinico Vittorio Emanuele (Catania, Sicilia, Italy) and derived from human PTC, harbors the *RET/PTC* rearrangement. The BCPAP cell line, also provided by Paolo Vigneri of Azienda Ospedaliero Universitaria Policlinico Vittorio Emanuele (Catania, Sicilia, Italy) and derived from human PTC, harbors the $BRAF^{V600E}$ mutation. Both cell lines were cultured in the RPMI 1940 (w/L-glutamine) medium (ThermoFisher Scientific, Waltham, MA, USA) and supplemented with 10% FBS, 100 U/mL penicillin and 1 µg/mL streptomycin at 37 ºC in a 5% CO_2 atmosphere.

6.2. Proliferation Assay (MTT Assay)

LDL incubation

For LDL analysis in Nthy-ori 3.1, CAL-62, TPC1, and BCPAP cells, approximately $4x10^3$–$1x10^4$ cells/well were seeded in 96-well microplates with the corresponding complete media supplemented with 10% FBS and 2% streptomycin/penicillin and maintained at 37 ºC in a 5% CO_2 atmosphere for 24 h. The day after, complete medium was replaced by deprived medium supplemented with 5% FBS and 2% streptomycin/penicillin. Consequently, exogenous LDL at 50, 100, or 200 µg/mL obtained from human serum was added alone or in combination with other reagents for 24 h, 48 h, and 72 h (depending on the experiment). The internal control corresponds to 5% FBS-alone condition.

DHEA treatment

For DHEA treatments (SKU 7000087 P) (Avanti, Polar Lipids, INC.) in Nthy-ori 3.1 and CAL-62 cells, approximately $4x10^3$ cells/well and $1x10^4$ were seeded, respectively, in 96-well microplates with the corresponding complete media supplemented with 10% of FBS, and 2% streptomycin/penicillin and maintained at 37 ºC in a 5% CO_2 atmosphere for 24 h. The day after, the complete medium was replaced by deprived medium supplemented with 5% LPDS and 2% streptomycin/penicillin. Consequently, DHEA at 40, 80, and 160 μM was added for 48 h. The internal control corresponds to 5% LPDS-alone condition.

27-HC incubation

For the 27-HC incubation experiment in Nthy-ori 3.1 cells, $4x10^3$ cells/well were seeded in 96-well microplates with RPMI 1640 (w/L-glutamine; ThermoFisher Scientific, Waltham, MA, USA) complete media supplemented with 10% FBS and 2% streptomycin/penicillin and maintained at 37 ºC in a 5% CO_2 atmosphere for 24 h. The day after, the complete medium was replaced by deprived RPMI 1640 (w/L-glutamine; ThermoFisher Scientific, Waltham, MA, USA) medium supplemented with 5% LPDS and 2% streptomycin/penicillin. Consequently, 27-HC (CAS: 20380-11-4, MedCHem Express, Monmouth Junction, NJ 08852, USA) at 6 and 12 μM was added for 48 h. The internal control corresponds to 5% LPDS-alone condition.

Vemurafenib treatment

For vemurafenib (PLX4032, Selleck Chemicals LLC, Houston, TX, USA) treatment in BCPAP cells, $4x10^3$ cells/well were seeded in 96-well microplates with complete RPMI 1640 (w/L-glutamine; ThermoFisher Scientific, Waltham, MA, USA) media supplemented with 10% FBS, and 2% streptomycin/penicillin and maintained at 37 ºC in a 5% CO^2 atmosphere for 24 h. The day after, the complete medium was replaced by deprived RPMI 1640 (w/L-glutamine; ThermoFisher Scientific, Waltham, MA, USA) medium supplemented with 5% FBS and 2% streptomycin/penicillin. Consequently, vemurafenib at 1 μM was added for 24 h, 48 h, and 72 h alone or in combination with other reagents, depending on the experiment. In the analysis studying vemurafenib effects, the LDL-alone treatment condition (200 μg/mL ApoB + DMSO 0.1%) was used as an internal control.

Finally, to determine the cell viability rate after each treatment, the thiazolyl blue tetrazolium bromide metabolic assay (MTT, Sigma, St. Louis, MO, USA) was used. Absorbance was determined at 560 nm with a microplate reader (xMark, Bio-Rad, Hercules, CA, USA). All conditions were performed in five replicates.

6.3. Migration Assay

Nthy-ori 3.1, CAL-62, TPC1, and BCPAP cells were plated in a 30- or 60-mm dish, depending on the assay, and grown with their corresponding medium supplemented with 10% FBS, 2% streptomycin/penicillin and maintained at 37 ºC in a 5% CO_2 atmosphere until 90% of confluency was reached. Afterwards, cells cultures were scratched with a pipette tip (10 µl) and washed twice with warm sterile PBS buffer to remove cellular debris. The wounds were photographed in a Leica DM IL Inverted Fluorescence Phase Contrast microscope (Leica, Wetzlar, Germany) at 0 h (t = 0), and this was done again in the same area after 13–16 h of cell incubation with the corresponding reagent and maintained at 37 ºC in a 5% CO_2 atmosphere. Image J software V1.53 (University of Wisconsin, Madison, WI, USA) was used to analyze the images[104]. The percentage of wound healing was determined based on three measurements of the wound area; each result was the mean of three independent experiments.

6.4. Adhesion Assay

BCPAP cells were seeded in a 60 mm dish at a density of $6x10^4$ cells/ dish with 5 mL of complete RPMI 1640 (w/L-glutamine; ThermoFisher Scientific, Waltham, MA, USA) media supplemented with 10% FBS and 2% streptomycin/penicillin and maintained at 37 ºC in a 5% CO_2 atmosphere for 24 h. The day after, the complete medium was replaced by deprived RPMI 1640 (w/L-glutamine; ThermoFisher Scientific, Waltham, MA, USA) medium supplemented with 5% FBS and 2% streptomycin/penicillin and treated with exogenous LDL at 200 µg/mL or only with 5% of FBS as a control for 16 h. Then, the supernatant was removed, and 50 µL of this supernatant medium was used to determine detached cell viability as well as to quantify detached cells through trypan blue staining in a TC20 Automated Cell Counter (Bio-Rad, Hercules, CA, USA). Afterwards, attached cells were trypsinized and the cell viability and the number of anchored cells were also determined by trypan blue staining in a TC20 Automated Cell Counter (Bio-Rad, Hercules, CA, USA). Finally, the percentage of viability and cells in suspension were calculated in comparison to the control (5% of FBS).

6.5. Protein Extraction and Western Blot

Nthy-ori 3.1, CAL-62, TPC1, and BCPAP cells were seeded in 30- or 60-mm diameter dishes. When they reached 70% confluence, the specific treatment was added for 24 h, 48 h, and 72 h. Then, cells were washed twice with cold PBS buffer and left in RIPA buffer (50 mM Tris-HCl, pH 7.5; 150 mM NaCl; 1% NP40; 0.5% sodium deoxycholate; 0.1% SDS; 1 mM EDTA) and supplemented with protease inhibitor cocktail (Roche Diagnostics, Minato City, Tokyo), phenylmethylsulfonyl fluoride (PMSF, Sigma, St. Louis, MO, USA), and sodium orthovanadate (Sigma, St. Louis, MO, USA) for 30 min. The next step involved vortexing the lysates and centrifuging them at 12,000 g for 15 minutes at 4 ºC. Pellets containing cellular debris were discarded, and protein quantification was conducted on the supernatants using the BCA protein assay reagent kit (ThermoFisher Scientific, Waltham, MA, USA). Afterwards, the protein extracts were mixed with a 4X Laemmli loading buffer (Sigma, St. Louis, MO, USA) and heated at 94 ºC for 4 min. Then, 20 µg of protein were size-separated on a 10% TGX Stain-Free precast gel (Bio-Rad, Hercules, CA, USA) and transferred to a 0.2 µm PVDF membrane (Bio-Rad, Hercules, CA, USA). The membrane was blocked with 3% dried milk in Tris buffer saline containing 0.05% of Tween-20 (TBST) for 45 min. Finally, membranes were incubated with optimized dilutions of the primary antibody (Table 4) overnight at 4 ºC with continuous shaking. The day after, the membranes were washed three times for 10 min with TBST buffer at room temperature and re-incubated with the IgG HRP-conjugated secondary antibody for 1 h (Table 4). Finally, the membranes were washed three times for 10 min with TBST buffer and analyzed using an Immun-StarWestern Chemiluminescence Kit (Bio-Rad, Hercules, CA, USA). Imaging and data analysis were performed following the protocol described in Taylor et al. TGX stain-free gels were activated for 1 min after SDS-electrophoresis, and images were captured using a ChemiDoc XRS Gel Documentation System (Bio-Rad, Hercules, CA, USA) and Image Lab software (version 6.0.1, Bio-Rad, Hercules, CA, USA). Data normalization analysis for each protein band was performed with the stain-free gel image saved before transferrin gel to PVDF membrane, and the background was adjusted in such a way that the total background was subtracted from the sum of the density of all the bands in each lane[105,106].

Antibody	Species	Dilution	Company (catalog#)
LDLR	Rabbit	1:200	Abcam EP1553Y
p44/42 MAPK (ERK 1/2)	Rabbit	1:1000	Cell signaling (#9102)
p-p44/42 MAPK (p-ERK 1/2)	Rabbit	1:1000	Cell signaling (#9101)
AKT	Rabbit	1:1000	Cell signaling (#4685)
p-AKT	Rabbit	1:1000	Cell signaling (#9271)
MTOR	Rabbit	1:200	Cell signaling (#2972)
p-MTOR	Rabbit	1:200	Cell signaling (#2971)
NF-κB	Rabbit	1:1000	Cell signaling (#3035)
Anti-rabbit secondary		1:5000	Promega (W4011)
Anti-mouse secondary		1:5000	Promega (W4021)

Table 4. Primary and secondary antibodies used.

7. DiI-Low-Density Lipoprotein Analyses

7.1. Labeling Low-Density Lipoprotein

LDL was labeled with 1,1'-Dioctadecyl-3,3,3',3'-Tetramethylindocarbocyanine Perchlorate (DiI, Invitrogen, Waltham, MA, USA), applying a modified procedure of the method described in Teupser et al.[107]

Firstly, a stock solution of DiI was prepared by dissolving 30 µg of DiI in 1 mL of DMSO. Then, DiI was added to the LDL solution, which had previously been dialyzed through a PD-10 column, to yield a final ratio of 300 µg of DiI to 1 mg of LDL (ApoB). Afterwards, it was incubated in a water bath for 18 h at 37 ºC under dark conditions with continuous shaking. The day after, the DiI-LDL solution was centrifuged for five 45-min rounds at 3,000 –3,500 g using an Amicon Ultra-4 Centrifugal Filter 50 kDa MWCO Millipore (15 mL; Sigma-Aldrich, Madrid, Spain) to isolate the DiI-labeled LDL. Then, the DiI-LDL was dialyzed in a PD-10 column against saline containing PBS and filter-sterilized (0.22 µm, Water Millex HV units).

The ApoB concentrations of LDL and DiI-LDL were determined using commercial kits adapted to a COBAS c501 autoanalyzer (Roche Diagnostics, Minato City, Tokyo). The standard solutions of DiI were prepared in isopropanol with a concentration range of 0–110 ng/mL. The standard curve of DiI-LDL was prepared in PBS with a concentration range of 0–1600 ng protein/mL. The fluorescence intensity of both standard curves was measured using a microplate reader, Synergy HT (BioTek Instrument, Winooski, VT, USA) at

λEx/EM = 485/530 nm. The specific activity of DiI-LDL was finally obtained as the amount of DiI (ng) integrated into 1 μg of LDL.

7.2. DiI-Low-Density Lipoprotein Uptake by Fluorometric Assay

TPC1 and BCPAP cells were seeded at a density of $3x10^4$ cells/dish in 30 mm dishes with 2 mL of complete RPMI 1640 (w/L-glutamine; ThermoFisher Scientific, Waltham, MA, USA) medium supplemented with 10% FBS and 2% streptomycin/penicillin and maintained at 37 ºC in a 5% CO_2 atmosphere for 24 h until 70% confluence was reached. The day after, the cells were treated with 5% FBS, as a control; or with 200 μg/mL DiI-LDL for 24 h, 48 h, and 72 h.

After incubation, the cells were placed on ice and washed three times with cold PBS 1X + 00.4% BSA and twice with cold PBS 1X. Then, 300 μL of lysis reagent (NaOH 0.1 M + 1 g/L SDS) was added and left with continuous shaking at room temperature for 30–60 min. Fluorescence intensity in 200 μL of the lysate was measured using a black microplate reader, Synergy HT (BioTek Instrument, Winooski, VT, USA) at λEx/EM = 485/530 nm. Protein quantification was determined in 10 μL of the lysate by BCA using BSA dissolved in lysis reagent as a standard (Thermofisher Scientific, Waltham, MA, USA) to normalize fluorescence measurements through cellular culture confluence. Additionally, the fluorescence of the standard curve of the DiI-LDL diluted in lysis reagent was measured to determine the specific fluorescence intensity of the DiI-LDL preparation used.

7.3. DiI-Low-Density Lipoprotein Uptake by Confocal Microscopy

TPC1 and BCPAP cells were seeded at a density of $3x10^4$ cells/dish in specific confocal 35 mm dishes (75856-742, Radnor, PA, USA) with 2 mL of complete RPMI 1640 (w/L-glutamine; ThermoFisher Scientific, Waltham, MA, USA) medium supplemented with 10% FBS and 2% streptomycin/penicillin and maintained at 37 ºC in a 5% CO_2 atmosphere for 24 h until 70% of confluence was reached. The day after, the cells were treated with 5% FBS, as a control, or with 200 μg/mL DiI-LDL for 24 h, 48 h, and 72 h. The nucleus and lysosomes were labeled with Hoechst and GFP (ThermoFisher Scientific,Waltham, MA, USA) 5 min and 16 h before confocal analysis, respectively.

The images of immune-stained cells were recorded on a Leica-inverted fluorescence confocal microscope (Leica TCS SP5-AOBS, Wetzlar, Germany). Cells were viewed with an HCX PL APO 63X oil/0.6–1.4 objective. Then, fluorescent images were acquired in a scan format of 1,024x1,024 pixels in a spatial dataset (xyz or xzy) and were processed using the Leica Standard Software TCS-AOBS (V2.7.3). Lysosomal quantification was carried out using Fiji software (ImageJ V1.53, University of Wisconsin, Madison, WI, USA)[104].

8. Transient Transfection Assay

8.1. siRNA-mediated Protein Knockdown

Downregulation of the CYP27A1 gene.

Nthy-ori 3.1 cells were plated at a density of $4x10^3$ cells/well in a 96-well plate one day prior to transfection. The following day, the cells were transiently transfected using JetPrime™ (Polyplus transfection) according to the manufacturer's instructions with either 5 nM pre-designed short interfering RNA (siRNA CYP27A1, ID106239, Ambion, Life Technologies, Carlsbad, CA, USA) or control siRNA purchased from Santa Cruz Biotechnology Inc. (sc-37007, Dallas, TX, USA) in RPMI supplemented with 10% FBS, 100 U/mL penicillin and 1µg/mL streptomycin medium for 24 h at 37 ºC in a 5% CO_2 atmosphere. Then, the transfected cells were treated with LDL (200 µM) plus 5% FBS or only 5% FBS as a control. After 48 h of incubation, the transfected cells were tested for MTT assay to analyze cellular proliferation.

8.2. Gene Overexpression

Overexpression of the CYP7B1 gene.

CAL-62 cells were plated at a density of $1x10^4$ cells in a 96-well plate with DMEM High Glucose 10% FBS, 100 U/mL penicillin and 1µg/mL streptomycin medium at 37º C in a 5% CO_2 atmosphere, one day prior to transfection. Then, the cells were transiently transfected using JetPrime™ (Polyplus transfection) according to the manufacturer's instructions with either 0.1 nM pre-designed *CYP7B1* (NM_004820.3) DNA ORF clone or control (pcDNA3.1+/ C-(K) DYK) purchased from GeneScript (Piscataway, NJ, USA) (OHu27221) and treated with LDL (200 µM), plus 5% FBS or only 5% FBS as a control for 48 h. After incubation, the transfected cells were tested for MTT assay (protocol detailed in Section 6.2).

For wound-healing assays, $5x10^4$ CAL-62 cells were plated in 6-well plates and transiently transfected with the same concentration described above. The wound-healing assay was performed as described in Section 6.3.

9. Quantitative RT-PCR Analyses

9.1. Tissue Collection

For RNA analysis, patients' thyroid tissue samples were collected, weighted and rapidly frozen in liquid nitrogen.

9.2. Cell Collection

For RNA extraction in cell culture, culture dishes were first kept on ice through all the extraction using TRIzol reagent (Invitrogen, Carlsbad, CA, USA). The culture medium was carefully aspirated, and then dishes were washed twice with cold, sterile PBS to remove the total amount of PBS before following to the RNA isolation steps. Afterwards, 500 μL of TRIzol reagent (Invitrogen, Carlsbad, CA, USA) was added to each culture dish, the lysate was pipetted up and down several times to homogenize, and the lysate was rapidly frozen in liquid nitrogen.

9.3. RNA Isolation

Total RNA from both tissue samples and cell line cultures was isolated using TRIzol reagent (Invitrogen, Carlsbad, CA, USA) according to the manufacturer's instructions. Afterwards, RNA concentration was determined using a NanoDrop2000 bioanalyzer (ThermoFisher Scientific, Waltham, MA, USA). The RNA concentration was determined at λ = 260 nm optical density (OD), considering that an A_{260} of 1.0 is equivalent to about 40 μg/mL of RNA.

To evaluate the purity of RNA, the ratio of absorbance at λ = 260 nm and λ = 280 nm was applied. A ratio of ~ 2.0 is commonly accepted as 'good' for RNA. A lower ratio could be related to the presence of protein, phenol, or other contaminants that absorb strongly at or near 280 nm.

9.4. cDNA Generation

One microgram of the total RNA was reverse transcribed to complementary DNA (cDNA). cDNA synthesis is performed due to the action of reverse transcriptase, an enzyme that creates single-stranded DNA from an RNA template in the presence of primers. cDNA was obtained using a first-strand cDNA synthesis kit (Roche Applied Science, Penzberg, Germany), and the cDNA samples were stored at –20 °C for use as a template in real-time quantitative polymerase chain reaction (PCR) analysis.

9.5. Quantitative real-time PCR

The quantitative real-time PCR (RT-PCR) was used to amplify cDNA products obtained from reverse-transcribed mRNA. A relative quantification method was applied in which internal genes named housekeeping genes are used to determine fold variations in the expression of specific genes.

The gene expression profiles were analyzed in an ABI PRISM 7900HF Sequence Detection System using a predesigned and labeled primer/probe set (Assays-on-Demand™ Gene Expression Assay, Applied Biosystems, Foster City, CA, USA). All the reactions were performed with 100 ng of cDNA in a total volume of 50 µl of TaqMan® Universal PCR Master Mix (Applied Biosystems, Waltham, MA, USA). Thermal cycling conditions involved 10 min at 95 ºC, 40 cycles at 95 ºC for 15 s, and 65 ºC for 1 min.

Specific human Taqman qPCR primers (Applied Biosystems, Waltham, MA, USA) were used to analyze gene expression of *CYP27A1* (Hs01017992_m1), *CYP7B1* (Hs01046431_m1), *HMGCR* (Hs00168352_m1), *LDL* receptor (LDLR; Hs01092524_m1), SCARB1 (Hs00969827_m1), *DHCR-24* (Hs00207388_m1), and *ABCA1* (Hs01059137_m1). The samples were analyzed in duplicate, and RNA from BTT was used as a group calibrator; negative controls were also included in all the reactions. The relative expression levels for each gene were calculated using the 2-ddCt method with SDS2.3 and Data Assist V2.1 software (Applied Biosystems).

The specific human *GAPDH* (NM_002046.3) was used as endogenous control gene (Applied Biosystems, Waltham, MA, USA).

10. Statistical Analysis

Results were expressed as mean ± SD or as mean ± SEM when indicated.

The one-way analysis of variance (ANOVA) test was utilized to compare continuous variables, and Tukey's multiple comparison post-test was applied to assess differences among the groups. Additionally, the Kruskal-Wallis multiple comparison test was employed to compare continuous variables that did not follow a Gaussian distribution, and Dunn's post-test was used to compare differences among the groups. Pearson's correlation analysis was conducted to examine the correlations between variables.

The differences between the two groups were compared using an unpaired two-tailed Student's t-test. To evaluate the effects of time and cell type on each dependent variable, a Two-way ANOVA with Sidak's multiple comparison post-test was applied.

Gene expression analysis was performed using the comparative CT (ddCt) method by DataAssist™ Software, and the results were adjusted as the p-value using the Benjamini–Hochberg false discovery rate (FDR). Genes showing an FDR <0.15 and more than two-fold difference in absolute values for both comparisons were considered differentially expressed.

GraphPad Prism 5.0 and 9.0 software (GraphPad, San Diego, CA, USA) were employed for the first and second publications, respectively, and values of $p < 0.05$ were considered statistically significant.

Chapter IV

- RESULTS -

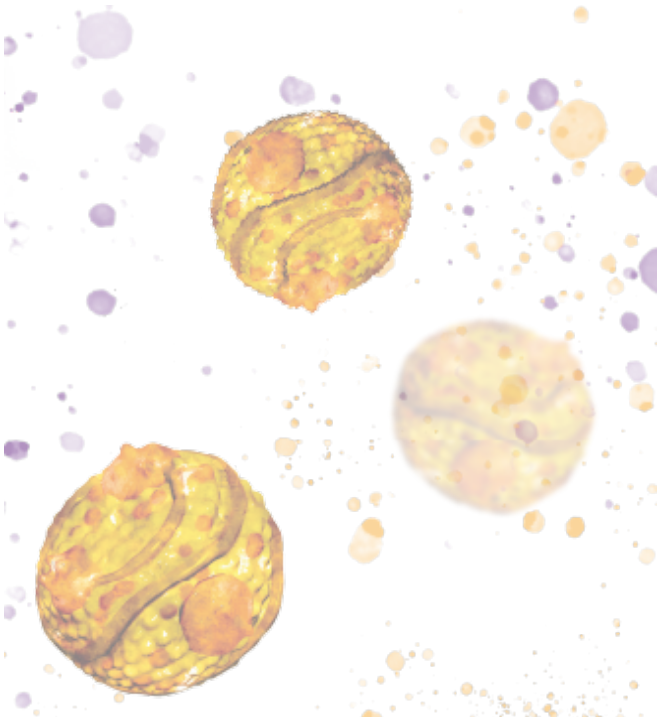

PUBLICATION I

Cholesterol and 27-Hydroxycholesterol Promote Thyroid Carcinoma Aggressiveness

Giovanna Revilla, Monica de Pablo Pons, Lucía Baila-Rueda, Annabel García-León, David Santos, Ana Cenarro, Marcelo Magalhaes, R. M. Blanco, Antonio Moral, José Ignacio Pérez, Gerard Sabé, Cintia González, Victoria Fuste, Enrique Lerma, Manuel dos Santos Faria, Alberto de Leiva, Rosa Corcoy, Joan Carles Escolà-Gil, Eugènia Mato*

*Corresponding authors

Scientific Reports

2019

SCIENTIFIC REPORTS

OPEN

Cholesterol and 27-hydroxycholesterol promote thyroid carcinoma aggressiveness

Received: 24 January 2019
Accepted: 4 July 2019
Published online: 16 July 2019

Giovanna Revilla[2,3], Monica de Pablo Pons[1,2], Lucía Baila-Rueda[4,5], Annabel García-León[2], David Santos[2,6], Ana Cenarro[5], Marcelo Magalhaes[8], R. M. Blanco[7], Antonio Moral[2,9,10], José Ignacio Pérez[9], Gerard Sabé[2], Cintia González[1,7], Victoria Fuste[2,11], Enrique Lerma[2,11], Manuel dos Santos Faria[8], Alberto de Leiva[2,7], Rosa Corcoy[1,7,10], Joan Carles Escolà-Gil[2,3,6] & Eugenia Mato[1,7]

Cholesterol mediates its proliferative and metastatic effects via the metabolite 27-hydroxycholesterol (27-HC), at least in breast and endometrial cancer. We determined the serum lipoprotein profile, intratumoral cholesterol and 27-HC levels in a cohort of patients with well-differentiated papillary thyroid carcinoma (PTC; low/intermediate and high risk), advanced thyroid cancers (poorly differentiated, PDTC and anaplastic thyroid carcinoma, ATC) and benign thyroid tumors, as well as the expression of genes involved in cholesterol metabolism. We investigated the gene expression profile, cellular proliferation, and migration in Nthy-ori 3.1 and CAL-62 cell lines loaded with human low-density lipoprotein (LDL). Patients with more aggressive tumors (high-risk PTC and PDTC/ATC) showed a decrease in blood LDL cholesterol and apolipoprotein B. These changes were associated with an increase in the expression of the thyroid's LDL receptor, whereas 3-hydroxy-3-methylglutaryl-CoA reductase and 25-hydroxycholesterol 7-alpha-hydroxylase were downregulated, with an intratumoral increase of the 27-HC metabolite. Furthermore, LDL promoted proliferation in both the Nthy-ori 3.1 and CAL-62 thyroid cellular models, but only in ATC cells was its cellular migration increased significantly. We conclude that cholesterol and intratumoral accumulation of 27-HC promote the aggressive behavior process of PTC. Targeting cholesterol metabolism could be a new therapeutic strategy in thyroid tumors with poor prognosis.

Cancer is a multifactorial disease that is associated with important metabolic disorders, one of which is the metabolism of cholesterol. Cholesterol molecules and their metabolites play important roles in normal cells, actively participating in the formation of cell membranes, as well as the cell cycle, and the tumoral cells require an increased supply of cholesterol. To meet these needs, these deregulated cells are able to promote two strategies cholesterol uptake from the bloodstream and *de novo* cholesterol biosynthesis[1–4]. In this context, hypercholesterolemia has been identified as a risk factor in the development or malignant drift of some solid tumors, such as in breast, colon, and prostate cancer[5–8]. In contrast, the inhibition of the cholesterol synthesis pathway can activate the mechanisms of cell differentiation[9].

[1]Department of Endocrinology-EDUAB-HSP, Hospital de la Santa Creu i Sant Pau, Barcelona, Spain. [2]Institut d'Investigacions Biomèdiques (IIB) Sant Pau, Hospital de la Santa Creu i Sant Pau, Barcelona, Spain. [3]Departament de Bioquímica, Biologia Molecular i Biomedicina, Universitat Autònoma de Barcelona, Barcelona, Spain. [4]Unidad Clínica y de Investigación en Lípidos y Arteriosclerosis, Hospital Universitario Miguel Servet, Instituto de Investigación Sanitaria Aragón (IIS Aragón), Zaragoza, Spain. [5]CIBER de Enfermedades Cardiovasculares, CIBERCV, Madrid, Spain. [6]CIBER de Diabetes y Enfermedades Metabólicas Asociadas, CIBERDEM, Madrid, Spain. [7]CIBER Bioingeniería, Biomateriales y Nanomedicina, CIBER-BBN, Madrid, Spain. [8]Service of Endocrinology, Clinical Research Center (CEPEC), Hospital of the Federal University of Maranhão (HUUFMA), São Luís, Maranhão, Brazil. [9]Department of General Surgery—Hospital de la Santa Creu i Sant Pau, Barcelona, Spain. [10]Medicine Department, Autonomous University of Barcelona (UAB), Barcelona, Spain. [11]Department of Anatomic Pathology—Hospital de la Santa Creu i Sant Pau, UAB, Barcelona, Spain. Joan Carles Escolà-Gil and Eugenia Mato contributed equally. Correspondence and requests for materials should be addressed to J.C.E.-G. (email: JEscola@santpau.cat) or E.M. (email: emato@santpau.cat)

	BTT	Low/intermediate-risk PTC	High-risk PTC	PDTC/ATC
Cholesterol (mmol/L)	4.933 ± 0.207	4.581 ± 0.159	3.832 ± 0.198*	3.793 ± 0.245*
Triglycerides (mmol/L)	1.563 ± 0.156	1.290 ± 0.105	0.824 ± 0.101**	0.936 ± 0.164
Phospholipids (mmol/L)	2.824 ± 0.101	2.558 ± 0.088	2.182 ± 0.112**	2.321 ± 0.131*
HDL Cholesterol (mmol/L)	1.673 ± 0.132	1.704 ± 0.106	1.515 ± 0.143	1.593 ± 0.267
LDL Cholesterol (mmol/L)	2.551 ± 0.165	2.293 ± 0.129	1.944 ± 0.222	1.775 ± 0.083*
ApoB (g/L)	0.990 ± 0.044	0.961 ± 0.037	0.748 ± 0.07**	0.714 ± 0.064*

Table 1. Patients' serum lipid profile according to histology pattern. Mean ± SEM of total cholesterol, triglycerides, phospholipids, low-density lipoprotein cholesterol, high-density lipoprotein cholesterol, apolipoprotein (apo) B in BTT ($n = 27$), low/intermediate-risk PTC ($n = 43$), high-risk PTC ($n = 12$), and PDTC/ATC ($n = 7$). Analysis of variance using ANOVA plus Tukey's post-hoc test (*$p < 0.05$, **$p < 0.01$). P-values are in comparison to BTT.

One feature of some malignant tumors is the existence of an imbalance between the accumulation of intracellular cholesterol and inhibition of the cholesterol storage machinery[10–12]. Other processes related to the malignant drift of the tumors, such as cell migration and metastasis, have been demonstrated to be dependent on intracellular accumulation of cholesterol[3,6,7]. Moreover, oxysterols are oxidized derivatives of cholesterol, and they are involved in the regulation of the cholesterol metabolism; oxysterols are associated with different chronic diseases, such as atherosclerosis, neurodegenerative diseases, and inflammatory bowel diseases[13]. Furthermore, the oxysterols have also been related to the development of cancer trough the hedgehog, WNT, and MAPK signaling pathways[14,15]. Different forms of oxysterols have been identified; the most important are 27-, 24-, and 7α-hydroxycholesterol. 27-hydroxycholesterol (27-HC), which is mainly synthesized in the liver, acts as a potent suppressor of cholesterol synthesis throughout the sterol regulatory element-binding proteins (SREBPs)[16]. 27-HC levels are controlled by two mitochondrial enzymes, namely sterol 27-hydroxylase (*CYP27A1)*—which is responsible for their synthesis—and 25-hydroxycholesterol 7-alpha-hydroxylase (*CYP7B1*), which is responsible for their catabolism[17]. Different studies have demonstrated the link among the levels of 27-HC, tumor proliferation and estrogen receptor expression in breast cancer[15,18–20]. The analysis of both genes in breast tumors with positive estrogen receptors showed that the prognosis and survival of patients were independent of the *CYP27A1* gene expression, while low expression levels of the *CYP7B1* gene were correlated with worse patient survival[15,19,21]. 27-HC can activate the liver X receptors (LXRs), which may regulate the target genes controlling cholesterol, glucose and fatty acid metabolism, as well as inflammatory responses and the expression of specific genes that control cell proliferation and metastasis processes[22,23].

Several epidemiological studies have investigated the link between dyslipidemias, high-fat diets, and cancer[24–26]. In thyroid cancer (TC), this relationship is still unknown, although some evidence in the last decade suggests that the body fat percentage, cholesterol levels, and adiposity could be associated with the increased incidence of TC, papillary subtype (PTC)[27,28]. However, the effects of the cholesterol metabolism and metabolite 27-HC on TC progression remain unknown. The objective of this study was to analyze the associations between cholesterol, intratumoral 27-HC levels, and TC tumors' malignancy.

Results

Low LDL-cholesterol levels in patients with high-risk PTC and dedifferentiated tumors. The serum lipid profiles of patients with different thyroid neoplasms are summarized in Table 1. Patients with high-risk PTC and PDTC/ATC tumors showed lower serum cholesterol levels (3.832 ± 0.198 mmo/L, $p = 0.0041$ and 3.793 ± 0.245 mmo/L, $p = 0.0293$, respectively) compared with those with BTT tumors (4.933 ± 0.207 mmo/L) and low/intermediate-risk PTC (4.581 ± 0.159 mmo/L). These changes were associated with a decrease in LDL cholesterol in high-risk PTC tumor patients (1.944 ± 0.222 mmo/L, $p = 0.0515$) and those with dedifferentiated PDTC/ATC tumors (1.775 ± 0.083 mmo/L, $p = 0.0274$) compared with those with BTT (2.551 ± 0.165 mmo/L) and low/intermediate-risk patients PTC (2.293 ± 0.129 mmo/L). The apoB levels were also decreased in patients with high-risk PTC tumors (0.748 ± 0.07 mmo/L, $p = 0.0068$) and PDTC/ATC (0.714 ± 0.064 mmo/L, $p = 0.011$). However, the HDL cholesterol levels did not differ among the groups analyzed. Moreover, the triglyceride levels were reduced in patients with all the types of malignant tumors, but significant changes were only found in the high-risk PTC group (0.824 ± 0.101 mmo/L, $p = 0.0015$).

The LDL receptor (LDLR) is upregulated in tumors with higher malignancy. The gene expression of the LDLR (specific receptor-mediated endocytosis of LDL) was upregulated in the PTC tumors with greater malignancy (high-risk PTC and PDTC/ATC) compared with the tumors with a minor degree of malignancy (low/intermediate-risk PTC and BTT; (Fig. 1). However, the tumorigenic-free cholesterol levels, esterified cholesterol, and triglycerides did not differ among all the groups analyzed (Supplementary Fig. S1). Moreover, the LDL uptake analysis in primary cell cultures displayed that the LDL-derived cholesterol uptake in the PDTC tumors was higher (13 ± 1.4%) than that of high-risk PTC and BTT tumorigenic cells (8.9 ± 0.3% and 8.4 ± 0.1%, respectively, $p \leq 0.01$ *vs* PDTC) (Supplementary Fig. S2).

HMGCR and CYP7B1 are strongly downregulated in PDTC and ATC tumors compared with BTT. The gene expression analysis of genes related with cholesterol metabolism and the oxysterol 27-HC in

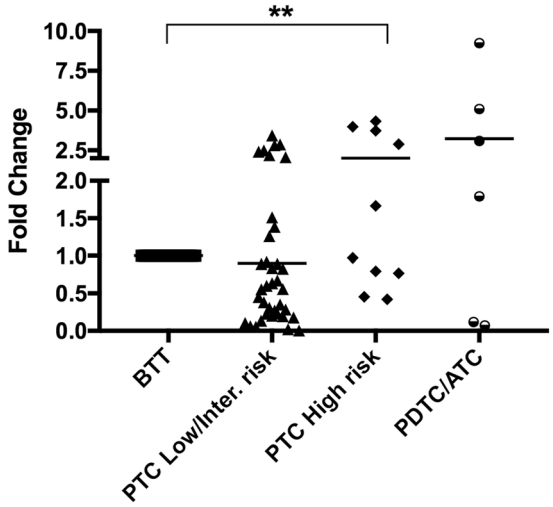

Figure 1. Analysis of the low density lipoprotein receptor (LDLR) gene expression by qRT-PCR in human thyroid tumors. BTT ($n = 26$), low/intermediate-risk PTC ($n = 37$), high-risk PTC ($n = 10$), PDTC/ATC ($n = 6$). Endogenous expression of the GAPDH gene has been used to normalize the data and BTT as calibrator. Statistical analysis: ANOVA test plus Tukey's post-test (**$p < 0.01$).

TC tumors are shown in Fig. 2; the expression of the HMGCR gene was downregulated in all types of malignant tumors compared to benign tumors, being higher in the PDTC/ATC ($p < 0.001$). Moreover, the differences were also significant when less aggressive PTC tumors or more indolent PTC tumors (low/intermediate risk) were compared with the aggressive PDTC and ATC tumors ($p < 0.05$, Fig. 2A). However, no differences were found between PTC with different degrees of malignancy. A similar expression profile was observed in the *CYP7B1* gene, which was also downregulated in all tumors, especially dedifferentiated PDTC/ATC ($p < 0.001$). The comparison between the malignant tumors exhibited a significant difference between the PTC (low/intermediate risk) and PDTC/ATC samples ($p < 0.01$; Fig. 2B). The gene expression analysis of the *LXR alpha* gene also displayed a similar gene expression pattern, although the downregulation detected was higher and significant in all groups analyzed (Fig. 2C). In contrast, the *CYP27A1* gene expression did not differ significantly among the groups (Fig. 2D).

The analysis of 24-Dehydrocholesterol reductase (24DHCR) and the scavenger receptor class B type 1 (SCARB1) genes showed that both genes tended to be downregulated when compared the most aggressive tumors with BTT group, although these changes were not significantly different (Supplementary Table 1).

To investigate whether LDL can produce similar effects *in vitro* to those found *in vivo*, two thyroid human cell lines with different genotypes (Nthy-ori 3.1 and CAL-62) were exposed to human LDL and the gene expression profile was analyzed. The comparison of both cell lines did not reveal significant changes in LDLR and CYP27A1 gene expression (Fig. 3A,C). However, a downregulation in HMGCR and CYP7B1 was detected in CAL-62 in comparison with Nthy-ori 3.1 (Fig. 3B,D).

PDTC/ATC tumors show higher levels of 27-hydroxycholesterol. The percentage of tumors with detectable levels of 27-HC was higher in the malignant tumors analyzed, with 20% in the low/intermediate-risk PTC samples (6 positive of the 30 total samples), with a mean of 3.73 ng/mg protein; 44% in the high-risk PTC samples (8 positive of 18 total samples), with a mean of 10.07 ng/mg protein; and 89% in the PDTC/ATC (8 positive of 9 total samples), with a mean of 89.42 ng/mg protein. In contrast, the percentage of detection in the BTT samples was 5% (2 of 40 total samples), with a mean of 16.38 ng/mg protein (Fig. 4A). Moreover, we observed a negative correlation between the CYP7B1 gene expression and the 27-HC concentration, showing higher levels of this sterol in the most aggressive samples analyzed (Fig. 4B).

LDL cholesterol promotes proliferation and migration in anaplastic thyroid cell lines without changing in MAPK, PI3K and mTOR signaling pathways. The Nthy-ori 3.1 cell line, derived from normal human primary thyroid follicular epithelial cells, was immortalized with a plasmid containing an origin-defective SV40 genome (SV-ori). The CAL-62 cell line, derived from a human thyroid anaplastic carcinoma (ATC), is an epithelial-like cells stabilized in culture. These cells do not show thyroglobulin expression, as well as, do not present any BRAF mutation[29]. LDL promoted a dose-related response in cellular proliferation in both Nthy-ori 3.1 and CAL-62 ($p < 0.01$), without significance between them (Fig. 5A). Nevertheless, the evaluation of wound healing capacity showed that LDL cholesterol promoted cell mobility in the CAL-62 cell line in a dose-related response; in contrast, LDL cholesterol did not induce significant changes in the cell mobility in the Nthy-ori 3.1 cells (Fig. 5B). The concentration of 27-HC measured in the LDL treated cells and non treated cell was 3.73 ± 1.69 ng 27HC/mg prot and 0.37 ± 0.53 ng 27HC/mg prot, respectively ($p = 0.01$), in CAL-62 cell line. However, the concentration of 27-HC in the Nthy-ori 3.1 cells treated with LDL was lower in comparison with CAL-62 cell line (0.7 ± 0.25 ng 27-HC/mg prot) and it was undetectable in non treated cell.

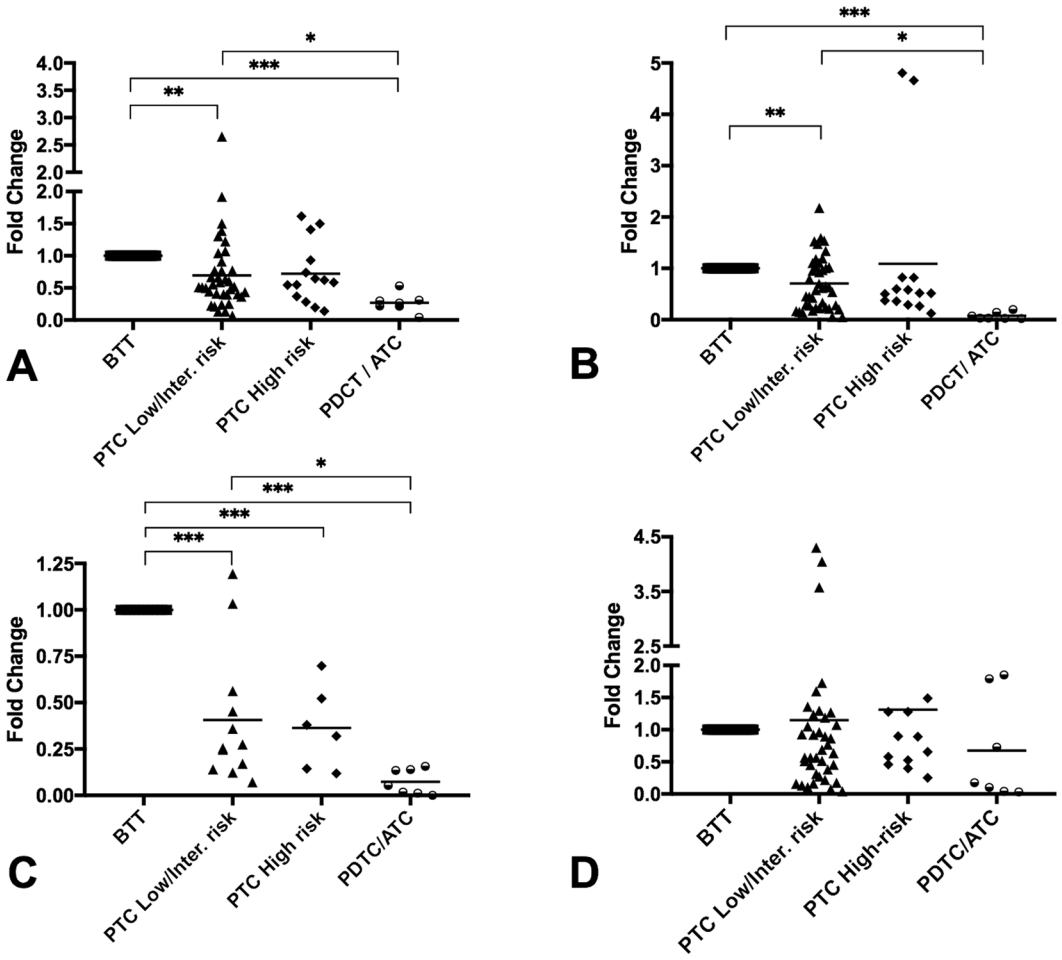

Figure 2. Analysis of the gene expressions by qRT-PCR in human thyroid tumors. (**A**) *HMGR* gene expression, (**B**) *CYP7B1* gene expression, (**C**) *LXR* gene expression, (**D**) *CYP27A1* gene expression. The patient cohort was divided into the following groups: BTT ($n = 32$), low/intermediate-risk PTC ($n = 37$), high-risk PTC ($n = 12$), and PDTC/ATC ($n = 7$). Endogenous expression of the *GADPH* gene was used to normalize the data, and BTT was used as calibrator tissue. Statistical analysis: ANOVA test plus Tukey's post-test (*$p < 0.05$, **$p < 0.01$, ***$p < 0.001$).

Finally, the effect of the LDL in the MAPK, PI3K and mTOR signaling was also investigated. A slight dose-dependent decrease of the P-Akt and ERK was found in both cell lines (Supplementary Fig. S3).

CYP7B1 overexpression and CYP27A1 silencing can modulate cellular proliferation rate. The overexpression of CYP7B1 in CAL-62 cell line treated with LDL arrested growth ($p = 0.001$) and decreased cellular migration with ($p = 0.02$) and without LDL treatment ($p = 0.02$) (Fig. 6A,B); nonetheless, Nthy-ori 3.1 cell line treated with 27-HC at 6 and 12 µM decreased the proliferation rate in both concentrations ($p = 0.001$), but promoted the migration rate ($p = 0.001$) without evidence of a dose-related response (Fig. 6C,D).

Furthermore, downregulation of CYP27A1 completely blocked LDL-mediated cell proliferation (Supplementary Fig. S4). In contrast, DHEA did not promote proliferation in CAL-62 cell line, whereas a moderate arrest growth was detected in a doses dependent manner in Nthy-ori 3.1 cell line (Supplementary Fig. S5).

Discussion

The role of cholesterol in cancer development is controversial; notwithstanding, several epidemiological studies have reported an association between serum cholesterol levels and a higher incidence of some types of solid tumors[18,26,30]. In this study, the patients bearing tumors with more aggressive behavior showed a significant decrease in serum LDL-cholesterol and apoB, without changing the HDL-cholesterol levels. These data are in consonance with different reports highlighting the importance of the uptake of systemic cholesterol as a mechanism modulating the tumoral process[31]. According to these data, we also detected overexpression of the LDLR in the subtypes of thyroid tumors with a more aggressive behavior. These data reinforce the hypothesis of these subtypes of tumors' higher systemic cholesterol uptake capacity in comparison with benign tumors. There is evidence in tumors that has demonstrated the role of LDL-cholesterol on the cell migration and metastasis[3,32]. The promotion of the migration process after incubation with LDL cholesterol in cells could support the idea of cholesterol's role in the tumor's metastatic promotion. On the other hand, different signaling pathways have been proposed as a mediator

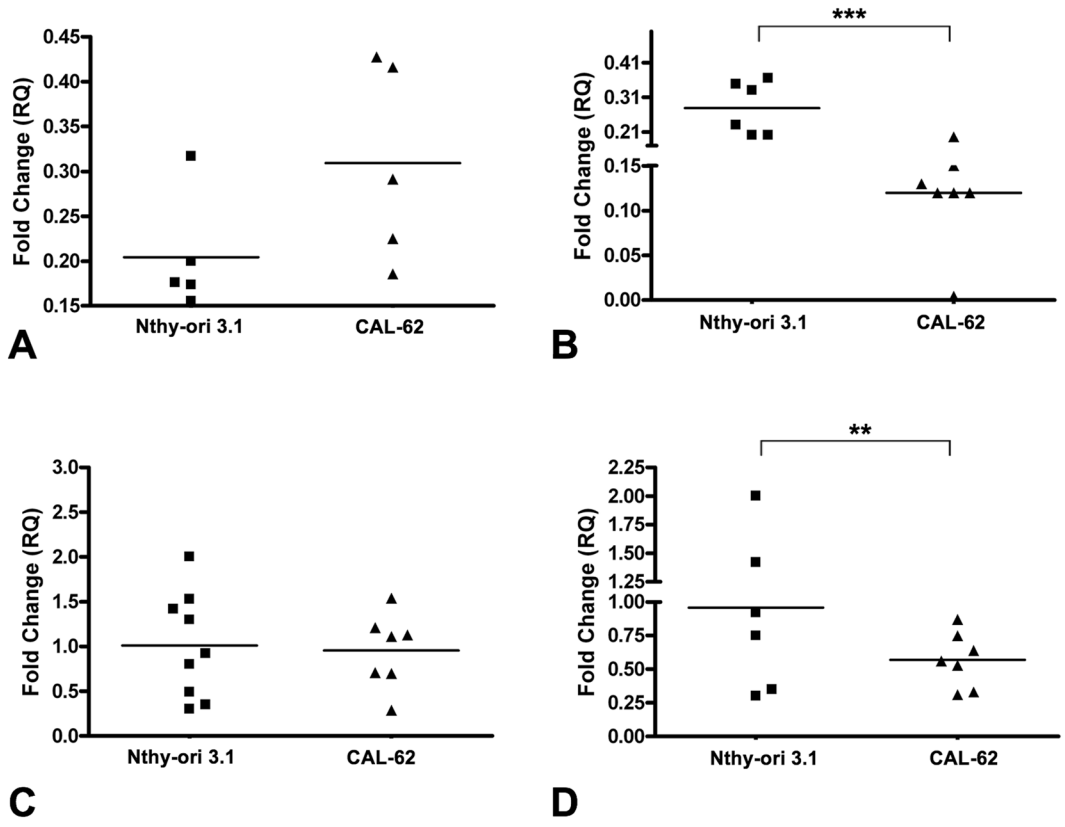

Figure 3. Analysis of the gene expression by qRT-PCR in thyroid cell lines (Nthy-ori 3.1 and CAL-62). (**A**) LDLR, (**B**) HMGR, (**C**) CYP27A1, and (**D**) CYP7B1. Endogenous expression of the GADPH gene was used to normalize the data. Statistical analysis: Student t-test (**$p < 0.01$, ***$p < 0.001$).

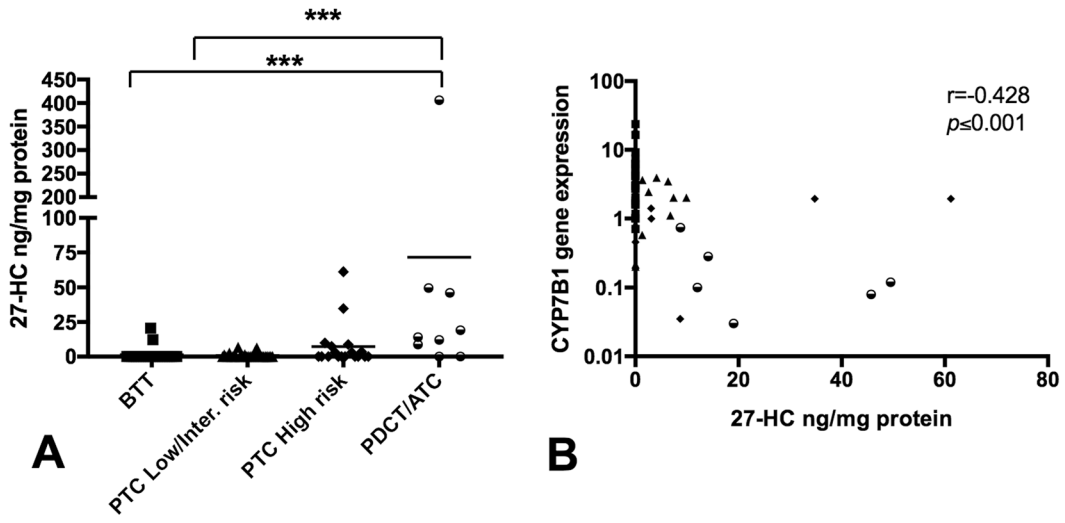

Figure 4. 27-hydroxycholesterol (27-HC) content and their relationship with the CYP7B1 gene expression in thyroid tumor tissue extracts. (**A**) The analysis of 27-HC was measured in 82 patients (n = 97 thyroid tissue samples) corresponding to BTT (n = 40), low/intermediate-risk PTC (n = 30), high-risk PTC (n = 18) and PDTC/ATC (n = 9). The results represent the mean ± SD of the measurements of individual thyroid tissue. (ANOVA) using the Kruskal–Wallis test and Dunn's post-test (***$p < 0.001$). (**B**) A correlation analysis was done in 73 samples in which 27-HC and CYP7B1 expression were analyzed in the same sample (27 BTT, 29 low/intermediate-risk PTC, 11 high-risk PTC and 6 PDTC/ATC samples). The graph illustrates the negative correlation between the CYP7B1 gene expression ($2^{-\Delta\Delta CT}$) and 27-hydroxycholesterol (27-HC) levels. CYP7B1 gene expression is showed log-transformed. R (−0.428), Pearson's correlation coefficient; $p \leq 0.001$.

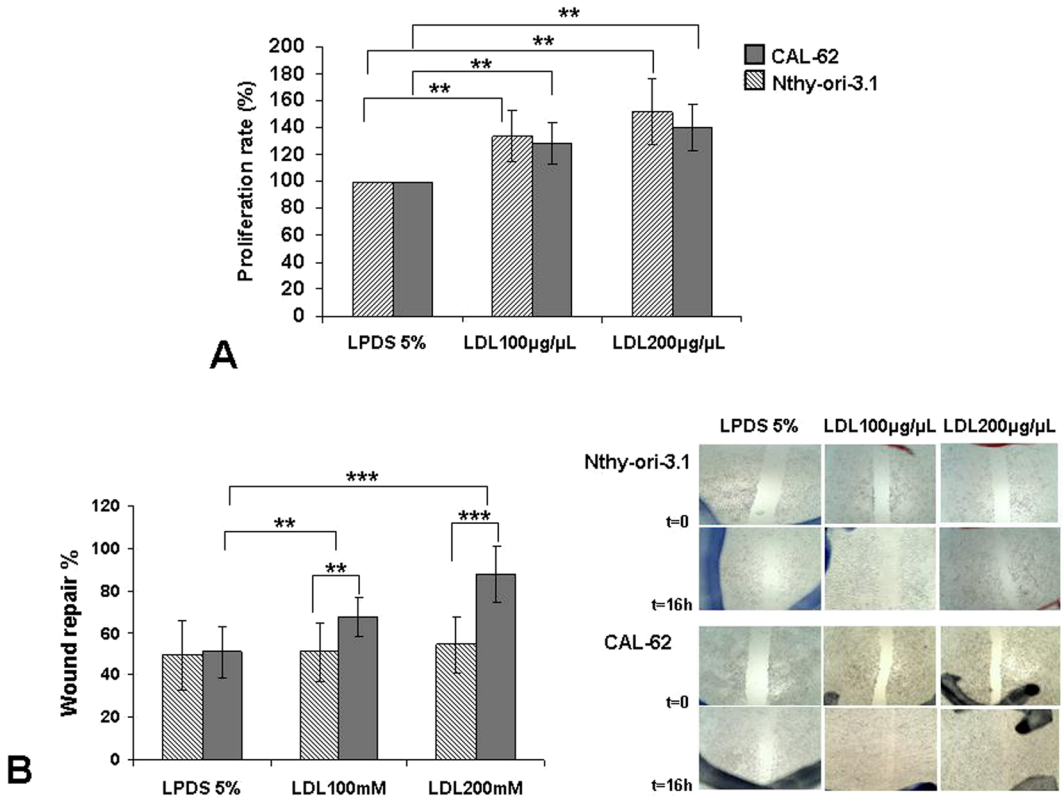

Figure 5. Exogenous administration of human low-density lipoprotein (LDL) in thyroid cell lines. (**A**) Percentage of cellular proliferation of the Nthy-ori 3.1 and CAL-62 cell lines. Both were treated for 24 h with LDL cholesterol (100 µg/mL and 200 µg/mL) compared with control cells maintained in basal conditions (5% LPDS). (**B**) Monolayer wound-induced migration assay. A line was scratched with a 200-µm plastic pipette tip in CAL-62 and Nthy-ori 3.1 cell lines; cultures were treated for 24 h with LDL cholesterol (100 mg/mL and 200 mg/mL). After 16 h, cells that had migrated to the wounded areas were photographed under a microscope for quantification of cell migration. Images are representative of three separate experiments. Quantitative analysis of wound-induced migration assay compared with control cells maintained in basal conditions (5% LPDS). The results are presented as mean ± SEM of eight experiments done in duplicate. The Kruskal–Wallis test was represented as a ± box plot, $n = 8$ separate experiments (**$p < 0.01$, ***$p < 0.001$).

in the control of development, progression, invasion and metastasis in thyroid cancer. Some of them, such as mitogen-activated protein kinase (MAPK), phosphoinositide 3-kinase (PI3K)/Akt, mTOR, has a strong relation with BRAF gene mutation, which are frequent in thyroid cancers[33]. The protein expression analyses did not show any change after LDL exposition in both CAL62 (wild-type BRAF and G12R KRAS mutation) and Nthy-ori 3.1 cell lines (no mutation has been reported). However, strong constitutive activation of these signaling transduction cascades under basal conditions were detected, indicating that the mechanisms by which LDL act are independent of these pathways. Additional cell lines harboring different oncogenic drivers should be investigated. In this context, SCARB1, which has been involved in tumor development[34,35], tended to be downregulated when compared the most aggressive tumors with BTT group, although these changes were not significantly different. This result rather indicates that this receptor seems no to be associated with the tumor's aggressiveness.

The regulation of the cholesterol metabolism in tumoral cells is complex. It is known that cancer cells have the capacity to increase intracholesterol via a feedback regulation mechanism of the HMGCR enzyme, which controls de novo cholesterol synthesis[36,37]. Importantly, the expression of this gene was downregulated in association with the degree of malignancies of the tumors. These changes may be related with similar free cholesterol levels found in the more aggressive tumors compared with those of benign tumors. It is noteworthy that the analyses in normal and ATC cell lines revealed a gene expression pattern like that found in the thyroid tumors from the patients. In contrast, one of the metabolites of cholesterol with greater relevance in both inflammatory and tumor processes is 27-HC, the most abundant oxysterol in the systemic circulation. In 2013, Nelson *et al.* demonstrated that 27-HC acted as an estrogen receptor agonist in breast cancer, inducing tumor growth and metastasis. These effects were reproduced in mice by overexpressing the CYP27A1 gene, which regulates 27-HC synthesis[18]. In contrast, decreased expression of CYP7B1 triggers accumulation of 27-HC, and CYP7B1 was downregulated in breast cancer compared with normal breast tissue[19,20]. In line with these findings, CYP7B1 was strongly downregulated in the aggressive tumor tissues (PTC high risk and PDTC/ATC) in relation to the benign tumors, in close association with the higher concentration of 27-HC. These data indicate that the accumulation of 27-HC in the thyroid cells may be promoting the development and progression of TC. In fact, downregulation of CYP7B1

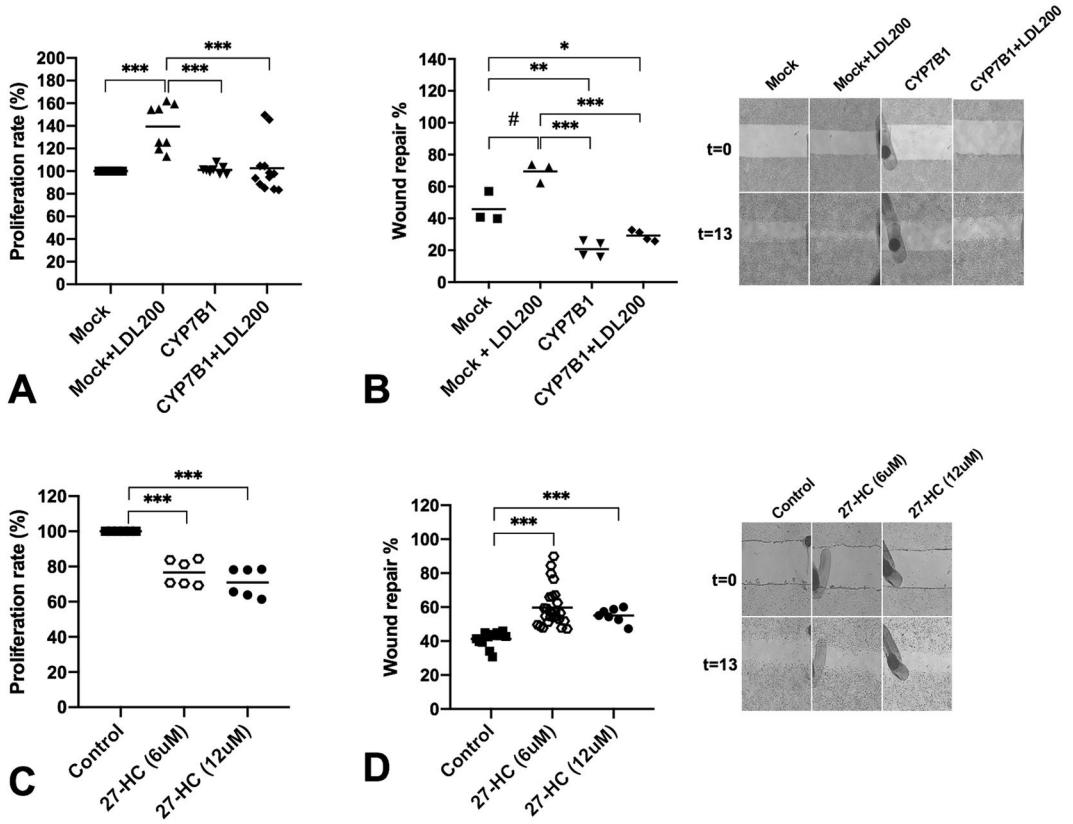

Figure 6. Overexpression of CYP7B1 gene in CAL-62 cells and exogenous administration of 27-HC in Nthy-ori 3.1 cell. (**A**) Percentage of cellular proliferation of the CAL-62 cells overexpressing CYP7B1 gene. Cells were treated for 24 h with or without LDL cholesterol (200 μg/mL) compared with control cells maintained in basal conditions (5% FBS). (**B**) Monolayer wound-induced migration assay in CAL-62 cells overexpressing CYP7B1 gene were scratched with a 200-μm plastic pipette tip and treated for 24 h with or without LDL cholesterol (200 μg/mL). After 13 h the wounded areas were photographed under a microscope for quantification of cell migration. Representative images of experiments. (**C**) Percentage of cellular proliferation of the Nthy-ori 3.1 cells treated with 27-HC at 6 and 12 μM for 48 h. (**D**) Monolayer wound-induced migration assay in Nthy-ori 3.1 cells gene were scratched with a 200-μm plastic pipette tip and treated for 48 h with 27-HC at 6 and 12 μM. After 13 h the wounded areas were photographed under a microscope for quantification of cell migration. Statistical analysis: ANOVA test plus Tukey's post-test (*,#$p < 0.05$, **$p < 0.01$, ***$p < 0.001$).

was also detected in the anaplastic cell line (CAL-62) and its overexpression reduced cell growth and migration. Furthermore, downregulation of CYP27A1 completely blocked LDL-mediated cell proliferation. However, 27-HC by itself only promoted cell migration in non tumoral cells. We also treated the cells with DHEA, which may be hydroxilated by CYP7B1[38] and it did not produce any effect in the cells with anaplastic phenotype. Nevertheless, in non-cancer cell (Nthy-ori 3.1 cells) we found a doses dependent decline in cell proliferation, as occurred with 27-HC. These results rather indicate a dual effect of 27-HC in cells with aggressive behaviors in contrast with immortalized cells with non tumoral phenotype. It should be noted that 27-HC increased ROS levels and reduced the antioxidant defense system levels in non pathological astrocytes, thereby affecting cell viability[39]. In addition, 27-HC may downregulate the expression of the nuclear factor E2-related factor 2 signaling pathways[40]. Moreover, in immortalized retinal pigment epithelial cell line (RPE cells), 27-HC also caused glutathione depletion, ROS generation, inflammation and apoptotic-mediated cell death[41].

It should be noted that 27-HC is also involved in the regulation of the nuclear receptor LXR expression. This gene, which controls the cell cycle progression, is also implicated in the mechanism for controlling the metastasis of the tumors of epithelial lineage[42,43]. Moreover, the LXR gene controls the mechanism to promote liver LDLR degradation and cholesterol conversion to bile acids via CYP7A1[44,45]. The downregulation of LXR could also be directly affecting the LDLR levels in the aggressive tumors. The DHCR24, which catalyzes the conversion of desmosterol into cholesterol and is considered a tumoral biomarker involved in proliferation, adhesion, cell migration and apoptosis[46,47], tended to be downregulated when compared the most aggressive tumors with BTT group, although these changes were not significantly different. Further investigation is needed to establish the role of desmosterol on thyroid cancer.

The expression of ATP Binding Cassette Subfamily A Member 1 (ABCA1), the main cholesterol efflux transporter from cells to HDL, was also determined. ABCA1 was upregulated in the most aggressive samples although this change was not significant in the PDTC group (Supplementary Table 1). We have recently reviewed the

potential role of ABCA1 on tumor development. ABCA1 regulates plasma membrane cholesterol content and fluidity which are critical determinants of its metastatic capacity. However, ABCA1 also inhibits the development of tumors by inhibiting cellular proliferation thereby highlighting the dual role of ABCA1 in regulating proliferation and metastasis[48]. Further studies are needed to establish the role of ABCA1 on thyroid cancer.

Several studies have shown the relationship between the levels of 27-HC and the expression of estrogen receptors in the breast tumors, demonstrating that this oxysterol is a selective modulator of them, having a role as an agonist or antagonist in the function of the cellular type[18,19]. In relation to epithelial-type thyroid cancer, these have a higher incidence in females. This characteristic probably suggests its relationship with the expression of estrogen receptors in the follicular thyroid epithelium. There are not enough reported data identifying the expression of these sexual steroid receptors and their relationship with the neoplastic follicular cells[49]. We explored the expression of the estrogen receptors (alpha and beta) in a series of samples, and the results showed that both benign and malignant tumors express both types of receptors. However, their expression was observed in undifferentiated tumors (Supplementary Table S2). These data are consistent with those observed in breast cancer, where estrogen receptor (ER)-negative tumors tend to grow faster and have a worse prognosis, whereas a lack of ER isoforms β expression would lead to a decrease in apoptosis[50,51]. This result contrasted with the potential effect of 27-HC as an endogenous ER ligand that promotes ER-positive breast tumor growth[19]. In contrast, 27-HC treatment reduced cell growth in Nthy-ori3.1 cells (ERα/ß negative). This effect is in agreement with the reported in prostate cancer cells in which 27-HC reduced intracellular cholesterol accumulation independent of the androgen receptors status[52]. These results suggest that 27-HC could promote a negative feedback control of cholesterol biosynthesis in normal immortalized follicular cells. Studies of the potential effects of 27-HC on ER-independent tumorigenic processes are warranted.

Of note, some experimental studies have shown the antineoplastic efficacy of statins but statins were associated with thyroid carcinoma in some clinical studies[53]. Furthermore, hepatic PCSK9 expression is modified in several diseases, including in thyroid cancer[54]: however, no large genetic studies and controlled cholesterol-lowering clinical trials have been carried out yet. In summary, our findings showed that cholesterol could be a key molecule in the thyroid carcinogenesis process, especially in terms of 27-OH, which may influence the development and progression of TC (Fig. 7). Therefore, targeting the transport of cholesterol and synthesis of 27-HC may be a therapeutic strategy for controlling TC development in the future. The causal association of cholesterol/27-HC and TC should be further investigated.

Material and Methods

Data sharing. The data, analytical methods, and study materials will be available to other researchers for purposes of reproducing the results or replicating the procedure upon reasonably request.

Patients. This study included a cohort of patients ($n = 89$) with a diagnosis of TC who were recruited at Hospital de la Santa Creu i Sant Pau (HSCSP) in Barcelona, Spain. In these patients, the following clinical information was collected: sex, age, unhealthy habits, no dyslipidemic pathology or statin treatment, and baseline TSH values (0.5–5 mlU/L). The tumors were classified according to the histopathological diagnosis, as follows: benign thyroid tumor (BTT), well-differentiated malignancies (PTC), and advanced thyroid cancers which include poorly differentiated and anaplastic thyroid carcinoma (PDTC/ATC). The AJCC/UICC TNM staging system (TNM) was used to subdivide the patients into two groups (low/intermediate and high risk; NCCN Guidelines Version 1. 2018, Staging Thyroid Carcinoma; Table 2). This study was approved by the ethics committee at HSCSP, and all patients gave written informed consent to participate. All research was performed in accordance with relevant guidelines/regulations.

Human tissue and serum samples. Surgical snap-frozen specimens and serum were obtained from patients recruited from January 2009 at HSCSP, as described above. These belonged to the sample collection registered at Instituto de Salut Carlos III (Spain; *C.000281*).

Lipid, lipoprotein, and apolipoprotein determinations. Serum lipid analyses were determined enzymatically using commercial kits adapted to a COBAS c501 autoanalyzer (Roche Diagnostics, Rotkreuz, Switzerland)[55]. High-density lipoprotein (HDL) cholesterol was measured in apoB-depleted serum obtained after precipitation with phosphotungstic acid and magnesium ions (Roche Diagnostics). The low-density lipoprotein (LDL) cholesterol was determined by the Friedewald formula[56]. The apoA-I and apoB concentrations were determined using nephelometric commercial kits (Roche Diagnostics)[55].

Thyroid 27-hydroxycholesterol (27-HC) levels. Frozen thyroid samples (n = 66) included in optimal cutting temperature (OCT) compound (Tissue-Tek, Sakura Europe, Alphen den Rijn, Netherlands) were sectioned and homogenized in 1 M NaOH. Protein concentration was measured using the BCA protein assay kit (Thermo Scientific S.L.U., Spain). Lipids were then extracted as described above, resuspended in 100 µl of methanol, and transferred to a vial with 6 µl of deuterium-labeled internal standard. The 27-HC levels were measured using high-performance liquid chromatography tandem mass spectrometry (HPLC-MS/MS)[57].

Human lipoproteins isolation: Low-density lipoprotein (LDL) and high-density lipoprotein (HDL). Human LDL (1.019–1.063 kg/L) and HDL (1.063–1.21 kg/L) were isolated by sequential ultracentrifugation of fasting plasma. Lipoprotein-depleted serum (LPDS) was prepared from fetal bovine serum (FBS) or charcoal/dextran-treated FBS (Gibco BRL, Life Technologies) by ultracentrifugation at a density > 1.21 kg/L.

Primary cell cultures and cellular low-density lipoprotein (LDL) cholesterol uptake. Human thyroid tissue obtained from intraoperative pieces were dissected in the Department of Pathology, washed with

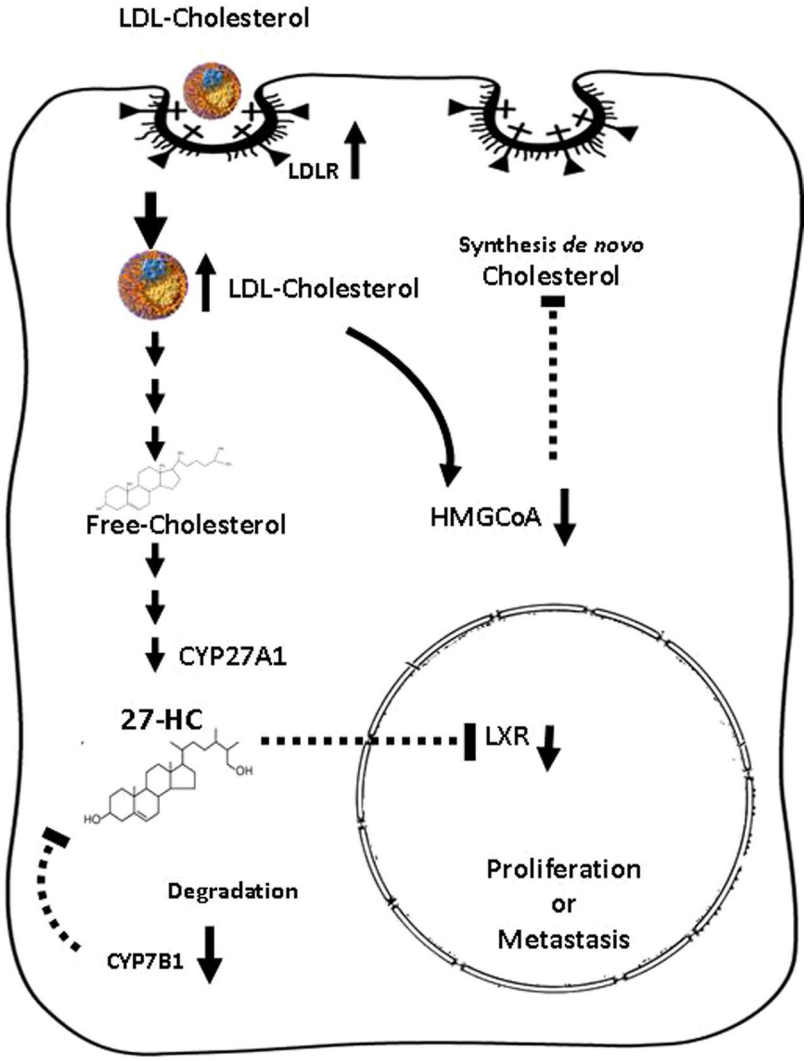

Figure 7. Schematic drawing of the hypothesis of the effect of uptake and intracellular pathways of LDL in the thyroid cells, based on our results. The LDL cholesterol molecules are internalized via endocytotic vesicles, transported and rapidly metabolized; they start to accumulate in the form of 27-HC due to the inhibition of their degradation in the aggressive forms of tumors. The oxysterol could diffuse into the nucleus region and interact with nuclear receptors and other molecular targets, promoting the proliferation or metastatic processes in the follicular cells. 3-hidroxi-3-metilglutaril-CoA (HMG-CoA) downregulation indicates a potential negative feedback in the *de novo* synthesis of cholesterol.

PBS Buffer, minced into small fragments and digested with collagenase type II (1 mg/mL, Gibco Invitrogen) in stir at 37 C for 1–3 h. The reaction was stopped by adding 10 mL of culture medium at room temperature and the digested tissues were centrifuged 1000 g for 10 min and washed two times in PBS Buffer salt solution. The cellular pellets were suspended with DMEM-F12 medium, transferred in cellular plates, and the medium was changed every two days. The cultures were maintained only six days. Finally, the cells were trypsinized, counted using an automated cell counter (TC10 Bio-Rad) and cell blocks with 10^5–10^6 cells were prepared by plasma-thrombin method. In order to check cell thyroid purity, thyroglobulin immunostaining with sections from cell blocks was done by peroxidase-anti-peroxidase (PAP) technique.

LDL particles (1.019–1.063 kg/L) were isolated by sequential ultracentrifugation at 100,000 g for 24 h from normolipidemic human plasma obtained in EDTA-containing vacutainer tubes and radiolabeled with [1,2-^{3}H] cholesteryl oleate (Perkin-Elmer), as previously reported[58]. Subsequently, radiolabeled LDL (0.45 μCi [1,2-^{3}H] cholesterol oleate/50 μg LDL-apoB) was dialyzed against phosphate-buffered saline (PBS) by gel filtration chromatography and incubated with 10^5 cells in DMEN-F12 supplemented with 5% LPDS for 16 h. Then, the medium was collected and centrifuged at 10,000 g for 10 min, and the cells were lysed with 0.1 M NaOH. The radioactivity was determined in the medium and cell lysates. [1, 2-^{3}H] LDL cholesterol uptake was expressed as the percentage of the radioactivity collected in the cells relative to the sum of radioactivity in cells and medium per μg of protein per cell.

Patient Demographics	Age at Diagnosis	
SEX	52.12 ± 5.65 (16–84)	n = 89
Female	50.8 ± 16.5 (34–75)	n = 77
Male	53.5 ± 14.7 (16–84)	n = 12
HISTOLOGY PATTERN		
Benign thyroid tumor (BTT)	52.92 ± 13.35 (29–81)	n = 27
Papillary thyroid carcinoma (PTC)	49.8 ± 16.4 (16–72)	n = 55
Low/intermediate Risk		n = 43
TNM staging		
I		n = 26
II		n = 17
High Risk	44.23 ± 19.6 (29–84)	
TNM staging		n = 12
III		n = 7
Advanced Thyroid Cancers:	61.5 ± 15.75 (34–82)	
PDTC		n = 5
Anaplastic thyroid carcinoma (ATC).		n = 2

Table 2. Clinical Description of the study Cohort. The age is represented as the mean ± standard deviation (minimum age–maximum age). Total subjects included in the study were classified, the AJCC/UICC TNM staging system (TNM) was used to subdivide the patients into two groups (low/intermediate and high risk; NCCN Guidelines Version.1 2018.

Total RNA isolation and first strand cDNA synthesis. Total RNA was isolated using the TRIZOL reagent according to the manufacturer's instructions (Invitrogen, Carlsbad, CA, USA). One microgram of the total RNA was reverse transcribed using a transcriptor first-strand cDNA synthesis kit (Roche Applied Science, Penzberg, Germany), and the cDNA samples were stored at −20 °C for use as a template in real-time polymerase chain reaction (PCR) analysis.

Gene expression profile. The gene expression profiles were analyzed in an ABI PRISM 7900HF Sequence Detection System, using a predesigned and labeled primer/probe set (Assays-on-Demand™ Gene Expression Assay, Applied Biosystems, Foster City, CA, USA). The Taqman qPCR primers (Applied Biosystems) used were as follows: CYP27A1 (Hs01017992_m1), CYP7B1 (Hs01046431_m1), HMGR (Hs00168352_m1), LDL receptor (LDLR; Hs01092524_m1), NR1H3 (Hs00172885_m1), SCARB1 (Hs00969827_m1), DHCR24 (Hs00207388_m1) and ABCA1 (Hs01059137_m1). All the reactions were performed with 100 ng of cDNA in a total volume of 50 µl of TaqMan® Universal PCR Master Mix (Applied Biosystems), and the relative expression levels for each gene were calculated using the 2- ddCt method, with SDS2.3 and Data Assist V2.1 software (Applied Biosystems). The samples were analyzed in duplicate, and RNA from BTT was used as a group calibrator; negative controls were also included in all the reactions.

Human thyroid cell lines and LDL, 27-HC and DHEA treatments. The Nthy-ori 3.1 cell line, derived from normal human primary thyroid follicular epithelial cells, was immortalized with a plasmid containing an origin-defective SV40 genome (SV-ori). This cell line was provided by Dr Pilar Santisteban (CSIC, Madrid), and the CAL-62 cell line, derived from a human thyroid anaplastic carcinoma (ATC), has a epithelial-like cells stabilized in culture. The cells do not show thyroglobulin expression and the most relevant cytogenetic data showed a gain of chromosome 20, with a translocation (14q), breakpoints of centrometric chromatine without presenting any BRAF mutation[29]. CAL-62 cell line was provided by Leibniz-Institut DSMZ GmbH (ACC 448). Nthy-ori 3.1 cell lines was cultured in RPMI 1640 (w/L-glutamine) and CAL-62 in Dulbecco's modified Eagle's medium (DMEM; Gibco, Invitrogen); both media were supplemented with 10% FBS and 2% streptomycin/penicillin. For treatment, 4,000 cells/well were seeded in 96-well microplates, and exogenous LDL obtained from human serum was added to the cultures at 200 µg/mL for 72 h, 27-HC at 6 and 12 µM for 48 h. For DHEA treatments (SKU 7000087 P) (Avanti, Polar Lipids, INC.), DHEA at 40, 80 and 160 uM was also added in both cells lines for 48 h.

To determine the cell viability rate, we used the thiazolyl blue tetrazolium bromide metabolic assay (MTT, Sigma, St. Louis, MO, USA). Absorbance was determined at 560 nm with a microplate reader (xMark, BIORAD). All conditions were performed in five replicates. Each experiment was repeated at least three times.

To determine cell migration, both cell lines (Nthy-ori 3.1 and CAL-62) were plated at high densities and grown to confluence at 90% O/N. Cells were scratched with a pipette tip (10 µl) and washed several times to remove the cellular debris.

The wounds were photographed in an inverted microscope at 0 h (t = 0), and this was done again in the same area after 16 h of cell incubation at 37 °C. The cultures were allowed to incubate in serum-free medium. Image J software was used to analyze the photographs. Here, the percentage of wound healing was determined based on three measurements of the wound area; each result was the mean of three independent experiments.

Transient transfection assay. *Overexpression of CYP7B1 gene in CAL-62 cell line.* Transfection in CAL-62 cell line was performed by JetPrime™ (Polyplus transfection) according to the manufacturer's instructions. Approximately 10,000 cells were plated in 96-well plates one day prior to transfection. The cells were transiently transfected with either 0.1 nM pre-designed CYP7B1 (NM_004820.3) DNA ORF clone or control (pcDNA3.1^{+}/C-(K)DYK) purchased from GeneScript (OHu27221) and treated with LDL 200 µM or without LDL as a control. After incubation for 48 h, the transfected cells were tested for MTT assay. For wound-healing assays, 50×10^3 cells were plated in 4-well plates, transiently transfected with the same concentration described above and the wound-healing assays were performed as described below. Each assay was performed in triplicate in at least three independent experiments.

Downregulation of CYP27A1 gene in Nthy-ori 3.1 cell line. siRNA transfection in Nthy-ori 3.1 cell line was performed by JetPrime™ (Polyplus transfection) according to the manufacturer's instructions. Approximately 4,000 cells were plated in 96-well plates one day prior to transfection. The following day, the cells were transiently transfected with either 5 nM pre-designed short interfering RNA (siRNA **CYP27A1**) (ID106239) (Ambion, Life Technologies) or control siRNA purchased from Santa Cruz Biotechnology, Inc. (sc-37007). The transfected cells were treated with LDL 200 µM or without LDL as a control. After incubation for 48 h, the transfected cells were tested for MTT assay. Each assay was performed in triplicate in at least three independent experiments.

Statistical analysis. Gene expression analysis was performed using the comparative CT (ddCt) method by DataAssist™ Software, and the results were adjusted as the *p*-value using the Benjamini–Hochberg false discovery rate (FDR). Genes showing an FDR <0.15 and more than twofold difference in absolute values for both comparisons were considered differentially expressed. One-way analysis of variance (ANOVA) with a Tukey's multiple comparison post-test or Kruskal–Wallis multiple comparison with Dunn's post-test was used to compare differences among the groups. Correlations between variables were analyzed using Pearson's correlation analysis. GraphPad Prism software V5.0 was employed, and values of $p < 0.05$ were considered statistically significant.

References

1. Martínez-Botas, J. *et al*. Dose-dependent effects of lovastatin on cell cycle progression. Distinct requirement of cholesterol and non-sterol mevalonate derivatives. *BBA-Mol Cell Biol. Lipids* **1532**, 185–194 (2001).
2. Fernández, C., Lobo, M., del, V. T., Gómez-Coronado, D. & Lasunción, M. A. Cholesterol is essential for mitosis progression and its deficiency induces polyploid cell formation. *Exp Cell Res.* **300**, 109–120, https://doi.org/10.1016/j.yexcr.2004.06.029 (2004).
3. Rodrigues dos Santos, C. *et al*. LDL- cholesterol signaling induces breast cancer proliferation and invasion. *Lipids Health Dis.* **13**, 16, https://doi.org/10.1186/1476-511X-13-16 (2014).
4. Furuya, Y. *et al*. Low-density lipoprotein receptors play an important role in the inhibition of prostate cancer cell proliferation by statins. *Prostate Int.* **4**, 56–60, https://doi.org/10.1016/j.prnil.2016.02.003 (2016).
5. Sánchez-Martín, C. C. *et al*. Cholesterol starvation induces differentiation of human leukemia HL-60 cells. *Cancer Res.* **67**, 3379–3386, https://doi.org/10.1158/0008-5472.CAN-06-4093 (2007).
6. Rodríguez-Acebes, S. *et al*. Desmosterol can replace cholesterol in sustaining cell proliferation and regulating the SREBP pathway in a sterol-Δ24-reductase-deficient cell line. *Biochem J.* **420**, 305–318, https://doi.org/10.1042/BJ20081909 (2009).
7. Antalis, C. J., Uchida, A., Buhman, K. K. & Siddiqui, R. A. Migration of MDA-MB-231 breast cancer cells depends on the availability of exogenous lipids and cholesterol esterification. *Clin Exp Metastas.* **28**, 733–741, https://doi.org/10.1186/1476-511X-13-16 (2011).
8. de Gonzalo-Calvo, D. *et al*. Intratumor cholesteryl ester accumulation is associated with human breast cancer proliferation and aggressive potential: a molecular and clinicopathological study. *BMC Cancer* **15**, 460, https://doi.org/10.1186/s12885-015-1469-5 (2015).
9. Istvan, E. S. & Deisenhofer, J. Structural mechanism for statin inhibition of HMGCoA reductase. *Science* **292**, 1160e4, https://doi.org/10.1126/science.1059344 (2001).
10. Clayman, R. V., Gonzalez, R., Elliott, A. Y., Gleason, D. E. & Dempsey, M. E. Cholesterol accumulation in heterotransplanted renal cell cancer. *J Urol.* **129**, 621–624 (1983).
11. Krycer, J., Kristiana, I. & Brown, A. Cholesterol Homeostasis in Two Commonly Used Human Prostate Cancer Cell-Lines, LNCaP and PC-3. *PLoS One* **4**, e8496, https://doi.org/10.1371/journal.pone.0008496 (2009).
12. Antalis, C. J. *et al*. High ACAT1 expression in estrogen receptor negative basal-like breast cancer cells is associated with LDL-induced proliferation. *Breast Cancer Res Treat.* **122**, 661–670, https://doi.org/10.1007/s10549-009-0612-x (2010).
13. Poli, G., Biasi, F. & Leonarduzzi, G. Oxysterols in the pathogenesis of major chronic diseases. *Redox Biol* **1**, 125–130, https://doi.org/10.1016/j.redox.2012.12.001 (2013).
14. Dash, R. C., Maschinot, C. R. & Hadden, M. K. A molecular dynamics approach to identify an oxysterol-based hedgehog pathway inhibitor. *BBA* **1861**, 168–177, https://doi.org/10.1016/j.bbagen.2016.11.003 (2017).
15. Kloudova, A., Guengerich, F. P. & Soucek, P. The role of Oxysterols in Human Cancer. *Trends Endocrinol Metab.* **28**, 485–496, https://doi.org/10.1016/j.tem.2017.03.002 (2017).
16. Lange, Y. *et al*. Regulation of fibroblast mitochondrial 27-hydroxycholesterol production by active plasma membrane cholesterol. *J Lipid Res.* **50**, 1881–1888, https://doi.org/10.1194/jlr.M900116 (2009).
17. Schroepfer, G. J. Oxysterols: modulators of cholesterol metabolism and other processes. *Physiol Rev.* **80**, 361–554, https://doi.org/10.1152/physrev.2000.80.1.361 (2000).
18. Nelson, E. R. *et al*. 27-Hydroxycholesterol links hypercholesterolemia and breast cancer pathophysiology. *Science* **342**, 1094–1098, https://doi.org/10.1126/science.1241908 (2013).
19. Wu, Q. *et al*. 27-Hydroxycholesterol promotes cell-autonomous, ER-positive breast cancer growth. *Cell Rep.* **14**, 637–645, https://doi.org/10.1016/j.celrep.2013.10.006 (2013).
20. Gibson, D. A., Collins, F., Cousins, F. L., Zufiaurre, A. E. & Saunders, T. K. The impact of 27-hydroxycholesterol on endometrial cancer proliferation. *Endocr Relat Cancer* **25**, 381–391, https://doi.org/10.1530/ERC-17-0449 (2018).
21. Kimbung, S. *et al*. Impact of 27-hydroxylase (CYP27A1) and 27-hydroxycholesterol in breast cancer. *Endocr Relat Cancer* **24**, 339–349, https://doi.org/10.1530/ERC-16-0533 (2017).
22. Steffensen, K. R. & Gustafsson, J. A. Putative metabolic effects of the liver×receptor (LXR). *Diabetes* **15**, S36–42, https://doi.org/10.2337/diabetes.53.2007 (2004).
23. Vedin, L., Lewandowski, S. A., Parini, P., Gustafsson, J. & Steffensen, K. R. The oxysterol receptor LXR inhibits proliferation of human breast cancer cells. *Carcinogenesis* **30**, 575–579, https://doi.org/10.1093/carcin/bgp029 (2009).

24. Michalaki, V. *et al.* Evaluation of serum lipids and high-density lipoprotein subfractions (HDL2, HDL3) in postmenopausal patients with breast cancer. *Mol Cell Biochem.* **268**, 19–24 (2005).
25. Iso, H., Ikeda, A., Inoue, M., Sato, S. & Tsugane, S. Serum cholesterol levels in relation to the incidence of cancer: the JPHC study cohorts. *Int. J. Cancer* **125**, 2679–2686, https://doi.org/10.1002/ijc.24668 (2009).
26. Kitahara, C. M. *et al.* Total cholesterol and cancer risk in a large prospective study in Korea. *J Clin Oncol.* **29**, 1592–1598, https://doi.org/10.1200/JCO.2010.31.5200J (2011).
27. Kim, H. J. *et al.* Associations between body mass index and clinico – pathologica l characteristics of papillary thyroid cancer. *Clin Endocrinol (Oxf).* **78**, 134–140, https://doi.org/10.1111/j.1365-2265.2012.04506.x (2013).
28. Xu, L. *et al.* Obesity and the Risk of Papillary Thyroid Cancer: A Pooled Analysis of Three Case–Control Studies. *Thyroid* **24**, 966–974, https://doi.org/10.1089/thy.2013.0566 (2014).
29. Gioanni, J. Characterization of a human cell line from an anaplastic carcinoma of the thyroid gland. *Bull Cancer* **78**, 1053–62 (1991).
30. Kuzu, O. F., Noory, M. A. & Robertson, G. P. The Role of Cholesterol in Cancer. *Cancer Res.* **76**, 2063–2070, https://doi.org/10.1158/0008-5472 (2016).
31. Beloribi-Djefaflia, S., Vasseur. & Guillaumond, F. Lipid metabolic reprogramming in cancer cells. *Oncogenesis* **5**, e189, https://doi.org/10.1038/oncsis (2016).
32. Xiangjian, L. *et al.* Emerging roles of lipid metabolism in cancer metastasis. *Mol Cancer* **16**, 76, https://doi.org/10.1186/s12943-017-0646-3 (2017).
33. Jin, S., Borkhuu, O., Bao, W. & Yang, Y.-T. Signaling Pathways in Thyroid Cancer and Their Therapeutic Implications. *J Clin Med Res.* **8**, 284–296 (2016).
34. Gutierrez-Pajares, J. L., Ben Hassen, C., Chevalier, S. & Frank, P. G. SR-BI: Linking Cholesterol and Lipoprotein Metabolism with Breast and Prostate Cancer. *Front Pharmacol* **7**, 338, https://doi.org/10.3389/fphar.2016.00338 (2016).
35. Singh, P., Saxena, R., Srinivas, G., Pande, G. & Chattopadhyay, A. Cholesterol biosynthesis and homeostasis in regulation of the cell cycle. *PLoS One* **8**, e58833, https://doi.org/10.1371/journal.pone.0058833 (2013).
36. Gustbée, E. *et al.* Tumor-specific expression of HMG-CoA reductase in a population-based cohort of breast cancer patients. *BMC Clinical Pathology* **15**, 8, https://doi.org/10.1186/s12907-015-0008-2 (2015).
37. Murtola, T. J. *et al.* The importance of LDL and cholesterol metabolism for prostate epithelial cell growth. *PloS ONE* **7**, e39445, https://doi.org/10.1371/journal.pone.0039445 (2012).
38. Stiles, A. R., McDonald, J. G., Bauman, D. R. & Russell, D. W. CYP7B1: One Cytochrome P450, Two Human Genetic Diseases, and Multiple Physiological Functions. *J Biol Chem* **284**, 28485–28489, https://doi.org/10.1074/jbc.R109.042168 (2009).
39. Chen, S. *et al.* 27-Hydroxycholesterol Contributes to Lysosomal Membrane Permeabilization-Mediated Pyroptosis in Co-cultured SH-SY5Y Cells and C6. *Cells. Front Mol Neurosci* **12**, 14, https://doi.org/10.3389/fnmol.2019.00014 (2019).
40. Ma, W. W. *et al.* The oxysterol 27-hydroxycholesterol increases oxidative stress and regulate Nrf2 signaling pathway in astrocyte cells. *Neurochem Res* **40**, 758–766, https://doi.org/10.1007/s11064-015-1524-2 (2015).
41. Dasari, B., Prasanthi, J. R. P., Marwarha, G., Singh, B. B. & Ghribi, O. The oxysterol 27-hydroxycholesterol increases β-amyloid and oxidative stress in retinal pigment epithelial cells. *BMC Opththalmol* **10**, 22, https://doi.org/10.1186/1471-2415-10-22 (2010).
42. Martin, K. O., Budai, K. & Javitt, N. B. Cholesterol and 27-hydroxycholesterol 7 alpha-hydroxylation: evidence for two different enzymes. *J Lipid Res.* **34**, 581–588 (1993).
43. Janowski, B. A. *et al.* Structural requirements of ligands for the oxysterol liver X receptors LXRα and LXRβ. *PNAS* **96**, 266–271, https://doi.org/10.1073/pnas.200367697 (1999).
44. Lehmann, J. M. *et al.* Activation of the nuclear receptor LXR by oxysterols defines a new hormone response pathway. *J Biol Chem.* **272**, 3137–3140 (1997).
45. Radhakrishnan, A., Ikeda, Y., Kwon, H. J., Brown, M. S. & Goldstein, J. L. Sterol-regulated transport of SREBPs from endoplasmic reticulum to Golgi: oxysterols block transport by binding to Insig. *PNAS* **104**, 6511–6518, https://doi.org/10.1073/pnas.0700899104 (2007).
46. Liu, X. P. *et al.* DHCR24 predicts poor clinicopathological features of patients with bladder cancer: A STROBE-compliant study. *Medicine (Baltimore)* **97**, e11830, https://doi.org/10.1097/MD.0000000000011830 (2018).
47. Zerentuk, E. J., Sharpe, L. J., Ikonen, E. & Brown, A. J. Desmosterol and DHCR24: unexpected new directions for a terminal step in cholesterol synthesis. *Prog Lipid Res* **52**, 666–80, https://doi.org/10.1016/j.plipres.2013.09.002 (2013).
48. Revilla, G., Corcoy, R., Moral, A., Escolà-Gil, J. C. & Mato, E. Cross-Talk between Inflammatory Mediators and the Epithelial Mesenchymal Transition Process in the Development of Thyroid Carcinoma. *Int J Mol Sci* **20**, 2466, https://doi.org/10.3390/ijms20102466 (2019).
49. Chen, G. G., Vlantis, A. C., Zeng, Q. & Van Hasselt, C. A. Regulation of cell growth by estrogen signaling and potential targets in thyroid cancer. *Curr Cancer Drug Tar.* **8**, 367–377 (2008).
50. Bieche, I. *et al.* Quantification of estrogen receptor [alpha] and [beta] expression in sporadic breast cancer. *Oncogene* **20**, 8109, https://doi.org/10.1038/sj.onc.1204917 (2001).
51. Castrellon, A. B. Novel strategies to improve the endocrine therapy of breast cancer. *Oncol Rev.* **11**, 323, https://doi.org/10.4081/oncol.2017.323 (2017).
52. Alfaqih, M. A. *et al.* CYP27A1 loss dysregulates cholesterol homeostasis in prostate càncer. *Cancer Res.* **77**, 1662–1673, https://doi.org/10.1158/0008-5472.CAN-16-2738 (2017).
53. Zhao, J. *et al.* Statins and Thyroid Carcinoma: a Meta-Analysis. *Cell Physiol Biochem* **47**, 1422–1431, https://doi.org/10.1159/000490832 (2018).
54. Schulz, R. & Schlüter, K. D. PCSK9 targets important for lipid metabolism. *Clin Res Cardiol Suppl* **12**, 2–11, https://doi.org/10.1007/s11789-017-0085-0 (2017).
55. Julve, J. *et al.* Human apolipoprotein A-II determines plasma triglycerides by regulating lipoprotein lipase activity and high-density lipoprotein proteome. *Arterioscler Thromb Vasc Biol.* **30**, 232–238, https://doi.org/10.1161/ATVBAHA.109.198226 (2010).
56. Friedewald, W., Levy, R. & Fredrickson, D. Estimation of the concentration of low-density lipoprotein cholesterol in plasma without use of the preparative ultracentrifuge. *Clin Chem.* **18**, 499–502 (1972).
57. Baila-Rueda, L. *et al.* Bile acid synthesis precursors in familial combined hyperlipidemia: the oxysterols 24S-hydroxycholesterol and 27-hydroxycholesterol. *Biochem Biophys Res Commun.* **446**, 731–735, https://doi.org/10.1016/j.bbrc.2013.12.131 (2014).
58. Escola-Gil, J. C. *et al.* The cholesterol content of western diets Plays a major role in the paradoxical increase in high-density lipoprotein cholesterol and upregulates the macrophage reverse cholesterol transport pathway. *Arterioscler Thromb Vasc Biol.* **31**, 2493–2499, https://doi.org/10.1161/ATVBAHA.111.236075 (2011).

Acknowledgements

This work was partly funded by the Ministerio de Sanidad y Consumo, Instituto de Salud Carlos III, and FEDER "Una manera de hacer Europa," grant FIS 16-00139 (to J.C.E.-G.), CIBERDEM, CIBERCV and CIBER-BBN (Instituto de Salud Carlos III). We especially want to thank all the patients who participated in this study and the Societat Catalana d'Endocrinologia i Nutrició (SCEN) (Ajut a la Investigació Bàsica/Clínica 2018) to financial support in part of the experiments shown of this paper.

Author Contributions

E.M. and J.C.E.-G. conceived and designed the study and drafted the manuscript. A.de L., R.C., C.G., M. dos S.F. and M.M., participated in the edition of the manuscript. G.R., M. de P.P., A.G.-L. and D.S. were responsible for performed the lipid and apolipoprotein analyses. G.R., M. de P.P., M.M., G.S. and R.M.B. carried out the *in vitro* experiments, gene and protein expression analysis. L.B.R. and A.C. carried out the 27-HC analysis. E.L. and V.F. performed the histopathological analysis. A.M., J.I.P. carried out the surgery of patients. All authors contributed to the data analysis and interpretation. All authors have critically revised the manuscript and approved of it prior to submission.

Additional Information

Supplementary information accompanies this paper at https://doi.org/10.1038/s41598-019-46727-2.

Competing Interests: The authors declare no competing interests.

Publisher's note: Springer Nature remains neutral with regard to jurisdictional claims in published maps and institutional affiliations.

PUBLICATION I: SUPPLEMENTARY DATA

Cholesterol and 27-Hydroxycholesterol Promote Thyroid Carcinoma Aggressiveness

Giovanna Revilla, Monica de Pablo Pons, Lucía Baila-Rueda, Annabel García-León, David Santos, Ana Cenarro, Marcelo Magalhaes, R. M. Blanco, Antonio Moral, José Ignacio Pérez, Gerard Sabé, Cintia González, Victoria Fuste, Enrique Lerma, Manuel dos Santos Faria, Alberto de Leiva, Rosa Corcoy, Joan Carles Escolà-Gil, Eugènia Mato*

*Corresponding authors

Scientific Reports

2019

Cholesterol and 27-hydroxycholesterol promote thyroid carcinoma aggressiveness

Giovanna Revilla[2,3], Monica de Pablo Pons[1,2], Lucía Baila-Rueda[4,5], Annabel García-León[2], David Santos[2,6], Ana Cenarro[5], Marcelo Magalhaes[8], R. M.ª Blanco[7],Antonio Moral[2,9,10], José Ignacio Pérez[9], Gerard Sabé[2], Cintia González[1,7], Victoria Fuste[2,11], Enrique Lerma[2,11], Manuel dos Santos Faria[8], Alberto de Leiva[2,7], Rosa Corcoy[1,7,10], Joan Carles Escolà-Gil[2,3,6*],and Eugenia Mato[1,7*]

Thyroid cholesterollevels

Frozen thyroid tissues (*n* = 66) were homogenized in 1 M NaOH, and lipids were extracted with isopropyl alcohol-hexane 2:3 (v/v); after the addition of Na_2SO_4, the hexane phase was isolated and dried with N_2. Lipid extracts were resuspended in chloroform, and free and esterified cholesterol was partitioned by thin layer chromatography. The chromatographic developing solution was heptane/diethylether/acetic acid (74:21:4, v/v/v). The spot corresponding to free and esterified cholesterol was quantified by densitometry against the standard of free cholesterol and cholesterol oleate using a computing densitometer[1].

Western Blot Analysis

Protein extracts from cell line CAL-62 and Nthy-ori 3.1 cell lines were obtained after homogenizingthe cells in a buffer containing 50 mm Tris-HCl (pH 7.5), 150 mm NaCl, 1% (v/v) Triton X-100, and a protease inhibitor mixture (Sigma). Proteins were quantified and 10 µg of total protein were separated by 12 or 7.5 % TGX Stain-Free polyacrylamide Starter kit (161-0174 Bio-Rad, Carson, CA), and transferred to PVDF membranes. The antibodies used to incubate the membranes were**:** Mouse Anti-ERK (pan ERK) Clone 16/ERK (pan ERK) (BD Bioscience610123) 1:10000, anti-Phospho-p44/42 MAPK (Erk1/2) (Thr202/Tyr204) (Cell Signaling 9101) 1:4000, anti-Akt (pan) (11E7) Rabbit mAb(Cell Signaling 4685) 1:2000, Anti-Phospho-Akt (Ser473) (D9E) XP® Rabbit (Cell Signaling 4060)1:2000, Anti-mTOR (Cell Signaling 2972)1:4000, Anti-Phospho-mTOR (Ser2448) antibody (Cell Signaling 2971) 1:4000. Chemiluminescence was revealed using an Immun-Star WesternC Chemiluminescence Kit (170-5070, Bio-Rad, Carson, CA).Imaging and data analysis:TGX Stain-Free gels were activated for 1' after SDS–electrophoresis, the images were captured by ChemiDOC™XRS Gel Documentation Systems (Bio-Rad, Herculles, CA) ImageLab software (version 5.1, Bio-Rad, Richmond, CA). The data normalization analysis was performed with stain free[2].

Gene expression of estrogen receptors

The expression of the estrogen receptors were performed by reversetranscriptase-polymerase chain reaction (*RT-PCR*) from 50ng of cDNA in a final volume of 25µl and specific primers. ERα: Forward5'*CAGGGGTGAAGTGGGGTCTGCTG*3', Reverse 5'*TGCCTCCCCGTGATGTAAT*3'(762-935bp) and temperature annealing (65ºC),ERβ**:** Forward*5'CCCTGCTGTGATGAATTACAG*3', Reverse 5'*CTTCTCTGTCTCCGCACAAG*3' (552bp) and temperature annealing (61ºC). The amplification was done with a Taqhotstart (BioThermStar DNA Polymerase, Gene Craft GC-045-0500)for 35 cycles (95 C 10 min and 95 C 1 min, 65 Cor 61 C 1 min, 72 C 1 min)with a final extension of 10 min at 72 C. The PCR products were subjected to electrophoresis in 1% agarose gel.

REFERENCES

1. de Gonzalo-Calvo, D. *et al.*Intratumor cholesteryl ester accumulation is associated with human breast cancer proliferation and aggressive potential: a molecular and clinicopathological study. *BMC Cancer***15,** 460; doi: 10.1186/s12885-015-1469-5 (2015).

2. Gürtler, A. *et al.* Stain-free technology as a normalization tool in western blot analysis. *Anal Biochem.***433,** 105–11; doi:10.1016/j.ab.2012.10.010 (2013).

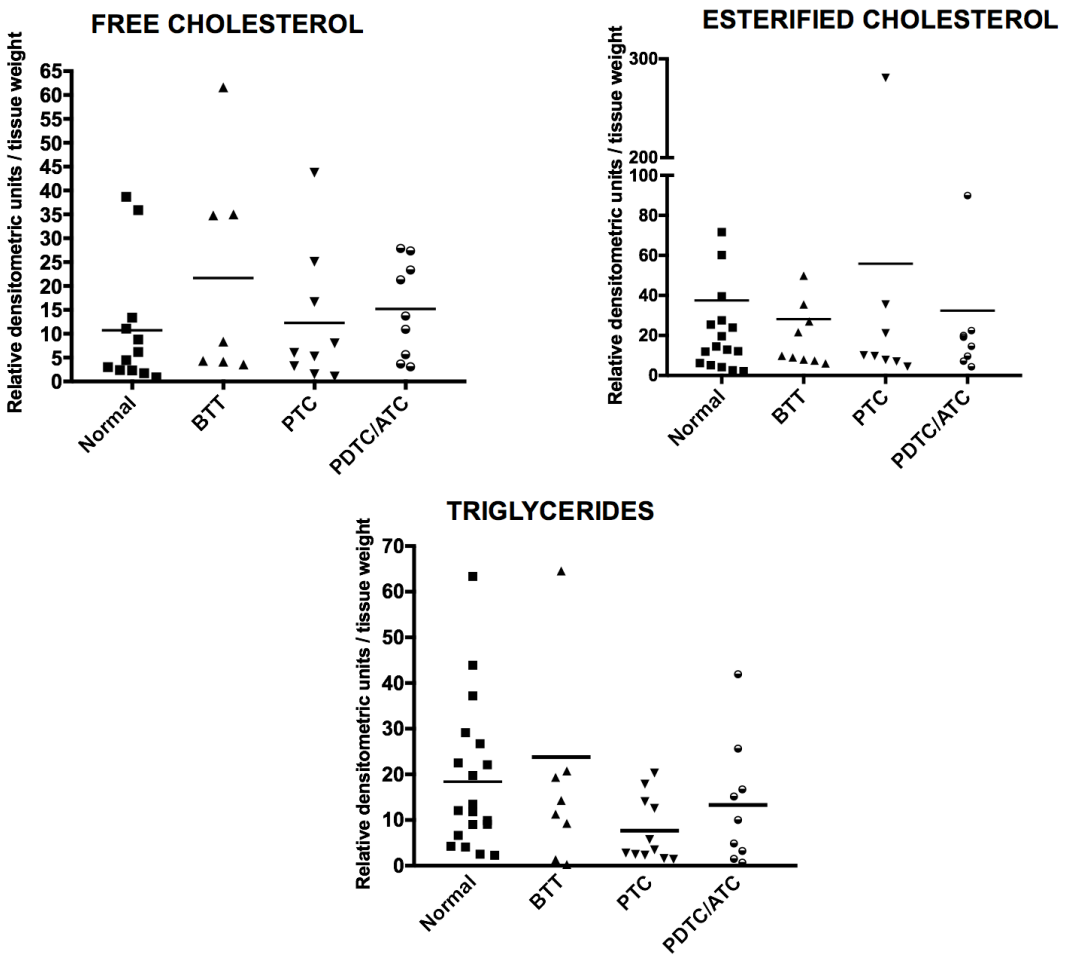

Supplementary Figure S1. Free Cholesterol, Esterified Cholesterol, and Triglycerides did not change in thyroid tumor tissue extracts and normal thyroid tissue.

Lipid extracts from BTT, PTC, PDTC,ATC and Normal Thyroid tissue (Normal) were determined by thin layer chromatography. Analysis of variance using ANOVA plus Tukey's post-hoc test did no shown significant differences.

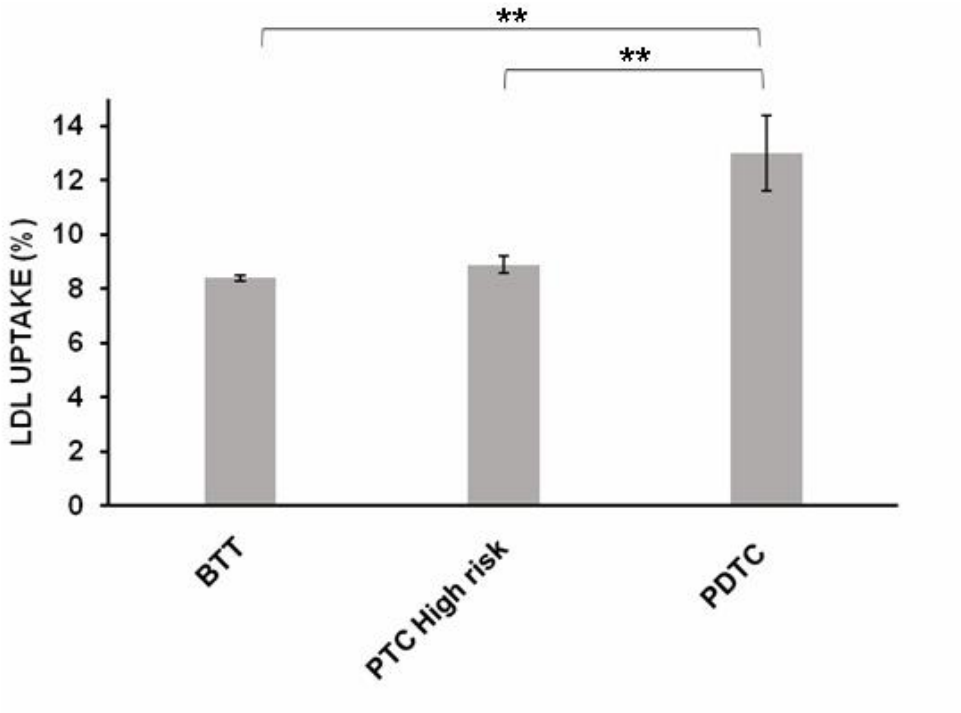

Supplementary Figure S2. Percentage of LDL uptake analysis in primary cell cultures; BTT, PTC High risk and PDTC. The results represent de mean ± SD. (ANOVA) using the Kruskal–Wallis test and Dunn's post-test (**p< 0.01).

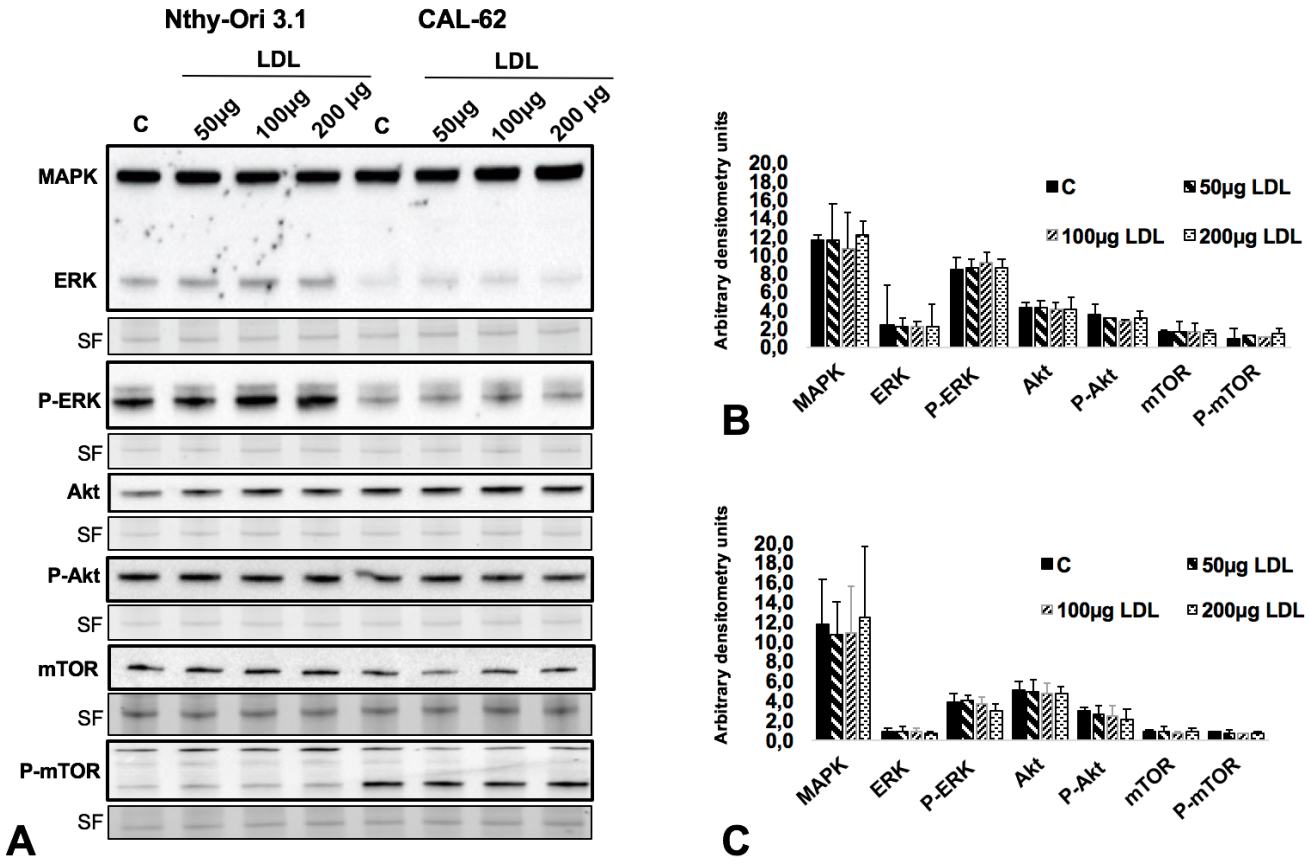

Supplementary Figure S3.LDL (50, 100 and 200 µM) incubated during 48h, does not promote changes in MAPK, PI3K and mTOR signaling pathways in both cells lines (CAL-62 and Nthy-ori 3.1). A) Representative Western blotof total proteinextractsfromCAL-62 and Nthy-ori 3.1 withantibodiesagainstAnti-ERK (pan ERK), anti-Phospho-p44/42 MAPK (Erk1/2)anti-Akt, Anti-Phospho-Akt, Anti-mTOR, Anti-Phospho-mTOR. **B-C)**Signals were normalized to stainfree (SF) gels and data presented asmean of integratedrelativedensityvaluefromNthy-ori 3.1 and CAL-62, respectively. Data areexpressed as mean ± SEM (*n* = 3).

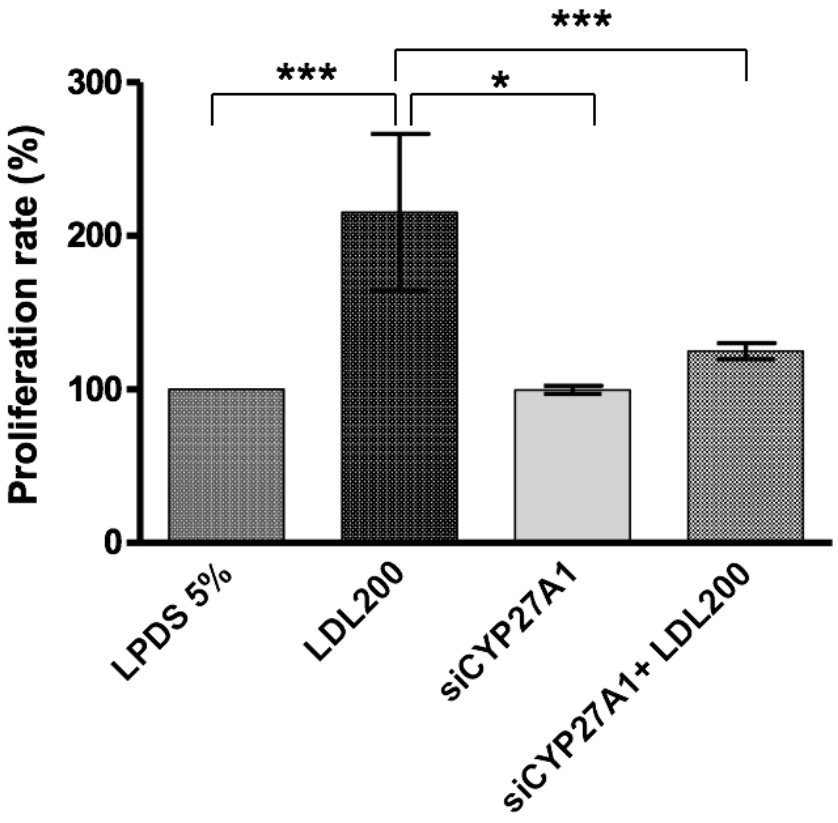

Supplementary Figure S4. Downregulation of CYP27A1 gene in Nthy-ori 3.1. Percentage of cellular proliferation of the Nthy-ori 3.1 cells with CYP27A1 downregulated. Cells were treated for 48 h with or without LDL cholesterol (200 µg/mL) compared with control cells maintained in basal conditions (5% LPDS). Statistical analysis: ANOVA test plus Tukey's post-test (*p<0.05, ***p<0.001).

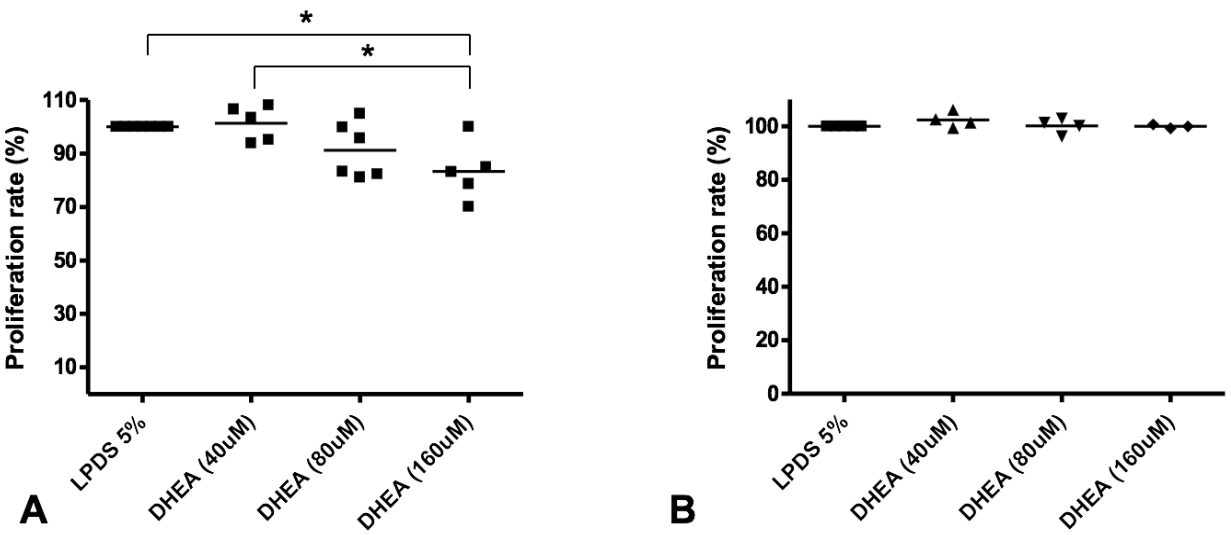

Supplementary Figure S5. Exogenous administration of DHEA in Nthy-ori 3.1 and CAL-62 cell lines. **A)** Percentage of cellular proliferation of the Nthy-ori 3.1 cells treated for 48 h with or without DHEA (40uM, 80uM and 160uM) compared with control cells maintained in basal conditions (5% LPDS). **B)** Percentage of cellular proliferation of the CAL-62 cells treated for 48 h with or without DHEA (40uM, 80uM and 160uM) compared with control cells maintained in basal conditions (5% LPDS). Statistical analysis: Kruskal-Wallis test and Dunn's Comparison post-test (*p< 0.05).

Supplementary Table 1: Gene Expression of ATP-binding cassette transporter 1 (ABCA1), 24-Dehydrocholesterol Reductase (DHEA) and Scavenger Receptor Class B (SCARB1) Member genes by qRT-PCR

		GENE	PTC		PTC HIGH RISK		PDTC	
Gene Name	**Gene Symbol**	**ID**	**(RQ)**	**(P-Value)**	**(RQ)**	**(P-Value)**	**(RQ)**	**(P-Value)**
ATP Binding Cassette Subfamily A Member 1	**ABCA1**	19	5.3007	0.0008	7.9018	0.0377	7.1117	0.5044
24-dehydrocholesterol reductase	**DHCR24**	1718	0.6044	0.5329	0.6297	0.5681	0.2775	0.2513
Scavenger receptor class B member 1	**SCARB1**	949	0.4356	0.3813	0.5038	0.5681	0.3138	0.2513

Differential gene expression was detected by qRT-PCR from human epithelial thyroid carcinoma, PTC (n=10), PTC HIGH RISK (n=16), PDTC/ATC (n=3). Data are presented as the fold change in target gene expression in tumours normalized to the BTT was the calibrator tissue (n=12) Statistical analysis: ANOVA test plus Tukey's post-test.

Supplementary Table 2: Gene Expression of Estrogen Receptor (ER)α and ERβ isoformsaccording to histologypattern

		BTT	PTC (low/ intermediate risk)	PTC (high risk)	PDTC/ATC
REα	**Positive**	24 (77.4%)	35 (87.5%)	10(66.7%)	2 (23%)**
	Negative	7 (22.6%)	5 (12.5%)	5 (33.3%)	7 (78%)**
REβ	**Positive**	27 (87.1%)	37 (92.5%)	9 (60.0%)	1 (11%)***
	Negative	4 (12.9%)	3 (7.5%)	6 (40.0%)	8 (89%)***

The analysis was measured in 89 patients (95 thyroid tissue samples): BTT (*n* = 27), high-risk PTC (*n* = 12), low/intermediate-risk PTC (*n* = 43), and PDTC/ATC (*n* = 7). *P*-values (**$p < 0.01$; *** $p < 0.001$), Fisher's exact test results comparing number of samples with and without REα and REβ expression in each tumor tissue type.

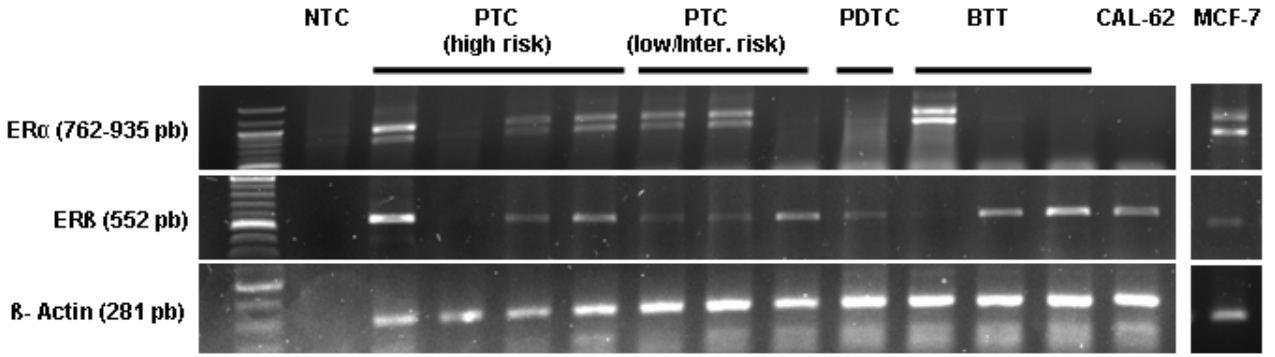

Representativeelectrophoresisagarose gel showing of the PCR amplicons results of the*oestrogen receptor*s isoforms (ERα and ERß)fromdifferenthumanthyroidtissuesamplesand MCF-7 cells. NTC (non template control)

PUBLICATION II

Low-Density Lipoprotein Receptor is a Key Driver of Aggressiveness in Thyroid Tumor Cells

Giovanna Revilla*; Lara Ruiz-Auladell; Nuria Fucui Vallverdú; Paula Santamaria; Antonio Moral; José Ignacio Pérez; Changda Li; Victoria Fusté; Enrique Lerma; Rosa Corcoy; Fabián Pitoia; Joan Carles Escolà-Gil; Eugènia Mato*

*Corresponding authors

International Journal of Molecular Sciences

2023

International Journal of
Molecular Sciences

MDPI

Article

Low-Density Lipoprotein Receptor Is a Key Driver of Aggressiveness in Thyroid Tumor Cells

Giovanna Revilla [1,2], Lara Ruiz-Auladell [1], Núria Fucui Vallverdú [1], Paula Santamaría [1,3], Antonio Moral [4,5], José Ignacio Pérez [4], Changda Li [1,2], Victoria Fuste [6], Enrique Lerma [6], Rosa Corcoy [1,3,5,7], Fabián Pitoia [8], Joan Carles Escolà-Gil [1,2,9,†] and Eugènia Mato [1,7,*,†]

1 Institut de Recerca de l'Hospital de la Santa Creu i Sant Pau, Institut d'Investigació Biomèdica (IIB) Sant Pau, 08041 Barcelona, Spain; grevilla@santpau.cat (G.R.)
2 Department of Biochemistry and Molecular Biology, Universitat Autònoma de Barcelona (UAB), 08025 Barcelona, Spain
3 Department of Endocrinology and Nutrition, Hospital de la Santa Creu i Sant Pau, 08041 Barcelona, Spain
4 Department of General Surgery, Hospital de la Santa Creu i Sant Pau, 08041 Barcelona, Spain
5 Department of Medicine, Universitat Autònoma de Barcelona (UAB), 08193 Bellaterra, Spain
6 Department of Pathological Anatomy, Hospital de la Santa Creu i Sant Pau, 08041 Barcelona, Spain
7 CIBER de Bioingeniería, Biomateriales y Nanomedicina (CIBER-BBN), 28029 Madrid, Spain
8 Division of Endocrinology, Hospital de Clínicas, University of Buenos Aires, Buenos Aires C1120 AAF, Argentina
9 CIBER de Diabetes y Enfermedades Metabólicas Asociadas (CIBERDEM), 28029 Madrid, Spain
* Correspondence: emato@santpau.cat
† These authors contributed equally to this work.

Abstract: We previously described the role of low-density lipoprotein (LDL) in aggressiveness in papillary thyroid cancer (PTC). Moreover, the MAPK signaling pathway in the presence of BRAF V600E mutation is associated with more aggressive PTC. Although the link between MAPK cascade and LDL receptor (LDLR) expression has been previously described, it is unknown whether LDL can potentiate the adverse effects of PTC through it. We aimed to investigate whether the presence of LDL might accelerate the oncogenic processes through MAPK pathway in presence or absence of BRAF V600E in two thyroid cell lines: TPC1 and BCPAP (wild-type and BRAF V600E, respectively). LDLR, PI3K-AKT and RAS/RAF/MAPK (MEK)/ERK were analyzed via Western blot; cell proliferation was measured via MTT assay, cell migration was studied through wound-healing assay and LDL uptake was analyzed by fluorometric and confocal analysis. TPC1 demonstrated a time-specific downregulation of the LDLR, while BCPAP resulted in a receptor deregulation after LDL exposition. LDL uptake was increased in BCPAP over-time, as well as cell proliferation (20% higher) in comparison to TPC1. Both cell lines differed in migration pattern with a wound closure of 83.5 ± 9.7% after LDL coculture in TPC1, while a loss in the adhesion capacity was detected in BCPAP. The siRNA knockdown of LDLR in LDL-treated BCPAP cells resulted in a p-ERK expression downregulation and cell proliferation modulation, demonstrating a link between LDLR and MAPK pathway. The modulation of BRAF-V600E using vemurafenib-impaired LDLR expression decreased cellular proliferation. Our results suggest that LDLR regulation is cell line-specific, regulating the RAS/RAF/MAPK (MEK)/ERK pathway in the LDL-signaling cascade and where BRAF V600E can play a critical role. In conclusion, targeting LDLR and this downstream signaling cascade, could be a new therapeutic strategy for PTC with more aggressive behavior, especially in those harboring BRAF V600E.

Keywords: thyroid cancer (TC); low-density lipoprotein receptor (LDLR); BRAF V600E; RAS/RAF/MAPK (MEK)/ERK pathway; low-density lipoprotein (LDL)

Citation: Revilla, G.; Ruiz-Auladell, L.; Fucui Vallverdú, N.; Santamaría, P.; Moral, A.; Pérez, J.I.; Li, C.; Fuste, V.; Lerma, E.; Corcoy, R.; et al. Low-Density Lipoprotein Receptor Is a Key Driver of Aggressiveness in Thyroid Tumor Cells. *Int. J. Mol. Sci.* **2023**, *24*, 11153. https://doi.org/10.3390/ijms241311153

Academic Editor: Antonio Lucacchini

Received: 29 May 2023
Revised: 30 June 2023
Accepted: 4 July 2023
Published: 6 July 2023

1. Introduction

Thyroid cancer (TC) is the most common malignancy of the human endocrine system, with papillary thyroid carcinoma (PTC) being the most frequent histological subtype.

The incidence of PTC has sharply increased in the last decade, accounting for 90% of all thyroid malignancies [1]. Despite most PTC having an excellent response to treatment after initial therapy, some subtypes may present with features that may determine a high risk of recurrence and even advanced disease, which eventually may become radioiodine refractory (RAI) [2].

The MAPK pathway is known for being critical in the development of many oncogenic diseases, such as melanoma, colon and breast cancer [3–5]. Various histological subtypes of TC present a constitutive activation of MAPK signaling pathway. RAS, RAF, MEK and ERK are the most relevant proteins in this pathway, and they are involved in cellular processes such as differentiation, proliferation and apoptosis [6]. Different studies of thyroid tumors have identified the activating mutation of BRAF as the main genetic alteration of this pathway, with the BRAF V600E hotspot mutation being the most frequently found genetic event. This oncogene is proposed to be the main early mutational event, occurring in about 50% of PTC diagnostics, and is consistently related to adverse prognostic evolution in tumors (>2 cm) [7,8]. BRAF V600E-driven tumors present high extracellular signal-regulated kinase phosphorylation, promoting unregulated cell proliferation and the inhibition of RAI responsive genes in TC through an aberrant activation of the MAPK pathway [9,10]. A recent report demonstrated a positive association between the presence of BRAF mutation, obesity and a greater risk of TC in tumors from patients with PTC [10].

Epidemiologic and experimental evidence have associated obesity/overweight and cholesterol levels as a risk factors of worse cancer progression, including TC [11–15]. Preclinical studies reported a higher low-density lipoprotein receptor (LDLR) expression in some malignant tumors such as colon cancer where low-density lipoprotein (LDL) increased the proliferation of these tumor cells through the MAPK signaling pathway [16].

Moreover, our group reported that cholesterol metabolite 27-hydroxycholesterol (27-HC) was accumulated in PTCs, promoting their aggressive behavior [17]. In this sense, we remark the association described between the LDLR expression and the abnormal lipidic metabolism as a factor of cancer progression and recurrence in hepatocellular carcinoma, lung cancer, breast cancer, colorectal cancer and prostate cancer [5,18]. The LDLR is a cell surface glycoprotein that plays an important role in regulating cholesterol homeostasis [19]. Elevated LDLR expression and LDL uptake in a wide range of tumors have been related to LDL-mediated cancer growth in mice [20,21]. Studies on pancreatic cancer elucidated that the blocking of LDLR reduces the proliferative and clonogenic potential of tumoral cells and decreases the activation of the ERK1/2 survival pathway sensitizing cells to chemotherapeutic drugs [22].

However, the potential molecular mechanisms that regulate this association in TC remain poorly understood. Different studies have established that the degree of MAPK signaling pathway activation determines the extent of LDLR transcription [5,23,24]. In this study, we aim to investigate whether BRAF V600E and LDL can potentiate the LDLR-mediated oncogenic processes via the RAS/RAF/MAPK (MEK)/ERK pathway.

2. Results

2.1. Differential Regulation of Low-Density Lipoprotein Receptor (LDLR) Protein Expression and Low-Density Lipoprotein (LDL) Uptake in Papillary Thyroid Carcinoma (PTC) Cell Lines with Different Mutational Status after LDL Incubation

To examine the protein expression kinetics of LDLR in response to LDL, TPC1 and BCPAP cells (wild-type and BRAF V600E, respectively) were treated under basal conditions (5% FBS), as a control, or with LDL (200 µg/mL ApoB) and harvested at 24 h, 48 h and 72 h to analyze LDLR protein expression via Western blotting. Figure 1A shows that LDL promoted a significant decrease in LDLR expression in TPC1, in comparison to BCPAP, where LDLR expression was maintained over the time. To determine the beginning of LDLR declining in TPC1 incubated with LDL, a time course at different times up to 12 h was carried out. In the initial 12 h period of exposure to LDL, TPC1 exhibited higher expression of LDLR protein, as it is demonstrated in Figure S1. However, subsequently, as depicted in Figure 1A, there was a gradual decline in expression levels until reaching

a significant threshold, albeit not being completely inhibited. To study the LDL uptake, LDL was labeled with 19-dioctadecyl-3,3,39,39-tetramethyl indocarbocyanine (DiI) for subsequent analysis using fluorescence spectrophotometry and confocal microscopy. As illustrated in Figures 1B and 2A, both cell lines were capable of acquiring DiI-LDL but displayed distinct uptake patterns. BCPAP demonstrated a progressive and higher uptake levels of DiI-LDL over time, in comparison to the TPC1 cell line, whose DiI-LDL uptake levels were significantly lower. Furthermore, considering the graph results of DiI-LDL uptake related to LDLR expression in TPC1, it is important to take into consideration the remnants of DiI-LDL acquired during the initial 12 h period, in which LDLR expression was higher, as well as the not complete abolition of LDLR expression at 24 h, 48 h and 72 h. Taking into account that aggregated LDL and oxidized LDL can be acquired through other receptors, such as LRP1 or LOX1, respectively, we initially tested whether the LDL showed any evidence of oxidation or aggregation (Figure S2).

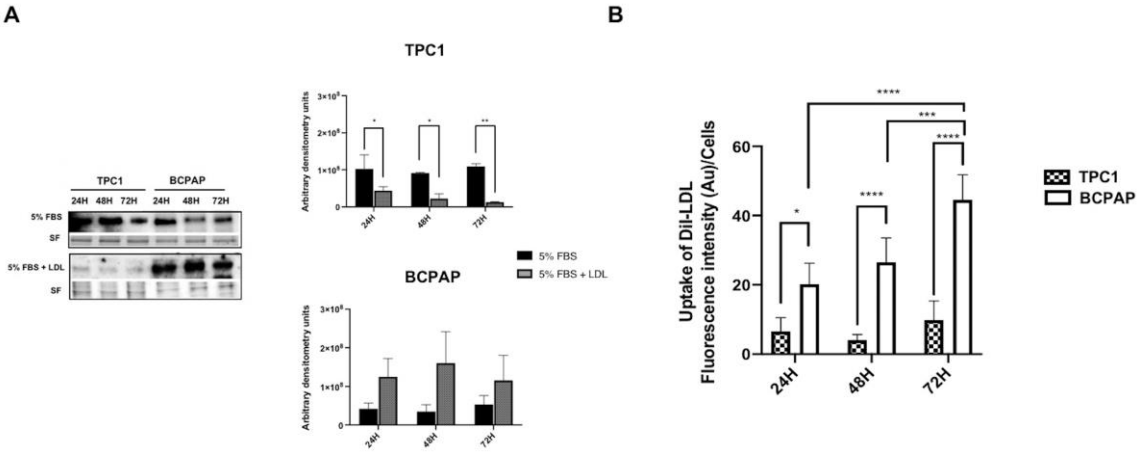

Figure 1. Low-density lipoprotein (LDLR) protein expression and 19-dioctadecyl-3,3,39,39-tetramethyl indocarbocyanine (DiI)-low-density lipoprotein (LDL) uptake in TPC1 and BCPAP cell lines. (**A**) Cells were treated with basal conditions (5% FBS) or LDL (200 µg/mL ApoB) and harvested at 24 h, 48 h and 72 h before analysis. Left panel: one representative blot is shown, and stain-free gel (SF) was used as the loading control. Graphs show densitometry of the Western blots relative to basal condition-treated cells (5% FBS) in comparison to LDL-treated cells. (**B**) Cells were exposed to DiI-LDL (200 µg/mL ApoB) for 24 h, 48 h and 72 h before analysis for mean fluorescence intensity by fluorescence spectrometer to compare LDL uptake between both cell lines. Statistical analysis: a two-way ANOVA test plus Sidak's multiple comparisons test were performed to compare the LDLR protein expression and DiI-LDL uptake between the two groups at each time point (* $p < 0.05$, ** $p < 0.002$, *** $p = 0.0003$, **** $p < 0.001$). Data are expressed as mean ± SEM of a minimum of three independent experiments (N = 3).

Confocal analysis demonstrated lysosome and LDL colocalization in both cell lines (Figure 2A,B). However, the cell lines displayed different intracellular distributions, with lysosomes being broadly distributed in the cytoplasm in the TPC1 cells, while in the BCPAP cells, these organelles were mainly localized throughout the perinuclear region (Figure 2A).

2.2. LDL Promotes Higher Proliferation Levels and Decreases Adhesion Capacity in the BCPAP Cell Line, in Comparison to the Constant Proliferation and Cellular Migration Promoted by LDL in the TPC1 Cell Line

To examine whether LDL regulates cellular proliferation and migration, TPC1 and BCPAP cell lines were maintained under basal conditions (5% FBS) as a control and were compared to cells incubated with LDL (200 µg/mL ApoB) for 24 h, 48 h and 72 h. As shown in Figure 3, LDL promoted cellular proliferation in both cell lines. However, in BCPAP cells, the percentage of proliferation was significantly higher over the time compared to TPC1 cells, which also displayed an increase in proliferation but to a lesser extent (127.1% ± 9.30;

181.0% ± 13.01; and 169.54% ± 28.43 in BCPAP cells incubated with LDL for 24 h, 48 h and 72 h, respectively, vs. 113.7% ± 7.84; 127.9% ± 11.86; and 156.4% ± 14.00 in TPC1 cells). These findings are consistent with the amount of internalized DiI-LDL observed in both cell lines (Figure 1B).

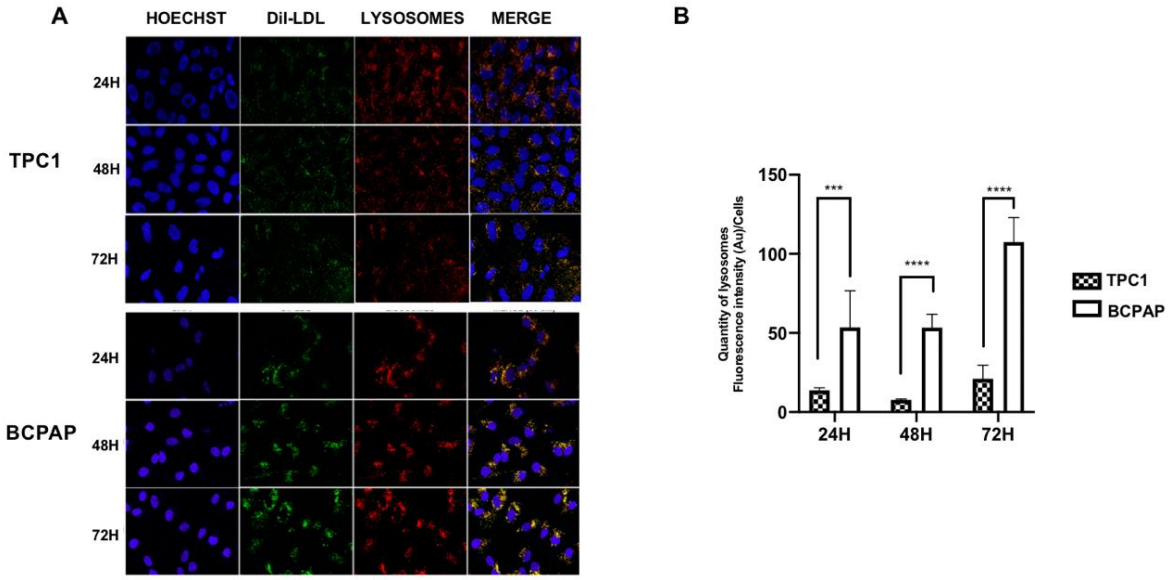

Figure 2. Confocal images of DiI-LDL uptake and lysosome quantification. (**A**) Confocal microscopy of Hoechst-stained (blue), DiI-LDL-stained (green) and lysosome-GFP (red) in TPC1 and BCPAP cell lines. Cells were treated for 24 h, 48 h and 72 h with DiI-LDL (200 µg/mL ApoB). The presence of colocalization of the red and green signals in the merged images is highlighted in yellow. The scale bar size was set to 50 µm. (**B**) Quantity of lysosomes in TPC1 and BCPAP cell lines after DiI-LDL (200 µg/mL ApoB) incubation for 24 h, 48 h and 72 h. Statistical analysis: a two-way ANOVA test plus Sidak's multiple comparisons test were performed to compare the lysosome quantification between the cell lines (*** $p < 0.0009$ and **** $p < 0.0001$). Data are expressed as mean ± SEM of three independent experiments (N = 3).

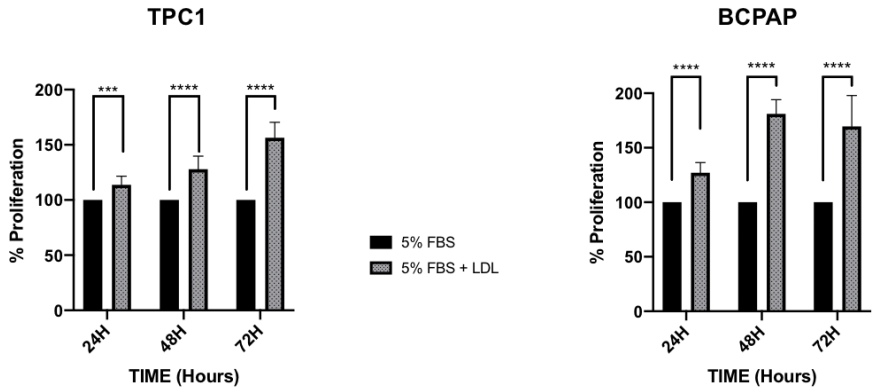

Figure 3. Percentage of cellular proliferation determined by MTT assay of the TPC1 and BCPAP cell lines. Cells were treated with basal conditions (5% FBS), as a control, or with LDL (200 µg/mL ApoB) for 24 h, 48 h and 72 h. Statistical analysis: a two-way ANOVA test plus Sidak's multiple comparisons test were performed to compare both groups. (*** $p < 0.0009$, **** $p < 0.001$). Data are expressed as mean ± SEM of three independent experiments (N = 3) carried out in quintuplicate.

To study the effect of LDL on cell migration, the wound-healing assay was performed by incubating TPC1 and BCPAP cell lines under basal conditions (5% FBS) or with LDL (200 µg/mL ApoB) for 16 h. The results presented in Figure 4 revealed significant differences between both cell lines. In the TPC1 cell line, the wound-repair percentage was

83.47% ± 2.36 compared to basal conditions (5% FBS), which was 22.35% ± 3.08 (Figure 4A). However, in the BCPAP cell line treated with LDL, there was a loss of cellular adhesion with a higher percentage of cell suspension (39.63% ± 2.14) compared to the control (16.80% ± 1.41, Figure 4B). Regarding the cell viability of these unanchored BCPAP cells under LDL treatment, trypan blue staining demonstrated 56.33% ± 4.33 viability compared to unanchored BCPAP cells maintained under basal conditions (29.50% ± 6.71, Figure S3).

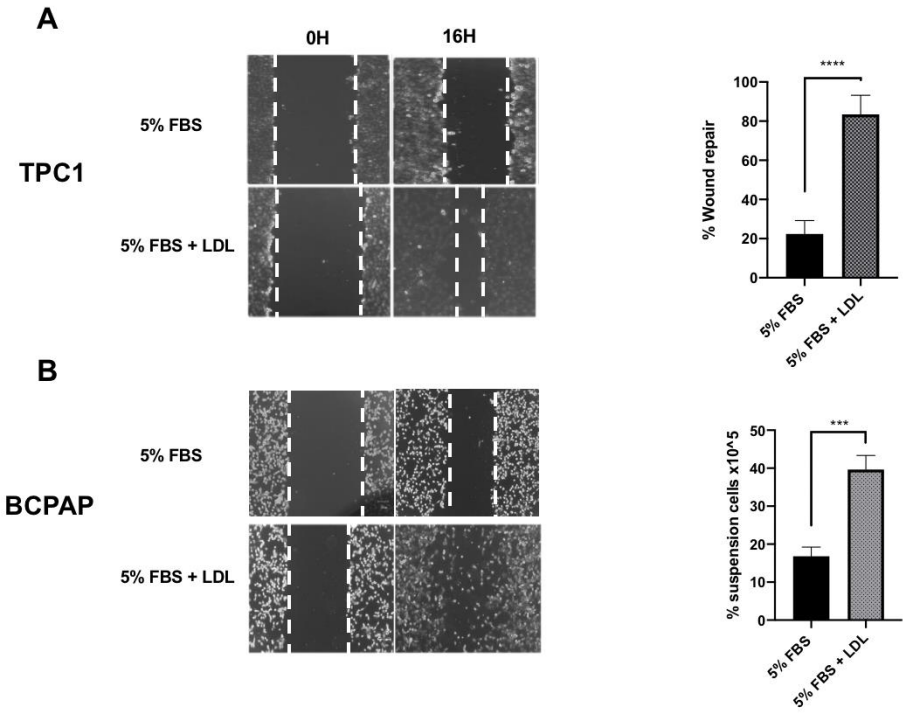

Figure 4. Effects of LDL on cellular migration. A line was scratched in both the TPC1 and BCPAP cell lines, and cultures were treated with 5% FBS, as a control, or with LDL (200 µg/mL ApoB) for 16 h. (**A**) The graph represents the percentage of wound-healing repair (**** $p < 0.0001$) in the TPC1 cell line treated with LDL (200 µg/mL ApoB) compared to the control at basal conditions (5% FBS). (**B**) The graph represents the percentage of suspension BCPAP cells treated with LDL (200 µg/mL ApoB) compared to the control at basal conditions (5% FBS). Images are at 10× resolution. Statistical analysis: an unpaired *t*-test was performed to compare the LDL-treated cells with the control condition (*** $p = 0.0009$, **** $p < 0.0001$). The results are presented as the mean ± SEM of three independent experiments.

2.3. LDL Enhances the RAS/RAF/MAPK (MEK)/ERK Pathway

As a next step towards understanding the mechanism of action of LDL in both cell lines, TPC1 and BCPAP, we analyzed the most relevant proteins of both PI3K-AKT and RAS-RAF-MAPK (MEK)/ERK pathways, two critical signaling pathways related to proliferation and migration, after LDL incubation (200 µg/mL ApoB) for 24 h, 48 h and 72 h.

In TPC1 cells, a moderate increase in p-ERK expression was observed after 24 h of LDL exposition in comparison to basal conditions (5% FBS), but without reaching significant levels, and followed by a progressive decrease over the time. Otherwise, no changes were detected in ERK expression when compared to basal conditions (5% FBS). Additionally, AKT expression was increased after LDL treatment but without reaching significant levels. Although p-AKT and p-MTOR levels did not suffer statistical modifications after LDL treatment in comparison to basal conditions (5% FBS), p-MTOR displayed a slight tendency to decrease at 48 h and 72 h after LDL exposure (Figure 5A). On the other hand, in BCPAP cell line, there was a significant increase in p-ERK expression after LDL incubation compared to basal conditions (5% FBS); otherwise, there were no changes in ERK expression. Moreover, AKT expression increased over time after LDL exposure, in comparison to basal conditions

(5% FBS). In contrast, cells incubated under basal conditions (5% FBS) demonstrated a significant increase in p-AKT, but only at 48 h. Finally, no changes were observed in terms of MTOR and p-MTOR over the time (Figure 5B). Interestingly, p-ERK expression was increased in both cell lines, particularly in the BCPAP cell line, demonstrating that LDL promoted a significant overactivation of the RAS/RAF/MAPK (MEK)/ERK pathway in the cell line harboring BRAF V600E (BCPAP).

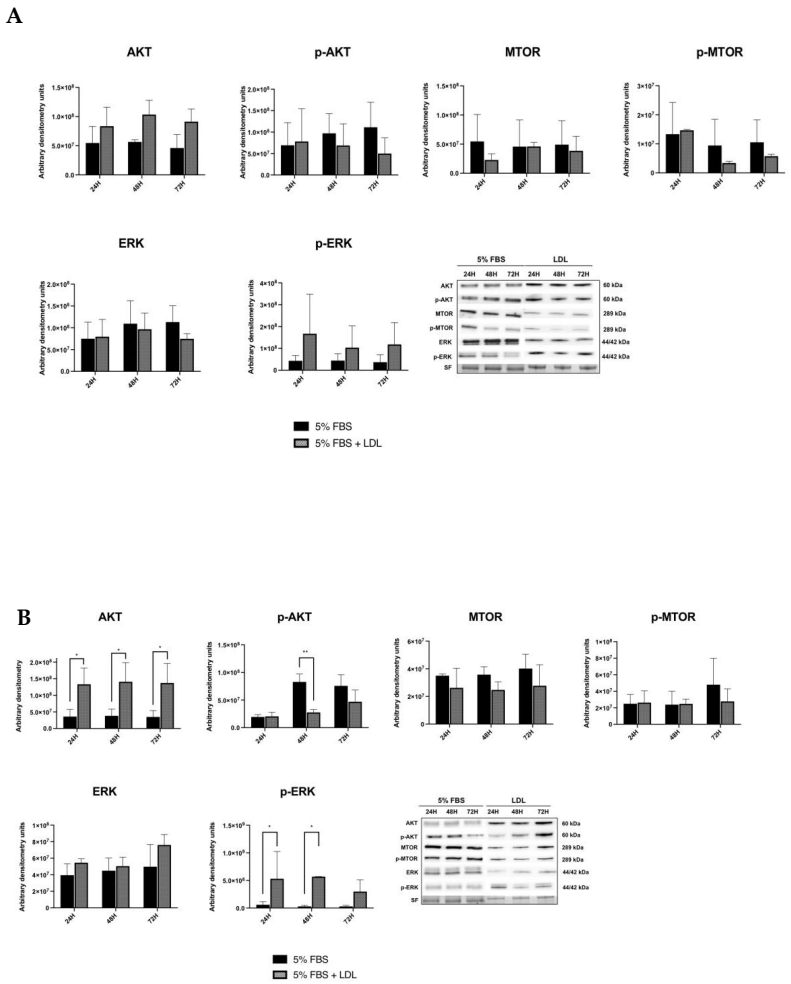

Figure 5. Western blot analysis for PI3K–AKT–MTOR and RAS/RAF/MAPK (MEK)/ERK pathways. (**A**) TPC1 cells were treated with basal conditions (5% FBS) or LDL (200 µg/mL ApoB) and harvested at 24 h, 48 h and 72 h. Last panel: representatives blots are shown. Stain-free (SF) gel was used as the loading control. Graphs show the densitometry of the Western blots relative to basal condition-treated cells in comparison to LDL-treated cells. (**B**) BCPAP cells were treated with basal conditions (5% FBS) or LDL (200 µg/mL ApoB) and harvested at 24 h, 48 h and 72 h. Last panel: representative blots are shown. Stain-free (SF) gel was used as the loading control. Graphs show densitometry of the Western blots relative to basal condition-treated cells in comparison to LDL-treated cells. Statistical analysis: two-way ANOVA test plus Sidak's multiple comparisons test (* $p < 0.01$, ** $p < 0.001$). Data are expressed as mean ± SEM of a minimum of three independent experiments (N = 3).

2.4. Vemurafenib Reduces Cellular Proliferation Promoted by LDL, Downregulating LDLR Expression and Impairing RAS/RAF/MAPK (MEK)/ERK Pathway Activation in BCPAP Cell Line

As shown in Figure 6, BCPAP cells were treated with vemurafenib (1 µM) with/without LDL (200 µg/mL ApoB) and were compared to the LDL-only treated condition at 24 h, 48 h and 72 h. Protein expression analysis revealed an increase in LDLR and p-ERK expression after LDL exposure, according with previous findings depicted in Figures 1A and 5B. Additionally, the treatment with vemurafenib by itself produced a significant decrease in both p-ERK

and LDLR protein expression. Importantly, vemurafenib completely counteracted the LDL-mediated effects on LDLR and p-ERK expression (Figure 6A,B).

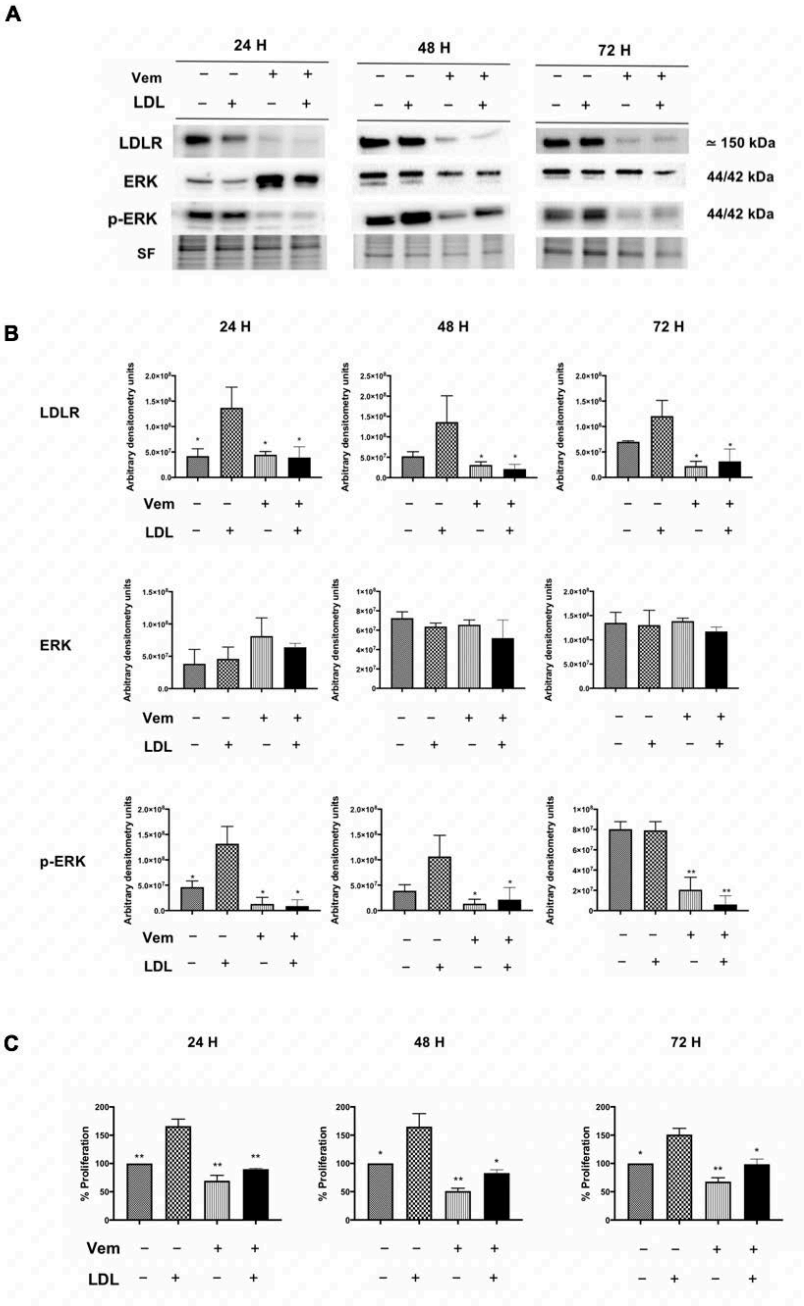

Figure 6. Western blot analysis of Ras/Raf/MAPK (MEK)/ERK pathway and cellular proliferation determined by MTT assay of BCPAP cell line after LDL (200 μg/mL ApoB) incubation and/or vemurafenib treatment (1 μM) compared to the LDL-only treatment condition (200 μg/mL ApoB + DMSO 0.1%) for 24 h, 48 h and 72 h. (**A**) Representative blots of LDLR, ERK and p-ERK are shown. Stain-free (SF) gel was used as the loading control. (**B**) Graphs show the densitometry analysis of the Western blots of LDLR, ERK and p-ERK after LDL (200 μg/mL ApoB) incubation and/or vemurafenib treatment (1 μM) for 24 h, 48 h and 72 h in comparison to the LDL-only treatment condition (200 μg/mL ApoB + DMSO 0.1%). (**C**) Proliferation percentage determined by

MTT assay in the BCPAP cell line after incubation with LDL (200 µg/mL ApoB) and/or vemurafenib treatment (1 µM) compared to the LDL-only treatment condition (200 µg/mL ApoB + DMSO 0.1%) at 24 h, 48 h and 72 h. Statistical analysis: one-way ANOVA test plus Tukey's multiple comparisons test (* $p < 0.01$, ** $p < 0.001$ vs. the LDL-alone condition). All data are expressed as mean ± SEM of three independent experiments (N = 3). Each MTT assay experiment was carried out in quintuplicate.

To assess the effects of vemurafenib on LDL-induced proliferation, the BCPAP cell line was treated with the same conditions described above and the proliferation was analyzed via MTT assay. As expected, incubation with LDL resulted in an increase in cellular proliferation compared to basal conditions (Figure 6C), as it has been previously reported in Figure 2. Vemurafenib also blocked the LDL-mediated increases in cell proliferation, reaching similar proliferation levels as the basal conditions (5% FBS, Figure 6C). Conversely, in the TPC1 cell line treated with LDL (control cell line), vemurafenib did not produce further changes in either LDLR expression or ERK phosphorylation or proliferation (Figure S4).

2.5. LDLR Is Required for LDL-Mediated Induction of RAS/RAF/MAPK (MEK)/ERK Pathway, LDL-Uptake and Cell Proliferation in the BCPAP Cell Line

In order to investigate whether LDL has a role as a coadjuvant with BRAF V600E in the cell proliferation, BCPAP cells were silenced for 48 h with a LDLR siRNA (siLDLR) before LDL treatment, resulting in an around 60% to 70% decrease in LDL uptake, LDLR gene expression, as well as LDLR protein expression (Figure 7A–C).

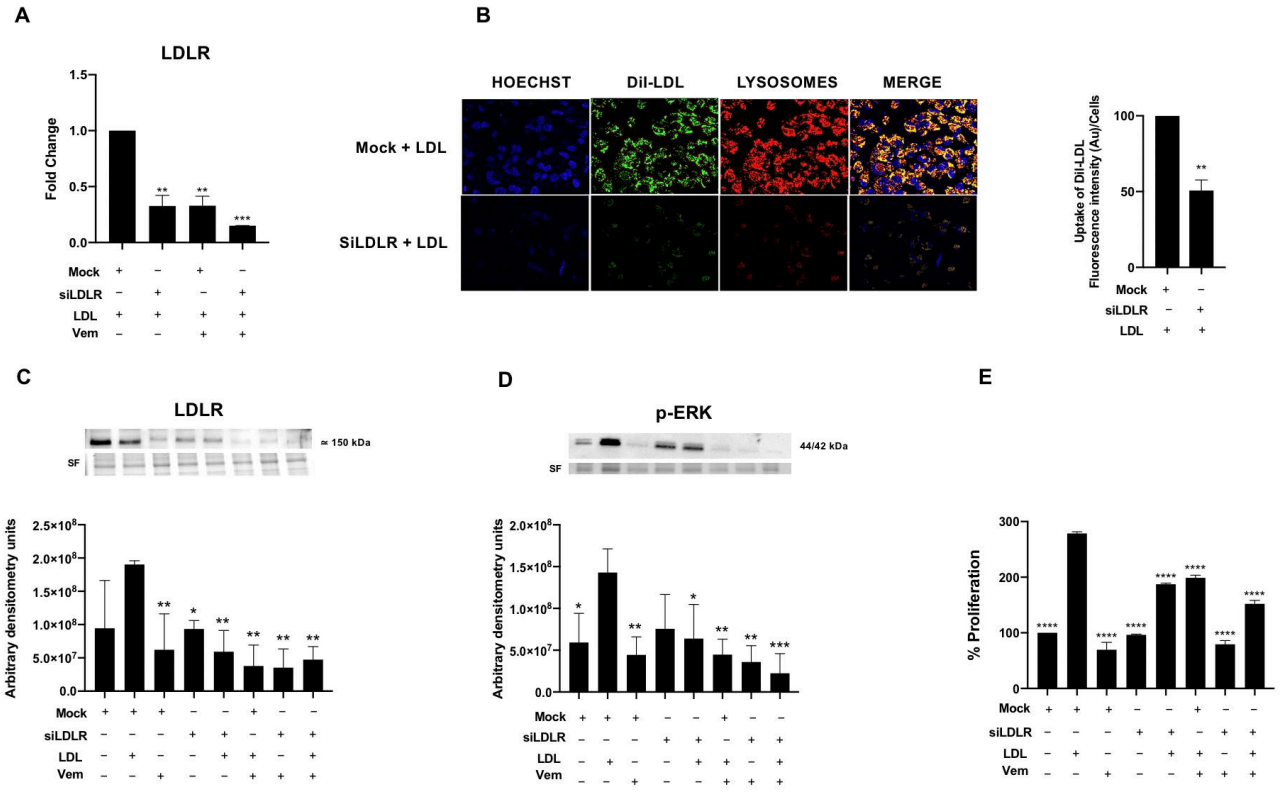

Figure 7. *LDLR* mRNA levels, confocal images and analysis of DiI-LDL uptake; LDLR and p-ERK expression; and cellular proliferation after siLDLR, vemurafenib (1 µM) and/or LDL (200 µg/mL ApoB) treatment compared to basal conditions for 24 h. (**A**) mRNA expression of *LDLR* after siLDLR for 48 h, LDL (200 µg/mL ApoB) and/or vemurafenib (1 µM) treatment in comparison to the LDL-only condition (LDL + DMSO 0.1% + Mock). (**B**) Confocal microscopy of Hoechst-stained (blue), DiI-LDL-stained (green) and lysosome-GFP (red) in BCPAP cell line after 24 h of DiI-LDL (200 µg/mL ApoB) treatment and with and without siLDLR for 48 h. The presence of colocalization of the red and green

signals in the merged images is highlighted in yellow. The scale bar size was set to 50 µm. Right graph: cells were exposed to DiI-LDL (200 µg/mL ApoB) for 24 h after siLDLR for 48 h in comparison to the LDL-only condition (Mock + LDL) and analyzed for mean fluorescence intensity by fluorescence spectrometer. Statistical analysis: an unpaired *t*-test plus Welch's correction were performed to compare both conditions (** $p = 0.066$). Data are expressed as mean ± SEM of a minimum of three independent experiments (n = 3). (**C**) Representative blot of LDLR is shown. Stain-free (SF) gel was used as the loading control. Graph shows the densitometry analysis of the Western blots of LDLR after siLDLR, LDL (200 µg/mL ApoB) incubation and/or vemurafenib treatment (1 µM) for 48 h, in comparison to the LDL-alone condition (LDL + DMSO 0.1% + Mock). (**D**) Representative blot of p-ERK is shown. Stain-free (SF) gel was used as the loading control. Graph shows the densitometry analysis of the Western blots of p-ERK after siLDLR, LDL (200 µg/mL ApoB) incubation and/or vemurafenib treatment (1 µM) for 48 h, in comparison to the LDL-only condition (LDL + DMSO 0.1% + Mock). (**E**) Proliferation percentage determined via MTT assay after incubation with LDL (200 µg/mL ApoB), vemurafenib treatment (1 µM) and/or siLDLR, compared to the LDL-only condition (LDL + DMSO 0.1% + Mock) at 48 h. Statistical analysis: one-way ANOVA test plus Tukey's multiple comparisons test (* $p < 0.01$, ** $p < 0.001$, *** $p = 0.0009$, **** $p < 0.0001$ vs. the LDL-only condition). All data are expressed as mean ± SEM of three independent experiments (N = 3). Each MTT assay experiment was carried out in quintuplicate.

Furthermore, as shown in Figure 7D, the knockdown of LDLR in BCPAP cells exposed to LDL resulted in a significant reduction in p-ERK expression compared to the LDL-alone treatment. In addition, LDL did not further upregulate p-ERK expression after silencing LDLR, suggesting that LDLR is the main driver of the LDL-mediated induction of the RAS/RAF/MAPK (MEK)/ERK pathway (Figure 7D). Interestingly, the LDLR knockdown in combination with vemurafenib treatment in BCPAP cells exposed to LDL resulted in a somewhat greater p-ERK protein expression decrease, implying a potential synergistic effect between LDLR and BRAF V600E. Otherwise, there were no changes in ERK expression (Figure S5). In line with these findings, LDLR knockdown also impaired cell proliferation in BCPAP cells exposed to LDL (Figure 7B,E). Further impaired cell proliferation was found when LDLR was knockdown in cells treated with vemurafenib (Figure 7E).

3. Discussion

Some epidemiological studies have demonstrated a relationship between obesity/overweight, cholesterol and a higher incidence rate, as well as worse prognosis, of certain solid tumors [11–15]. Moreover, it has been described the potential therapeutic effect of targeting lipid metabolism using classic lipid-lowering drugs, such as statins, in cancer therapy to prevent LDL effects on tumor progression [25]. Although the link between lipid metabolism and tumor aggressiveness is complex and not yet fully understood, several reports have identified these connections in certain solid tumors. Furthermore, there is evidence that the oncogenes and tumor suppressor genes have important roles as the drivers of alterations in lipid metabolism in cancer [17,26–30].

In TC, we previously identified a decrease in LDL levels in the serum of patients with a more aggressive histological pattern, whereas in their tumoral tissue, there was an upregulation in the expression of the *LDLR* and a decrease in the *3-hydroxy-3-methylglutaryl-CoA reductase (HMG-CoA)* gene expression, responsible for the biosynthesis of cholesterol. Moreover, we also observed an intratumoral increase in the 27-HC metabolite together with a downregulation of the 25-HC 7-alpha-hydroxylase (CYP7B1) enzyme that controls its degradation [17]. In this line, it is known that the most common histological pattern of well-differentiated TC corresponds to PTC, and the subtype with aggressive behavior and worse prognosis in patients is associated with the presence of the BRAF V600E mutation [31–33]. The BRAF V600E belongs to the RAS/RAF/MAPK (MEK)/ERK pathway, which is the most important signaling cascade related with proliferation, differentiation and apoptosis, and promotes ERK hyperactivation that is critical in cancer development and progression [34]. Moreover, LDL was shown to activate the RAS/RAF/MAPK

(MEK)/ERK pathway, promoting oncogenic processes in tumors such as colorectal cancer, as well as in endothelial dysfunction in atherosclerosis [35,36].

Considering the current evidence of the association between LDL and tumor progression, and the effect of LDL on MAPK activation [37], we aimed to study the role of LDL in PTC cells and the connection with BRAF V600E mutation as a metabolic trigger of the tumor aggressiveness. Thus, we analyzed the LDL-associated uptake through the LDLR, as well as the signaling pathways related to the presence or absence of the BRAF V600E mutation in two TC cell lines: TPC1 and BCPAP.

The most important findings of our study show that the LDLR expression and LDL uptake were differentially regulated in the presence versus the absence of the BRAF V600E mutation, with the BCPAP cell line showing poor LDLR regulation. Moreover, due to this LDLR expression in BCPAP cell line, the LDL uptake was significantly higher in comparison to TPC1. On the other hand, the amount of LDL uptake in TPC1 cells was maintained over the time due to a not complete inhibition of the LDLR expression in the cell membrane, as well as the LDL particles taken up during the first 12 h of LDL exposure, where LDLR expression was higher (Figure S1). In addition, the BCPAP cell line displayed a higher proliferation percentage and an increase in the loss of cellular adhesion compared to the TPC1 cell line. Similar independent studies were performed on anaplastic thyroid cancer (ATC) cell lines, CAL-62 and 8505C (wild type and harboring BRAF V600E, respectively), exposed to LDL conditions and showed comparable results regarding LDLR protein expression, LDL uptake, cellular proliferation and MAPK signaling pathway (Figure S6).These data are in accordance with previous studies that demonstrates LDL capacity to induce the proliferation, migration and loss of adhesion in breast cancer cells [38]. Nevertheless, these differences between both cell lines after LDL treatment could be related to its different mutational status. Different reports highlight how lipid metabolic dysregulation due to high systemic cholesterol uptake could lead to an important metabolic alteration in tumoral processes. This supports the suggestion that cholesterol plays a critical role in tumor metastatic promotion with the presence of the BRAF mutation [39–44].

Moreover, the lysosomal distribution pattern differed between both cell lines. The lysosome distribution of BCPAP cell line was more juxtanuclear; meanwhile, in the TPC1 cell line, the lysosomes were distributed throughout the cytoplasm. These results may suggest a higher interaction with the endoplasmic reticulum (ER) and Golgi in BCPAP cell line, in comparison to TPC1, as a consequence of different metabolic signaling inputs due to their differential capacity for LDL uptake [45]. It is well known that the LDL uptake is released to the lysosomes for their degradation, as well as the delivery of free cholesterol. However, our findings are in line with the newly reported roles of lysosomes in relation to tumoral cells, indicating a potential connection with other important organelles, such as the ER, mitochondria and nucleus, which are crucial in the cholesterol metabolism of cancer cells [45,46]. The lysosomal system has emerged as an important factor in invasion, dissemination and survival related to oncogenic processes [47]; for that reason, further investigation should be considered to clarify its role in TC progression.

To elucidate the signal transduction pathway, through which LDL promoted the proliferation, adhesion and migration processes in TC cell lines, we studied the most relevant transduction pathways involved in these processes in TC, namely the PI3K-AKT and RAS-RAF-MAPK (MEK)/ERK signaling cascades. In accordance with Velarde V. et al., who established a crosstalk between native LDL and ERK phosphorylation through the MAPK pathway in vascular smooth muscle cells [48], our results also demonstrated an increase in p-ERK expression after LDL exposure. However, the BCPAP cell line demonstrated a greater increase in ERK phosphorylation, suggesting the hyperactivation of the RAS/RAF/MAPK (MEK)/ERK pathway due to its higher levels of LDL uptake. These results were also observed in the ATC cell line, 8505C, harboring the BRAF V600E mutation (Figure S6D). Therefore, the RAS/RAF/MAPK (MEK)/ERK pathway could be considered an LDL-related signaling pathway. On the other hand, regarding the PI3K-AKT pathway, both cell lines, TPC1 and BCPAP, resulted in a higher phosphorylation of AKT when cells

were nutrient-deprived (5% FBS) in comparison to LDL conditions, being significant in BCPAP cell line. These findings are directly in line with previous studies in cancer cells that suggest an activation of PI3K-AKT by increasing AKT phosphorylation to survive stressful environments promoted by serum starvation [49,50].

Importantly, we also investigated whether BRAF V600E partial suppression through vemurafenib decreases its oncogenic effects by modulating LDLR expression and MAPK signaling cascade in BCPAP cell line. We found that BRAF V600E-mediated oncogenic signaling was partially blocked by vemurafenib in the BCPAP cell line treated with LDL, causing a decrease in the p-ERK signaling pathway. Consequently, proliferation decreased, as has also been reported by Xing et al., in TC cell lines [51]. Interestingly, we observed a link between the RAS/RAF/MAPK (MEK)/ERK and LDL signaling pathways when vemurafenib was able to induce a strong LDLR downregulation, as well as to attenuate cell proliferation promoted by LDL exposure in the BCPAP cell line. These results show, for the first time to our knowledge, that vemurafenib could also regulate the recycling or gene transcription of *LDLR* in the BCPAP cell line. Otherwise, no significant changes were found, either in LDLR or p-ERK in the TPC1 cell line used as a control, and the cytotoxic effects of this drug can be discarded. Moreover, the combination of siRNA-mediated targeting *LDLR* plus vemurafenib in LDL-treated conditions can trigger a significant reduction in the LDL-induced ERK phosphorylation, as well as cellular proliferation, suggesting a synergistic effect between LDL and BRAF mutation in TC. In this sense, similar results in regard to a synergic effect between LDL-signaling and BRAF V600E were described in melanoma, colorectal and lung cancer cells [5,52–54]. Nevertheless, further research is needed to better understand the role of vemurafenib in lipid metabolism.

In summary, our findings support the suggestion that LDLR plays an important role in the RAS/RAF/MAPK (MEK)/ERK signaling cascade in TC and suggest a synergy between LDL-mediated receptor uptake and BRAF V600E in TC, which could lead to a worse prognosis in the clinical setting of hypercholesterolemia (Figure 8). Further investigation is needed in terms of using cholesterol-lowering drugs in combination with RAS/RAF/MAPK (MEK)/ERK inhibitors as a possible therapeutic strategy for PTC with aggressive behavior.

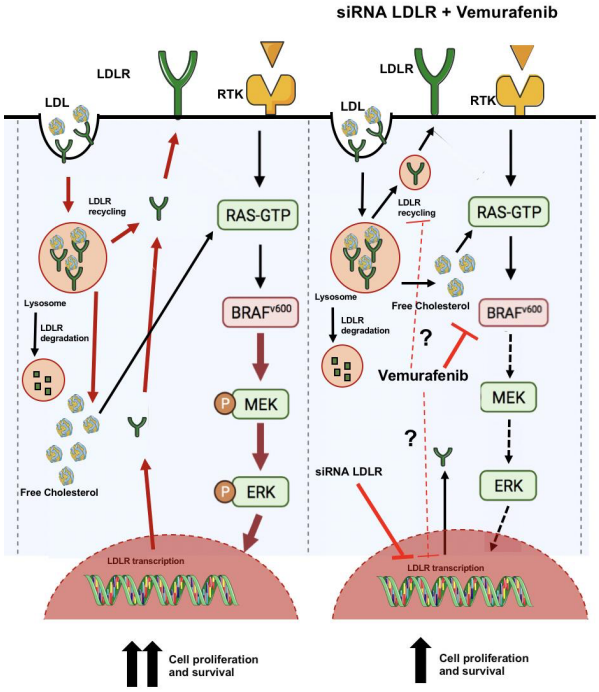

Figure 8. Schematic illustration of the hypothesis that proposes a crosstalk between RAS/RAF/MAPK (MEK)/ERK pathway and LDL-mediated receptor uptake in BCPAP cell line. In the presence of LDL,

a cell line harboring a BRAF mutation (BCPAP) can increase proliferation and worsens its behavior by increasing the activation of the RAS/RAF/MAPK (MEK)/ERK pathway. Vemurafenib treatment at 1uM, which enters to the cell by passive diffusion, interrupts the B-Raf/MEK step, as well as downregulating LDLR expression. Additionally, siRNA LDLR downregulates LDLR expression, decreasing LDL uptake and modulating RAS/RAF/MAPK (MEK)/ERK pathway overactivation. Black arrows mean the normal activation of the pathway, red arrows are used when the pathway is overactivated and dashed arrows symbolize when the pathway is inhibited. Part of the Servier Medical Art by Servier is licensed under a Creative Commons Attribution 3.0 Unported License (https://smart.servier.com/image-set-download/ (accessed on 9 November 2022)).

4. Materials and Methods

4.1. Cell Lines and Cell Culture

The experiments were carried out on cell lines derived from human PTC, TPC1 (bearing RET/PTC rearrangement) and BCPAP (bearing the BRAF V600E oncogene). Both cell lines were provided by Paolo Vigneri of Azienda Ospedaliero Universitaria Policlinico Vittorio Emanuele Catania, Catania, Sicilia, IT. Cells were cultured in RPMI 1940 medium (ThermoFisher Scientific, Waltham, MA, USA) supplemented with 10% FBS, 100 U/mL penicillin and 1 µg/mL streptomycin at 37 °C in a 5% CO_2 atmosphere.

4.2. Human LDL Isolation

Human LDL (1.019–1.063 kg/L) was isolated via the sequential ultracentrifugation of fasting plasma. ApoB levels were determined enzymatically and by immunoturbidimetric assays, respectively, applying commercial kits adjusted to a COBAS c501 autoanalyzer (Roche Diagnostics, Minato City, Tokyo) [55,56]. Human LDL particles were not oxidatively modified during their isolation and the experimental procedure. The oxidative modification of human LDL was measured via the monitoring of the formation of conjugated dienes at 234 nm at 37 °C with a BioTek Synergy HT spectrophotometer (BioTek Synergy, Winooski, VT, USA). As a positive control, LDL was also oxidized by adding $CuSO_4$ (2.5 mol/L) to wells containing LDL (0.1 mg of apoB/mL). At the end of the process, an aliquot of native LDL oxLDL and the substance oxidized for 2 h (partially oxidized LDL) were stained with Sudan Black and run on an agarose gel (0.5%) for 40 min to evaluate their integrity and charge properties (Figure S2).

4.3. Labeling LDL with DiI

LDL was labeled with DiI perchlorate-conjugated LDL (Invitrogen, Waltham, MA, USA), applying a modified procedure of the method described in Teupser et al. [57]. A stock solution of DiI was prepared by dissolving 3 mg DiI in 1 mL DMSO and then was added to the LDL solution to yield a final ratio of 150 µg DiI to 1 mg LDL. Then, it was incubated for 18 h at 37 °C under dark conditions followed by five rounds of centrifugation at 3000–3500× *g* for 45 min, using ultra centrifugal filter units (15 mL; Merck, Darmstadt, Germany) in order to isolate the DiI-labeled LDL. Then, DiI-LDL was dialyzed against saline containing phosphate-buffered saline (PBS) and filter-sterilized (0.25 µm, Water Millex HV units). The ApoB concentrations of LDL and DiI-LDL were determined using commercial kits adapted to a COBAS c501 autoanalyzer (Roche Diagnostics, Minato City, Tokyo). The standard solutions of DiI were prepared in isopropanol with a concentration range of 0–110 ng/mL. The standard curve of DiI-LDL was prepared in saline with a concentration range of 0–1600 ng protein/mL. A spectrofluorometer with excitation and emission wavelengths set at 549 and 564 nm was used to obtain fluorescence measurements. The specific activity of DiI-LDL was finally obtained as the amount of DiI (ng) integrated into 1 µg of LDL.

4.4. Analysis of Lipoprotein Uptake by a Fluorometric Assay

LDLR activity and LDL uptake were analyzed measuring the DiI-LDL. Specifically, 3×10^4 cells were seeded in 30 mm dishes with RPMI 1940 (ThermoFisher Scientific,

Waltham, MA, USA) and 10% FBS. The day after, the cells were treated with 5% FBS, as a control, and with 200 µg/mL DiI-LDL for 24 h, 48 h and 72 h. For the fluorometric assay, after incubation, the cells were placed on ice and washed three times with cold PBS 1X + 00.4% BSA and twice with cold PBS 1X. Then, 300 µL of lysis reagent (NaOH 0.1 M + 1 g/L SDS) was added and left under consistent shaking at room temperature for 30–60 min. A spectrofluorometer with excitation and emission wavelengths set at 549 and 564 nm was used to measure the fluorescence in 200 µL of the lysate on black microtiter plates. Protein quantification was determined in 10 µL by BCA using BSA dissolved in lysis reagent as a standard (Thermofisher Scientific, Waltham, MA, USA) in order to normalize fluorescence measurements through cellular culture confluence. Additionally, the fluorescence of the DiI-LDL diluted in lysis reagent was measured to determine the specific fluorescence intensity of the DiI-LDL preparation used.

4.5. Analysis of Lipoprotein Uptake by Confocal Microscopy

Specifically, 3×10^4 cells were seeded in 30 mm confocal dishes (VWR, Radnor, PA, USA) with RPMI 1940 and 10% FBS. The day after, the cells were treated with 5% FBS, as a control, and with 200 µg/mL DiI-LDL for 24 h, 48 h and 72 h. Nucleus and lysosomes were labeled with Hoechst and GFP (ThermoFisher Scientific, Waltham, MA, USA) 5 min and 16 h before confocal analysis, respectively. Images of immunostained cells were recorded on a Leica-inverted fluorescence confocal microscope (Leica TCS SP5-AOBS, Wetzlar, Germany). Cells were viewed with HCX PL APO 63X oil/0.6–1.4 objective. Fluorescent images were acquired in a scan format of 1024 × 1024 pixels in a spatial dataset (xyz or xzy) and were processed using the Leica Standard Software TCS-AOBS (V2.7.3). Lisosomal quantification has been carried out using Fiji software (ImageJ V1.53, University of Wisconsin, Madison, WI, USA) [58].

4.6. Quantitative Real-Time PCR

Total RNA was isolated using the TRIZOL reagent according to the manufacturer's instructions (Invitrogen, Waltham, MA, USA). A total of 1 µg of the total RNA was reverse-transcribed using a transcriptor first-strand cDNA synthesis kit (Roche Applied Science, Penzberg, Germany), and the cDNA samples were stored at –20 °C for use as a template in real-time polymerase chain reaction (PCR) analysis. The gene expression profiles were analyzed in an ABI PRISM 7900HF Sequence Detection System, using a predesigned and labeled primer/probe set (Assays-on-Demand™ Gene Expression Assay, Applied Biosystems, Foster City, CA, USA). The Taqman qPCR primers (Applied Biosystems, Foster City, CA, USA) used were as follows: human HMGCR (Hs00168352_m1), human LDL receptor (LDLR; Hs01092524_m1) and human GAPDH (NM_002046.3). All the reactions were performed with 100 ng of cDNA in a total volume of 50 µL of TaqMan® Universal PCR Master Mix (Applied Biosystems, Foster City, CA, USA), and the relative expression levels for each gene were calculated using the 2^{-ddCt} method, with SDS2.3 and Data Assist V2.1 software (Applied Biosystems, Foster City, CA, USA), and GAPDH was used as the normalizing gene.

4.7. Protein Extraction and Western Blot

TPC1 and BCPAP cells were seeded in 60 mm plates and treated with or without LDL (200 µg/mL ApoB) for 24 h, 48 h and 72 h when they reached a 70% of confluence. In terms of inhibitor treatment, the BCPAP cells were treated with 5% FBS and 0.01% DMSO as a control, with LDL (200 µg/mL ApoB) or with vemurafenib (1 µM) (PLX4032, Selleck Chemicals LLC, Houston, TX, USA) for 24 h, 48 h and 72 h. The TPC1 and BCPAP cells were lysed in RIPA buffer (50 mM Tris-HCl, pH 7.5; 150 mM NaCl; 1% NP40; 0.5% sodium deoxycholate; 0.1% SDS; 1 mM EDTA) supplemented with protease inhibitor cocktail (Roche Diagnostics, Minato City, Tokyo), phenylmethylsulfonyl fluoride (PMSF, Sigma, St. Louis, MO, USA) and sodium orthovanadate (Sigma). Lysates were centrifuged at 12,000× *g* for 15 min at 4 °C and a BCA protein assay reagent kit (ThermoFisher Scientific,

Waltham, MA, USA) was used to obtain the protein concentrations from the supernatants. Afterwards, the protein extracts were mixed with a 4X Laemmli loading buffer and heated at 94 °C for 4 min. Then, 20 µg of protein was size-separated on a 10% TGX Stain-Free precast gel (Bio-Rad, Hercules, CA, USA), transferred to a 0.2 µm PVDF membrane (Bio-Bio-Rad, Hercules, CA, USA) and the membrane were blocked with 3% dried milk in Tris-buffered saline containing 0.05% of Tween-20 (TBST buffer) for 15 min. Finally, membranes were incubated with optimized dilutions of the primary antibody (Table S1) overnight at 4 °C. Thereafter, the membranes were washed three times for 10 min with TBST buffer and re-incubated with the IgG HRP-conjugated secondary antibody for 1 h (Supplementary Table S1). Finally, the membranes were washed three times for 10 min with TBST buffer and analyzed using an Immun-Star Western Chemiluminescence Kit (Bio-Rad, Hercules, CA, USA). Imaging and data analysis were performed following the protocol described in Taylor et al. and Neris, R.L.S., et al. TGX Stain-free gels were activated for 1 min after SDS-electrophoresis. Images were captured using a ChemiDoc XRS Gel Documentation System (Bio-Rad, Hercules, CA, USA) and Image Lab software (version 6.0.1, Bio-Rad, Hercules, CA, USA). Data normalization analysis for each protein band was performed with the stain-free gel image saved, and the background was adjusted in such a way that the total background was subtracted from the sum of the density of all the bands in each lane [59,60].

4.8. MTT Assay

In terms of the MTT assay, 4.000 cells/well were seeded in quintuplicates in 96-well microplates and treated with 5% FBS and 0.01% DMSO as a control, with LDL (200 µg/mL ApoB) or with vemurafenib (PLX4032, Selleck Chemicals LLC, Houston, TX, USA) (1 µM) for 24 h, 48 h and 72 h. The proliferation viability was measured using a 20-µL MTT solution (5 mg/mL) of 3-(4,5-dimethyl-2-thiazolyl)-2,5-diphenyl-2-H-tetrazolium bromide (MTT; Sigma-Aldrich, St. Louis, MO, USA) and incubation at 37 °C for 4 h; then, 50 µL DMSO was added to each well and they were incubated at 37 °C for 10 min. The absorbance at 490 nm was obtained to calculate the cell proliferation rate using a microplate reader (xMark, Bio-Rad, Hercules, CA, USA).

4.9. Migration and Adhesion Assay

To analyze the cell migration and adhesion, both cell lines (TPC1 and BCPAP) were seeded at high densities until 70% confluence was reached. In terms of migration capacity, the cells were scratched using a 10 uL pipette tip and washed with PBS 1X. The wounds were photographed at 0 h (t = 0) and after 16 h with or without LDL incubation (200 µg/mL ApoB) and 5% FBS at 37 °C using an inverted microscope and analyzed with Image J software V1.53 (University of Wisconsin, Madison, WI, USA) [58]. The percentage of wound-healing was obtained from a minimum of three measurements of the wound area, and each result was the mean of three independent experiments. In terms of the adhesion assay, the cells were treated with or without LDL (200 µg/mL ApoB) and 5% FBS and then incubated for 24 h, 48 h and 72 h. Afterwards, the percentages of viable suspension cells in the supernatant were counted using the automated Cell Counter (Bio-Rad, Hercules, CA, USA) together with trypan blue exclusion assay for a direct identification and enumeration of live (unstained) and dead (blue) cells in a given population.

4.10. Transient Transfection Assay

To knockdown LDLR expression, a siRNA transfection in BCPAP cell line was performed via JetPrimeTM (Polyplus transfection, VWR, Radnor, PA, USA), according to the manufacturer's instructions. Approximately 1.5×10^5 cells were seeded in 30 mm plates for protein and RNA extraction one day prior to transfection. Cells were transfected with either 80 nM pre-designed short, interfering RNA for human LDLR (siLDLR) (IDs4) (Ambion, Life Technologies, Carlsbad, CA, USA) or control siRNA (Mock-siRNA) purchased from Santa Cruz Biotechnology, Inc. (sc-37007) (Dallas, TX, USA) in RPMI 1940 medium

(ThermoFisher Scientific, Waltham, MA, USA) supplemented with 10% FBS, 100 U/mL penicillin and 1 µg/mL streptomycin. After 48 h, the transfection media was replaced with RPMI 1940 medium (ThermoFisher Scientific, Waltham, MA, USA) supplemented with 5% FBS, 100 U/mL penicillin and 1 µg/mL streptomycin, the cells were transfected again with the corresponding siRNA (siLDLR or Mock-siRNA) and treated for 48 h with 5% FBS and 0.1% DMSO, as a control; LDL (200 µg/mL ApoB) and 1µM of vemurafenib (PLX4032, Selleck Chemicals LLC, Houston, TX, USA), when corresponds. The 1 µM dose of vemurafenib (PLX4032, Selleck Chemicals LLC, Houston, TX, USA) was chosen in accordance with previous studies in BCPAP cell lines in order to just modulate the RAS/RAF/MAPK (MEK)/ERK signaling pathway without promoting cellular toxic effects [61,62].

The following steps after siRNA transfection for lipoprotein uptake analysis by fluorometric assay and confocal analysis in the BCPAP cell line are described in Sections 4.4 and 4.5, respectively.

For MTT assay (MTT; Sigma-Aldrich, St. Louis, MO, USA), 3×10^3 cells were plated in 96-well plate and transiently transfected with 5nM siRNA LDLR or Mock-siRNA, following the same steps described above.

4.11. Statistical Analysis

GraphPad Prism version 9.0 (GraphPad Inc., San Diego, CA, USA), with a p-value < 0.05 denoting statistical significance, was used for the statistical analysis. The two-way ANOVA test as well as Sidak's multiple comparisons test were used to evaluate the effects of time and cell type on each dependent variable. The analysis of more than two groups was performed via one-way ANOVA with Tukey's post hoc test where applicable. Differences between the two groups were analyzed via an unpaired two-tailed Student's t-test.

Supplementary Materials: The supporting information can be downloaded at: https://www.mdpi.com/article/10.3390/ijms241311153/s1.

Author Contributions: Conceptualization, G.R. and E.M.; methodology, G.R., L.R.-A., N.F.V., P.S. and C.L.; writing—original draft, G.R. and E.M.; writing—review and editing, G.R., E.M., J.C.E.-G., R.C., A.M., J.I.P., V.F., F.P. and E.L.; project administration, G.R. and E.M.; funding acquisition, E.M. All authors have read and agreed to the published version of the manuscript.

Funding: This work was partly funded by "The Ministerio de Sanidad y Consumo, Instituto de Salud Carlos III", Madrid (Spain) and FEDER, "Una manera de hacer Europa", grant FIS PI19/00136. Additionally, Revilla, G., was granted by a PhD fellowship co-financed by "Instituto Salud Carlos III, Madrid, Spain" (PFIS) and Fondo Social Europeo (FSE), grant FI19/00007.

Institutional Review Board Statement: Not applicable.

Informed Consent Statement: Not applicable.

Data Availability Statement: Not applicable.

Acknowledgments: We would like to acknowledge David Santos and Núria Puig for technical support. We acknowledge the contribution of Esther Peña from microscopy facility at the Institut de Recerca of Hospital Sant Pau (IIB Sant Pau). This study was carried out as part of the PhD program in Biochemistry, Molecular Biology and Biomedicine at the Universitat Autònoma de Barcelona (UAB).

Conflicts of Interest: The authors declare no conflict of interest.

References

1. Noone, A.-M.; Cronin, K.A.; Altekruse, S.F.; Howlader, N.; Lewis, D.R.; Petkov, V.I.; Penberthy, L. Cancer Incidence and Survival Trends by Subtype Using Data from the Surveillance Epidemiology and End Results Program, 1992–2013. *Cancer Epidemiol. Biomark. Prev.* **2017**, *26*, 632–641. [CrossRef] [PubMed]
2. Coca-Pelaz, A.; Shah, J.P.; Hernandez-Prera, J.C.; Ghossein, R.A.; Rodrigo, J.P.; Hartl, D.M.; Olsen, K.D.; Shaha, A.R.; Zafereo, M.; Suarez, C.; et al. Papillary Thyroid Cancer—Aggressive Variants and Impact on Management: A Narrative Review. *Adv. Ther.* **2020**, *37*, 3112–3128. [CrossRef] [PubMed]

3. Zhang, H.; Liu, J.; Dang, Q.; Wang, X.; Chen, J.; Lin, X.; Yang, N.; Du, J.; Shi, H.; Liu, Y.; et al. Ribosomal Protein RPL5 Regulates Colon Cancer Cell Proliferation and Migration through MAPK/ERK Signaling Pathway. *BMC Mol. Cell Biol.* **2022**, *23*, 48. [CrossRef]
4. Jiang, W.; Wang, X.; Zhang, C.; Xue, L.; Yang, L. Expression and Clinical Significance of MAPK and EGFR in Triple-negative Breast Cancer. *Oncol. Lett.* **2020**, *19*, 1842–1848. [CrossRef]
5. Scully, T.; Kase, N.; Gallagher, E.J.; LeRoith, D. Regulation of Low-Density Lipoprotein Receptor Expression in Triple Negative Breast Cancer by EGFR-MAPK Signaling. *Sci. Rep.* **2021**, *11*, 17927. [CrossRef]
6. Lavoie, H.; Gagnon, J.; Therrien, M. ERK Signalling: A Master Regulator of Cell Behaviour, Life and Fate. *Nat. Rev. Mol. Cell Biol.* **2020**, *21*, 607–632. [CrossRef]
7. Nucera, C.; Goldfarb, M.; Hodin, R.; Parangi, S. Role of B-RafV600E in Differentiated Thyroid Cancer and Preclinical Validation of Compounds against B-RafV600E. *Biochim. Biophys. Acta BBA Rev. Cancer* **2009**, *1795*, 152–161. [CrossRef] [PubMed]
8. Silver, J.A.; Bogatchenko, M.; Pusztaszeri, M.; Forest, V.-I.; Hier, M.P.; Yang, J.W.; Tamilia, M.; Payne, R.J. BRAF V600E Mutation Is Associated with Aggressive Features in Papillary Thyroid Carcinomas $\leq$ 1.5 cm. *J. Otolaryngol. Head Neck Surg.* **2021**, *50*, 63. [CrossRef]
9. Anand, N.; Agrawal, T.; Gupta, A.; Shukla, S.; Pradhan, R.; Husain, N. Diagnostic Efficacy of Brafv600e Immunocytochemistry in Thyroid Aspirates in Bethesda Category Iv and Papillary Thyroid Carcinoma. *J. Cytol.* **2021**, *38*, 113. [CrossRef]
10. Rahman, S.T.; Pandeya, N.; Neale, R.E.; McLeod, D.S.A.; Bain, C.J.; Baade, P.D.; Youl, P.H.; Allison, R.; Leonard, S.; Jordan, S.J. Obesity Is Associated with *BRAF* ^{V600E} -Mutated Thyroid Cancer. *Thyroid* **2020**, *30*, 1518–1527. [CrossRef]
11. Feigelson, H.S.; Bodelon, C.; Powers, J.D.; Curtis, R.E.; Buist, D.S.M.; Veiga, L.H.S.; Bowles, E.J.A.; Berrington de Gonzalez, A.; Gierach, G.L. Body Mass Index and Risk of Second Cancer among Women with Breast Cancer. *JNCI J. Natl. Cancer Inst.* **2021**, *113*, 1156–1160. [CrossRef]
12. Huang, B.; Song, B.; Xu, C. Cholesterol Metabolism in Cancer: Mechanisms and Therapeutic Opportunities. *Nat. Metab.* **2020**, *2*, 132–141. [CrossRef] [PubMed]
13. Yan, A.; Jia, Z.; Qiao, C.; Wang, M.; Ding, X. Cholesterol Metabolism in Drug-resistant Cancer (Review). *Int. J. Oncol.* **2020**. [CrossRef] [PubMed]
14. Matrone, A.; Ferrari, F.; Santini, F.; Elisei, R. Obesity as a Risk Factor for Thyroid Cancer. *Curr. Opin. Endocrinol. Diabetes Obes.* **2020**, *27*, 358–363. [CrossRef] [PubMed]
15. Kitahara, C.M.; Pfeiffer, R.M.; Sosa, J.A.; Shiels, M.S. Impact of Overweight and Obesity on US Papillary Thyroid Cancer Incidence Trends (1995–2015). *JNCI J. Natl. Cancer Inst.* **2020**, *112*, 810–817. [CrossRef]
16. Mayengbam, S.S.; Singh, A.; Pillai, A.D.; Bhat, M.K. Influence of Cholesterol on Cancer Progression and Therapy. *Transl. Oncol.* **2021**, *14*, 101043. [CrossRef]
17. Revilla, G.; de Pons, M.P.; Baila-Rueda, L.; García-León, A.; Santos, D.; Cenarro, A.; Magalhaes, M.; Blanco, R.M.; Moral, A.; Ignacio Pérez, J.; et al. Cholesterol and 27-Hydroxycholesterol Promote Thyroid Carcinoma Aggressiveness. *Sci. Rep.* **2019**, *9*, 10260. [CrossRef]
18. Siemianowicz, K.; Gminski, J.; Stajszczyk, M.; Wojakowski, W.; Goss, M.; Machalski, M.; Telega, A.; Brulinski, K.; Magiera-Molendowska, H. Serum LDL Cholesterol Concentration and Lipoprotein Electrophoresis Pattern in Patients with Small Cell Lung Cancer. *Int. J. Mol. Med.* **2000**, *5*, 55–62. [CrossRef] [PubMed]
19. Go, G.-W.; Mani, A. Low-Density Lipoprotein Receptor (LDLR) Family Orchestrates Cholesterol Homeostasis. *Yale J. Biol. Med.* **2012**, *85*, 19–28.
20. Gallagher, E.J.; Zelenko, Z.; Neel, B.A.; Antoniou, I.M.; Rajan, L.; Kase, N.; LeRoith, D. Elevated Tumor LDLR Expression Accelerates LDL Cholesterol-Mediated Breast Cancer Growth in Mouse Models of Hyperlipidemia. *Oncogene* **2017**, *36*, 6462–6471. [CrossRef]
21. Huang, J.; Li, L.; Lian, J.; Schauer, S.; Vesely, P.W.; Kratky, D.; Hoefler, G.; Lehner, R. Tumor-Induced Hyperlipidemia Contributes to Tumor Growth. *Cell Rep.* **2016**, *15*, 336–348. [CrossRef]
22. Guillaumond, F.; Bidaut, G.; Ouaissi, M.; Servais, S.; Gouirand, V.; Olivares, O.; Lac, S.; Borge, L.; Roques, J.; Gayet, O.; et al. Cholesterol Uptake Disruption, in Association with Chemotherapy, Is a Promising Combined Metabolic Therapy for Pancreatic Adenocarcinoma. *Proc. Natl. Acad. Sci. USA* **2015**, *112*, 2473–2478. [CrossRef] [PubMed]
23. Mehta, K.D. Role of Mitogen-Activated Protein Kinases and Protein Kinase C in Regulating Low-Density Lipoprotein Receptor Expression. *Gene Expr.* **2002**, *10*, 153–164. [CrossRef]
24. Abidi, P.; Zhang, F.; Li, C.; Liu, J. Blockage of the ERK Signaling Pathway Abrogates the SCAP Ligand-Induced Transcriptional Activation of the LDL Receptor Gene in HepG2 Cells. *Int. J. Mol. Med.* **2005**, *16*, 779–785. [CrossRef] [PubMed]
25. Deng, C.-F.; Zhu, N.; Zhao, T.-J.; Li, H.-F.; Gu, J.; Liao, D.-F.; Qin, L. Involvement of LDL and Ox-LDL in Cancer Development and Its Therapeutical Potential. *Front. Oncol.* **2022**, *12*, 803473. [CrossRef]
26. Le, A.; Udupa, S.; Zhang, C. The Metabolic Interplay between Cancer and Other Diseases. *Trends Cancer* **2019**, *5*, 809–821. [CrossRef]
27. Gyamfi, J.; Kim, J.; Choi, J. Cancer as a Metabolic Disorder. *Int. J. Mol. Sci.* **2022**, *23*, 1155. [CrossRef] [PubMed]
28. Butler, L.M.; Perone, Y.; Dehairs, J.; Lupien, L.E.; De Laat, V.; Talebi, A.; Loda, M.; Kinlaw, W.B.; Swinnen, J.V. Lipids and Cancer: Emerging Roles in Pathogenesis, Diagnosis and Therapeutic Intervention. *Adv. Drug Deliv. Rev.* **2020**, *159*, 245–293. [CrossRef]

29. Labbé, D.P.; Zadra, G.; Yang, M.; Reyes, J.M.; Lin, C.Y.; Cacciatore, S.; Ebot, E.M.; Creech, A.L.; Giunchi, F.; Fiorentino, M.; et al. High-Fat Diet Fuels Prostate Cancer Progression by Rewiring the Metabolome and Amplifying the MYC Program. *Nat. Commun.* **2019**, *10*, 4358. [CrossRef]
30. Zhang, F. Dysregulated Lipid Metabolism in Cancer. *World J. Biol. Chem.* **2012**, *3*, 167. [CrossRef]
31. Gan, X.; Shen, F.; Deng, X.; Feng, J.; Lu, J.; Cai, W.; Peng, L.; Zheng, W.; Wang, W.; Huang, P.; et al. Prognostic Implications of the BRAF-V600E Mutation in Papillary Thyroid Carcinoma Based on a New Cut-off Age Stratification. *Oncol. Lett.* **2020**, *19*, 631–640. [CrossRef]
32. Yang, K.; Wang, H.; Liang, Z.; Liang, J.; Li, F.; Lin, Y. BRAFV600E Mutation Associated with Non–Radioiodine-Avid Status in Distant Metastatic Papillary Thyroid Carcinoma. *Clin. Nucl. Med.* **2014**, *39*, 675–679. [CrossRef]
33. Li, J.; Liang, J.; Zhao, T.; Lin, Y. Noninferior Response in BRAFV600E Mutant Nonmetastatic Papillary Thyroid Carcinoma to Radioiodine Therapy. *Eur. J. Nucl. Med. Mol. Imaging* **2016**, *43*, 1034–1039. [CrossRef] [PubMed]
34. Guo, Y.; Pan, W.; Liu, S.; Shen, Z.; Xu, Y.; Hu, L. ERK/MAPK Signalling Pathway and Tumorigenesis (Review). *Exp. Ther. Med.* **2020**, *19*, 1997–2007. [CrossRef] [PubMed]
35. Catar, R.; Chen, L.; Zhao, H.; Wu, D.; Kamhieh-Milz, J.; Lücht, C.; Zickler, D.; Krug, A.W.; Ziegler, C.G.; Morawietz, H.; et al. Native and Oxidized Low-Density Lipoproteins Increase the Expression of the LDL Receptor and the LOX-1 Receptor, Respectively, in Arterial Endothelial Cells. *Cells* **2022**, *11*, 204. [CrossRef] [PubMed]
36. Wang, C.; Li, P.; Xuan, J.; Zhu, C.; Liu, J.; Shan, L.; Du, Q.; Ren, Y.; Ye, J. Cholesterol Enhances Colorectal Cancer Progression via ROS Elevation and MAPK Signaling Pathway Activation. *Cell. Physiol. Biochem.* **2017**, *42*, 729–742. [CrossRef]
37. Jenkins, A.J.; Velarde, V.; Klein, R.L.; Joyce, K.C.; Phillips, K.D.; Mayfield, R.K.; Lyons, T.J.; Jaffa, A.A. Native and Modified LDL Activate Extracellular Signal-Regulated Kinases in Mesangial Cells. *Diabetes* **2000**, *49*, 2160–2169. [CrossRef]
38. Rodrigues Dos Santos, C.; Domingues, G.; Matias, I.; Matos, J.; Fonseca, I.; De Almeida, J.M.; Dias, S. LDL-Cholesterol Signaling Induces Breast Cancer Proliferation and Invasion. *Lipids Health Dis.* **2014**, *13*, 16. [CrossRef]
39. Luo, X.; Cheng, C.; Tan, Z.; Li, N.; Tang, M.; Yang, L.; Cao, Y. Emerging Roles of Lipid Metabolism in Cancer Metastasis. *Mol. Cancer* **2017**, *16*, 76. [CrossRef]
40. Fu, Y.; Zou, T.; Shen, X.; Nelson, P.J.; Li, J.; Wu, C.; Yang, J.; Zheng, Y.; Bruns, C.; Zhao, Y.; et al. Lipid Metabolism in Cancer Progression and Therapeutic Strategies. *MedComm* **2021**, *2*, 27–59. [CrossRef]
41. Matsushita, Y.; Nakagawa, H.; Koike, K. Lipid Metabolism in Oncology: Why It Matters, How to Research, and How to Treat. *Cancers* **2021**, *13*, 474. [CrossRef] [PubMed]
42. Valvo, V.; Iesato, A.; Kavanagh, T.R.; Priolo, C.; Zsengeller, Z.; Pontecorvi, A.; Stillman, I.E.; Burke, S.D.; Liu, X.; Nucera, C. Fine-Tuning Lipid Metabolism by Targeting Mitochondria-Associated Acetyl-CoA-Carboxylase 2 in *BRAF* ^{V600E} Papillary Thyroid Carcinoma. *Thyroid* **2021**, *31*, 1335–1358. [CrossRef] [PubMed]
43. Li, J.; Gu, D.; Lee, S.S.-Y.; Song, B.; Bandyopadhyay, S.; Chen, S.; Konieczny, S.F.; Ratliff, T.L.; Liu, X.; Xie, J.; et al. Abrogating Cholesterol Esterification Suppresses Growth and Metastasis of Pancreatic Cancer. *Oncogene* **2016**, *35*, 6378–6388. [CrossRef] [PubMed]
44. Rashkovan, M.; Albero, R.; Gianni, F.; Perez-Duran, P.; Miller, H.I.; Mackey, A.L.; Paietta, E.M.; Tallman, M.S.; Rowe, J.M.; Litzow, M.R.; et al. Intracellular Cholesterol Pools Regulate Oncogenic Signaling and Epigenetic Circuitries in Early T-Cell Precursor Acute Lymphoblastic Leukemia. *Cancer Discov.* **2022**, *12*, 856–871. [CrossRef]
45. Zhao, Q.; Gao, S.M.; Wang, M.C. Molecular Mechanisms of Lysosome and Nucleus Communication. *Trends Biochem. Sci.* **2020**, *45*, 978–991. [CrossRef]
46. Bartel, K.; Pein, H.; Popper, B.; Schmitt, S.; Janaki-Raman, S.; Schulze, A.; Lengauer, F.; Koeberle, A.; Werz, O.; Zischka, H.; et al. Connecting Lysosomes and Mitochondria—A Novel Role for Lipid Metabolism in Cancer Cell Death. *Cell Commun. Signal.* **2019**, *17*, 87. [CrossRef]
47. Machado, E.R.; Annunziata, I.; Van De Vlekkert, D.; Grosveld, G.C.; d'Azzo, A. Lysosomes and Cancer Progression: A Malignant Liaison. *Front. Cell Dev. Biol.* **2021**, *9*, 642494. [CrossRef]
48. Velarde, V.; Jenkins, A.J.; Christopher, J.; Lyons, T.J.; Jaffa, A.A. Activation of MAPK by Modified Low-Density Lipoproteins in Vascular Smooth Muscle Cells. *J. Appl. Physiol.* **2001**, *91*, 1412–1420. [CrossRef]
49. Gao, M.; Liang, J.; Lu, Y.; Guo, H.; German, P.; Bai, S.; Jonasch, E.; Yang, X.; Mills, G.B.; Ding, Z. Site-Specific Activation of AKT Protects Cells from Death Induced by Glucose Deprivation. *Oncogene* **2014**, *33*, 745–755. [CrossRef]
50. Fathy, M.; Awale, S.; Nikaido, T. Phosphorylated Akt Protein at Ser473 Enables HeLa Cells to Tolerate Nutrient-Deprived Conditions. *Asian Pac. J. Cancer Prev.* **2017**, *18*, 3255. [CrossRef]
51. Xing, J.; Liu, R.; Xing, M.; Trink, B. The BRAFT1799A Mutation Confers Sensitivity of Thyroid Cancer Cells to the BRAFV600E Inhibitor PLX4032 (RG7204). *Biochem. Biophys. Res. Commun.* **2011**, *404*, 958–962. [CrossRef]
52. Theodosakis, N.; Langdon, C.G.; Micevic, G.; Krykbaeva, I.; Means, R.E.; Stern, D.F.; Bosenberg, M.W. Inhibition of Isoprenylation Synergizes with MAPK Blockade to Prevent Growth in Treatment-resistant Melanoma, Colorectal, and Lung Cancer. *Pigment Cell Melanoma Res.* **2019**, *32*, 292–302. [CrossRef] [PubMed]
53. Bose, C.; Bhuvaneswaran, C.; Udupa, K.B. Altered Mitogen-Activated Protein Kinase Signal Transduction in Human Skin Fibroblasts during In Vitro Aging: Differential Expression of Low-Density Lipoprotein Receptor. *J. Gerontol. A. Biol. Sci. Med. Sci.* **2004**, *59*, B126–B135. [CrossRef] [PubMed]

54. Jin, S.; Borkhuu, O.; Bao, W.; Yang, Y.-T. Signaling Pathways in Thyroid Cancer and Their Therapeutic Implications. *J. Clin. Med. Res.* **2016**, *8*, 284–296. [CrossRef]
55. Julve, J.; Escolà-Gil, J.C.; Rotllan, N.; Fiévet, C.; Vallez, E.; de la Torre, C.; Ribas, V.; Sloan, J.H.; Blanco-Vaca, F. Human Apolipoprotein A-II Determines Plasma Triglycerides by Regulating Lipoprotein Lipase Activity and High-Density Lipoprotein Proteome. *Arterioscler. Thromb. Vasc. Biol.* **2010**, *30*, 232–238. [CrossRef]
56. Friedewald, W.T.; Levy, R.I.; Fredrickson, D.S. Estimation of the Concentration of Low-Density Lipoprotein Cholesterol in Plasma, without Use of the Preparative Ultracentrifuge. *Clin. Chem.* **1972**, *18*, 499–502. [CrossRef] [PubMed]
57. Teupser, D.; Thiery, J.; Walli, A.K.; Seidel, D. Quantitative Spectrofluorometry of DiI-Lipoprotein Uptake. *Biochim. Biophys Acta* **1996**, *1303*, 193–198. [CrossRef] [PubMed]
58. Schindelin, J.; Arganda-Carreras, I.; Frise, E.; Kaynig, V.; Longair, M.; Pietzsch, T.; Preibisch, S.; Rueden, C.; Saalfeld, S.; Schmid, B.; et al. Fiji: An open-source platform for biological-image analysis. *Nat. Methods* **2012**, *9*, 676–682. [CrossRef]
59. Taylor, S.C.; Posch, A. The Design of a Quantitative Western Blot Experiment. *BioMed Res. Int.* **2014**, *2014*, 1–8. [CrossRef]
60. Neris, R.L.S.; Dobles, A.M.C.; Gomes, A.V. Western Blotting Using In-Gel Protein Labeling as a Normalization Control: Advantages of Stain-Free Technology. In *Proteomic Profiling*; Posch, A., Ed.; Methods in Molecular Biology; Springer: New York, NY, USA, 2021; Volume 2261, pp. 443–456. [CrossRef]
61. Montero-Conde, C.; Ruiz-Llorente, S.; Dominguez, J.M.; Knauf, J.A.; Viale, A.; Sherman, E.J.; Ryder, M.; Ghossein, R.A.; Rosen, N.; Fagin, J.A. Relief of Feedback Inhibition of *HER3* Transcription by RAF and MEK Inhibitors Attenuates Their Antitumor Effects in *BRAF*-Mutant Thyroid Carcinomas. *Cancer Discov.* **2013**, *3*, 520–533. [CrossRef]
62. Byeon, H.K.; Na, H.J.; Yang, Y.J.; Ko, S.; Yoon, S.O.; Ku, M.; Yang, J.; Kim, J.W.; Ban, M.J.; Kim, J.-H.; et al. Acquired Resistance to BRAF Inhibition Induces Epithelial-to-Mesenchymal Transition in BRAF (V600E) Mutant Thyroid Cancer by c-Met-Mediated AKT Activation. *Oncotarget* **2017**, *8*, 596–609. [CrossRef] [PubMed]

PUBLICATION II: SUPPLEMENTARY DATA

Low-Density Lipoprotein Receptor is a Key Driver of Aggressiveness in Thyroid Tumor Cells

Giovanna Revilla*; Lara Ruiz-Auladell; Nuria Fucui Vallverdú; Paula Santamaria; Antonio Moral; José Ignacio Pérez; Changda Li; Victoria Fusté; Enrique Lerma; Rosa Corcoy; Fabián Pitoia; Joan Carles Escolà-Gil; Eugènia Mato*

*Corresponding authors

International Journal of Molecular Sciences

2023

Table S1. List of antibodies used for Western Blot studies

Antibody	Species	Dilution	Company (catalog#)
LDLR	Rabbit	1:200	Abcam EP1553Y
p44/42 MAPK (ERK 1/2) = **total ERK**	Rabbit	1:1000	Cell signaling (#9102)
P-p44/42 MAPK MAPK (ERK 1/2) = **p-ERK**	Rabbit	1:1000	Cell signaling (#9101)
AKT	Rabbit	1:1000	Cell signaling (#4685)
p-AKT	Rabbit	1:1000	Cell signaling (#9271)
MTOR	Rabbit	1:200	Cell signaling (#2972)
p-MTOR	Rabbit	1:200	Cell signaling (#2971)
NF-κB	Rabbit	1:1000	Cell signaling (#3035)
Anti-rabbit secondary antibody		1:5000	Promega (W4011)
Anti-mouse secondary antibody		1:5000	Promega (W4021)

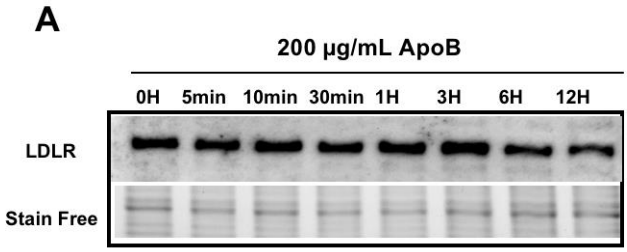

Figure S1. Western blot analysis showing the time course of Low-Density lipoprotein (LDLR) protein expression in the TPC1 cell line after low-density lipoprotein (LDL) (200 µg/mL ApoB) incubation for 5 min, 10 min, 30 min, 1 h, 3 h, 6 h and 12 h . Western blot Stain-Free gel was used as the loading control.

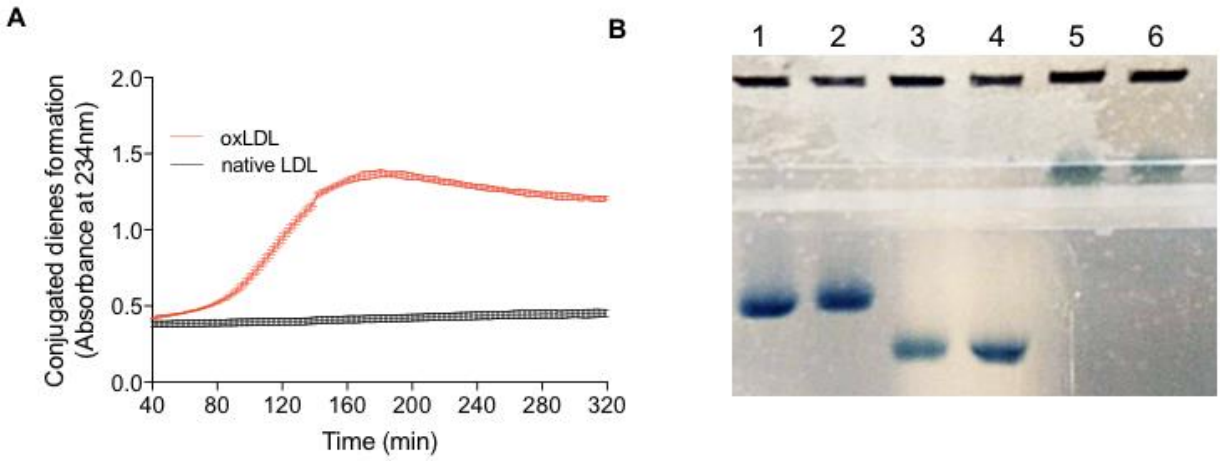

Figure S2. A) Diene formation curves of native LDL incubated with media and LDL after being under specific oxidation conditions. (B) Electrophoretic mobility of native LDL and LDL after being exposed to oxidation or partially oxidized as shown in panel A. 1 & 2: partially oxidated LDL; 3 & 4: oxidated LDL; 5 & 6: native LDL (used in our experiments).

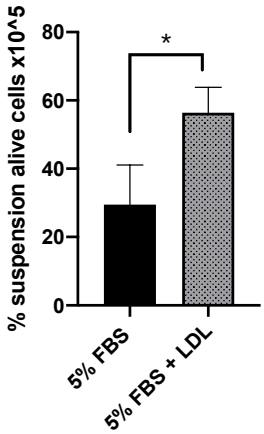

Figure S3. The graph represents the percentage of suspension alive BCPAP cells treated with LDL (200 µg/mL ApoB) compared to the suspension alive BCPAP cells at basal conditions (5% FBS). Statistical analysis: An unpaired t-test was performed to compare the LDL-treated cells with the control condition (*p = 0.0284). The results corresponded to the mean ± SEM of three independent experiments.

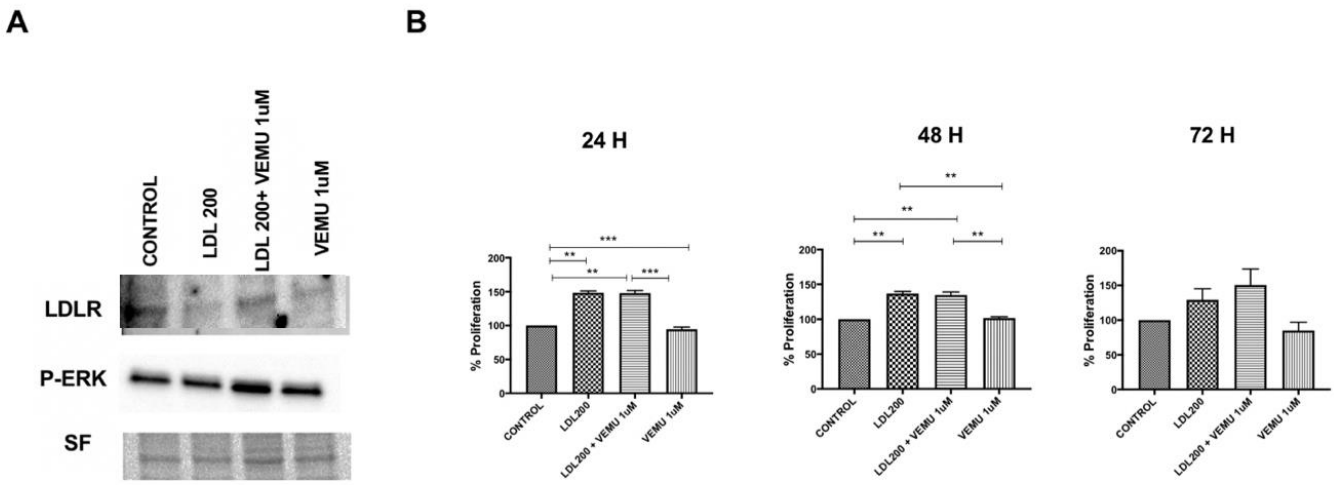

Figure S4. Western blot protein expression panel and MTT assay of TPC1 cell lines after LDL (200 µg/mL ApoB) incubation and vemurafenib treatment (1 µM). (A) Western blot protein expression panel of LDLR, and p-ERK after LDL (200 µg/mL ApoB) incubation and vemurafenib treatment (1 µM) for 24 h. Stain-Free (SF) gel was used as the loading control. (B) Proliferation percentage determined via MTT assay in the TPC1 cell line after LDL (200 µg/mL ApoB) incubation and vemurafenib treatment (1 µM) compared to the control condition (5% FBS) at 24 h, 48 h, and 72 h. Statistical analysis: One-way ANOVA test plus Tukey's multiple comparisons test (*$p < 0.01$, **$p < 0.001$, ***$p = 0.0008$). Data are expressed as mean ± SEM ($n = 3$) of three independent experiments carried out in quintuplicate.

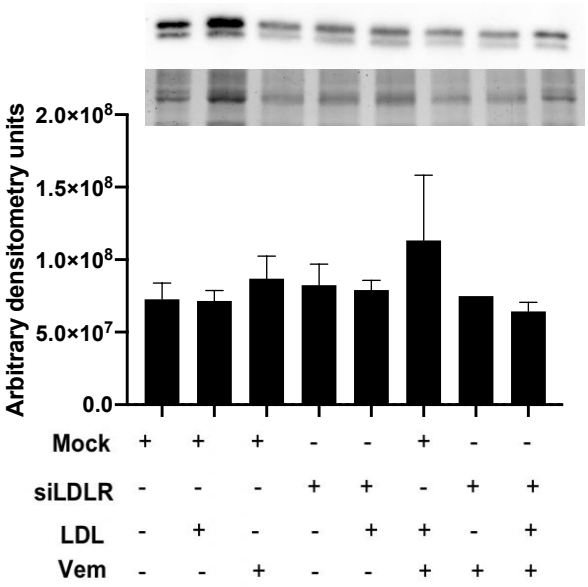

Figure S5. ERK protein expression panel in BCPAP cell line treated with LDL, siLDLR and/or vemurafenib. Representative blot is shown of ERK. Stain-Free (SF) gel was used as the loading control. Graph shows densitometry analysis of the Western Blots of ERK after siLDLR, LDL (200 μg/mL ApoB) incubation and/or vemurafenib treatment (1 μM) for 48 h in comparison to LDL-alone condition (LDL + DMSO 0,1% + Mock).

SUPPLEMENTARY MATERIAL: Cell lines and cell culture

The supplementary experiments depicted in Figure S6 were carried out on cell lines derived from anaplastic human thyroid carcinoma, CAL-62 (bearing KRAS p.G12), and 8505C (bearing the BRAF V600E oncogene). Both cell lines were provided by Paolo Vigneri of Azienda Ospedaliero Universitaria Policlinico Vittorio Emanuele Catania, Catania, Sicilia, IT. CAL-62 cells were cultured in DMEM High Glucose and 8505C cells were cultured in RPMI 1940, both mediums were supplemented with 10% FBS, 100 U/ml penicillin, and 1 μg/ml streptomycin at 37 °C in a 5% CO2 atmosphere.

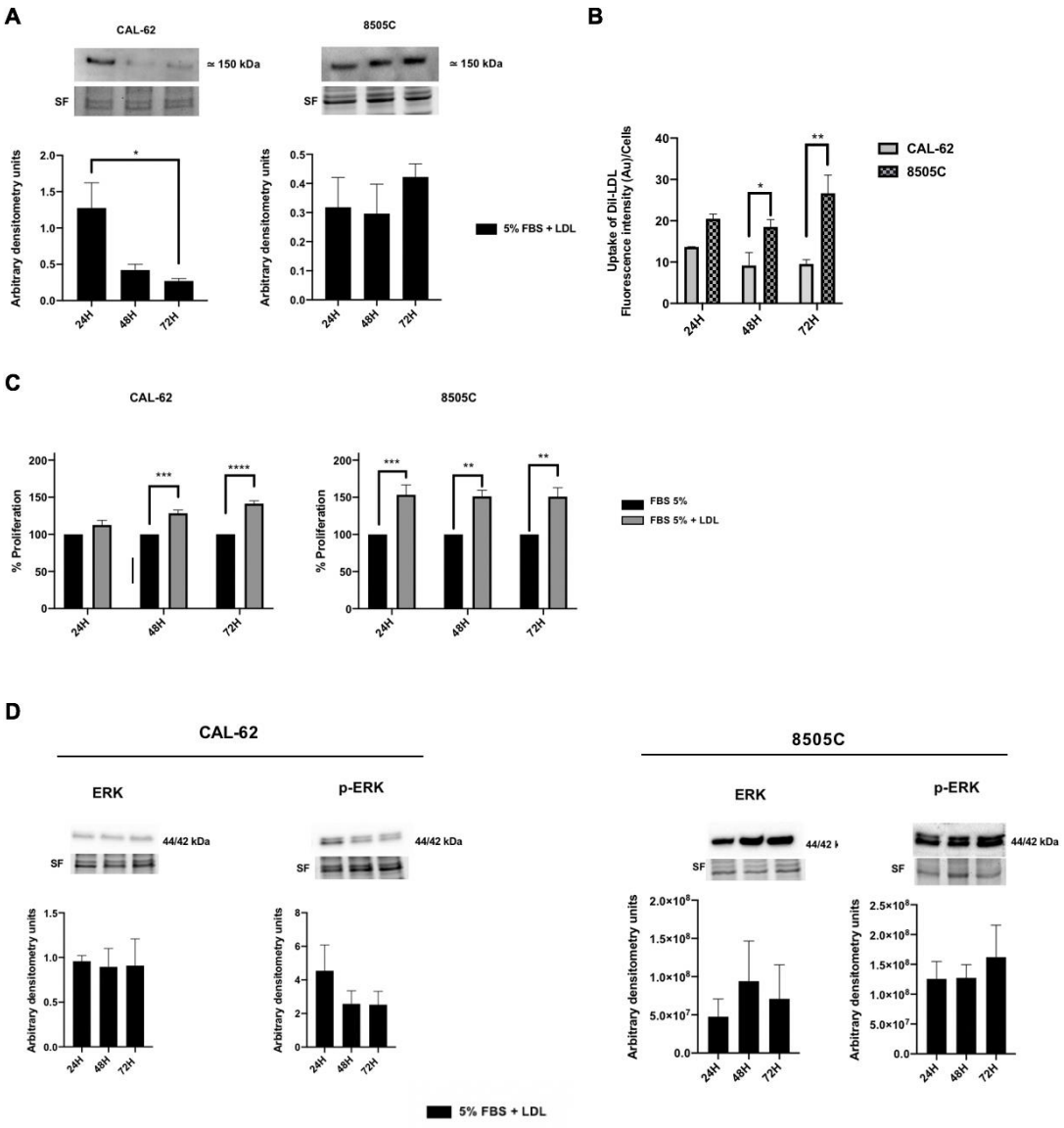

Figure S6. LDLR protein expression, 19-dioctadecyl-3,3,39,39-tetramethyl indocarbocyanine (DiI)-LDL uptake, percentage of cellular proliferation and RAS/RAF/MAPK (MEK)/ERK pathway expression in CAL-62 and 8505C cell lines. A) Cells were treated with LDL (200 µg/mL ApoB) and harvested at 24 h, 48 h, and 72 h before analysis. One representative blot is shown: Stain-Free gel (SF) was used as the loading control. Graphs show densitometry of the Western Blots relative to LDL-treated cells. Statistical test: A one-way ANOVA test plus Tukey's multiple comparisons test (*p = 0.032). Data are expressed as mean ± SEM of a minimum of three independent experiments (n = 3). (B) Cells were exposed to DiI-LDL (200 µg/mL ApoB) for 24 h, 48 h, and 72 h before analysis for mean fluorescence intensity by fluorescence spectrometer to compare LDL uptake between both cell lines. Statistical analysis: A two-way ANOVA

test plus Sidak's multiple comparisons test were performed to compare the DiI-LDL uptake between the two groups at each time point (*p < 0.03, **p < 0.002). Data are expressed as mean ± SEM of a minimum of three independent experiments (n = 3). C) Percentage of cellular proliferation determined by MTT assay of the CAL-62 and 8505C cell lines. Cells were treated with basal conditions (5% FBS), as a control, or with LDL (200 μg/mL ApoB) for 24 h, 48 h, and 72 h. Statistical analysis: A two-way ANOVA test plus Sidak's multiple comparisons test were performed to compare both groups (***p = 0.0007, ****p < 0.001). Data are expressed as mean ± SEM of three independent experiments (n = 3) carried out in quintuplicate. D) Western blot analysis for RAS/RAF/MAPK (MEK)/ERK pathways. CAL-62 and 8505C cells were treated with LDL (200 μg/mL ApoB) and harvested at 24 h, 48 h, and 72 h. Representatives blots are shown. SF gel was used as the loading control. Graphs show densitometry of the Western Blots. Statistical analysis: A one-way ANOVA test plus Tukey's multiple comparisons test. Data are expressed as mean ± SEM of a minimum of three independent experiments (n = 3).

Chapter V

- GENERAL DISCUSSION -

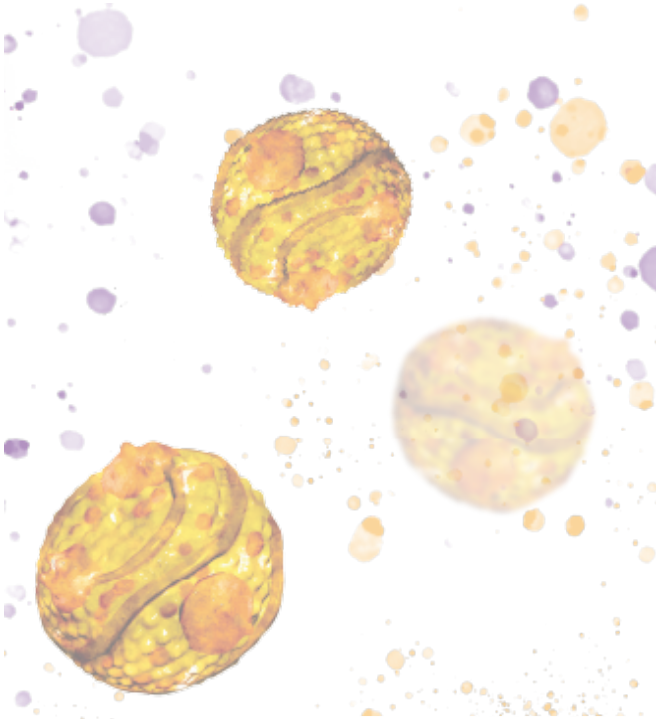

1. The Role of Cholesterol in Cancer Progression: Impact of both Cholesterol Biosynthesis and Dietary/Dyslipidemia-related Cholesterol on Tumor Development.

Cancer is a multifactorial disease affected by many important metabolic disorders, with the reprogramming of lipid metabolism an emerging hallmark of cancer[108,109]. The etiopathogenesis of this disease is primarily driven by gene mutations that promote a constitutive activation of growth factor receptors, downstream signaling cascades, as well as a rewiring of metabolic processes that supply cancer with resources and energy to thrive in a specific microenvironment[109].

The role of cholesterol in cancer was first described in the 1900s, and it has been implicated in the etiology of cancer as a disease even before DNA mutations. These first studies reported that cholesterol crystallization in normal cells promoted malignancy, and they noticed increased levels of cholesterol in tumor tissues and altered levels in patients' blood. Moreover, the mevalonate pathway has an important role in oncogenesis and drug resistance[110]. In this regard, highly proliferative cancer cells demonstrate a strong lipid and cholesterol avidity which they satisfy by either increasing the acquisition of exogenous (or dietary) lipids and lipoproteins or through the overactivation of their endogenous synthesis[65,108].

Taken together, this provides an interesting link with diet and obesity that has been supported by several epidemiological studies. Diets rich in saturated fat and cholesterol, obesity and dyslipidemias such as hypercholesterolemia, have been associated with increased risk of many cancers and may lead to increased cancer-related mortality[109]. Obesity is considered one of the most important risk factors for several types of cancer, accounting for more than 14% and 20% of cancer deaths in men and women, respectively. However, due to its complexity and multifactorial nature, it is yet to describe the exact link between them. Some of the mechanisms of action proposed in the context of cancers are by inducing the inflammation through cytokines, insulin resistance, hypercholesterolemia, TME disruption, and increasing the local production of sex hormones biosynthesis, such as estrogen in the adipose tissue[72,88]. Nevertheless, the relationship between cholesterol metabolism and its main metabolite 27-HC on TC progression remains poorly understood. In this context, the

effects of LDL and 27-HC studied in this project exploit the actively-targeted strategy towards cholesterol metabolism in TC tumors with aggressive behavior[63,64,102,111,112].

2. The deregulation of cholesterol metabolite 27-HC homeostasis promotes TC malignancy.

The extensive analysis of serum lipid profiles as well as the tumor samples of patients studied in the first publication yielded considerable differences in terms of cholesterol-related factors depending on tumors histological patterns. Patients suffering from tumors with more aggressive behavior demonstrated a significant decrease in serum LDL-C and ApoB; together with an overexpression of the *LDLR* gene expression and increased intratumoral levels of 27-HC in tumors samples with worse prognosis. Similar findings were reported by Niendorf A. et al., who observed that increased expression of LDLR in colon cancer cells led to decreased blood cholesterol levels[113]. These data underline the potential association of serum lipid level with cancer risk, pathology, and prognosis as well as reinforce our hypothesis that the most malignant tumors present higher systemic cholesterol uptake, which can modulate tumoral processes[114–116]. It is well known that the regulation of the cholesterol metabolism is complex. Therefore, one feature of some malignant tumors is the existence of an imbalance between the intracellular accumulation of cholesterol and the inhibition of cholesterol storage machinery[117–119].

Our results demonstrated that the tumor tissue expression of the *HMGCR* gene, the rate-limiting enzyme of the mevalonate pathway and responsible for the '*novo*' biosynthesis, was downregulated in tumors with higher levels of 27-HC, which corresponded to PDTC and ATC. In our case, the most malignant tumors attempted to counterbalance the significant increase in cholesterol uptake via the LDLR by reducing the '*novo*' biosynthesis. A relationship has been established between the levels of 27-HC and the expression of ER, confirming that this oxysterol acts as an agonist or antagonist selective modulator of these receptors depending on the cell type[120]. In relation to epithelial-type TC, it is notable that there is a higher incidence of this cancer type in females. This observation likely indicates a potential connection with the expression of ER in the follicular thyroid epithelium. However, there is a lack of sufficient reported data identifying the expression of these sexual steroid receptors and their association with neoplastic follicular cells[121]. In our study, we investigated the expression of estrogen receptors (alpha and beta) in a series of tumor samples, and the findings revealed that both benign and malignant tumors exhibited expression of both receptor types. These results align with observations in breast cancer, where ER-negative

tumors tend to exhibit faster growth and a worse prognosis. Furthermore, the absence of ER isoform β expression may lead to a decrease in apoptosis. Interestingly, these findings contrast with the potential effect of 27-HC as an endogenous ligand for ER, which has been implicated in promoting the growth of ER-positive breast tumors[91,122]. Thus, studies of the potential effects of 27-HC on ER-independent tumorigenic processes are warranted. Furthermore, the most malignant tumors exhibited an elevated accumulation of 27-HC, primarily attributed to the reduced expression of CYP7B1, the key enzyme responsible for 27-HC degradation[91,122].

In recent years, research interests have focused on the role of oxysterols in tumor growth and metastasis, with special attention toward 27-HC, the most abundant oxysterol in the systemic human circulation[88]. Moreover, research on the 27-HC signaling axis has revealed that the overexpression of the *CYP27A1* gene and the downregulation of the *CYP7B1* gene have been associated with a poorer prognosis in certain types of cancer[123,124]. In this context, the most aggressive tissues analyzed in our study (PTC high risk and PDTC/ATC) demonstrated a strong downregulation of *CYP7B1* in comparison to benign tumors, closely correlated with high concentrations of 27-HC. Moreover, it is important to mention that 27-HC is also involved in the regulation of the nuclear receptor *LXR* expression. This gene plays a role in controlling cell cycle progression and is implicated in metastasis processes as well. Interestingly, the *LXR* gene is responsible for regulating LDLR degradation in the liver and the conversion of cholesterol to bile acids through CYP27A1. Our data has shown that the most malignant tumors exhibited downregulated levels of *LXR*, which could directly impact LDLR degradation and promote increased LDL uptake capacity of tumors[125–127]. All these findings together indicate that the accumulation of 27-HC in thyroid cells may promote the progression of TC. However, it is worth noting the potential dual effect of 27-HC as it has been observed that this cholesterol metabolite can downregulate the expression of Nrf-2 signaling pathways, leading to the promotion of ROS generation, inflammation, and apoptotic-mediated cell death. Hence, it appears that the effect of 27-HC is cell-line-specific, and further studies on this oxysterol should be conducted to establish its precise role in the progression of TC[128–131].

3. LDLR is a key driver of aggressiveness in thyroid tumor cells.

Taking everything into consideration, a clear relationship between malignancy and high LDL uptake is evident in TC. This leads us to propose LDLR as one of the cornerstones in the relationship between TC and cholesterol. Preclinical studies reported a higher LDLR expression in some malignant tumors such as colon cancer, where LDL increased the proliferation of these tumor cells through the activation of oncogenic signaling cascades[40]. In tumorigenic processes, LDL is a critical lipoprotein that transfers cholesterol from the liver to peripheral tissues. Cancer cells present high demands of energy associated with the rapid growth of tumors that supply increasing LDLR expression in the cell membrane surface. Therefore, circulating LDL binds to LDLR, and it is internalized through endocytosis, hydrolyzed by lipases, and finally free cholesterol is released for cell utilization. Some recent studies have found that LDLR is over-expressed in several types of cancers such as hepatocellular carcinoma, lung cancer, breast cancer, colorectal cancer, prostate cancer, and so on. Additionally, this lipid metabolism abnormality could lead to increased ROS levels that promote a gradual increment in oxidative stress. Consequently, intracellular LDL becomes oxidized (ox-LDL) which can further promotes DNA damage in cancers resulting in malignant transformation and carcinogenesis[52]. Our *in vitro* studies have determined that in a high LDL environment, the LDL could promote cellular proliferation and migration in a dose-dependent manner in both papillary (TPC1 and BCPAP) and anaplastic cell lines (CAL-62 and 8505C), through LDLR. Consistent with these findings, the *in vivo* analysis conducted in a xenograft mouse model of ATC, included in the Annex II of this dissertation, demonstrated that mice fed a high-fat diet exhibited larger and more highly vascularized tumors compared to mice fed a conventional diet. Obesity induced by a high-fat diet not only stimulated thyroid tumor growth but also promoted anaplastic change in the TC in a mouse model that spontaneously develops TC, ThrbPV/PVPten+/− mice, via the STAT3 signaling pathway[132].

4. LDLR-signaling pathway is directly linked to MAPK signaling pathway in a synergic effect with *BRAF*^{V600E} mutation.

Several signaling pathways involved in processes such as proliferation and migration, including the Wnt, Hedgehog, and mTORC1 pathways, among others, have been extensively studied for their susceptibility to modulation via elevated cholesterol levels[133]. However, it seems that the impact of LDL on these signaling cascades is cancer-type-specific. In the

present thesis, we carried out a study to elucidate the LDL-signaling transduction pathway of potentiated proliferation, loss of adhesion and migration processes in human tumoral thyroid cell lines with different degrees of aggressiveness. In this context, we analyzed the effects of LDL on the most relevant signaling pathways, namely PI3K/AKT/mTOR and RAS-RAF-MAPK (MEK) ERK, that present the most frequent mutations in TC. Our results in papillary cell lines TPC1 (bearing *RET/PTC* rearrangement) and BCPAP (bearing the $BRAF^{V600E}$ oncogene) as well as in anaplastic cell lines CAL-62 (harboring *KRAS* mutation) and 8505C (bearing the $BRAF^{V600E}$ oncogene) after LDL incubation resulted in an increase of p-ERK protein expression. Interestingly, cell lines harboring *BRAF* mutation, namely BCPAP and 8505C, presented a totally deregulated LDLR, what promoted a continuous and higher LDL uptake and a consequently greater increase in malignancy. Alternatively, TPC1 and CAL-62 cell lines (both wild-type for *BRAF* mutation) were capable of regulating LDLR expression to prevent excessive intracellular cholesterol levels. However, this LDLR regulation did not completely prevent the promotion of LDL-induced proliferation and migration, although to a lesser extent compared to cells bearing *BRAF* mutation. All these data are in line with previous studies performed by Velarde V. et al., who established a crosstalk between native LDL and ERK phosphorylation through the MAPK pathway in vascular smooth muscle cells[134].

Following our studies on the BCPAP cell line, we further confirmed a clear connection between these two factors by simultaneously modulation of the LDLR and MAPK pathway using a siRNA and vemurafenib (a MEK inhibitor), respectively.

Firstly, we found that $BRAF^{V600E}$-mediated oncogenic signaling was partially blocked by vemurafenib in the BCPAP cell line treated with LDL, causing a decrease in the p-ERK signaling pathway. Consequently, proliferation decreased, as expected, following the same results reported by Xing et al., in different TC cell lines[135]. Interestingly, we observed a connection between the RAS/RAF/MAPK (MEK)/ERK and LDL signaling pathways when vemurafenib induced significant downregulation of LDLR and attenuated cell proliferation promoted by LDL exposure in the BCPAP cell line. These findings suggest that vemurafenib can regulate the gene transcription of *LDLR* in the BCPAP cell line, which, to our knowledge, is a novel observation. In contrast, no significant changes were observed in LDLR or p-ERK levels in the TPC1 cell line, which was used as a control. This suggests that vemurafenib has an indirect effect on LDLR expression, probably mediated via *BRAF* mutation, and it rules out the possibility of cytotoxic effects of the drug. Moreover, the combination of siRNA-mediated targeting of LDLR along with vemurafenib under LDL-

treated conditions led to a significant reduction in LDL-induced ERK phosphorylation and cellular proliferation. These results indicate a synergistic effect between LDL and the *BRAF* mutation in TC. Similar synergistic effects between LDL signaling and $BRAF^{V600E}$ have been described in melanoma, colorectal, and lung cancer cells[68,136–138].

5. Current targeted therapy studies for TC and future perspectives of using statins in combination with TKI for high-risk PTC.

To date, when there is no other choice of cure with the conventional therapy, the most suitable systemic treatment for iodine-refractory DTC, ATC, and MTC is using TKI. Nevertheless, despite this therapeutic alternative, these tumors require a multimodal treatment approach, including surgery, radioiodine therapy, and external beam radiotherapy, to optimize the patient's chances of improved survival.

Sorafenib and lenvatinib, both members of the multikinase inhibitors family that block VEGFR, were approved for TC with bad prognosis in 2015 by the European Medicine Agency (EMA; https://www.ema.europa.eu/) and are the first choice of oncologists in this context. However, when tumors become resistant to these drugs, there is no established strategy to guide the treatment.

In this scenario and due to the fact that up to 50% of people with PTC carry the $BRAF^{V600E}$ mutation, it has been hypothesized that the use of the BRAF inhibitor, vemurafenib, which is already approved and widely used for patients with melanoma bearing this mutation, could provide another treatment option[139,140].

Regarding TC, vemurafenib has been the first drug to show a dramatic response in ATC patients; and for this reason, we chose this inhibitor when we proposed the study included in the present dissertation[141]. Currently, vemurafenib is under phase II clinical trials for PTC and ATC patients bearing the *BRAF* mutation, resulting in an improvement of long-term patient survival and restoring RAI uptake and efficacy[142,143]. However, it is important to mention that despite the benefit of BRAF inhibition in BRAF-mutated tumors, some patients eventually acquired resistance to this therapy after a certain period of time, and approximately 65% of patients treated with vemurafenib developed serious adverse events such as fatigue, diarrhea, pneumonia and squamous cell carcinomas, sometimes even resulting in patient death[143]. For that reason, this treatment warrants further investigation in

a phase III setting to better define the patient profile that can benefit from this therapy to minimize the side effects. In this context, other *BRAF*^{V600E}–targeting drugs are under current investigation such as the treatment using dabrafenib alone or in combination with trametinib. These inhibitors are yielding impressive results that include improving the long-term survival, duration of response, and overall survival of ATC, although they are not exempt from side effects similar to vemurafenib. Nevertheless, thus far no cases of death have been reported due to its use[144,145].

Drug repositioning/rediscovery is a novel strategy aimed at identifying new and advanced uses for preapproved drugs or existing medications. In this context, after confirming the potential role of cholesterol in tumor progression, studies of possible benefits in combining statins with conventional oncogenic treatments are emerging. Currently, there are some discrepancies about the antineoplastic efficacy of statins. While it is true that some studies associate the use of statins with an increased risk of TC, many others not only refute this association but also present promising results associated with antineoplastic effects and reduced cancer-related mortality[146–148]. It is important to highlight the study conducted by Zeybek, ND. et al., which demonstrated that in primary human cellular cultures of PTC cells and cell lines (such as BCPAP) exposed to rosuvastatin, the drug exhibited the ability to induce vacuolization, autophagosomes, and eventually apoptosis[149]. Furthermore, research on ATC cell lines revealed similar effects on proliferation, migration, and apoptosis when using lovastatin. Interestingly, in mice models, the combination of lovastatin with TKI treatments showed even greater effects. These findings underscore the potential of statins as a therapeutic option in the treatment of TC[149–151]. Treatments using statins in combination with TKI report promising results in lung cancer, but no studies have been published using TKI inhibitors in combination with statins in TC[152].

Overall, this thesis presents compelling evidence that LDL and its metabolite 27-HC play an important role in the progression of TC. Additionally, LDL can induce synergistic effects on *BRAF*-mutant tumors by hyperactivating the MAPK pathway, potentially leading to a worse prognosis and as described in previous studies, facilitating the high-risk PTC transition to ATC or to tumors with a high-risk of developing recurrent disease and increasing resistance to RAI.

In summary, future research should concentrate on a more in-depth study of the molecular pathways and resistance mechanisms and should explore the potential of combining targeted therapy with statins for high-risk PTC patients.

Chapter VI

- CONCLUSIONS -

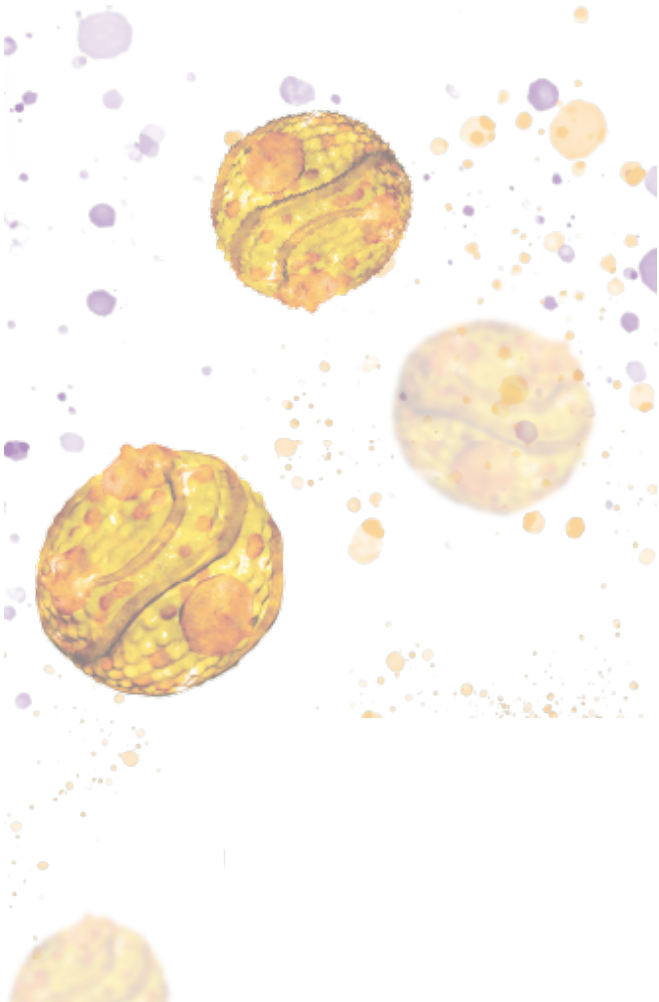

<u>Publication 1:</u> Cholesterol and 27-Hydroxycholesterol Promote Thyroid Carcinoma Aggressiveness.

- Low LDL-C levels in serum, *LDLR* upregulation, and *HMGCR* downregulation in tumors samples were linked with high-risk PTC and dedifferentiated tumors (PDTC/ATC).
- Cholesterol and intratumoral accumulation of 27-HC promoted the aggressive behavior of PTC.
- LDL promoted similar levels of cell proliferation in both the benign thyroid cell line (Nthy-ori 3-1) and in the ATC cell line. Nevertheless, LDL only was able to promote migration in the ATC cell line.
- Targeting the enzymes: *CYP27A1* and *CYP7B1*, which are responsible for the formation and degradation of 27-HC, respectively, could be a new therapeutic strategy to regulate tumor cell proliferation.

<u>Publication 2:</u> Low-Density Lipoprotein Receptor is a Key Driver of Aggressiveness in Thyroid Tumor Cells.

- LDLR expression was differentially regulated in TC cell lines with different $BRAF^{V600E}$ status, modulating the LDL uptake and leading to variations in the cellular processes, such as proliferation, migration, and adhesion ability.
- Vemurafenib, a drug targeting $BRAF^{V600E}$ mutation, partially blocked *BRAF* mutant oncogenic effects in TC cell lines and downregulated LDLR expression, attenuating LDL-induced cell proliferation and suggesting a synergistic effect between LDL and the $BRAF^{V600E}$ mutation in TC.
- LDL plays a role as a co-adjuvant with $BRAF^{V600E}$ in promoting oncogenic processes in BCPAP cells by hyperactivating the RAS/RAF/MAPK (MEK)/ERK signaling cascade.

GENERAL CONCLUSIONS:

- LDL and intratumoral accumulation of 27-HC promote the aggressive behavior process of PTC.

- Targeting LDLR and cholesterol metabolism together with the RAS/RAF/MAPK (MEK)/ERK signaling cascade could be a new therapeutic strategy for PTC with more aggressive behavior, especially in those harboring *BRAF*^{V600E}.

- REFERENCES -

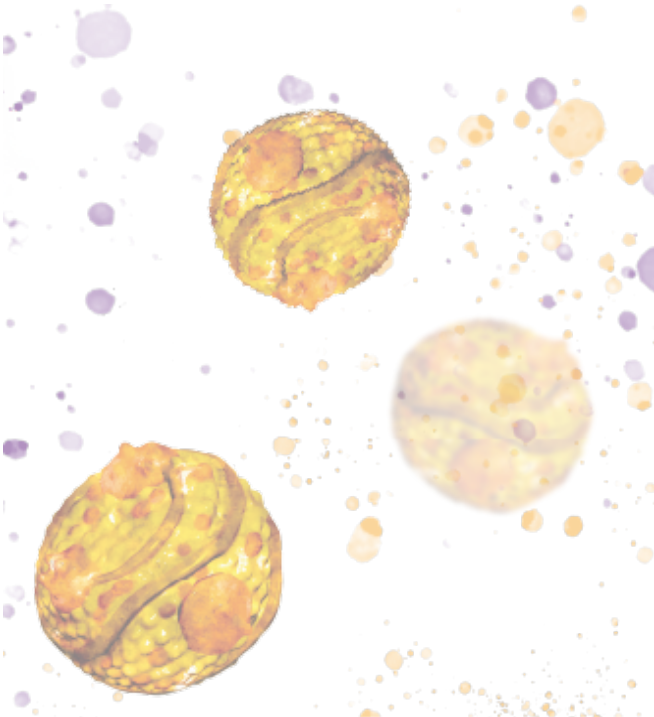

REFERENCES

1. Khan YS, Farhana A. Histology, Thyroid Gland. In: *StatPearls*. StatPearls Publishing; 2023. Accessed July 25, 2023. http://www.ncbi.nlm.nih.gov/books/NBK551659/

2. Parameswaran R, Brooks S, Sadler GP. Molecular pathogenesis of follicular cell derived thyroid cancers. *Int J Surg Lond Engl*. 2010;8(3):186-193. doi:10.1016/j.ijsu.2010.01.005

3. Armstrong M, Asuka E, Fingeret A. Physiology, Thyroid Function. In: *StatPearls*. StatPearls Publishing; 2023. Accessed July 25, 2023. http://www.ncbi.nlm.nih.gov/books/NBK537039/

4. Gomes-Lima C, Burman KD. Reverse T_3 or perverse T_3? Still puzzling after 40 years. *Cleve Clin J Med*. 2018;85(6):450-455. doi:10.3949/ccjm.85a.17079

5. Christofer Juhlin C, Mete O, Baloch ZW. The 2022 WHO classification of thyroid tumors: novel concepts in nomenclature and grading. *Endocr Relat Cancer*. 2023;30(2):e220293. doi:10.1530/ERC-22-0293

6. Kim MJ, Won JK, Jung KC, et al. Clinical Characteristics of Subtypes of Follicular Variant Papillary Thyroid Carcinoma. *Thyroid Off J Am Thyroid Assoc*. 2018;28(3):311-318. doi:10.1089/thy.2016.0671

7. Jannin A, Escande A, Al Ghuzlan A, et al. Anaplastic Thyroid Carcinoma: An Update. *Cancers*. 2022;14(4):1061. doi:10.3390/cancers14041061

8. Lamartina L, Grani G, Arvat E, et al. 8th edition of the AJCC/TNM staging system of thyroid cancer: what to expect (ITCO#2). *Endocr Relat Cancer*. 2018;25(3):L7-L11. doi:10.1530/ERC-17-0453

9. Kitahara CM, Schneider AB. Epidemiology of Thyroid Cancer. *Cancer Epidemiol Biomark Prev Publ Am Assoc Cancer Res Cosponsored Am Soc Prev Oncol*. 2022;31(7):1284-1297. doi:10.1158/1055-9965.EPI-21-1440

10. Bogović Crnčić T, Ilić Tomaš M, Girotto N, Grbac Ivanković S. Risk Factors for Thyroid Cancer: What Do We Know So Far? *Acta Clin Croat*. 2020;59(Suppl 1):66-72. doi:10.20471/acc.2020.59.s1.08

11. Hieu TT, Russell AW, Cuneo R, et al. Cancer risk after medical exposure to radioactive iodine in benign thyroid diseases: a meta-analysis. *Endocr Relat Cancer*. 2012;19(5):645-655. doi:10.1530/ERC-12-0176

12. Rahman ST, Pandeya N, Neale RE, et al. Obesity Is Associated with *BRAF*^{V600E}-Mutated Thyroid Cancer. *Thyroid*. 2020;30(10):1518-1527. doi:10.1089/thy.2019.0654

13. Luzón-Toro B, Fernández RM, Villalba-Benito L, Torroglosa A, Antiñolo G, Borrego S. Influencers on Thyroid Cancer Onset: Molecular Genetic Basis. *Genes*. 2019;10(11):913. doi:10.3390/genes10110913

14. Singh A, Ham J, Po JW, Niles N, Roberts T, Lee CS. The Genomic Landscape of Thyroid Cancer Tumourigenesis and Implications for Immunotherapy. *Cells*. 2021;10(5):1082. doi:10.3390/cells10051082

15. Pozdeyev N, Gay LM, Sokol ES, et al. Genetic Analysis of 779 Advanced Differentiated and Anaplastic Thyroid Cancers. *Clin Cancer Res*. 2018;24(13):3059-3068. doi:10.1158/1078-0432.CCR-18-0373

16. Nikiforov YE. Thyroid carcinoma: molecular pathways and therapeutic targets. *Mod Pathol Off J U S Can Acad Pathol Inc*. 2008;21 Suppl 2(Suppl 2):S37-43.

doi:10.1038/modpathol.2008.10

17. Barreno LRQ, Mello JBHD, Barros-Filho MC, et al. Characterization of BRAF mutation in patients older than 45 years with well-differentiated thyroid carcinoma. *Braz J Otorhinolaryngol.* 2022;88(4):523-528. doi:10.1016/j.bjorl.2020.07.007

18. Quintero-Fabián S, Arreola R, Becerril-Villanueva E, et al. Role of Matrix Metalloproteinases in Angiogenesis and Cancer. *Front Oncol.* 2019;9:1370. doi:10.3389/fonc.2019.01370

19. Fallahi P, Ferrari SM, Galdiero MR, et al. Molecular targets of tyrosine kinase inhibitors in thyroid cancer. *Semin Cancer Biol.* 2022;79:180-196. doi:10.1016/j.semcancer.2020.11.013

20. Mohamad Pakarul Razy NH, Wan Abdul Rahman WF, Win TT. Expression of Vascular Endothelial Growth Factor and Its Receptors in Thyroid Nodular Hyperplasia and Papillary Thyroid Carcinoma: A Tertiary Health Care Centre Based Study. *Asian Pac J Cancer Prev APJCP.* 2019;20(1):277-282. doi:10.31557/APJCP.2019.20.1.277

21. McKelvey BA, Umbricht CB, Zeiger MA. Telomerase Reverse Transcriptase (TERT) Regulation in Thyroid Cancer: A Review. *Front Endocrinol.* 2020;11:485. doi:10.3389/fendo.2020.00485

22. Salvatore D, Santoro M, Schlumberger M. The importance of the RET gene in thyroid cancer and therapeutic implications. *Nat Rev Endocrinol.* 2021;17(5):296-306. doi:10.1038/s41574-021-00470-9

23. Armstrong MJ, Yang H, Yip L, et al. *PAX8/PPARγ* Rearrangement in Thyroid Nodules Predicts Follicular-Pattern Carcinomas, in Particular the Encapsulated Follicular Variant of Papillary Carcinoma. *Thyroid.* 2014;24(9):1369-1374. doi:10.1089/thy.2014.0067

24. Mishra P, Laha D, Grant R, Nilubol N. Advances in Biomarker-Driven Targeted Therapies in Thyroid Cancer. *Cancers.* 2021;13(24):6194. doi:10.3390/cancers13246194

25. Grani G, Ramundo V, Verrienti A, Sponziello M, Durante C. Thyroid hormone therapy in differentiated thyroid cancer. *Endocrine.* 2019;66(1):43-50. doi:10.1007/s12020-019-02051-3

26. Biondi B, Cooper DS. Thyroid Hormone Suppression Therapy. *Endocrinol Metab Clin North Am.* 2019;48(1):227-237. doi:10.1016/j.ecl.2018.10.008

27. Biondi B, Cooper DS. Benefits of Thyrotropin Suppression Versus the Risks of Adverse Effects in Differentiated Thyroid Cancer. *Thyroid.* 2010;20(2):135-146. doi:10.1089/thy.2009.0311

28. Haugen BR, Alexander EK, Bible KC, et al. 2015 American Thyroid Association Management Guidelines for Adult Patients with Thyroid Nodules and Differentiated Thyroid Cancer: The American Thyroid Association Guidelines Task Force on Thyroid Nodules and Differentiated Thyroid Cancer. *Thyroid Off J Am Thyroid Assoc.* 2016;26(1):1-133. doi:10.1089/thy.2015.0020

29. Schlumberger M, Brose M, Elisei R, et al. Definition and management of radioactive iodine-refractory differentiated thyroid cancer. *Lancet Diabetes Endocrinol.* 2014;2(5):356-358. doi:10.1016/S2213-8587(13)70215-8

30. Porter A, Wong DJ. Perspectives on the Treatment of Advanced Thyroid Cancer: Approved Therapies, Resistance Mechanisms, and Future Directions. *Front Oncol.* 2021;10:592202. doi:10.3389/fonc.2020.592202

31. Brose MS, Nutting CM, Jarzab B, et al. Sorafenib in radioactive iodine-refractory,

locally advanced or metastatic differentiated thyroid cancer: a randomised, double-blind, phase 3 trial. *The Lancet*. 2014;384(9940):319-328. doi:10.1016/S0140-6736(14)60421-9

32. Schlumberger M, Tahara M, Wirth LJ, et al. Lenvatinib versus Placebo in Radioiodine-Refractory Thyroid Cancer. *N Engl J Med*. 2015;372(7):621-630. doi:10.1056/NEJMoa1406470

33. Chapman PB, Hauschild A, Robert C, et al. Improved Survival with Vemurafenib in Melanoma with BRAF V600E Mutation. *N Engl J Med*. 2011;364(26):2507-2516. doi:10.1056/NEJMoa1103782

34. Kim KB, Cabanillas ME, Lazar AJ, et al. Clinical Responses to Vemurafenib in Patients with Metastatic Papillary Thyroid Cancer Harboring BRAF ^{V600E} Mutation. *Thyroid*. 2013;23(10):1277-1283. doi:10.1089/thy.2013.0057

35. Dadu R, Shah K, Busaidy NL, et al. Efficacy and Tolerability of Vemurafenib in Patients with BRAFV600E -Positive Papillary Thyroid Cancer: M.D. Anderson Cancer Center Off Label Experience. *J Clin Endocrinol Metab*. 2015;100(1):E77-E81. doi:10.1210/jc.2014-2246

36. Fröhlich E, Wahl R. Nanoparticles: Promising Auxiliary Agents for Diagnosis and Therapy of Thyroid Cancers. *Cancers*. 2021;13(16):4063. doi:10.3390/cancers13164063

37. Yao Y, Zhou Y, Liu L, et al. Nanoparticle-Based Drug Delivery in Cancer Therapy and Its Role in Overcoming Drug Resistance. *Front Mol Biosci*. 2020;7:193. doi:10.3389/fmolb.2020.00193

38. Xu H, Zhou S, Tang Q, Xia H, Bi F. Cholesterol metabolism: New functions and therapeutic approaches in cancer. *Biochim Biophys Acta BBA - Rev Cancer*. 2020;1874(1):188394. doi:10.1016/j.bbcan.2020.188394

39. Kulig W, Cwiklik L, Jurkiewicz P, Rog T, Vattulainen I. Cholesterol oxidation products and their biological importance. *Chem Phys Lipids*. 2016;199:144-160. doi:10.1016/j.chemphyslip.2016.03.001

40. Mayengbam SS, Singh A, Pillai AD, Bhat MK. Influence of cholesterol on cancer progression and therapy. *Transl Oncol*. 2021;14(6):101043. doi:10.1016/j.tranon.2021.101043

41. Patel KK, Kashfi K. Lipoproteins and cancer: The role of HDL-C, LDL-C, and cholesterol-lowering drugs. *Biochem Pharmacol*. 2022;196:114654. doi:10.1016/j.bcp.2021.114654

42. Huang B, Song B liang, Xu C. Cholesterol metabolism in cancer: mechanisms and therapeutic opportunities. *Nat Metab*. 2020;2(2):132-141. doi:10.1038/s42255-020-0174-0

43. King RJ, Singh PK, Mehla K. The cholesterol pathway: impact on immunity and cancer. *Trends Immunol*. 2022;43(1):78-92. doi:10.1016/j.it.2021.11.007

44. Griffiths WJ, Wang Y. Sterols, Oxysterols, and Accessible Cholesterol: Signalling for Homeostasis, in Immunity and During Development. *Front Physiol*. 2021;12:723224. doi:10.3389/fphys.2021.723224

45. Chen L, Ma MY, Sun M, et al. Endogenous sterol intermediates of the mevalonate pathway regulate HMGCR degradation and SREBP-2 processing. *J Lipid Res*. 2019;60(10):1765-1775. doi:10.1194/jlr.RA119000201

46. Xue L, Qi H, Zhang H, et al. Targeting SREBP-2-Regulated Mevalonate Metabolism for Cancer Therapy. *Front Oncol*. 2020;10:1510. doi:10.3389/fonc.2020.01510

47. Williams KJ. Molecular processes that handle — and mishandle — dietary lipids. *J*

Clin Invest. 2008;118(10):3247-3259. doi:10.1172/JCI35206

48. Chackalamannil S, Rotella D, Ward SE, eds. *Comprehensive Medicinal Chemistry III*. 3rd edition. Elsevier; 2017.

49. Real JT, Ascaso JF. Metabolismo lipídico y clasificación de las hiperlipemias. *Clínica E Investig En Arterioscler*. 2021;33:3-9. doi:10.1016/j.arteri.2020.12.008

50. Opplt JJ, Holzberg ES. Ultracentrifugal subclasses of low and intermediate density lipoproteins. *J Lipid Res*. 1994;35(3):510-523.

51. Martínez-Oliván J, Arias-Moreno X, Velazquez-Campoy A, Millet O, Sancho J. LDL receptor/lipoprotein recognition: endosomal weakening of ApoB and ApoE binding to the convex face of the LR5 repeat. *FEBS J*. 2014;281(6):1534-1546. doi:10.1111/febs.12721

52. Deng CF, Zhu N, Zhao TJ, et al. Involvement of LDL and ox-LDL in Cancer Development and Its Therapeutical Potential. *Front Oncol*. 2022;12:803473. doi:10.3389/fonc.2022.803473

53. Bayly GR. Lipids and disorders of lipoprotein metabolism. In: *Clinical Biochemistry: Metabolic and Clinical Aspects*. Elsevier; 2014:702-736. doi:10.1016/B978-0-7020-5140-1.00037-7

54. Benito-Vicente A, Uribe K, Jebari S, Galicia-Garcia U, Ostolaza H, Martin C. Validation of LDLr Activity as a Tool to Improve Genetic Diagnosis of Familial Hypercholesterolemia: A Retrospective on Functional Characterization of LDLr Variants. *Int J Mol Sci*. 2018;19(6):1676. doi:10.3390/ijms19061676

55. Morris SM, Cooper JA. Disabled-2 Colocalizes with the LDLR in Clathrin-Coated Pits and Interacts with AP-2: Dab2 Interacts with AP-2. *Traffic*. 2001;2(2):111-123. doi:10.1034/j.1600-0854.2001.020206.x

56. Islam MM, Hlushchenko I, Pfisterer SG. Low-Density Lipoprotein Internalization, Degradation and Receptor Recycling Along Membrane Contact Sites. *Front Cell Dev Biol*. 2022;10:826379. doi:10.3389/fcell.2022.826379

57. Sirinian MI, Belleudi F, Campagna F, et al. Adaptor Protein ARH Is Recruited to the Plasma Membrane by Low Density Lipoprotein (LDL) Binding and Modulates Endocytosis of the LDL/LDL Receptor Complex in Hepatocytes. *J Biol Chem*. 2005;280(46):38416-38423. doi:10.1074/jbc.M504343200

58. Qin Y, Ting F, Kim MJ, et al. Phosphatidylinositol-(4,5)-Bisphosphate Regulates Plasma Cholesterol Through LDL (Low-Density Lipoprotein) Receptor Lysosomal Degradation. *Arterioscler Thromb Vasc Biol*. 2020;40(5):1311-1324. doi:10.1161/ATVBAHA.120.314033

59. Friedman JR, DiBenedetto JR, West M, Rowland AA, Voeltz GK. Endoplasmic reticulum–endosome contact increases as endosomes traffic and mature. Hegde RS, ed. *Mol Biol Cell*. 2013;24(7):1030-1040. doi:10.1091/mbc.e12-10-0733

60. Bartuzi P, Billadeau DD, Favier R, et al. CCC- and WASH-mediated endosomal sorting of LDLR is required for normal clearance of circulating LDL. *Nat Commun*. 2016;7:10961. doi:10.1038/ncomms10961

61. Yang H xian, Zhang M, Long S yin, et al. Cholesterol in LDL receptor recycling and degradation. *Clin Chim Acta*. 2020;500:81-86. doi:10.1016/j.cca.2019.09.022

62. Gu J, Zhu N, Li HF, et al. Cholesterol homeostasis and cancer: a new perspective on the low-density lipoprotein receptor. *Cell Oncol*. 2022;45(5):709-728. doi:10.1007/s13402-022-00694-5

63. Iso H, Ikeda A, Inoue M, Sato S, Tsugane S, JPHC Study Group. Serum cholesterol levels in relation to the incidence of cancer: The JPHC study cohorts. *Int J Cancer*. 2009;125(11):2679-2686. doi:10.1002/ijc.24668

64. Kim HJ, Kim NK, Choi JH, et al. Associations between body mass index and clinico-pathological characteristics of papillary thyroid cancer. *Clin Endocrinol (Oxf)*. 2013;78(1):134-140. doi:10.1111/j.1365-2265.2012.04506.x

65. Antalis CJ, Uchida A, Buhman KK, Siddiqui RA. Migration of MDA-MB-231 breast cancer cells depends on the availability of exogenous lipids and cholesterol esterification. *Clin Exp Metastasis*. 2011;28(8):733-741. doi:10.1007/s10585-011-9405-9

66. Stranzl A, Schmidt H, Winkler R, Kostner GM. Low-density lipoprotein receptor mRNA in human breast cancer cells: Influence by PKC modulators. *Breast Cancer Res Treat*. 1997;42(3):195-205. doi:10.1023/A:1005754026205

67. Rudling MJ, Stahle L, Peterson CO, Skoog L. Content of low density lipoprotein receptors in breast cancer tissue related to survival of patients. *BMJ*. 1986;292(6520):580-582. doi:10.1136/bmj.292.6520.580

68. Scully T, Kase N, Gallagher EJ, LeRoith D. Regulation of low-density lipoprotein receptor expression in triple negative breast cancer by EGFR-MAPK signaling. *Sci Rep*. 2021;11(1):17927. doi:10.1038/s41598-021-97327-y

69. Wang Y, Yutuc E, Griffiths WJ. Cholesterol metabolism pathways – are the intermediates more important than the products? *FEBS J*. 2021;288(12):3727-3745. doi:10.1111/febs.15727

70. Kloudova A, Guengerich FP, Soucek P. The Role of Oxysterols in Human Cancer. *Trends Endocrinol Metab TEM*. 2017;28(7):485-496. doi:10.1016/j.tem.2017.03.002

71. Griffiths WJ, Wang Y. Oxysterols as lipid mediators: Their biosynthetic genes, enzymes and metabolites. *Prostaglandins Other Lipid Mediat*. 2020;147:106381. doi:10.1016/j.prostaglandins.2019.106381

72. Asghari A, Umetani M. Obesity and Cancer: 27-Hydroxycholesterol, the Missing Link. *Int J Mol Sci*. 2020;21(14):4822. doi:10.3390/ijms21144822

73. Brown AJ, Sharpe LJ, Rogers MJ. Oxysterols: From physiological tuners to pharmacological opportunities. *Br J Pharmacol*. 2021;178(16):3089-3103. doi:10.1111/bph.15073

74. Olkkonen VM, Béaslas O, Nissilä E. Oxysterols and their cellular effectors. *Biomolecules*. 2012;2(1):76-103. doi:10.3390/biom2010076

75. Kimbung S, Inasu M, Stålhammar T, et al. CYP27A1 expression is associated with risk of late lethal estrogen receptor-positive breast cancer in postmenopausal patients. *Breast Cancer Res*. 2020;22(1):123. doi:10.1186/s13058-020-01347-x

76. Cho H, Shen Q, Zhang LH, et al. CYP27A1-dependent anti-melanoma activity of limonoid natural products targets mitochondrial metabolism. *Cell Chem Biol*. 2021;28(10):1407-1419.e6. doi:10.1016/j.chembiol.2021.03.004

77. Kim D, Lee KM, Lee C, et al. Pathophysiological role of 27-hydroxycholesterol in human diseases. *Adv Biol Regul*. 2022;83:100837. doi:10.1016/j.jbior.2021.100837

78. Griffiths WJ, Abdel-Khalik J, Crick PJ, Yutuc E, Wang Y. New methods for analysis of oxysterols and related compounds by LC–MS. *J Steroid Biochem Mol Biol*. 2016;162:4-26. doi:10.1016/j.jsbmb.2015.11.017

79. Canagarajah BJ, Hummer G, Prinz WA, Hurley JH. Dynamics of cholesterol exchange in the oxysterol binding protein family. *J Mol Biol*. 2008;378(3):737-748. doi:10.1016/j.jmb.2008.01.075

80. Komati R, Spadoni D, Zheng S, Sridhar J, Riley K, Wang G. Ligands of Therapeutic Utility for the Liver X Receptors. *Molecules*. 2017;22(1):88. doi:10.3390/molecules22010088

81. Zhao C, Dahlman-Wright K. Liver X receptor in cholesterol metabolism. *J Endocrinol*. 2010;204(3):233-240. doi:10.1677/JOE-09-0271

82. Rashkovan M, Albero R, Gianni F, et al. Intracellular Cholesterol Pools Regulate Oncogenic Signaling and Epigenetic Circuitries in Early T-cell Precursor Acute Lymphoblastic Leukemia. *Cancer Discov*. 2022;12(3):856-871. doi:10.1158/2159-8290.CD-21-0551

83. Bełtowski J. Liver X Receptors (LXR) as Therapeutic Targets in Dyslipidemia. *Cardiovasc Ther*. 2008;26(4):297-316. doi:10.1111/j.1755-5922.2008.00062.x

84. Repa JJ, Liang G, Ou J, et al. Regulation of mouse sterol regulatory element-binding protein-1c gene (SREBP-1c) by oxysterol receptors, LXRα and LXRβ. *Genes Dev*. 2000;14(22):2819-2830. doi:10.1101/gad.844900

85. Dambal S, Alfaqih M, Sanders S, et al. 27-Hydroxycholesterol Impairs Plasma Membrane Lipid Raft Signaling as Evidenced by Inhibition of IL6-JAK-STAT3 Signaling in Prostate Cancer Cells. *Mol Cancer Res MCR*. 2020;18(5):671-684. doi:10.1158/1541-7786.MCR-19-0974

86. Raza S, Meyer M, Goodyear C, Hammer KDP, Guo B, Ghribi O. The cholesterol metabolite 27-hydroxycholesterol stimulates cell proliferation via ERβ in prostate cancer cells. *Cancer Cell Int*. 2017;17(1):52. doi:10.1186/s12935-017-0422-x

87. Ma L, Cho W, Nelson ER. Our evolving understanding of how 27-hydroxycholesterol influences cancer. *Biochem Pharmacol*. 2022;196:114621. doi:10.1016/j.bcp.2021.114621

88. Nelson ER, Wardell SE, Jasper JS, et al. 27-Hydroxycholesterol Links Hypercholesterolemia and Breast Cancer Pathophysiology. *Science*. 2013;342(6162):1094-1098. doi:10.1126/science.1241908

89. Russell D. Oxysterol biosynthetic enzymes. *Biochim Biophys Acta BBA - Mol Cell Biol Lipids*. 2000;1529(1-3):126-135. doi:10.1016/S1388-1981(00)00142-6

90. Baek AE, Yu YRA, He S, et al. The cholesterol metabolite 27 hydroxycholesterol facilitates breast cancer metastasis through its actions on immune cells. *Nat Commun*. 2017;8(1):864. doi:10.1038/s41467-017-00910-z

91. Wu Q, Ishikawa T, Sirianni R, et al. 27-Hydroxycholesterol Promotes Cell-Autonomous, ER-Positive Breast Cancer Growth. *Cell Rep*. 2013;5(3):637-645. doi:10.1016/j.celrep.2013.10.006

92. Zhu D, Shen Z, Liu J, et al. The ROS-mediated activation of STAT-3/VEGF signaling is involved in the 27-hydroxycholesterol-induced angiogenesis in human breast cancer cells. *Toxicol Lett*. 2016;264:79-86. doi:10.1016/j.toxlet.2016.11.006

93. Sierralta W. 27-Hydroxycholesterol induces the transition of MCF7 cells into a mesenchymal phenotype. *Oncol Rep*. Published online April 28, 2011. doi:10.3892/or.2011.1284

94. Shen Z, Zhu D, Liu J, et al. 27-Hydroxycholesterol induces invasion and migration of breast cancer cells by increasing MMP9 and generating EMT through activation of

STAT-3. *Environ Toxicol Pharmacol*. 2017;51:1-8. doi:10.1016/j.etap.2017.02.001

95. Faubert B, Solmonson A, DeBerardinis RJ. Metabolic reprogramming and cancer progression. *Science*. 2020;368(6487):eaaw5473. doi:10.1126/science.aaw5473

96. Zhao J, Tian Y, Yao J, et al. Hypercholesterolemia Is an Associated Factor for Risk of Differentiated Thyroid Cancer in Chinese Population. *Front Oncol*. 2021;10:508126. doi:10.3389/fonc.2020.508126

97. Xiao X, Huang Y, Sadeghi F, et al. Carbohydrate, Lipid, and Apolipoprotein Biomarkers in Blood and Risk of Thyroid Cancer: Findings from the AMORIS Cohort. *Cancers*. 2023;15(2):520. doi:10.3390/cancers15020520

98. Lu J, Zhang Y, Sun M, et al. Multi-Omics Analysis of Fatty Acid Metabolism in Thyroid Carcinoma. *Front Oncol*. 2021;11:737127. doi:10.3389/fonc.2021.737127

99. Xu M, Sun T, Wen S, et al. Characteristics of lipid metabolism-related gene expression-based molecular subtype in papillary thyroid cancer. *Acta Biochim Biophys Sin*. 2020;52(10):1166-1170. doi:10.1093/abbs/gmaa092

100. Wen S, Luo YI, Wu W, et al. Identification of lipid metabolism-related genes as prognostic indicators in papillary thyroid cancer. *Acta Biochim Biophys Sin*. 2021;53(12):1579-1589. doi:10.1093/abbs/gmab145

101. Li C, Peng X, Lv J, et al. SREBP1 as a potential biomarker predicts levothyroxine efficacy of differentiated thyroid cancer. *Biomed Pharmacother*. 2020;123:109791. doi:10.1016/j.biopha.2019.109791

102. Xu L, Port M, Landi S, et al. Obesity and the Risk of Papillary Thyroid Cancer: A Pooled Analysis of Three Case–Control Studies. *Thyroid*. 2014;24(6):966-974. doi:10.1089/thy.2013.0566

103. Radding CM, Steinberg D. STUDIES ON THE SYNTHESIS AND SECRETION OF SERUM LIPOPROTEINS BY RAT LIVER SLICES. *J Clin Invest*. 1960;39(10):1560-1569. doi:10.1172/JCI104177

104. Schindelin J, Arganda-Carreras I, Frise E, et al. Fiji: an open-source platform for biological-image analysis. *Nat Methods*. 2012;9(7):676-682. doi:10.1038/nmeth.2019

105. Taylor SC, Posch A. The Design of a Quantitative Western Blot Experiment. *BioMed Res Int*. 2014;2014:1-8. doi:10.1155/2014/361590

106. Neris RLS, Dobles AMC, Gomes AV. Western Blotting Using In-Gel Protein Labeling as a Normalization Control: Advantages of Stain-Free Technology. In: Posch A, ed. *Proteomic Profiling*. Vol 2261. Methods in Molecular Biology. Springer US; 2021:443-456. doi:10.1007/978-1-0716-1186-9_28

107. Teupser, D.; Thiery, J.; Walli, AK.; Seidel, D. Quantitative Spectrofluorometry of DiI-Lipoprotein Uptake. Biochim Biophys Acta 1996, 1303, 193–198.

108. Beloribi-Djefaflia S, Vasseur S, Guillaumond F. Lipid metabolic reprogramming in cancer cells. *Oncogenesis*. 2016;5(1):e189-e189. doi:10.1038/oncsis.2015.49

109. Butler LM, Perone Y, Dehairs J, et al. Lipids and cancer: Emerging roles in pathogenesis, diagnosis and therapeutic intervention. *Adv Drug Deliv Rev*. 2020;159:245-293. doi:10.1016/j.addr.2020.07.013

110. Guerra B, Recio C, Aranda-Tavío H, Guerra-Rodríguez M, García-Castellano JM, Fernández-Pérez L. The Mevalonate Pathway, a Metabolic Target in Cancer Therapy. *Front Oncol*. 2021;11:626971. doi:10.3389/fonc.2021.626971

111. Michalaki V, Koutroulis G, Koutroulis G, Syrigos K, Piperi C, Kalofoutis A. Evaluation of serum lipids and high-density lipoprotein subfractions (HDL2, HDL3) in postmenopausal patients with breast cancer. *Mol Cell Biochem*. 2005;268(1-2):19-24. doi:10.1007/s11010-005-2993-4

112. Kitahara CM, Berrington De González A, Freedman ND, et al. Total Cholesterol and Cancer Risk in a Large Prospective Study in Korea. *J Clin Oncol*. 2011;29(12):1592-1598. doi:10.1200/JCO.2010.31.5200

113. Niendorf A, Nägele H, Gerding D, Meyer-Pannwitt U, Gebhardt A. Increased LDL receptor mRNA expression in colon cancer is correlated with a rise in plasma cholesterol levels after curative surgery. *Int J Cancer*. 1995;61(4):461-464. doi:10.1002/ijc.2910610405

114. Yuan F, Wen W, Jia G, Long J, Shu XO, Zheng W. Serum Lipid Profiles and Cholesterol-Lowering Medication Use in Relation to Subsequent Risk of Colorectal Cancer in the UK Biobank Cohort. *Cancer Epidemiol Biomarkers Prev*. 2023;32(4):524-530. doi:10.1158/1055-9965.EPI-22-1170

115. Lin F, Zheng R, Yu C, Su Y, Yan X, Qu F. Predictive role of serum cholesterol and triglycerides in cervical cancer survival. *Int J Gynecol Cancer*. 2021;31(2):171-176. doi:10.1136/ijgc-2020-001333

116. Pih GY, Gong EJ, Choi JY, et al. Associations of Serum Lipid Level with Gastric Cancer Risk, Pathology, and Prognosis. *Cancer Res Treat*. 2021;53(2):445-456. doi:10.4143/crt.2020.599

117. Sánchez-Martín CC, Dávalos A, Martín-Sánchez C, De La Peña G, Fernández-Hernando C, Lasunción MA. Cholesterol Starvation Induces Differentiation of Human Leukemia HL-60 Cells. *Cancer Res*. 2007;67(7):3379-3386. doi:10.1158/0008-5472.CAN-06-4093

118. Rodríguez-Acebes S, de la Cueva P, Fernández-Hernando C, et al. Desmosterol can replace cholesterol in sustaining cell proliferation and regulating the SREBP pathway in a sterol-Δ24-reductase-deficient cell line. *Biochem J*. 2009;420(2):305-318. doi:10.1042/BJ20081909

119. De Gonzalo-Calvo D, López-Vilaró L, Nasarre L, et al. Intratumor cholesteryl ester accumulation is associated with human breast cancer proliferation and aggressive potential: a molecular and clinicopathological study. *BMC Cancer*. 2015;15(1):460. doi:10.1186/s12885-015-1469-5

120. Vini R, Rajavelu A, Sreeharshan S. 27-Hydroxycholesterol, The Estrogen Receptor Modulator, Alters DNA Methylation in Breast Cancer. *Front Endocrinol*. 2022;13:783823. doi:10.3389/fendo.2022.783823

121. Chen G, Vlantis A, Zeng Q, Van Hasselt C. Regulation of Cell Growth by Estrogen Signaling and Potential Targets in Thyroid Cancer. *Curr Cancer Drug Targets*. 2008;8(5):367-377. doi:10.2174/156800908785133150

122. Bièche I, Parfait B, Laurendeau I, Girault I, Vidaud M, Lidereau R. Quantification of estrogen receptor α and β expression in sporadic breast cancer. *Oncogene*. 2001;20(56):8109-8115. doi:10.1038/sj.onc.1204917

123. Avena P, Casaburi I, Zavaglia L, et al. 27-Hydroxycholesterol Binds GPER and Induces Progression of Estrogen Receptor-Negative Breast Cancer. *Cancers*. 2022;14(6):1521. doi:10.3390/cancers14061521

124. Kimbung S, Chang C yi, Bendahl PO, et al. Impact of 27-hydroxylase (CYP27A1) and 27-hydroxycholesterol in breast cancer. *Endocr Relat Cancer*. Published online July

2017:339-349. doi:10.1530/ERC-16-0533

125. Janowski BA, Grogan MJ, Jones SA, et al. Structural requirements of ligands for the oxysterol liver X receptors LXRα and LXRβ. *Proc Natl Acad Sci*. 1999;96(1):266-271. doi:10.1073/pnas.96.1.266

126. Venkateswaran A, Laffitte BA, Joseph SB, et al. Control of cellular cholesterol efflux by the nuclear oxysterol receptor LXRα. *Proc Natl Acad Sci*. 2000;97(22):12097-12102. doi:10.1073/pnas.200367697

127. Lehmann JM, Kliewer SA, Moore LB, et al. Activation of the Nuclear Receptor LXR by Oxysterols Defines a New Hormone Response Pathway. *J Biol Chem*. 1997;272(6):3137-3140. doi:10.1074/jbc.272.6.3137

128. Bilotta MT, Petillo S, Santoni A, Cippitelli M. Liver X Receptors: Regulators of Cholesterol Metabolism, Inflammation, Autoimmunity, and Cancer. *Front Immunol*. 2020;11:584303. doi:10.3389/fimmu.2020.584303

129. Ma WW, Li CQ, Yu HL, et al. The Oxysterol 27-Hydroxycholesterol Increases Oxidative Stress and Regulate Nrf2 Signaling Pathway in Astrocyte Cells. *Neurochem Res*. 2015;40(4):758-766. doi:10.1007/s11064-015-1524-2

130. Dasari B, Prasanthi JR, Marwarha G, Singh BB, Ghribi O. The oxysterol 27-hydroxycholesterol increases β-amyloid and oxidative stress in retinal pigment epithelial cells. *BMC Ophthalmol*. 2010;10(1):22. doi:10.1186/1471-2415-10-22

131. Gibson DA, Collins F, Cousins FL, Esnal Zufiaurre A, Saunders PTK. The impact of 27-hydroxycholesterol on endometrial cancer proliferation. *Endocr Relat Cancer*. 2018;25(4):381-391. doi:10.1530/ERC-17-0449

132. Kim WG, Park JW, Willingham MC, Cheng S yann. Diet-Induced Obesity Increases Tumor Growth and Promotes Anaplastic Change in Thyroid Cancer in a Mouse Model. *Endocrinology*. 2013;154(8):2936-2947. doi:10.1210/en.2013-1128

133. Halimi H, Farjadian S. Cholesterol: An important actor on the cancer immune scene. *Front Immunol*. 2022;13:1057546. doi:10.3389/fimmu.2022.1057546

134. Gao M, Liang J, Lu Y, et al. Site-specific activation of AKT protects cells from death induced by glucose deprivation. *Oncogene*. 2014;33(6):745-755. doi:10.1038/onc.2013.2

135. Xing J, Liu R, Xing M, Trink B. The BRAFT1799A mutation confers sensitivity of thyroid cancer cells to the BRAFV600E inhibitor PLX4032 (RG7204). *Biochem Biophys Res Commun*. 2011;404(4):958-962. doi:10.1016/j.bbrc.2010.12.088

136. Theodosakis N, Langdon CG, Micevic G, et al. Inhibition of isoprenylation synergizes with MAPK blockade to prevent growth in treatment-resistant melanoma, colorectal, and lung cancer. *Pigment Cell Melanoma Res*. 2019;32(2):292-302. doi:10.1111/pcmr.12742

137. Bose C, Bhuvaneswaran C, Udupa KB. Altered Mitogen-Activated Protein Kinase Signal Transduction in Human Skin Fibroblasts During In Vitro Aging: Differential Expression of Low-Density Lipoprotein Receptor. *J Gerontol A Biol Sci Med Sci*. 2004;59(2):B126-B135. doi:10.1093/gerona/59.2.B126

138. Jin S, Borkhuu O, Bao W, Yang YT. Signaling Pathways in Thyroid Cancer and Their Therapeutic Implications. *J Clin Med Res*. 2016;8(4):284-296. doi:10.14740/jocmr2480w

139. Hu L, Zhang J, Tian M, et al. Pharmacological inhibition of Ref-1 enhances the therapeutic sensitivity of papillary thyroid carcinoma to vemurafenib. *Cell Death Dis*. 2022;13(2):124. doi:10.1038/s41419-022-04550-0

140. Vemurafenib Active in Iodine-Refractory Thyroid Cancer. *Cancer Discov*. 2016;6(10):OF4-OF4. doi:10.1158/2159-8290.CD-NB2016-105

141. Lang M, Longerich T, Anamaterou C. Targeted therapy with vemurafenib in BRAF(V600E)-mutated anaplastic thyroid cancer. *Thyroid Res*. 2023;16(1):5. doi:10.1186/s13044-023-00147-7

142. Dunn LA, Sherman EJ, Baxi SS, et al. Vemurafenib Redifferentiation of *BRAF* Mutant, RAI-Refractory Thyroid Cancers. *J Clin Endocrinol Metab*. 2019;104(5):1417-1428. doi:10.1210/jc.2018-01478

143. Brose MS, Cabanillas ME, Cohen EEW, et al. Vemurafenib in patients with BRAFV600E-positive metastatic or unresectable papillary thyroid cancer refractory to radioactive iodine: a non-randomised, multicentre, open-label, phase 2 trial. *Lancet Oncol*. 2016;17(9):1272-1282. doi:10.1016/S1470-2045(16)30166-8

144. Busaidy NL, Konda B, Wei L, et al. Dabrafenib Versus Dabrafenib + Trametinib in *BRAF* -Mutated Radioactive Iodine Refractory Differentiated Thyroid Cancer: Results of a Randomized, Phase 2, Open-Label Multicenter Trial. *Thyroid*. Published online July 5, 2022:thy.2022.0115. doi:10.1089/thy.2022.0115

145. Chang CF, Yang MH, Lee JH, et al. The impact of BRAF targeting agents in advanced anaplastic thyroid cancer: a multi-institutional retrospective study in Taiwan. *Am J Cancer Res*. 2022;12(11):5342-5350.

146. Kim SY, Song YS, Wee JH, et al. Evaluation of the relationship between previous statin use and thyroid cancer using Korean National Health Insurance Service-Health Screening Cohort data. *Sci Rep*. 2021;11(1):7912. doi:10.1038/s41598-021-87297-6

147. Nielsen SF, Nordestgaard BG, Bojesen SE. Statin Use and Reduced Cancer-Related Mortality. *N Engl J Med*. 2012;367(19):1792-1802. doi:10.1056/NEJMoa1201735

148. Zhao J, Xu C, Yao J, Yu C, Liao L, Dong J. Statins and Thyroid Carcinoma: a Meta-Analysis. *Cell Physiol Biochem Int J Exp Cell Physiol Biochem Pharmacol*. 2018;47(4):1422-1431. doi:10.1159/000490832

149. Zeybek ND, Gulcelik NE, Kaymaz FF, et al. Rosuvastatin induces apoptosis in cultured human papillary thyroid cancer cells. *J Endocrinol*. 2011;210(1):105-115. doi:10.1530/JOE-10-0411

150. Zhong WB, Wang CY, Chang TC, Lee WS. Lovastatin Induces Apoptosis of Anaplastic Thyroid Cancer Cells via Inhibition of Protein Geranylgeranylation and de Novo Protein Synthesis. *Endocrinology*. 2003;144(9):3852-3859. doi:10.1210/en.2003-0098

151. Wang CY, Shui HA, Chang TC. Dual Effects for Lovastatin in Anaplastic Thyroid Cancer: The Pivotal Effect of Transketolase (Tkt) on Lovastatin and Tumor Proliferation. *J Investig Med*. 2018;66(5):1-9. doi:10.1136/jim-2017-000634

152. Hung MS, Chen IC, Lee CP, et al. Statin improves survival in patients with EGFR-TKI lung cancer: A nationwide population-based study. Souglakos J, ed. *PLOS ONE*. 2017;12(2):e0171137. doi:10.1371/journal.pone.0171137

- ANNEXES -

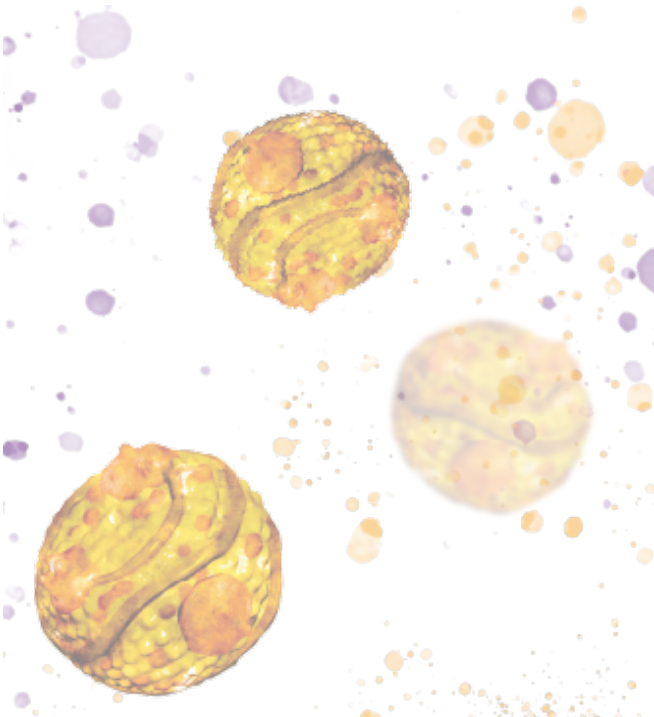

ANNEX I: List of publications and conferences

The following published research articles were included in the present thesis:

1- **Revilla G,** Pons MP, Baila-Rueda L, García-León A, Santos D, Cenarro A, Magalhaes M, Blanco RM, Moral A, Ignacio Pérez J, Sabé G, González C, Fuste V, Lerma E, Faria MDS, de Leiva A, Corcoy R, Carles Escolà-Gil J, Mato E. Cholesterol and 27-hydroxycholesterol promote thyroid carcinoma aggressiveness. Sci Rep. 2019 Jul 16;9(1):10260. doi: 10.1038/s41598-019-46727-2. PMID: 31311983; PMCID: PMC6635382.

2- **Revilla G,** Ruiz-Auladell L, Vallverdú NF, Santamaría P, Moral A, Pérez JI, Li C, Fuste V, Lerma E, Corcoy R, Pitoia F, Escolà-Gil JC, Mato E. Low-Density Lipoprotein Receptor Is a Key Driver of Aggressiveness in Thyroid Tumor Cells. Int J Mol Sci. 2023 Jul 6;24(13):11153. doi: 10.3390/ijms241311153. PMID: 37446330; PMCID: PMC10342163.

Other co-authored articles not included in this thesis:

3- Garcia-Rendueles MER, Krishnamoorthy G, Saqcena M, Acuña-Ruiz A, **Revilla G,** de Stanchina E, Knauf JA, Lester R, Xu B, Ghossein RA, Fagin JA. Yap governs a lineage-specific neuregulin1 pathway-driven adaptive resistance to RAF kinase inhibitors. Mol Cancer. 2022 Dec 7;21(1):213.

4- Hueso M, Griñán R, Mallen A, Navarro E, Purqueras E, Gomá M, Sbraga F, Blasco-Lucas A, **Revilla G,** Santos D, Canyelles M, Julve J, Escolà-Gil JC, Rotllan N. MiR-125b downregulates macrophage scavenger receptor type B1 and reverse cholesterol transport. Biomed Pharmacother. 2022 Feb;146:112596. doi: 10.1016/j.biopha.2021.112596. Epub 2021 Dec 28. PMID: 35062066.

5- **Revilla G.,** Hasan N., Caruana P., Rodriguez, F., Saez-Espinosa, V., Changda Li., Sainz M., Escolà-Gil JC., Pedraz JL., Corcoy R., Cespedes M V., Puras G. and Mato E. Reformulation of Lenvatinib encapsulated in PLGA nanoparticles with and without anti-EGFR conjugation: In vitro and in vivo proof of concept for treatment of thyroid cancer with aggressive behavior. *(Under Submission).*

Reviews:

6- **Revilla G**, Corcoy R, Moral A, Escolà-Gil JC, Mato E. Cross-Talk between Inflammatory Mediators and the Epithelial Mesenchymal Transition Process in the Development of Thyroid Carcinoma. Int J Mol Sci. 2019 May 18;20(10):2466. doi: 10.3390/ijms20102466. PMID: 31109060; PMCID: PMC6566886.

7- **Revilla G**, Cedó L, Tondo M, Moral A, Pérez JI, Corcoy R, Lerma E, Fuste V, Reddy ST, Blanco-Vaca F, Mato E, Escolà-Gil JC. LDL, HDL and endocrine-related cancer: From pathogenic mechanisms to therapies. Semin Cancer Biol. 2020; 26:S1044-579X(20)30248-0.

Book Chapters:

8- **Revilla, G.** Mato, E. Escolà, JC et al; The role of ATP-binding cassette transporter genes in the metastatic process of epithelial thyroid carcinoma with aggressive behavior; Unraveling the Complexities of Metastasis; Elsevier.

Selected Conferences:

- **Revilla, G.,** Mato, E., Garcia-León, A., Escolà, JC et al., Evidence of altered cholesterol metabolism in the aggressive behavior of epithelial thyroid neoplasia. World Congress on Thyroid Cancer; 2017 July; Boston, Massachusetts (United States of America).

- **Revilla, G.,** Mato, E. "Té implicacions el metabolisme del colesterol en el comportament agressiu de la neoplàsia tiroïdal d'estirp epitelial? III Jornada d'actualització de càncer de tiroides. Consorci per l'estudi de càncer de tiroides (CECat); 2018 Barcelona (Spain).

- **Revilla, G.** "Key role of cholesterol and 27-hydroxycholesterol in thyroid carcinoma agressiveness". XVI Jornada Científica del Departament de Bioquímica i Biologia Molecular. Universitat Autònoma de Barcelona; 2019 Barcelona (Spain).

- **Revilla, G.,** Santamaría, P., Moral, A., Pérez, J.I.,Fuste, V., Lerma, E., Corcoy, R., Pitoia, F., 9; Li, C., Escolà-Gil, J. C., Mato, E. Role of Braf V600E Mutation in LDL-Mediated Signaling Pathways Increases Aggressiveness in Thyroid Tumor Cells' . World Congress on Thyroid Cancer; 2023 June; London (United Kingdom).

ANNEX II: Effect of Cholesterol Intake on Thyroid Tumor Progression: Xenograft Mouse Model of Anaplastic Thyroid Cancer (CAL-62)

SUMMARY

Thyroid cancer of epithelial origin is the most common endocrine neoplasm, with a steadily increasing incidence over the last decade. These solid tumors exhibit diverse histological patterns, ranging from well-differentiated forms with favorable prognoses to undifferentiated and/or refractory tumors with poor prognoses. Clinical and experimental evidence links cholesterol, a crucial component of lipid bilayers that determines their physical and functional properties, and its metabolites with the process of tumor aggressiveness in some solid tumors.

The objective of this study was to analyze cholesterol intake in relation to tumor progression using a xenograft mouse model of anaplastic thyroid cancer (CAL-62). Two groups of animals were administered high-fat diets differing in cholesterol content, while a third group was maintained on a regular diet for comparison. The lipid profile was analyzed, and tumors were characterized at the tissue level to determine the percentage of necrotic area, the mitotic index, and neovascularization. At the protein expression level, LDL receptor expression, oncogenic signaling pathways (PI3K/AKT/mTOR/MEK/ERK), and SREBP isoforms (SREBP1 and SREBP2) were evaluated.

Results showed that dietary cholesterol intake led to the following changes compared to a low-cholesterol diet: 1. A systemic increase in LDL and triglycerides, 2. Larger and more viable tumors with a higher mitotic index and increased angiogenesis, 3. Reduced expression of LDLR, p-AKT, and P-mTOR proteins, along with activation of the MAPK/ERK pathway, 4. Lower levels of SREBP isoforms 1 and 2 in comparison to animals on a low-cholesterol diet, suggesting regulation in cholesterol synthesis and transport at the tumor tissue level.

In conclusion, these results suggest a link between systemic cholesterol levels and increased tumor aggressiveness, associated with a poorer prognosis for these tumors.

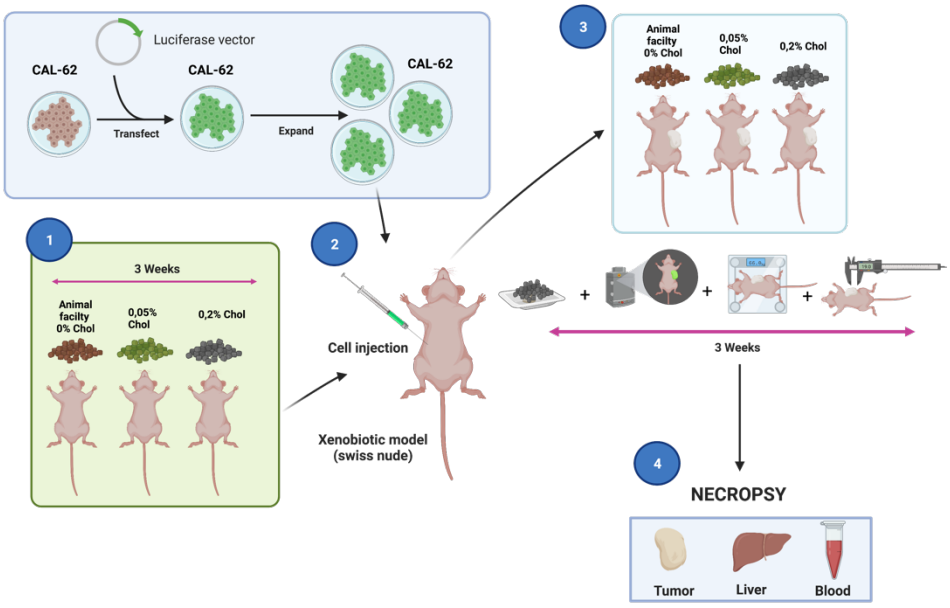

Figure 1: Chronological outline of the *in vivo* protocol in Swiss Nude mice. Created with BioRender.com

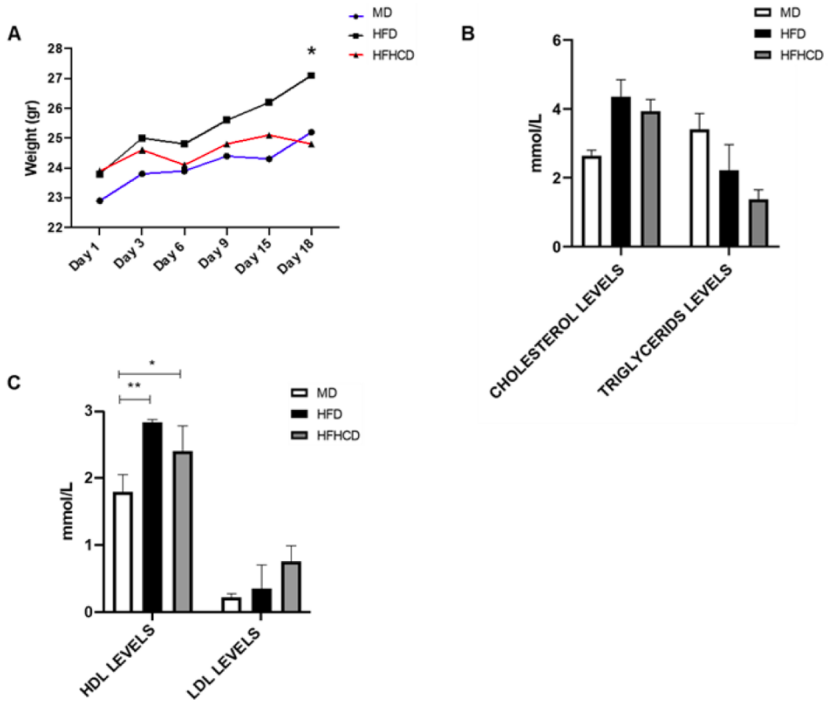

Figure 2. Analysis of weight and serum samples of Swiss Nude-CAL-62 mice with different types of diets. A. Analysis of mouse weight from day 1 to 18. Mice fed MD, HFC, and HFHCD diets. B. mmol/L of cholesterol and triglyceride levels. C. mmol/L of HDL and LDL levels. (**p=0.001) Statistical analysis: Tukey's method for multiple comparisons.

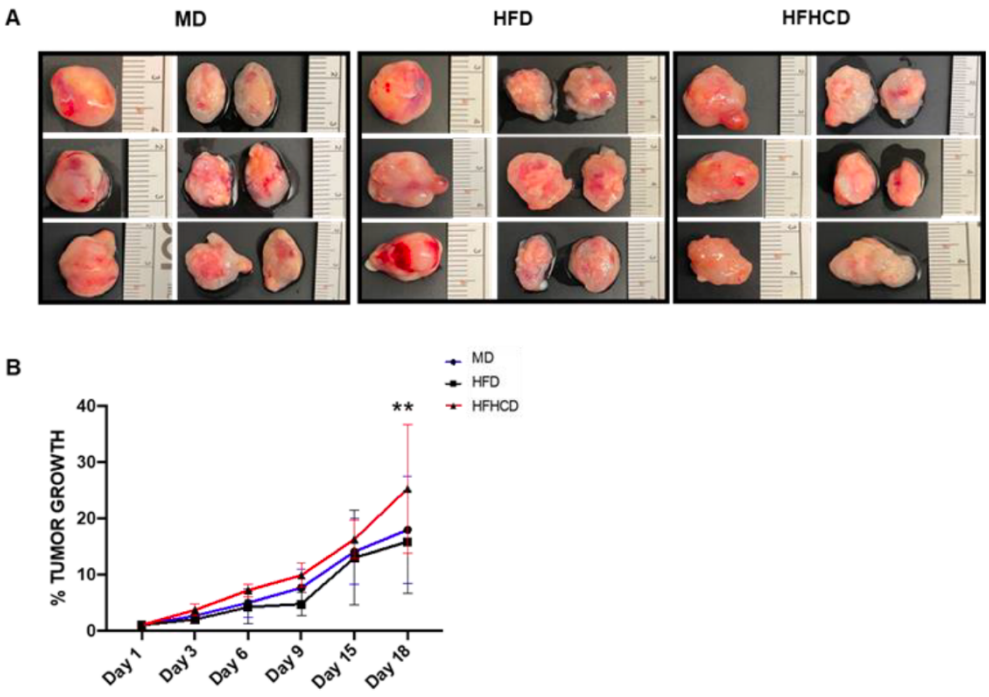

Figure 3. Tumor samples in the xenograft model of CAL-62 anaplastic thyroid tumor cells in Swiss Nude CAL-62 mice. A. Macroscopic observation of tumor specimens extracted from treated animals, showing different areas of fibrosis/necrosis. B. Tumor growth percentage from day 1 to 18. (**$p<0.058$ between HFD and HFHCD tumors) Statistical analysis: Tukey's method for multiple comparisons.

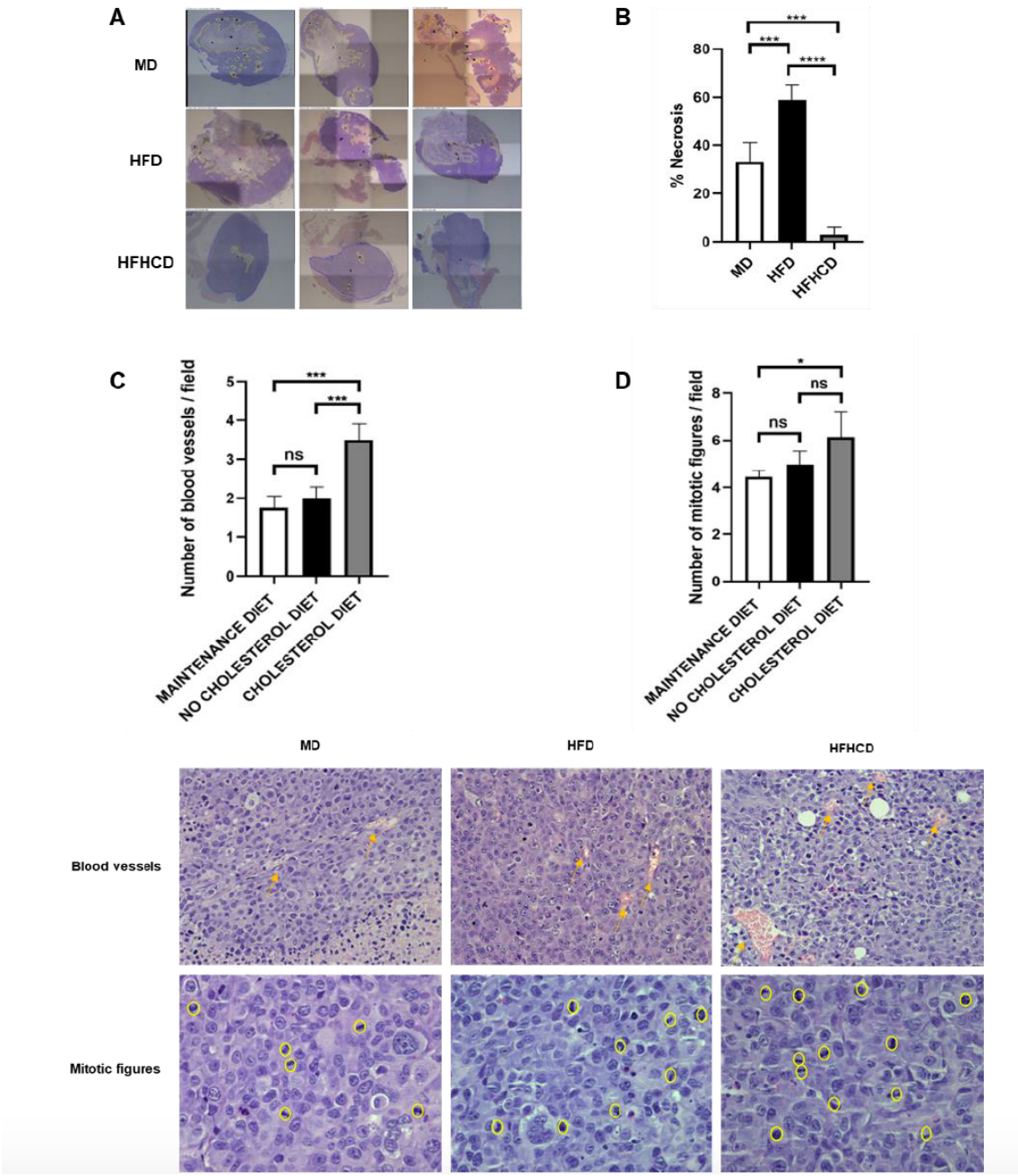

Figure 4. Histological analysis of tumor samples in the xenograft model of CAL-62 anaplastic thyroid tumor cells in Swiss Nude CAL-62 mice. A. Histological analysis showing areas of active tumor tissue and fibrosis. B. Percentage of necrotic tumor tissue. C. Count of mitotic figures per field at 40X magnification (14 total fields). D. Count of blood vessels per field at 20X magnification (12 total fields). E. Histological analysis showing the count of blood vessels and mitotic figures per field at 20X magnification. Data are expressed as mean ± SEM. (*p=0.02, ***p=0.001, ****p<0.0001) Statistical analysis: One-way ANOVA, Tukey's method for multiple comparisons.

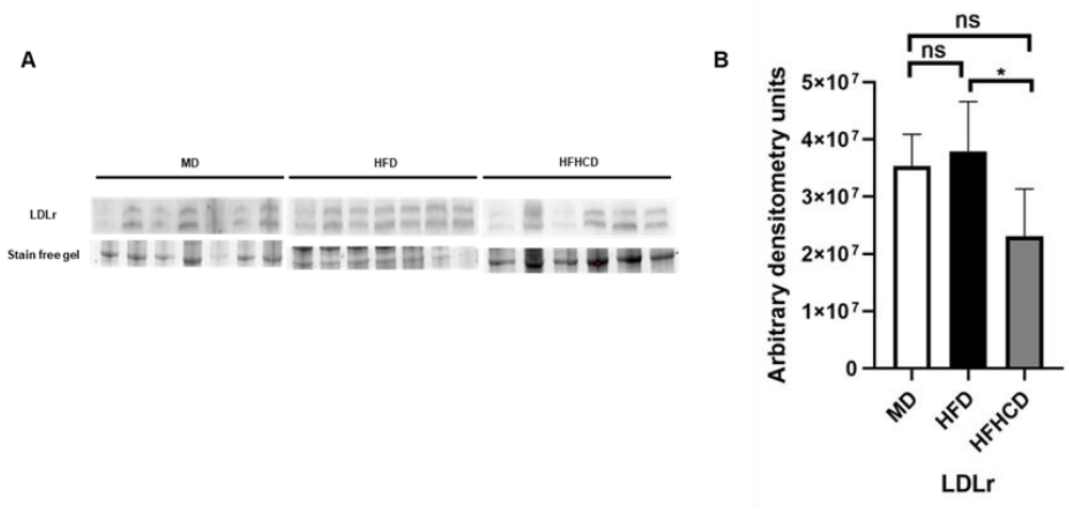

Figure 5. Protein expression of LDLR in tumors of the Swiss Nude-CAL-62 xenograft model with MD, HFC, and HFHCD diets. LDLR expression decreases in Swiss Nude CAL-62 mice administered with the HFHCD diet. Signals were normalized relative to Stain-Free gels, and data are presented as mean of the integrated relative density value for each group of mice. Data are expressed as mean ± SEM. (*p=0.02) Statistical analysis: One-way ANOVA, Tukey's method for multiple comparisons.